THE UNIVERSITY *of* EDINBURGH

This thesis has been submitted in fulfilment of the requirements for a postgraduate degree (e. g. PhD, MPhil, DClinPsychol) at the University of Edinburgh. Please note the following terms and conditions of use:

- This work is protected by copyright and other intellectual property rights, which are retained by the thesis author, unless otherwise stated.
- A copy can be downloaded for personal non-commercial research or study, without prior permission or charge.
- This thesis cannot be reproduced or quoted extensively from without first obtaining permission in writing from the author.
- The content must not be changed in any way or sold commercially in any format or medium without the formal permission of the author.
- When referring to this work, full bibliographic details including the author, title, awarding institution and date of the thesis must be given.

Interactions of organic carbon and nitrogen cycles with phytoplankton in a changing Southern Ocean

Ben J. Fisher

Thesis submitted in fulfilment of the requirements for the degree of

Doctor of Philosophy

University of Edinburgh

2024

Declaration

I declare that the thesis has been composed by myself and that the work has not be submitted for any other degree or professional qualification. I confirm that the work submitted is my own, except where work which has formed part of jointly-authored publications has been included. My contribution and those of the other authors to this work have been explicitly indicated below. I confirm that appropriate credit has been given within this thesis where reference has been made to the work of others.

The work presented in Chapter 2 is currently in revision at *Biogeosciences* as "Biogeochemistry of climate driven shifts in Southern Ocean primary producers" by **Ben J. Fisher,** Alex J. Poulton*, Michael P. Meredith*, Kimberlee Baldry, Oscar Schofield, and Sian F. Henley*. This study was conceived by BJF and SFH. I carried out all model analysis, coding and data processing and led the writing of the article. MPM contributed towards the writing of the physical oceanography and sea ice sections of the article. KB provided input on conducting comparative model analysis. AJP and OS contributed towards the biological interpretation. All authors provided feedback on the submitted article.

The work presented in Chapter 3 is currently in submission to *Global Biogeochemical Cycles* as "The structure of Southern Ocean phytoplankton communities influences molecular level variability in dissolved organic matter composition" by **Ben J. Fisher**, Michael Seidel, Alex J. Poulton, Nicole Waite, Miah Manning, Michael Cappola, Thorsten Dittmar, Oscar Schofield, Sian F. Henley*. This study was conceived by BJF. I wrote the funding proposal, conducted all fieldwork and lab work, completed data analysis and led the writing of the article. MS and TD provided lab training and sample analysis facilities for FT-ICR-MS. OS facilitated fieldwork, with NW, MM and MC contributing towards sampling efforts in the field. AJP and SFH provided supervision and helped with writing the article, all authors gave feedback on the submitted article.

The work presented in Chapter 4 has not currently been submitted for publication. This work was performed by **Ben J. Fisher**, Andrew Smith, Sharon McNeill, Alex J. Poulton* and Sian F. Henley*. The experiments in this chapter were designed by BJF, AJP and SFH. I co-developed analysis of enriched liquid phase nitrate and ammonium isotopes with AS as part of a NERC Environmental Isotope Facility grant, written by myself and awarded to SFH due to eligibility criteria. SM provided technical assistance in the analysis of particulate nitrogen isotopes at SAMS.

* denotes a supervisor

Ben J. Fisher

June 2024

Abstract

Marine phytoplankton are the foundation of the Southern Ocean ecosystem and carbon cycle. Carbon fixation during summertime photosynthesis produces organic matter and drives the Southern Ocean towards being a seasonal carbon sink. Consequently, the Southern Ocean sequesters a disproportionately large amount of anthropogenic carbon and heat relative to its size. However, increased heat uptake is having widespread environmental impacts on the Southern Ocean, including reduced sea ice concentrations, increased sea surface temperatures, and increased variability in nutrient supply resulting from changes to stratification. These multiple stressors feedback on marine phytoplankton and can influence rates of growth and nutrient uptake, alongside potential ecological changes in community composition and size class.

This thesis takes a multi-methods approach, combining model evaluation, laboratory experiments and *in situ* sampling to further our understanding of how Southern Ocean phytoplankton will respond to the projected effects of climate change, and the subsequent impacts for carbon and nitrogen cycling. Earth system model outputs from the coupled model intercomparison project (CMIP6) were analysed for properties of Southern Ocean phytoplankton, physics and biogeochemistry to examine the extent of projected change under a high emission, low mitigation pathway (SSP5-8.5). Productivity across the Southern Ocean was shown to increase by 30% over the 21st century, against a backdrop of global decreases in net primary productivity. Since most CMIP6 models have simplistic representations of phytoplankton, there is widespread inter-model variability in the extent to which productivity will increase across the different latitudinal zones of the Southern Ocean. However, ensemble means suggest that diatoms and picophytoplankton (2-20 µm) will increase at roughly similar rates across much of the Subantarctic and Transitional zones, while growth of picophytoplankton is expected to exceed that of diatoms in the coastal Antarctic zones. The greatest source of variability was identified as being from light concentrations (>15000 (µE m^{-2} s^{-1})^2), particularly close to ice shelves. Uncertainties in light supply leads to variability in phytoplankton growth in this iron and light limited system. Projected changes in phytoplankton growth were analysed from the perspective of the Southern Ocean Observing System to identify spatial and temporal frames whereby targeting of additional sampling may be most beneficial in resolving uncertainties for future generations of model development.

To understand how potential ecological changes in the composition of phytoplankton communities will impact the carbon cycle, sites were sampled along the West Antarctic Peninsula (WAP) to analyse the molecular composition of dissolved organic matter (DOM) associated with different phytoplankton types. DOM was analysed by ultrahigh resolution FT-ICR-MS to identify possible molecular fingerprints of phytoplankton types. Analysis of the stable carbon isotope ($\delta^{13}C$) and stoichiometric data allowed for the identification of different DOM sources and transformation processes. Smaller classes of phytoplankton (<20 µm),

including cryptophytes and flagellates, were most abundant in the warmer northern peninsula region and were associated with fresher forms of DOM. In comparison, larger diatoms were associated with aged DOM, which had a higher degree of degradation and was depleted in carbon and nitrogen compared to the bulk pool. All forms of DOM were rapidly transformed below the euphotic zone, resulting in a recalcitrant background pool of DOM at depth. If future Southern Ocean phytoplankton communities shift towards a smaller size class, a greater amount of organic matter is likely to be partitioned to the dissolved phase, potentially weakening the organic carbon sink.

Since nutrient requirements differ between phytoplankton types, one consequence of shifts in community composition could be changes to nutrient utilisation. Utilisation of nitrogenous nutrients are of particular interest because the Southern Ocean exports nutrients across the global ocean, ~75% of which is limited by nitrogen outside of high nutrient zones. An experiment was conducted whereby different Southern Ocean phytoplankton species in culture were incubated with isotopic tracers (^{15}N) to measure the uptake of nitrate, ammonium and urea. This showed that at realistic nutrient concentrations for the WAP during summer, all species have a preference for ammonium, accounting for >50% of total nitrogen uptake. The greatest amount of variability in nitrogen uptake existed at the species level between the pennate diatoms *Fragilariopsis cylindrus* and *Pseudo-nitzschia subcurvata*, perhaps due to growth limitation in one species. This study further investigated variability in the application of the ^{15}N tracer method by adapting an existing chemical method from the freshwater literature to work in seawater. This was successfully applied to show that a titanium mediated conversion is effective for determining the isotopic composition of ^{15}N enriched NH_4^+in seawater, allowing for the correction of ammonium uptake rates for ammonium regeneration. Accounting for ammonium regeneration increased ammonium uptake rates by 52% (± 16%), suggesting the importance of ammonium for phytoplankton may be greater than previously thought.

Taken together, the results of this thesis demonstrate that physical change in the Southern Ocean resulting from climate driven environmental change, will increase overall primary productivity and variability in the abundance of different phytoplankton size fractions across the latitudinal zones of the Southern Ocean. Biogeochemical implications of this ecological shift could manifest through increased DOM partitioning reducing export efficiency and more variability in nitrogenous nutrient uptake. Improving consistency in nutrient uptake methodologies and targeting additional observations to regions of existing uncertainties could help to resolve knowledge gaps in our understanding of phytoplankton-biogeochemical coupling in this large and climatically sensitive region.

Lay Summary

The Southern Ocean is a key regulator of global climate, playing a disproportionately large role for its size in absorbing heat and carbon released by human activities. However, heat uptake by the Southern Ocean has led to warming at up to five times the global average in some water masses. This is concerning because increased ocean temperatures leads to reductions in sea ice concentrations, which are intimately linked to ecosystems of the Southern Ocean. Marine phytoplankton are the primary producers of the Southern Ocean food web, they require light to fix carbon dioxide to organic carbon, which can act as a food source to larger organisms. When sea ice retreats in the spring and summer, light availability to the Southern Ocean increases and marine phytoplankton grow in to large blooms, taking up nutrients and forming biological organic carbon in the process.

Under climate change conditions, we could expect changes to phytoplankton populations of the Southern Ocean including changes in concentrations of phytoplankton across different regions, and shifts in the type of phytoplankton which form the population. This can have downstream impacts on nutrient and carbon cycling if different types of phytoplankton utilise nutrients or release carbon at different rates. Since whales, penguins and other Antarctic species rely on krill, which in turn feed on phytoplankton, as a primary food source, we may also experience wider ecological consequences from disturbance to phytoplankton populations. Ecosystems could become much less efficient if phytoplankton blooms move earlier in the season in response to the earlier retreat of sea ice, this disturbs the feeding patterns of migratory predators because phytoplankton and zooplankton stocks will have dissipated by the time these predators reach the Southern Ocean. With reduced energy availability, predator populations such as whales will struggle to survive and reproduce to the same extent as when phytoplankton blooms align with their migratory patterns.

This thesis first examines the projected physical, chemical and biological changes in the Southern Ocean as a result of a continued climate change scenario using global scale models. The rate of carbon production, as well as the amount of nutrients required for growth stand out as the two key variables in models which influence the global carbon cycle and also differ with phytoplankton type. Further experiments aimed to better understand these relationships by conducting a ship-based survey seeking to associate organic carbon with differing states of reactivity as being products of different phytoplankton types. Additionally, the amount of nitrogen-containing nutrients used for growth by different phytoplankton species was determined, after developing a method required to accurately measure this. Our collective understanding gained from these experiments and model projections can be used to improve our ability to better project the response of fragile Southern Ocean environments and ecosystems to continued climate change.

Acknowledgements

In retrospect, starting a field-based research project about the Southern Ocean amidst a global pandemic was perhaps not the best timing. My PhD journey has been challenging, at times frustrating, but most importantly rewarding. I will always remember the experience of joining my first research cruise to the Southern Ocean, seeing the vast glacial landscape, penguin colonies and pods of whales for the first time. None of what has been achieved in this thesis would have been possible without the continuous support of my supervisors, friends, colleagues, and family to whom I owe an enormous debt of gratitude.

When I first met my supervisor, Dr Sian Henley, at a meeting while I was a master's student in Leeds and proposed starting a PhD, I'm not sure either of us could have predicted what the next 4 years would have in store. I am immensely grateful for the friendly way in which we have been able to work together during my PhD. I also express thanks to Prof. Alex Poulton and Prof. Michael Meredith for their useful input as supervisors throughout my PhD. Following many pandemic related revisions to my PhD plan, much of the work included in this PhD involved experiments which were brand new to me and my supervisors. I have benefited from the generosity of many collaborators who have lent their time and expertise to help me with setting up these experiments.

I thank Dr Michael Seidel and Prof. Thorsten Dittmar at the University of Oldenburg for hosting me on multiple visits to their group to learn the solid phase extraction protocol and analyse DOM samples. Dr Andrew Smith at the NERC Environmental Isotope Facility was invaluable in helping me to develop the method for isotopic analysis of enriched ammonium in seawater. I am grateful to Prof. Oscar Schofield for allowing me to join his group on the Palmer LTER cruise, and acknowledge the scientists and crew of LMG23-01, in particular, Nicole Waite, Michael Cappola and Miah Manning were incredibly helpful in assisting me with sampling. At Edinburgh, I thank Prof. Sinéad Collins for her help in setting up my culture experiments, Dr Ulrike Baranowski for helping with $\delta^{13}C$ analysis, and Dr Gavin Sim for lab support and his great ability to always find the obscure chemicals I needed.

My friends and colleagues in the PhD office have been a constant source of support throughout my PhD. It would be impossible to acknowledge everybody, however I especially thank Sophie, David, Sally, Siobhan and Freddie for their friendship over the years. Outside of Edinburgh, I was fortunate to meet Patrick and Jess from the University of Washington, who made the GEOTRACES Summer School and Ocean Sciences Meeting such fun experiences, thanks also for letting me stay at your house!

Finally, I acknowledge NERC for funding my PhD through the E4 DTP and Environmental Isotope Facility Grant. Antarctic Science International supported my fieldwork and sample analysis, along with travel and logistical support from NSF. The Scottish Alliance for Geoscience, Environment and Society (SAGES) provided COVID funding support and travel funding. I am also grateful for conference grants from the Challenger Society, GEOTRACES, EGU and European Association of Geochemistry

List of Abbreviations

^{15}N: Isotopically enriched nitrogen

AABW: Antarctic Bottom Water

AAIW: Antarctic Intermediate Water

AASW: Antarctic Surface Water

ACC: Antarctic Circumpolar Current

AI_{Mod}: Modified Aromaticity Index

APCC: Antarctic Peninsula Coastal Current

ASF: Antarctic Slope Front

ASL: Amundsen Sea Low

CDW: Circumpolar Deep Water

Chl: Chlorophyll

CMIP(6): Coupled Model Intercomparison Project

CRM: Certified Reference Material

DBE: Double Bond Equivalent

DOC: Dissolved Organic Carbon

DOM: Dissolved Organic Matter

DON: Dissolved Organic Nitrogen

DSW: Dense Shelf Water

FT-ICR-MS: Fourier Transform Ion Cyclotron Resonance Mass Spectrometry

HNLC: High Nutrient Low Chlorophyll

ICP-MS: Inductively Coupled Plasma Mass Spectrometry

I_{DEG}: Degradation Index

LCDW: Lower Circumpolar Deep Water

MDL: Method Detection Limit

MLB_L: Molecular Lability Boundary

NADW: North Atlantic Deep Water

NPQ: Non-Photochemical Quenching

OA: Ocean Acidification

OM: Organic Matter

Palmer LTER: Palmer Long Term Ecological Research Program

PF: Polar Front

PN: Particulate Nitrogen

POC: Particular Organic Carbon

POM: Particular Organic Matter

PPL: Priority Pollutant (Cartridges)

RFU: Relative Fluorescence Units

SAF: Subantarctic Front

SAM: Southern Annular Mode

SAMW: Subantarctic Mode Water

SASW: Subantarctic Surface Water

SB: Southern Boundary of the ACC

SF: Southern Front

Si*: (The concentration of silicic acid – the concentration of nitrate)

SOCAT: Surface Ocean CO_2 Atlas

SOCCOM: Southern Ocean Carbon and Climate Observations and Modelling

SOOS: Southern Ocean Observing System

SPE: Solid Phase Extraction

STF: Subtropical Front

UCDW: Upper Circumpolar Deep Water

UNFCCC: United Nations Framework Convention on Climate Change

WAP: West Antarctic Peninsula

WW: Winter Water

Contents

1. Introduction

1.1 Physical oceanography of the Southern Ocean

The Southern Ocean south of 50°S has an open ocean area of up to 38.66 x10^6 km^2 during austral summer (Arrigo et al., 1998). The Antarctic Circumpolar Current (ACC) forms the major circulation pattern, with the lack of land barriers in the mid to high latitudes allowing the ACC to connect the Southern Ocean to all the other major ocean basins (**Figure 1.1**) forming the global overturning circulation (Rintoul et al., 2001). Subsequently, this overturning circulation distributes heat, nutrients, and freshwater across the thermohaline gradient. Therefore, changes in Southern Ocean heat and carbon uptake, along with modulation of the export of excess nutrients has the ability to influence global ocean productivity.

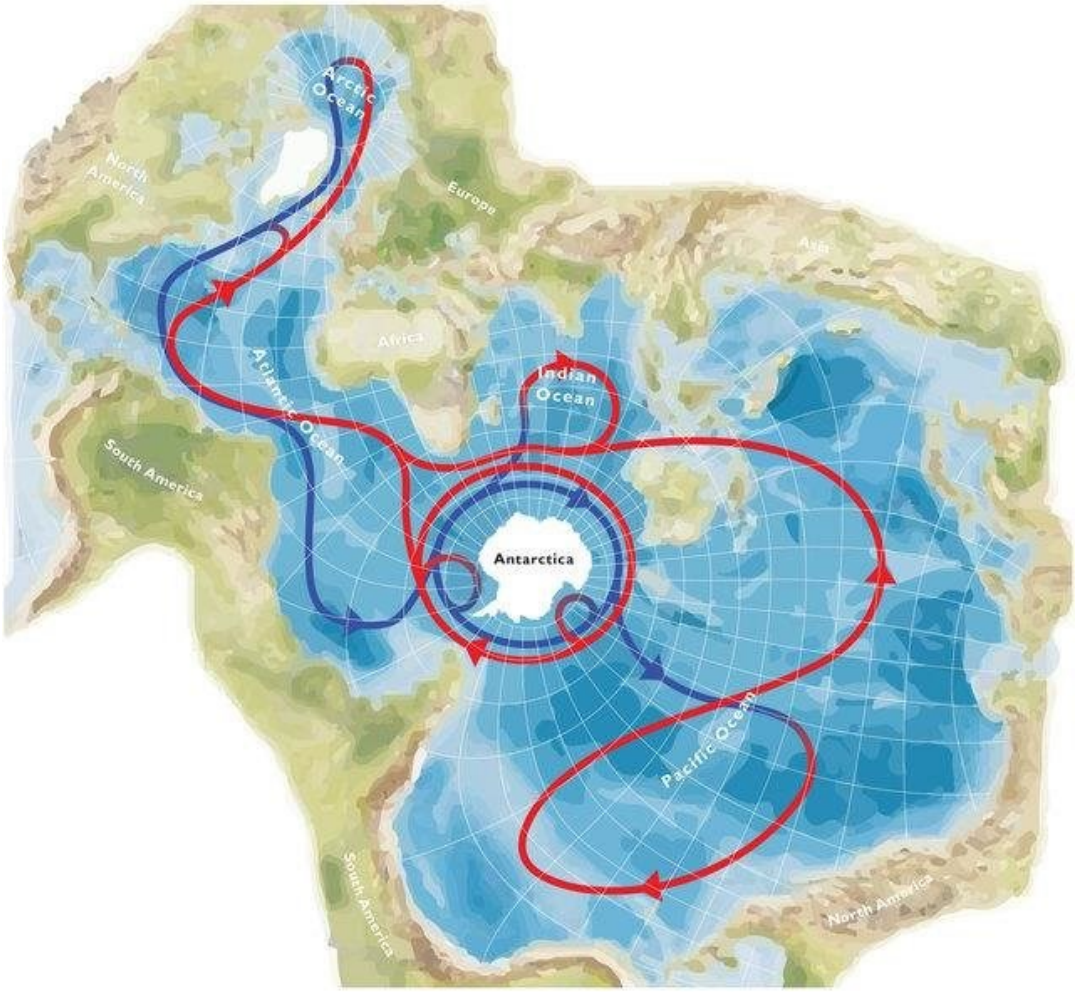

Figure 1.1: Spilhaus projection of the Southern Ocean, the upper-layer circulation is shown in red and lower-level in blue, reproduced from (Meredith, 2019).

1.1.1 **Water masses**

Surface waters of the Southern Ocean are latitudinally separated in to fronts by differences in temperature and salinity (**Figure 1.2**, **Table 1.1**). Closest to the continent, the Antarctic Slope Front represents the boundary between fresh shelf water and more saline circumpolar deep water carried by the ACC (Carter et al., 2008). Between the Southern ACC front and Polar fronts, cold, fresh Antarctic Surface Water (ASSW) meets Subantarctic Surface Water (SASW), as SASW cools while travelling south it sinks below the AASW, the mixing of the two water masses ultimately produces Antarctic Intermediate Water (AAIW). New AAIW is produced in regions of the southwest Atlantic and southeast Pacific, where it sinks below Subantarctic Mode Water (SAMW) (Carter et al., 2008). Mesoscale diapycnal mixing with SAMW results in a denser form of AAIW which can be returned to 'new' AAIW through Ekman pumping in to the mixed layer south of the PF before being advected northward by Ekman transport (Li et al., 2022).

As part of the overturning circulation, Circumpolar Deep Water is upwelled towards the southern boundary of the ACC. Due to air and ice interactions, this CDW is converted to a less dense form, producing Upper Circumpolar Deep Water (UCDW) (Meredith and Brandon, 2017). UCDW plays an important role in ice-ocean interactions as the upwelling of warm deep water on to the shelf contributes towards basal ice shelf and glacier melt (Meredith and Brandon, 2017). The more saline Lower Circumpolar Deep Water (LCDW) originates from North Atlantic Deep Water (NADW) and generally resides off the shelf, but can also contribute heat to glacial melt in regions of low nominal shelf depth (Martinson and McKee, 2012). Alongside heat, the high nutrient concentrations found in UCDW are important for stimulating productivity. Prézelin et al. (2000) found that UCDW intrusions on to the continental shelf of the West Antarctic Peninsula (WAP) were responsible for enhanced biological production, specifically diatom dominated communities which supported krill populations.

Antarctic Bottom Water (AABW) is formed from Dense Shelf Water (DSW) along the continental margin. DSW develops during winter when sea ice formation causes brine rejection producing cool dense water which sinks along the continental shelf. The mixing of DSW with CDW forms AABW, which is exported along the ACC. The deep-water nature of AABW, along with its export from the continent means that this is a highly important water

mass for the sequestration of carbon and heat in deep waters on the scale of centuries (de Lavergne et al., 2017). Properties of AABW are sensitive to climate dynamics, with salinity, density and thickness closely linked to sea ice formation. Against a backdrop of long-term freshening of AABW over previous decades (e.g. Purkey and Johnson, 2013, Menezes et al., 2017), wind forcing resulting from a combination of a positive Southern Annular Mode (SAM) and El Niño during 2015-2018 caused increased sea ice formation in the Ross Sea, producing a more saline and dense AABW (Aoki et al., 2020, Silvano et al., 2020).

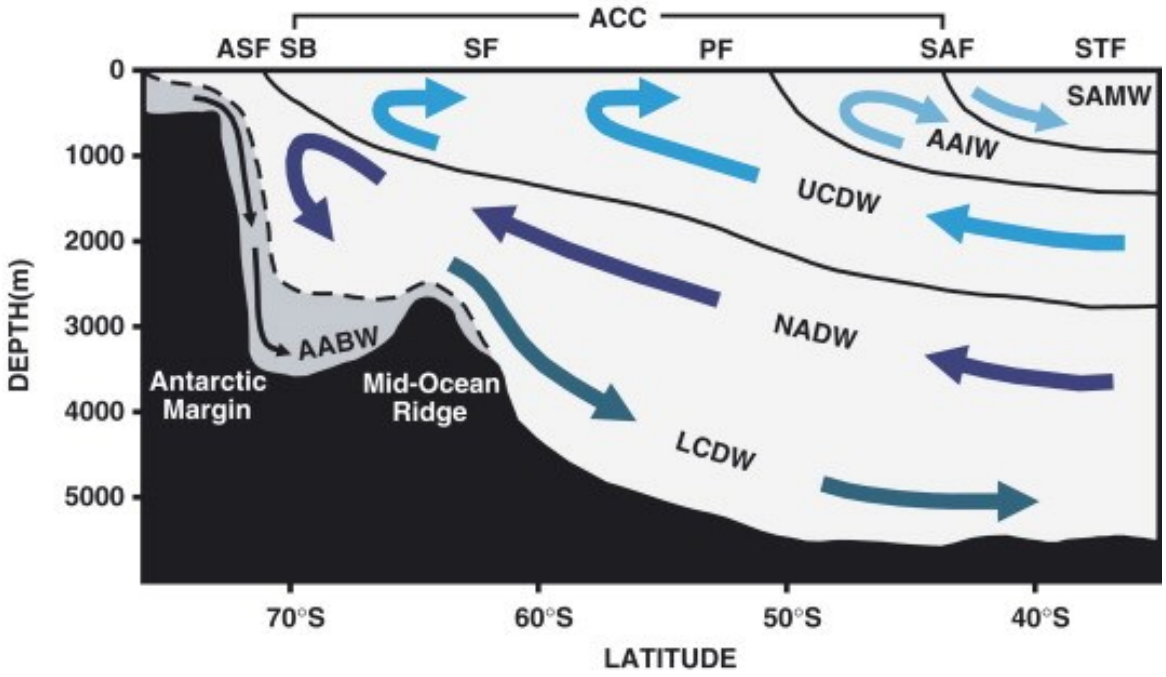

Figure 1.2: Water masses of the Southern Ocean and their transport. Abbreviations: SAMW- Subantarctic Mode Water, AAIW- Antarctic Intermediate Water, UCDW- Upper Circumpolar Deep Water, LCDW- Lower Circumpolar Deep Water, NADW- North Atlantic Deep Water, AABW- Antarctic Bottom Water. Fronts: ASF- Antarctic Slope Front, SB- Southern Boundary of the ACC, SF- Southern Front, PF- Polar Front, SAF- Subantarctic Front, STF- Subtropical Front. Figure reproduced from (Carter et al., 2008).

A cold surface layer of water forms over autumn and winter (winter water) which is low in temperature and salinity (**Table 1.1**). Winter water experiences the largest seasonal variability in volume, reaching a maximum in October and a minimum in March (Evans et al., 2018). In the sea-ice sector of the Southern Ocean, the formation of a freshwater layer results in shoaling of the mixed layer following a seasonal cycle (Nardelli et al., 2017). During subsequent deepening of the mixed layer, remaining winter water from the prior year is first entrained to the mixed layer resulting in an initial cooling and buoyancy loss between

January and May before entrainment of the warmer UCDW between May and October increases buoyancy again (Pellichero et al., 2017). The balance between winter water and UCDW inputs to the winter mixed layer is a strong influence on heat content and is an important determinant of sea-ice formation (Gordon, 1991, Gordon and Huber, 2012).

Table 1.1: Water mass properties (depth, salinity and temperature) for the Southern Ocean.

Water Mass	Depth	Salinity (g kg^{-1})	Temperature	Reference
Winter Water	0-100m	33.8-34.0	-1.5°C	Dierssen et al. (2002)
Antarctic Bottom Water	1500-4000m	34.45-34.72	-0.9 to 0°C	Talley et al. (2011)
Antarctic Intermediate Water	500-1200m	34.2-34.5	3-7°C	Yao et al. (2017)
Upper Circumpolar Deep Water	200-550m	34.62-34.68	1.55-2.10°C	Moffat et al. (2009)
Lower Circumpolar Deep Water	500-1600m	~34.73	1.25-1.57°C	Moffat et al. (2009)
Subantarctic Mode Water	200-1000m	34.1-34.8	5.2-10.3°C	(Bushinsky and Cerovecki, 2023)

1.1.2 **Sea ice dynamics**

Antarctic sea ice has been strongly variable over the last 50 years, in contrast to declining Arctic sea ice concentrations associated with a warming climate (Yadav et al., 2020, Cai et al., 2021). Antarctic sea ice underwent a period of steady growth between 1978 and 2010 on the order of 1.2 ±0.2% per decade (Comiso, 2010). Within this time period, spatial variability existed within the trend of increasing area, the Ross Sea, Weddell Sea and Indian Ocean

sector (**Figure 1.3**) experienced growth, while the Bellingshausen and Amundsen Seas jointly underwent a decline of -8200 ± 1200 km^2 yr^{-1} (Parkinson and Cavalieri, 2012). Some authors proposed this spatial variability to be a result of a co-occurrence between a strong El Niño (La Niña) and a negative (positive) Southern Annular Mode (Stammerjohn et al., 2008). With El Niño causing increases in sea ice in the Bellingshausen region and decreases in the Ross Sea due to warm northerly winds and inverse trends resulting from the dominance of cold southerly winds in La Niña years (Yuan, 2004). SAM interacts with the El Niño Southern Oscillation (ENSO), producing the most favourable sea ice conditions for sea ice growth outside of the Bellingshausen region when La Niña co-occurs with a positive SAM, such conditions were attributed to a record high sea ice extent in 2008 (Pezza et al., 2011).

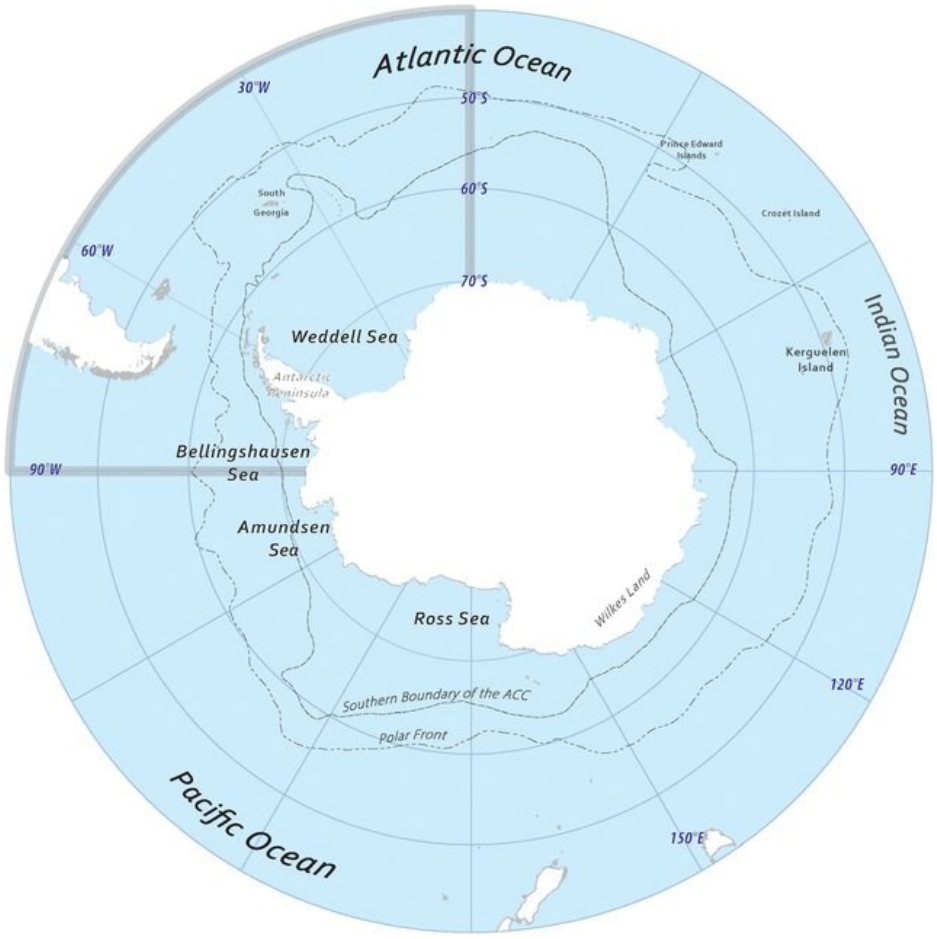

Figure 1.3: Geography of the regions and seas of the Southern Ocean. The two major frontal systems, the Antarctic Circumpolar Current and Polar Front are indicated, along with the seas and oceanic sectors. Figure reproduced from Sylvester et al. (2021)

Recently however, the overall trend of increasing sea ice has rapidly reversed, leading to a record low sea ice extent in 2022 and then again in 2023 (**Figure 1.4**) despite an ongoing combination of La Niña and positive SAM. These reductions in sea ice have been linked to a particularly deep Amundsen Sea Low (ASL), where strong winds resulting from this low pressure system lead to the breakup of sea ice (Turner et al., 2022). Multiple studies propose that we have entered a new state for Antarctic sea ice, where subsurface oceanic warming plays a greater role in determining sea ice extent (Raphael and Handcock, 2022, Purich and Doddridge, 2023). However, within the context of periods of strong multidecadal variability in Antarctic sea ice over the last 40 years (Parkinson, 2019), continued monitoring over the coming years will be required to determine whether the current trends represent an oscillation or a fundamental shift in sea ice behaviour.

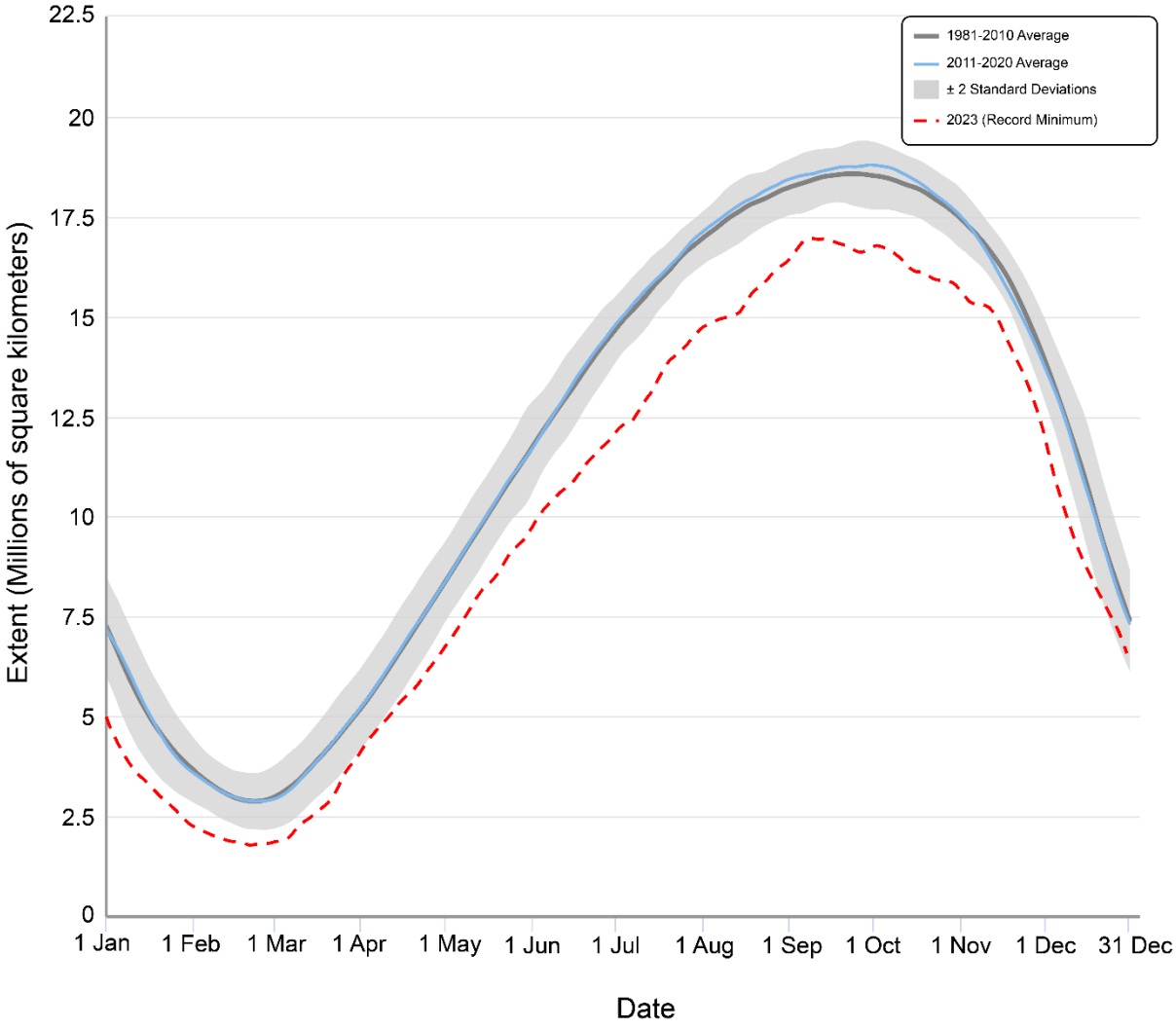

Figure 1.4: Antarctic sea ice extent, representative of the area of ocean with at least 15% sea ice cover. The grey line represents the mean sea ice extent from 1981-2010, plus or minus 2 standard deviations, shown by the grey shaded area. The blue line represents the 2011-2020 average and the red dashed line the 2023 sea ice extent, the record minimum since 1981. Figure based on data provided by the National Snow and Ice Data Center, Boulder CO.

Beyond driving deep ocean circulation through the formation of AABW, sea ice plays an important role in heat and CO_2 exchange across the air-sea interface. Sea ice cover may be expected to reduce exchange of CO_2 between the atmosphere and the ocean as the ice acts as a physical barrier, reducing outgassing via capping and minimising the influence of wind driven mixing on the ocean. However, the concurrent rejection of CO_2 with brine during sea ice formation is estimated to account for a flux of 186 Tg C yr^{-1} being exported to depth (Rysgaard et al., 2011). Combined with multiple studies demonstrating the permeability of sea ice to gas exchange (e.g. Delille et al., 2007, Rysgaard et al., 2007) the contribution of sea ice to CO_2 uptake could account for up to 58% of the Southern Ocean CO_2 flux (Delille et al., 2014). Despite the potential importance of sea-ice to the Southern Ocean carbon cycle,

Watts et al. (2022) have highlighted the lack of data on air-sea CO_2 exchange in the marginal ice zone, in particular the lack of consistent methodology between studies means that gas exchange associated with multi-year ice, polynyas and eddy covariance remain poorly understood. Under climate change, outgassing of CO_2 can be expected to increase with more intense storm events (Nicholson et al., 2022) and reduced sea ice concentrations will make a greater amount of the ocean surface available for gas exchange (Shadwick et al., 2021). In addition to the physical exchange of inorganic carbon with the atmosphere, biological carbon uptake is sensitive to changes in sea ice cover (Chierici et al., 2004, Fransson et al., 2004). During the seasonal sea ice retreat, the stratification induced by the influx of fresh meltwater promotes phytoplankton blooms where dissolved inorganic carbon (DIC) is drawn down by biological carbon export, leading to a reduction in seawater pCO_2. Net Primary Productivity (NPP) and phytoplankton community composition, particularly greater abundance of diatoms and haptophytes, have been associated with larger changes in the seawater pCO_2 value across the West Antarctic Peninsula (−43.60 ± 39.06 µatm in the diatom dominated southern WAP vs 21.71 ± 22.39 µatm in the north) (Moreau et al., 2012, Hauri et al., 2015), and Indian sector (Jabaud-Jan et al., 2004, Takao et al., 2020). However, with most of these studies relying on remote sensing of primary productivity, understanding the extent of the role of biological carbon export in determining the ΔpCO_2 is spatially and temporally limited to summer (Takao et al., 2020), likely missing the biological uptake of CO_2 during periods of ice breakup.

1.1.3 **Stratification and wind driven mixing**

The mixed layer depth (MLD) is determined by the strength of vertical mixing and varies in space and time in responses to atmospheric forcing, the layer thickness quantifies the volume of water which is available for direct exchange of heat and CO_2 with the atmosphere (Dong et al., 2008). In the Southern Ocean, westerly winds enhance the northward export of sea ice in the Southern Ocean, promoting freshwater injection at more northerly latitudes, and enhancing stratification (Haumann et al., 2016). Glacial discharge is likely to have the greatest impact on stratification in the Amundsen and Bellingshausen Seas, with freshwater reaching as far west as the Ross Sea (Levermann et al., 2014, Meredith et al., 2019). The combined effect of these factors on MLD can impact primary productivity, since stratification changes the nutrient and light availability to phytoplankton. Under climate change, shoaling

of mixed layers within the seasonal sea ice zone from increased stratification is expected to increase light availability (as phytoplankton become more concentrated near the surface), and deplete nutrient concentrations (Boyd et al., 2008).

Increased near-surface wind strength has also been linked to reduced upper-ocean stratification and deeper mixed layers around the Southern Ocean (Carranza and Gille, 2015, Sallee et al., 2021). However this is counteracted near to the coast by the stabilising influences of buoyancy forcing (Shi et al., 2020). A substantial proportion of the extra energy resulting from zonal wind strengthening is imparted to the mesoscale eddy field (Meredith and Hogg, 2006, Hogg and Munday, 2014, Hogg et al., 2015). This intensification of the eddies may lead to regional enhancements in vertical mixing and nutrient supply, especially where it is co-located with regions of rugged bathymetry (Sheen et al., 2014) and sedimentary sources of iron (Kahru et al., 2007, Ellwood et al., 2020, Uchida et al., 2020). Such changes to nutrient supply could stimulate greater biological export of carbon. For example, at a larger scale, intensified wind driven mixing has been seen to increase supply of deep iron-rich water to the Weddell Sea gyre, stimulating dense phytoplankton blooms and increasing krill stocks (Moreau et al., 2023). The occurrence of synoptic storm events has also been associated with deepening of the mixed layer (du Plessis et al., 2017) and increases of up to 60% in summer primary productivity in the Subantarctic (Nicholson et al., 2016), through nutrient exchange to the surface layer by turbulent subsurface mixing.

1.2 Southern Ocean Ecosystems

1.2.1 The microbial loop

In the Southern Ocean, photosynthesis by marine phytoplankton in the euphotic zone represents the major source of organic matter (OM) to the ecosystem. In turn, this fuels the microbial loop, providing energy to protozoa, bacteria and viruses, degrading OM and liberating nutrients in the process. The Southern Ocean is known to be a region of high biomass and low export because of strong grazing by krill populations in the Antarctic region, in contrast to deeper penetration of the OM flux through the ocean in the Subantarctic where carbonate production plays a greater role in productivity (Lam and Bishop, 2007). Consequently, the flux of OM to benthos is low and where this does occur, is observed to be a seasonal 'pulse' (Smith and Comiso, 2008, Smith Jr et al., 2013), comprised of intrinsically recalcitrant material (Cho et al., 2020), with low bioavailability to sustain

microbial communities. Therefore, the pelagic microbial loop is the major energy sink for new productivity in the Southern Ocean, with an organic transfer efficiency of ~50% (**Figure 1.5**).

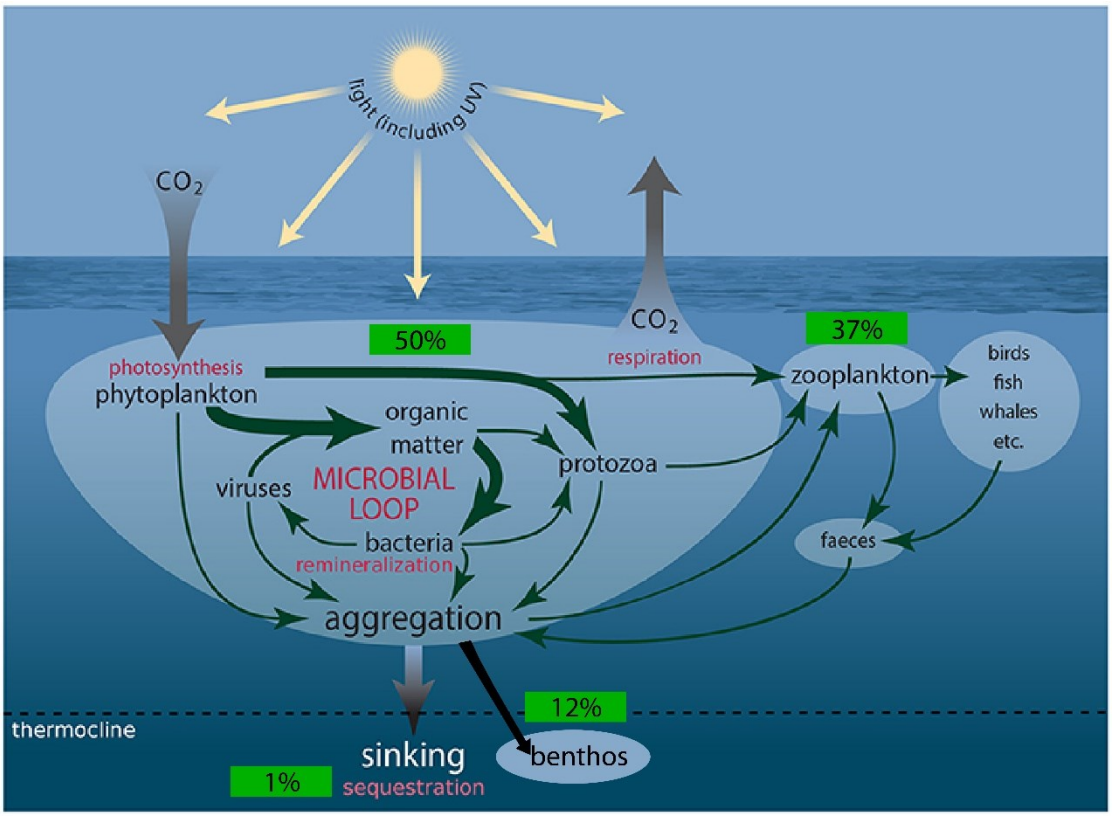

Figure 1.5: Production, trophic transfer and sequestration of organic matter in the Southern Ocean, with a focus on dynamics within the microbial loop. Figure adapted from Deppeler and Davidson (2017), with the approximate organic matter transfer efficiency shown in green boxes, with values derived from Henley et al. (2020) and references therein.

Microbial community composition in the Southern Ocean is driven by nutrient availability, (nitrate and phosphate), (Wilkins et al., 2013b, Signori et al., 2014), salinity (Evans et al., 2011), and physical perturbations by advection (Wilkins et al., 2013a) or proximal distribution by krill (Clarke et al., 2018). Seasonality also plays a substantial role in mediating microbial interactions with phytoplankton and prokaryotes, with greater abundances and diversity of microbial prokaryotes during summertime phytoplankton blooms where dissolved organic matter (DOM) availability can be greater (Castillo et al., 2022 and references therein), in part due to photodegradation of organic compounds during periods of increased light availability (Cory and Kling, 2018).

Nanoprotozoa (2–20 μm) include heterotrophic nanoflagellates and dinoflagellates; mixotrophic behaviour in some flagellate species allows for both autotrophic production and heterotrophic consumption of similar sized prey (Moorthi et al., 2009), as well as 27-95% of bacterial production (Thomson et al., 2010). Subsequently, they form an important part of the pelagic ecosystem in allowing for the trophic transfer of regenerated productivity (Froneman and Perissinotto, 1996).

Viral activity has been observed to be greater during blooms (Gowing et al., 2004), potentially due to a feedback whereby the release of organics and nutrients from phytoplankton lysis (Fuhrman, 1999, Evans and Brussaard, 2012), stimulates new phytoplankton growth and increases the abundance of hosts which can become infected (Castillo et al., 2022). The lysis of phytoplankton cells by viruses reduces the efficiency of carbon export by shunting intracellular nutrients and organic matter away from grazers and towards decomposers (Suttle, 2007). Viral lysis was shown to account for the majority (58%) of seasonal phytoplankton losses at the Rothera time series station on the WAP, with a particular impact on smaller and non-silicified phytoplankton types such as cryptophytes and *Phaeocystis spp.* (Biggs et al., 2021). This variable impact of viruses on different phytoplankton types highlight the importance of species composition in driving ecosystem and carbon dynamics, with species more vulnerable to lysis being less likely to be efficiently grazed, reducing the export efficiency of their organic content.

Early studies differentiated phytoplankton types based on size fraction, with species <2 μm considered to be picophytoplankton, those in the range of 2-20 μm being nanophytoplankton and individuals > 20 μm assigned to the microphytoplankton (e.g. Jochem et al., 1995, Gall et al., 2001). At the global scale, this approach provides a high-level understanding of the likely contributors towards primary productivity since cyanobacteria such as *Prochlorococcus* and *Synechococcus* fall in to the pico- category, while diatoms exist within the >2μm category. However, in the cold-water conditions of the Southern Ocean where cyanobacteria are low in abundance, the main phytoplankton types (diatoms, cryptophytes, dinoflagellates and haptophytes) can all span both the nano and micro phytoplankton categories, so size fractionation can obscure differential environmental responses or rates between phytoplankton types. Chemical methods based on pigment proxies (e.g. CHEMTAX (Mackey et al., 1996) and *phytoclass* (Hayward et al., 2023)), or *in* situ

imaging techniques of water samples (e.g. Imaging Flow Cytobot (Olson and Sosik, 2007)) have allowed for a more in depth understanding of group specific biogeography (Hayward et al., 2024).

Diatoms are a key contributor to the Southern Ocean carbon cycle because of their widespread abundance, relatively high carbon content, and ability to rapidly export organic matter due to low buoyancy resulting from silicification. High silicic acid concentrations across the Southern Ocean support dense summertime diatom blooms (Henley et al., 2020), with iron and manganese being the main limiting nutrients (Pausch et al., 2019). Where iron supply is greater, larger chain forming diatom species such as *Eucampia antarctica*, and *Fragilariopsis kerguelensis* are seen to dominate the community composition (Laubscher et al., 1993, Boyd et al., 2000, Salter et al., 2007). High nutrient low chlorophyll (HNLC) iron limited regions are more favourable towards smaller diatoms, for example Timmermans et al. (2001) found that the small diatom *Chaetoceros brevis* is adapted to slow growth and is not iron limited under HNLC iron concentrations, this diatom could only become iron limited by reducing the bioavailability of iron through siderophore binding. However, some large diatom species may be able to access complexed iron through evolved bio-reduction pathways, unique to polar diatom species (Strzepek et al., 2011). Additionally, there is growing evidence that large Southern Ocean diatoms have physiologically adapted to the environmental low iron and light concentrations, having larger photosynthetic antennae (Alderkamp et al., 2019) and reducing iron demand through lower than expected chlorophyll (Chl) and carbon to cell volume ratios in *E. antarctica* and *Proboscia inermis* (Strzepek et al., 2019).

Antarctic cryptophytes are a group of small sized phytoplankton (~10 µm) (Mcminn and Hodgson, 1993) gaining attention for their increasing abundance on the WAP between 2008-2018 (Mendes et al., 2023) where they have begun to outgrow other phytoplankton types in sea-ice influenced regions (e.g. Mendes et al., 2018a, Mendes et al., 2018b). Advection (Moline and Prezelin, 1996), diatom grazing (Garibotti et al., 2003b) and low salinity stable water columns from sea-ice and glacial inputs (e.g. Moline et al., 2004, Schofield et al., 2017, Brown et al., 2019) have previously been attributed as drivers of cryptophyte growth. *Geminigera cryophila* is the main cryptophyte species present in the Southern Ocean and is available in culture, such that multiple studies have sought to understand drivers of

cryptophyte abundance using *G. cryophila* as a model (McKie-Krisberg et al., 2015, Trimborn et al., 2019, Mendes et al., 2023). From light exposure experiments, Mendes et al. (2023) attributed the occurrence of cryptophytes in the shallow highly stratified surface layer to a good tolerance for high and variable light concentrations. In contrast, Trimborn et al. (2019) found that tolerance of high light conditions only occurs under simultaneous high pCO_2 conditions, with high light causing growth inhibition at ambient pCO_2, these authors conclude that "*G. cryophila* may be potential winners of climate change".

The haptophyte *Phaeocystis antarctica* is a large colony forming species (up to 2 mm), which can substantially impact carbon and nitrogen cycles because of high rates of CO_2 and nitrate drawdown alongside rapid size associated carbon export (Arrigo et al., 1999). Differing from diatom populations, *Phaeocystis spp.* can also enzymatically convert the organosulfur compound dimethylsulfoniopropionate (DMSP) to volatile dimethylsulfide (DMS) (Van Boekel et al., 1993), contributing to the outward air-sea flux of sulphur. The relative abundance of *Phaeocystis spp.* over diatoms has been linked to mixed layer depth, with *Phaeocystis spp.* generally being more tolerant of deeper mixed layers (Arrigo et al., 1999). *Phaeocystis* blooms usually form earlier in the season during sea ice retreat, and are the main genera present in massive under ice prymnesiophyte blooms (Saggiomo et al., 2021). The iron requirement for *Phaeocystis* colony formation (Garcia et al., 2009, Bender et al., 2018) could explain its appearance in the early period of the growth season, before the re-supply of iron supply over winter has been depleted by uptake. *P. antarctica* may also have an advantage over other species by their ability to sequester iron from a wide range of organic complexes (Strzepek et al., 2011), including iron held in humic-like exopolymeric substances (Fourquez et al., 2023). The apparent early season preference of *P. antarctica* is consistent with proteomic signatures of combined iron-manganese co-limitation in *P. antarctica* during the late growth season (Wu et al., 2019). Nutrient induced succession of phytoplankton communities has implications for determining the fate of organic matter, including the balance of organic carbon supply to heterotrophic microbial communities.

1.2.2 **Phytoplankton phenology**

During winter, the Southern Ocean experiences extended periods of severe light limitation, from a combination of sea ice cover and the polar night, consequently, primary productivity in the region is tightly coupled to seasonal cycles. Despite the low light concentrations

during winter (<1 E m^{-2} d^{-1}), under ice productivity during winter begins the accumulation of biomass before the onset of sea-ice retreat (Arteaga et al., 2020). Productivity within sea ice accounts for 9-25% of the total productivity within the sea-ice zone (Arrigo et al., 1997), but may play a relatively larger role during winter because of the lower impact of light attenuation relative to below ice phytoplankton. During the early spring sea ice retreat, seeding of phytoplankton has been presumed to start the open water productivity cycle, with sea ice diatoms among the first phytoplankton types to dominate (Petrou et al., 2016). However this perspective is somewhat controversial, with Lizotte (2001) concluding that the seeding hypothesis is largely based on similarities in the composition of sea ice and early season sea ice zone phytoplankton, but does not account for how processes within sea ice (e.g. physical stress, and strong variability in salinity) could impact the viability of cells released from thawing sea ice. A potential explanation for the increase in diatom-based productivity at the start of the season, beyond alleviation of light limitation, could be the release of nutrients by thawing land-fast sea ice (Henley et al., 2023).

The emergence of sea ice diatoms in spring can be attributed to their ability to adapt to changes in high light concentrations through physiological photoprotection adaptations. The sea ice diatom *Fragilariopsis cylindrus* produces more photoprotective xanthophyll pigments than the haptophyte *P. antarctica* (Kropuenske et al., 2009, Arrigo et al., 2010, Kropuenske et al., 2010), the higher concentration of xanthophyll allows for effective non photochemical quenching (NPQ), dissipating excess light energy and protecting photosystem II from damage (Olaizola et al., 1994). For species such as *P. antarctica* where NPQ is less effective, the cells are more dependent on protein mediated repair processes to their photosynthetic apparatus (Kropuenske et al., 2009, Kropuenske et al., 2010). The high concentration of photoprotective pigments in *F. cylindrus* correlates with a reduced concentration of photosynthetic pigments (i.e. chlorophyll), therefore, while sea ice diatoms have an advantage in high and variable light environments, this is a trade off against a lower capacity for photosynthesis and growth (Arrigo et al., 2010). As sea ice concentrations reduce through early summer, open water area increases and light conditions stabilise; this can allow diatom species that partition more of their pigment content towards growth (Lavaud et al., 2007), alongside species which prefer the light conditions associated with stable mixed layers (e.g. *P. antarctica* (Arrigo et al., 2010)), to succeed the sea ice diatom dominated population.

Summertime blooms consist of a mixed community between *P. antarctica* colonies and diatoms (e.g. DiTullio and Smith, 1996, Arrigo et al., 1999, Poulton et al., 2007, Smith et al., 2014). At the Southern Ocean scale, a modelling approach suggests the balance of the community between these two phytoplankton types is driven by temperature and iron availability, with iron limitation more adversely impacting *Phaeocystis* and temperature limitation having a greater limiting effect on diatoms (Nissen and Vogt, 2021). The succession from a diatom based to *Phaeocystis* based community has also been linked to silicic acid limitation, following the export of silicic acid from the surface by sinking diatoms (Salter et al., 2007). Iron availability can additionally act as a control on the Si:C stoichiometry of sinking diatoms. Under conditions of iron limitation across the Subantarctic, thicker shelled diatom species experience growth limitation, and have produce less organic carbon from photosynthesis. This drives the export of emptier silica shells (high Si:C) in contrast to carbon dense mucosal export (low Si:C) in iron fertilised regions where organic carbon production is unimpeded (Assmy et al., 2013) .

Due to a combination of a low grazing pressure from krill for *Phaeocystis* and colony aggregation (Schoemann et al., 2005), *Phaeocystis* can act as a vector for nutrients and carbon. Studies disagree on the fate of this carbon and nutrients, with some authors proposing that the aggregation and sinking of colonies transfers organic matter to deep waters while others suggest that the biomass is remineralised in the mesopelagic (Nissen and Vogt, 2021 and references therein). The fate is likely to be a factor of density, and will depend on whether communities are comprised of low-density solitary cells or large colonies, up to 3cm in size, which will rapidly sink. Regardless of the eventual fate of this nutrient-rich organic matter, the uptake of nutrients during the formation of large *Phaeocystis* and diatom mixed blooms results in nutrient limitation, terminating the *Phaeocystis* bloom (Wang and Moore, 2011), with iron limitation impacting *Phaeocystis* through reductions in growth rate, cell size, cellular iron quotas and photosynthetic efficiency (Koch et al., 2018).

The late season phytoplankton community is comprised of a smaller size class of species, such as cryptophytes, which increase in abundance after the peak in primary productivity (**Figure 1.6**). The abundance of cryptophytes is linked to the light conditions of well stratified water columns (see **1.2.2**), which are increasingly common in coastal regions following

freshwater input from summertime glacial melt. However, work in culture indicates that cryptophytes are highly sensitive to iron limitation (Camoying et al., 2022), suggesting that for cryptophytes to occupy this niche, iron must be resupplied either by remineralisation of *Phaeocystis* in the mesopelagic (Reigstad and Wassmann, 2007, Yang et al., 2016) or through terrigenous inputs of iron in glacial run off (Alderkamp et al., 2012).

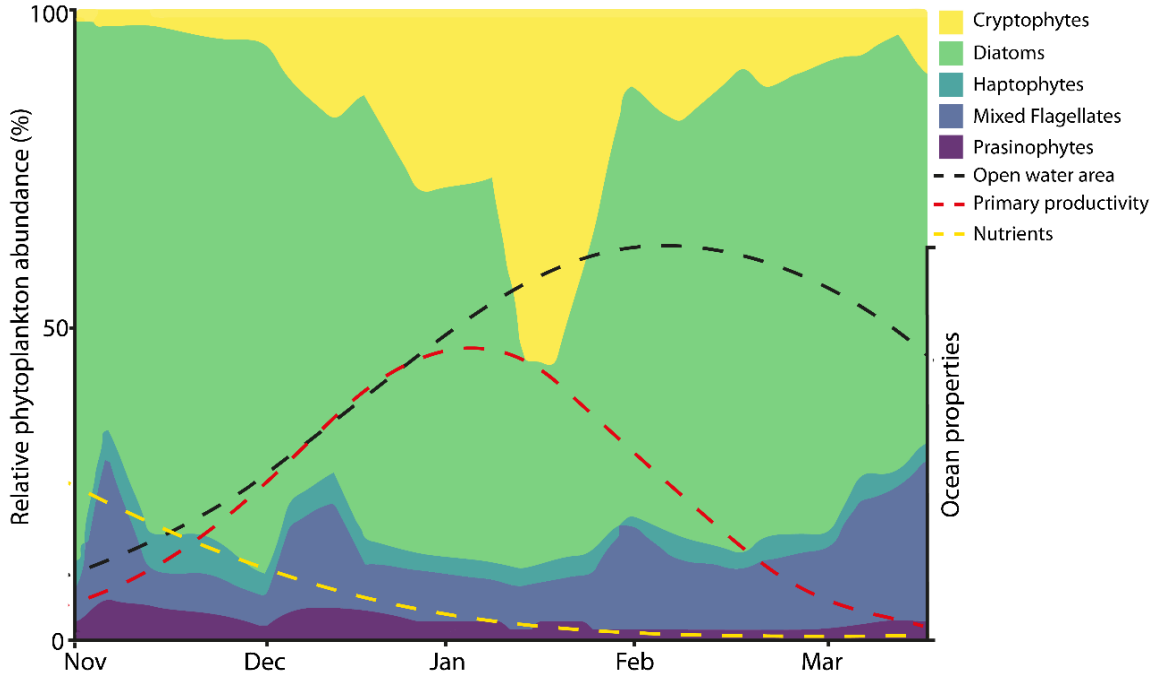

Figure 1.6: Timing of changes in relative abundance (by number) of phytoplankton groups along the west Antarctic Peninsula overlayed with timing of transitions in open water area, primary productivity and macronutrients for the seasonal sea ice zone. Figure adapted from phytoplankton composition provided by Cimino et al. (2023), ocean property timing is adapted from Petrou et al. (2016) based on (Arrigo et al., 2008).

Although this description of phytoplankton succession is generalised for the seasonal sea ice zone of the WAP, it should be noted that patterns of succession are spatially variable, typically along a north-south gradient with the timing of group succession linked to sea ice retreat (Garibotti et al., 2003a). The close relationship with sea ice also results in temporal variability on the decadal scale with shifts in sea ice dynamics being historically dictated by the phases of ENSO and SAM (see **1.1.2**). Resolving the spatial, temporal and climate variability to determine a clear phenology of phytoplankton succession alongside the physical, biological and chemical drivers remains a key challenge for the field.

1.2.3 **Higher trophic levels**

As phytoplankton are the major source of OM to Southern Ocean ecosystems, shifts in the phytoplankton community composition can have major implications for energy transfer through higher trophic levels. Key to the trophic transfer of primary productivity is the grazing efficiency of Antarctic krill (*Euphausia superba*) (Atkinson et al., 2004); krill effectively graze on diatom populations (Saba et al., 2014), and are themselves consumed by a range of predators including penguins and whales. This short food chain acts as an efficient shuttle of energy since there are fewer opportunities for energy to be lost in transfer. Along the WAP, in years where cryptophytes were more abundant, the zooplankton community shifted from krill towards salps *(Salpa thompsoni)* (Moline et al., 2004). The balance between krill and salps influences higher trophic levels because salps are far less efficient at transferring energy compared to protein and fat rich krill (Böckmann et al., 2021). Salp blooms have been observed as a common feature on the northern WAP since 2010 (Bernard et al., 2012) and the shift from krill towards salps in this region have been linked to declines in Adélie penguin populations (Trivelpiece et al., 2011). Conversely, regions with high chlorophyll concentrations support penguin diets which are rich in krill (Saba et al., 2014).

Krill are discriminate grazers which prefer a diatom-dominated diet, with poor grazing efficiency on non-diatom phytoplankton species (e.g. cryptophytes (Haberman et al., 2003)). This preference for diatoms could be a passive physiological restriction (e.g., filter feeding mesh size) or an active selection in response to chemical or physical stimuli using receptors (Pauli et al., 2021 and references therein). In contrast salps are non-selective in their feeding behaviour, utilising all types of phytoplankton (Pakhomov et al., 2002).

Marine mammals and krill also play an important role in nutrient recycling within the surface Southern Ocean, particularly for the major limiting nutrient, iron. Antarctic krill is estimated to act as a reservoir for ~24% of the iron in surface waters (Nicol et al., 2010), because krill do not sink or migrate they can effectively retain iron in the upper ocean. As the major food source to baleen whales, this iron is transferred through the ecosystem during the summer breeding season before release through defecation, where whale faeces are enriched in iron by a factor of up to 10 million compared to seawater (Ratnarajah et al., 2014). Sperm whales have also been postulated to act as a shuttle for the return of deep water iron to the surface by consumption of prey at depth and subsequent release in the surface, this process could

account for the transfer of ~50 tonnes Fe yr^{-1} (Lavery et al., 2010). Southern Ocean whale populations are still recovering from the industrial whaling era; the role of whales in recycling iron in the surface suggests they may make an increasingly important contribution to sustaining phytoplankton populations as the demand for iron by phytoplankton will increase with longer sea ice free growing seasons. The composition of phytoplankton stimulated by any change in iron concentrations may then have an important feedback on Southern Ocean ecosystems as krill grazing of this larger, iron fertilised, phytoplankton population will return energy to predators through trophic transfer. The balance between krill and salp populations stands out as a key constraint on the efficiency of energy transfer in the phytoplankton-zooplankton-predator Antarctic food chain. Changes in the food chain which subsequently impact the composition or abundance of macroecological species can play a key role in the distribution of nutrients and carbon across the global ocean (Murphy et al., 2021). The movement of migratory species from the Southern Ocean represents a variable pathway for nutrient and carbon export, independent of ocean circulation. This demonstrates the intimate link between biogeochemical cycling with ecology and the potential for regional Southern Ocean processes to have global scale impacts.

1.3 Southern Ocean Biogeochemistry

1.3.1 Carbon cycle

The Southern Ocean has accounted for at least 43% (± 3%) of anthropogenic CO_2 uptake in recent decades (Frölicher et al., 2015). When aged deep water is upwelled to the surface, the difference in pCO_2 between the atmosphere and the surface drives the air-sea flux, this exchange can be further influenced by physical drivers such as wind, sea ice, storms, and mesoscale processes, including eddies (Rysgaard et al., 2011, Delille et al., 2014, Keppler and Landschutzer, 2019, Shadwick et al., 2021, Nicholson et al., 2022).

Chemically, pCO_2 of the ocean surface is determined from the concentration of dissolved inorganic carbon [DIC] and total alkalinity, the acid buffering capacity of the ocean (Lueker et al., 2000). At warmer temperatures pCO_2 increases as CO_2 solubility decreases, in the Southern Ocean where temperature is seasonal this results in summertime reductions in the air-sea CO_2 flux, counteracting the increased biological uptake of DIC over the growth season (Lenton et al., 2013, Mongwe et al., 2018). The uptake of CO_2 by the Southern Ocean is greatest in the Subtropics where wintertime exchange driven by seasonal cooling is strong

compared to south of the polar front where sea ice capping inhibits gas exchange (**Figure 1.7**). The Subantarctic acts as a net CO_2 source, with outgassing being the dominant signal between May and October (**Figure 1.7**). In this region Ekman transport of water masses across front systems and mesoscale processes drive the outgassing (Yang et al., 2024), and the impact of storms has also been shown to be particularly acute in the Subantarctic (Nicholson et al., 2022).

CO_2 solubility also increases when salinity decreases, the freshening of surface waters associated with summertime meltwater input therefore reduces the pCO_2 of waters in the seasonal sea ice zone, allowing for a greater air-sea CO_2 flux (Legge et al., 2017, Kiuchi et al., 2021). However, the competing effects of temperature, salinity and biological productivity (since freshening also impacts nutrient concentrations) makes pCO_2 difficult to resolve over spatial and temporal scales (Nomura et al., 2014). Gray (2024) highlights that current approaches towards understanding pCO_2 dynamics place an overreliance on zonal averaging, which results in the loss of fine scale variability by averaging these positive and negative values over large areas. This makes it more difficult to determine differences pCO_2 between different sectors of the Southern Ocean. Additionally, mesoscale and microscale turbulent processes can have significant, but to-date poorly characterised, impacts on Southern Ocean gas exchange.

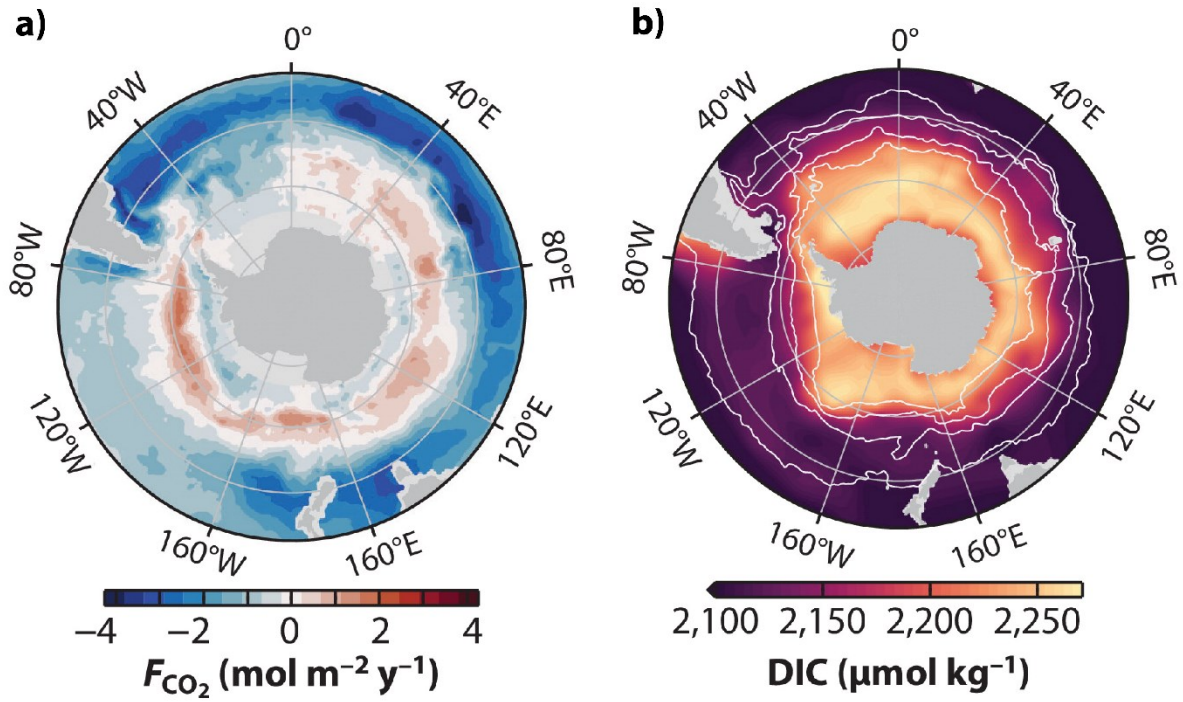

Figure 1.7: Inorganic carbon properties of the Southern Ocean adapted from Gray (2024). A) Air-sea flux of CO_2 from the Surface Ocean CO_2 Atlas (SOCAT) and Southern Ocean Carbon and Climate Observations and Modelling (SOCCOM) datasets. B) Dissolved inorganic carbon concentration at 200 m from the Global Ocean Data Analysis project.

The contribution of biological productivity to CO_2 drawdown drives the Southern Ocean from being a source of CO_2 during winter to a summertime sink (Bakker et al., 1997). Climate models project that the importance of biological production to CO_2 drawdown will increase in a warming Southern Ocean (Ito and Follows, 2013, Hauck et al., 2015). This has been attributed to an increase in the Revelle factor, which describes an ocean with a lower buffering capacity, such that the same amount of biological uptake of DIC will drive a greater disequilibrium in the air-sea pCO_2 (Hauck and Volker, 2015). Phytoplankton community structure can impart variability on the CO_2 uptake from biological productivity (see **1.1.2**), therefore linking ecosystems to CO_2 modelling efforts will be important for understanding future changes in Southern Ocean CO_2 uptake.

1.3.2 Organic Matter

The uptake of CO_2 by phytoplankton communities is not only important for balancing atmospheric exchange, but also in fuelling organic matter production through photosynthesis for energy supply across the wider ecosystem (1.2.3). The organic carbon cycle is essential for the coupling of CO_2 uptake by marine phytoplankton with long term

carbon sequestration, the DOM inventory is the largest pool of reduced carbon in the ocean (662 ±32 PgC), over 95% of which is termed as refractory (Hansell, 2013). Marine phytoplankton produce dissolved organic carbon (DOC) through exudation, as a result of cell lysis, or by microbial decomposition of particulate organic carbon resulting from cell death. The balance between DOC and particulate organic carbon (POC) production by phytoplankton is postulated to vary with species and nutrient availability, but plays a key role in determining the fate of organic molecules since larger particulate organics are more efficiently exported from the surface ocean, resulting in the quicker sequestration of carbon. Changes to the balance between DOC and POC could also be important for nutrient remineralisation and bacterial composition in the microbial pump.

The molecular composition of DOM has been used as an indicator of lability, with saturated aliphatic molecules seen as the products of fresh DOM release which then become transformed over time to unsaturated aromatic compounds which persist over the long term as part of the refractory pool (Dittmar et al., 2021). Multiple theories have been proposed to describe the biogeochemical and ecological processes which lead to the persistence of refractory DOM in the ocean. These most commonly include one of intrinsic recalcitrance, whereby molecular properties (e.g., aromatic structures) confer stability, or emergent recalcitrance, arising from the concept that the energy required to break down organic structures by heterotrophs results in lower energetic returns as these structures become more degraded (Dittmar et al., 2021). Therefore, under the emergent recalcitrance theory these structures of DOM persist because there is no net energy gain to be made from further transforming these compounds. As DOM compounds undergo a continuous series of biological, chemical and physical transformations, the molecular level structure of these compounds can be used to generate a "fingerprint", which can be used to determine the extent of degradation and lability of a compound. Coupling this with isotopic (e.g. $\delta^{13}C$) and stoichiometric (C,H,N,O,S,P) properties of DOM compounds can provide a holistic profile of organic carbon dynamics (e.g. Ksionzek et al., 2016, Phillips et al., 2022). These multi-parameter approaches allow for identification of sources of organic carbon (marine vs terrestrial), longevity in the surface layer, probable fates of compounds, and some identification of biological interactions. DOM composition can therefore act as a powerful

tool for understanding the fine-scale relationship between biological communities and carbon export dynamics.

Within the context of uncertainties in the Southern Ocean carbon cycle linked to changing biological productivity regimes, this thesis advances our understanding of the biological carbon cycle by focusing on the relationship between phytoplankton communities and DOM production. This represents a crucial link in the carbon sequestration pathway and this thesis aims to resolve the fate of dissolved organics based on the presence of different phytoplankton types across a section of the WAP. Connecting the biological uptake of CO_2 through to the fate of organic matter via the phytoplankton intermediary is a key challenge in furthering our understanding of the timescales of carbon longevity in the surface ocean and transfer efficiency to the deep ocean.

1.3.3 **Nitrogen cycle**

Nitrogen is a bio-essential element for all life, required for amino and nucleic acid synthesis. In phytoplankton, nitrogen has further importance in photosynthesis and is seen to closely associate with chlorophyll in ratios of 0.34 to 2.47 µg chl:µmol N (Moreau et al., 2020 and references therein), with nitrogen deficiencies resulting in cellular chlorosis (Yentsch and Vaccaro, 2003). Consequently, nitrogen limits productivity across much of the global ocean (Browning and Moore, 2023), but is generally replete in the Southern Ocean (south of 40°S), although sporadic nitrate (NO_3^-) limitation has occasionally been observed during large blooms along the WAP where uptake outpaces resupply (Henley et al., 2017, Henley et al., 2018).

Across the high productivity shelf environments, nutrient supply to phytoplankton in the photic zone is dominated by the upwelling of CDW. The accumulation of nutrients over winter results in concentrations of 20-35 µmol NO_3^- L^{-1} in the surface layer of the coastal ocean at the onset of summertime productivity (Henley et al., 2017). During the period where nitrate is at a high, ammonium (NH_4^+) is at a low, with concentrations of <1 µmol NH_4^+ L^{-1} at the start of summer across much of the Southern Ocean (Savoye et al., 2004, Henley et al., 2017, Henley et al., 2020), due to wintertime heterotrophic consumption.

Phytoplankton display a preference for NH_4^+ as their nitrogen source because NO_3^- assimilation requires an additional reduction step to produce NH_4^+ so is less energetically

favourable compared to direct NH_4^+ uptake (as reviewed in Glibert et al., 2016). Under Southern Ocean conditions in early summer, the low NH_4^+ concentrations would be presumed to drive the system in to NO_3^- uptake, yet across different seasons and different regions of the Southern Ocean, uptake of NH_4^+ still accounts for a large proportion of nitrogen assimilation even when [NH_4^+] <1 μmol NH_4^+ L^{-1} (Philibert et al., 2015, Smith et al., 2022, Flynn et al., 2023). Different phytoplankton types are proposed to have diverse preferences for their nitrogen source, in particular diatoms have been shown to assimilate a large fraction of their nitrogen as NO_3^- under conditions of high NH_4^+ availability (Glibert et al., 2016). This correlates with NO_3^- being the greatest source of nitrogen to the large microplankton class in the Atlantic sector of the Southern Ocean (Flynn et al., 2023). Dissolved organic nitrogen in the form of urea has also been considered as a source of nitrogen to phytoplankton and appears to make a substantial contribution to nitrogen uptake over summer (Joubert et al., 2011, Thomalla et al., 2011), but less so during winter where urea concentrations are low (Smith et al., 2022). However, the utilisation of NH_4^+ and urea appear somewhat interchangeable under conditions where the concentration of urea exceeds [NH_4^+] (Smith et al., 2022).

The balance between the uptake of nitrogen sources is important in determining the contribution of new (NO_3^- mediated) and regenerated (NH_4^+ & urea mediated) productivity (Dugdale and Goering, 2003). Ammonium and urea are considered to facilitate 'regenerated' productivity because NO_3^- is initially reduced to NH_4^+ by phytoplankton and then released from phytoplankton cells by exudation or during remineralisation, this can be seen in the summertime depletion in NO_3^- and increase in NH_4^+ in cross seasonal timeseries (e.g. Henley et al., 2017). The ratio between new and new + regenerated productivity (*f* ratio) is particularly relevant in the Southern Ocean because assimilation of nitrogen from NO_3^- requires a greater amount of iron to reduce the NO_3^- than is required by phytoplankton types which directly utilise regenerated nitrogen (Dortch, 1990). Therefore, in the Southern Ocean, iron limitation can inhibit NO_3^- uptake. According to the new productivity paradigm, NO_3^- uptake must be balanced by productivity losses, so limitation of NO_3^- uptake also limits biological carbon export (Eppley and Peterson, 1979, Dugdale and Goering, 2003, Flynn et al., 2023). Productivity from regenerated nitrogen sources has no overall impact on CO_2

sequestration.

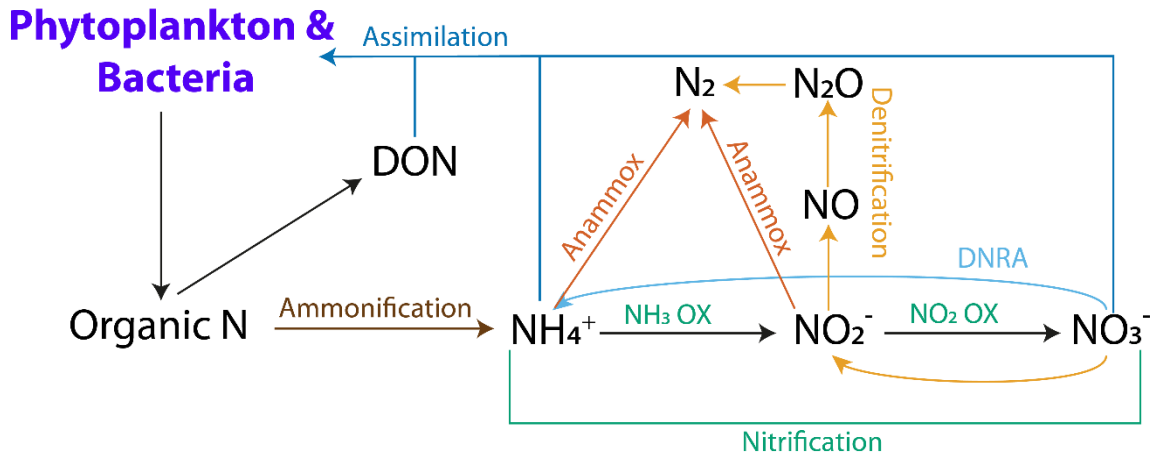

Figure 1.8: Simplified schematic of nitrogen recycling processes relevant to the Southern Ocean. DNRA represents dissimilatory nitrate reduction to ammonium. NH_3 OX and NO_2 OX represent biological ammonia and nitrite oxidation carried out by ammonia oxidising archaea and nitrite oxidising bacteria respectively.

Mdutyana et al. (2020) suggest that the *f* ratio cannot be applied to accurately describe the carbon export resulting from the balance between new and regenerated productivity in the Southern Ocean because it does not account for a significant amount of summertime NPP fuelled by wintertime nitrification. Nitrification describes the two-stage regeneration of NO_3^- from NH_4^+ (via a NO_2^- intermediary) through ammonium oxidation and nitrite oxidation (**Figure 1.8**). These are decoupled processes with nitrite oxidation being the rate limiting step, either because nitrite oxidising bacteria require a minimum nitrite concentration to be maintained, making the process inherently inefficient, or through iron limitation of nitrite oxidation (Mdutyana et al., 2020). Nitrate regeneration can be theoretically accounted for in a corrected *f* ratio where nitrification is subtracted from the numerator (per Fernández I et al. (2005)) but determining the true rate of nitrification is difficult because it relies on interpreting the change in both substrates of the oxidations (NH_4^+ and NO_2^-) despite widely varying rates of these two reactions across different environmental settings (Mdutyana et al., 2020, Mdutyana et al., 2022). Accounting for nitrification in the calculation of the *f* ratio is a key step required for resolving the impact of biological productivity on Southern Ocean CO_2 sequestration, particularly at the finer scale over seasonal transitions and in coastal upwelling regions where nutrient concentrations are most variable.

A similar problem exists in accounting for the rate of NH_4^+ regeneration, where the production and removal of NH_4^+ is poorly understood (Smith et al., 2022). This matters in the

Southern Ocean because NH_4^+ concentrations remain high over winter (e.g. Philibert et al., 2015, Henley et al., 2020, Mdutyana et al., 2020), suggesting strong NH_4^+ regeneration alongside NH_4^+ uptake, which sustains wintertime heterotrophic activity, resulting in the Southern Ocean being a seasonal CO_2 source to the atmosphere. Smith et al. (2022) attribute this trend to heterotrophic regeneration of NH_4^+ which exceeds the rate of removal due to temperature, light and iron limitation of phytoplankton and nitrifiers. Within the context of a Southern Ocean subject to rapid and widespread seasonal changes in temperature, light and nutrients, we could expect the balance between NH_4^+ regeneration and assimilation to change in the future, with implications for CO_2 sequestration. However, our current understanding of NH_4^+ regeneration rates are largely limited to interpretating changes in NH_4^+ concentrations or from balancing the NH_4^+ stock against measured uptake rates. While some authors proposed mathematical methods for accounting for NH_4^+ regeneration within the context of $^{14}NH_4^+$ regeneration by phytoplankton diluting the $^{15}NH_4^+$ isotope dilution in ^{15}N labelled uptake experiments (Kanda et al., 1987, Gilbert et al., 2003), recent methodical advances have improved the ease of determining the rate of NH_4^+ regeneration.

This thesis focuses on nitrogen cycling through the methodological lens of NH_4^+ regeneration in ^{15}N labelled uptake experiments. ^{15}N labelled experiments are the primary method by which the uptake of nitrogen containing compounds by phytoplankton communities is measured. Briefly, a known concentration of ^{15}N labelled NO_3^-, NH_4^+, Urea or Dissolved Free Amino Acids at <10% of the ambient nutrient concentration is added to a bottle of sampled seawater (e.g. Moschonas et al., 2017). After a brief incubation period (usually <6 hours) the sample is filtered and the $^{15}N/^{14}N$ composition of the filter can be used to calculate the uptake rate of the labelled nutrient. A longstanding issue with this approach in determining NH_4^+ uptake is that the phytoplankton release non-isotopically labelled NH_4^+ during the course of the incubation which dilutes the $^{15}NH_4^+$ signal by an unknown, but potentially large, factor (Dugdale and Goering, 2003, Gilbert et al., 2003). Therefore, all uncorrected NH_4^+ uptake experiments are inherently an underestimate of the true rate of NH_4^+ uptake. As discussed previously, when the CO_2 source or sink state of the ocean is dependent on accurate balancing of NH_4^+ regeneration and uptake, these known methodological errors must be tackled to provide the most accurate assessment of nutrient uptake and therefore biological carbon potential.

One approach to mitigate isotope dilution is to use short incubations of 3-6 hours, such that no substantial amount of NH_4^+ regeneration can occur in this time (e.g. Moschonas et al., 2017, Mdutyana et al., 2020, Flynn et al., 2023). However, this is based on a presumption, and some studies show NH_4^+ regeneration rates on an hourly scale of up to 0.43 mmol N-NH_4^+ m^{-3} d^{-1} in the Southern Ocean (Goeyens et al., 1991b). Additionally, by using a short incubation over only one period of the day, we might not be accounting for any diel effects of changing light conditions on NH_4^+ uptake, a process known to influence nitrate uptake rates (Koike et al., 1986, Cochlan et al., 1991).

This thesis addresses this problem, by applying a new chemical method for the extraction of ^{15}N enriched aqueous NH_4^+ and subsequent stable isotope analysis to measure the change in the ^{15}N source pool over the course of a lengthened 24-hour uptake experiment, using a suite of model phytoplankton species isolated in the Southern Ocean. This chapter provides a new basis for the accurate determination of NH_4^+ uptake, accounting for the regeneration effect. This tool can be applied in the environmental setting and used towards efforts in balancing heterotrophic NH_4^+ regeneration and community assimilation, with implications for interpretating biological carbon production and CO_2 sequestration.

1.3.4 **Other macronutrients**

In addition to nitrogenous nutrients, phosphate (PO_4^{3-}) and silicic acid are essential molecules for phytoplankton metabolism. Concentrations of PO_4^{3-} are depleted during the growth season (Henley et al., 2017) but Southern Ocean phytoplankton do not experience PO_4^{3-} limitation (Henley et al., 2020). Silicic acid concentrations are variable across the Southern Ocean, with greater concentrations south of the Polar Frontal Zone (Franck et al., 2000) providing ample Si availability along the coastal shelves, fuelling diatom blooms. However, some studies suggest that silicic acid can become seasonally co-limiting alongside iron in the Subantarctic (Boyd et al., 1999, Franck et al., 2000, Hutchins et al., 2001, Sedwick et al., 2002).

The uptake rates of PO_4^{3-} and silicic acid in Southern Ocean phytoplankton are influenced by iron limitation. Under low iron concentrations the decreased growth rate of diatoms can result in a depletion of PO_4^{3-} relative to cellular stocks of micronutrients (Cullen et al., 2003). This is particularly relevant for cadmium because Cd:P ratios of planktonic foraminifera are used as a palaeoproxy for reconstructing historical phosphate dynamics. However,

Timmermans et al. (2004) found phosphate consumption to be uncorrelated with iron availability in four separate Southern Ocean phytoplankton species during culture experiments. Hendry et al. (2008) attribute water mass mixing, variability in micronutrient concentrations and changes in phytoplankton composition as contributory factors to the Cd:P ratio.

When iron is added to phytoplankton communities which are deficient in both iron and silicic acid (e.g. north of the polar front), Si:N and Si:C ratios are seen to decrease (Hutchins and Bruland, 1998, Takeda, 1998), usually resulting in organic rich diatoms, but the continued limitation of silicic acid prevents growth of the overall community (Boyd et al., 2000, Marchetti et al., 2009). In their experiment, Hutchins et al. (2001) note that removal of iron limitation does not always result in an elevated Si:N, with iron stimulated growth of lightly silicified haptophytes maintaining a low Si:N ratio in their experiment, highlighting the importance of a holistic understanding of nutrient utilisation rates and community composition. Physiochemical interactions can also interact with nutrient stoichiometry, with increased Si:N ratios of sinking biogenic material observed under ocean acidification conditions due to slower Si dissolution rates (Petrou et al., 2019, Taucher et al., 2022).

Since iron and light limit productivity in the Southern Ocean, macronutrients are incompletely assimilated over the growth season. Subsequently, excess quantities of macronutrients become available for export to the global ocean, for example by transport in Subantarctic Mode Water to upwelling regions (Sarmiento et al., 2004). Consequently, Southern Ocean macronutrient export has been estimated to account for 62 (±5%) of upper ocean nitrate and phosphate supply (Fripiat et al., 2021). Therefore, changes in the uptake of macronutrients by Southern Ocean phytoplankton could alter the concentration and timing of nutrient leakage outside of the ACC. For example, decreased Si dissolution under acidifying conditions would reduce silicic acid concentrations in the surface ocean (Taucher et al., 2022), and the Si:N ratio of nutrients supplied to the Subantarctic and beyond. This could result in a restructuring the balance between diatoms and non-silicifying phytoplankton across silicic acid limited regions of the global ocean which depend on the supply of Southern Ocean nutrients (Nissen et al., 2021).

1.3.5 **Micronutrients**

The role of micronutrients, particularly iron, has been discussed within the context of the upwelling of water masses (1.1.3), limitation of phytoplankton growth (1.2.2), nutrient recycling by higher trophic levels (1.2.3), control of nitrogen uptake (1.3.2) and influence on macronutrient stoichiometry (1.3.3). These intimate links with all aspects of Southern Ocean biogeochemistry demonstrate the importance of iron as the primary limiting nutrient on productivity, yet phytoplankton require a diverse set of trace metals for cellular functions, to act as electron donors/acceptors in metabolic reactions or to combat toxicity (e.g., the formation of reactive oxygen species). The individual roles of the most important micronutrients (iron, zinc, cobalt, manganese and cadmium) are extensively reviewed in Sunda (2012). Non-metallic micronutrients, such as vitamin B12 also play an important role in fuelling phytoplankton growth, additions of B12 have been shown to increase chlorophyll concentrations and elicit changes in community composition in combination with iron (Bertrand et al., 2007). Iron, and more recently manganese (Pausch et al., 2019, Wu et al., 2019, Browning et al., 2021, Balaguer et al., 2022, Browning and Moore, 2023), have attracted the most attention among the micronutrients for their joint role in growth limitation; consequently, most modelling efforts towards understanding pathways of trace metal supply and loss rates focus on iron. This discussion on micronutrient supply is therefore based on iron, but other important metals are assumed to be supplied via the same core mechanisms in varying ratios relative to iron.

The major pathways that contribute towards bioavailable trace metal deposition in the Southern Ocean include atmospheric (dust) sources (e.g. Jickells et al., 2005), sedimentary supply (e.g. Lam et al., 2006, Tagliabue et al., 2008, Lancelot et al., 2009), and liberation from sea ice, icebergs and glacial melt (e.g. Raiswell et al., 2008, Hopwood et al., 2019). Across different regions of the Southern Ocean, different mechanisms contribute to the supply of bioavailable iron utilised by phytoplankton, atmospheric deposition is greatest north of the subtropical front and decreases towards the continent (Cassar et al., 2007). While sedimentary supply is weak in the open ocean, it is the major pathway for iron supply south of the polar front, including on the shelves where supply rates vary between 4.3 and >100 μmol Fe m^{-2} d^{-1}, varying with depth (Wadley et al., 2014 and references therein). The sedimentary iron supply to the high productivity continental shelves during summer

accounts for up to 90% of phytoplankton growth, with icebergs contributing the remainder (Lancelot et al., 2000). Consequently, iron supply from sediments accounts for 1.4-9 times as much export productivity as atmospheric deposition at the basin scale (Tagliabue et al., 2009). Bioavailability of iron (and other trace metals) must also be considered alongside a simple balance of utilisation against supply since scavenging of iron through ligand complexation or mineral adsorption can remove it from the dissolved phase. Wadley et al. (2014) find the major sources of iron on the shelves (iceberg and sediment supply) to be scavenged to a greater degree than dust or sea ice derived iron. Within the context of a changing climate, wind driven changes to eddy formation and upwelling have the potential to substantially alter the supply of sedimentary iron to the surface (1.1.3). The added effect of warming on increasing basal ice melt has been projected to increase iron supply to shelf surface waters on the order of ~50-60% by the end of the century (Dinniman et al., 2023).

1.4 Observations in the Southern Ocean

1.4.1 **Observational time series**

Chapter 3 of this thesis builds on the Palmer Antarctic Long Term Ecological Research program (Palmer LTER), one of several well-established ecological monitoring programs on the WAP, alongside the Rothera Time Series (RaTS). The Palmer LTER is a wide-ranging program monitoring physical, biological, chemical and ecological change across the ocean, land and atmosphere of WAP. Palmer LTER was established in 1990 and conducts year-round monitoring from Palmer Station on Anvers Island (64.77° S, 64.05° W) in addition to an annual cruise during austral summer covering an area of ~180,000 km^2. A detailed explanation of the sampling grid used during the Palmer LTER annual cruise and the oceanographic setting is provided in Chapter 3. The large spatial extent of the LTER is useful in understanding climate change on the rapidly warming WAP as the north of the Peninsula has experienced the greatest amount of change, now representing a more maritime climate, while the south of the Peninsula remains a more typical polar environment. These spatial differences create a wide range of environmental niches which can be useful for studying the

climate tolerance of different phytoplankton species and understanding long term change in biogeography.

Outside of the WAP, and not utilised in this thesis, there is a growing effort by the international community towards observing changes in Southern Ocean water masses using autonomous technologies. These approaches involve networks of gliders, autonomous underwater vehicles, (bio)argo floats, animal borne sensors and mooring arrays, and are particularly advantageous for capturing changes during the understudied winter months where sea ice cover prevents ship access. Chapter 2 explores how targeted increases in observational capacity from both *in situ* and autonomous observations can help to support improving the representation of the Southern Ocean in earth system models.

1.4.2 **Southern Ocean phytoplankton in global climate modelling**

The Southern Ocean already plays a disproportionate role in CO_2 and heat uptake relative to its size, and under continued warming the importance of regional biological carbon export is projected to increase against a global decline. Therefore, accurately modelling biogeochemical cycling within the Southern Ocean is of growing importance in accounting for global scale change in the carbon-climate system within earth system models. Chapter 2 works towards this aim by providing the first assimilation of Southern Ocean biogeochemical performance among the Coupled Model Intercomparison Project 6 (CMIP6) ensemble members, the class of models used for global stocktake assessments by the Intergovernmental Panel on Climate Change (IPCC) and United Nations Framework Convention on Climate Change (UNFCCC).

Compared to regional or ecological models the most significant limitation of the CMIP6 class models is resolving small scale change (<50km resolution) or complex processes. Computationally, increasing resolution or adding additional parameters is challenging because of the requirement to propagate these seemingly minor changes over the global ocean, land and atmosphere under multiple different climate scenarios with a monthly frequency to the end of the century. For example, in CMIP6 the entire global phytoplankton population is encoded by 1-4 explicit phytoplankton groups which use mostly fixed values for key parameters including nutrient uptake rates and chlorophyll:carbon ratios. This is a gross oversimplification because it presumes that a diatom in the tropical Pacific Ocean

behaves in the same way as a diatom in the Southern Ocean despite the fact that different nutrient limitations can drive changes in the cellular stoichiometry of diatoms.

Between CMIP5 and CMIP6 there was no improvement in the representation of ocean chlorophyll (deviation of models from observations) despite a decade of model development (Seferian et al., 2020). The lack of complexity in phytoplankton communities could account for some of this, if perhaps, we have reached the limit for how well a few explicit tracers can represent a diverse global population of marine phytoplankton. Ecosystem models used to investigate phytoplankton biogeography typically use many more phytoplankton types because they explicitly account for variation in size class (unlike CMIP6 models). For example, Dutkiewicz et al. (2015) and Dutkiewicz et al. (2020) develop a model including 35 plankton types, 11 of which are diatoms, revealing a climate driven decrease in the size class of Southern Ocean phytoplankton by the end of the century (Henson et al., 2021). This is beyond the current capabilities of CMIP6 class models but would have profound implications for biological carbon export, silicic acid drawdown and pelagic nutrient remineralisation. When representing phytoplankton at the global scale, a fine balance must be found between adequate community complexity and computational capacity. Thinking about phytoplankton through the lens of adaptive physiological processes rather than explicit tracers with fixed properties could be one pathway to achieving this. Multiple studies have indicated that improving inclusion of phytoplankton physiology, mostly in relation to variable nutrient stoichiometry, could help reduce modelling bias in the Southern Ocean (Kwiatkowski et al., 2018, Person et al., 2018)

In addition to developing and simplifying our understanding of key phytoplankton physiological processes, sampling bias is particularly acute in the Southern Ocean and may contribute towards a substantial degree of uncertainty in model outputs (Bushinsky et al., 2019). Autonomous year-round measurements can reduce the degree of uncertainty in pCO_2 by almost an order of magnitude (Henson et al., 2024), but many essential biogeochemical measurements required to understand phytoplankton dynamics (pigments, nutrient uptake rates, iron concentrations) cannot currently be determined remotely. Chapter 2 aims to use the existing projections of Southern Ocean biological change to identify episodes (spatial regions or temporal periods) with the largest expected changes or largest variability between models. Through the existing observing frameworks, based on the Southern Ocean

Observing System, this chapter considers where and when additional Southern Ocean observations may provide the greatest benefit in resolving model uncertainty. Additionally, processes currently missing from modelling efforts but that have a potential to strongly impact our understanding of phytoplankton in a changing climate are highlighted as targets for development. Collectively, the ambition of this chapter is to begin a conversation between the modelling and observational communities about how we can avoid stagnation in the progress between CMIP eras and ensure that our observational capacity is utilised to its fullest extent in an effort to understand how climate driven changes in the Southern Ocean will influence the global carbon cycle and climate.

1.5 Thesis overview and objectives

1.5.1 Thesis aims

The overall purpose of this thesis is to address how the multi-factorial response of the Southern Ocean to climate change will impact Southern Ocean phytoplankton, specifically in regards to their biological carbon export and nitrogen acquisition. This is a very large topic area covering a multitude of biogeochemical and ecological processes over a vast ocean basin which contains endless ecological niches and regions subject to the effects of fine scale mesoscale dynamics. When coupling this with seasonal variability in sea ice and decadal scale phase shifts in ENSO and SAM it becomes increasingly apparent that there can be no "one size fits all" solution to resolving these important questions at the whole ocean scale.

Therefore, the overarching aim of this thesis is to experimentally target poorly understood mechanisms which couple Southern Ocean phytoplankton ecology to biogeochemical cycling, with a view towards improving the mechanistic representation of Southern Ocean biogeochemistry in Earth System Models.

The specific aims of this thesis are to:

1. Quantify the magnitude of modelled change in the Southern Ocean with a warming climate and determine the extent of variability in primary productivity and related variables across space and time.
2. Understand the importance of phytoplankton communities in the Southern Ocean carbon cycle through elucidating the extent to which phytoplankton type acts as a control on the molecular composition of dissolved organic matter.

3. Establish how changing phytoplankton species composition could impact nutrient stocks by determining the rate of uptake for a range of nutrients across different Southern Ocean phytoplankton species.

1.5.2 Thesis structure

These aims are explored throughout the thesis and further elaborated upon with chapter specific sub-aims. Chapter 2 targets aim 1 by taking a whole ocean view of biogeochemical and physical change in the Southern Ocean. Providing the first biogeochemical assessment of the Southern Ocean from the latest CMIP6 models, this chapter establishes our current best state of knowledge as to how we might expect carbon production, primary productivity, iron and light limitation of phytoplankton, and mixed layer depth to respond to a warming planet. While this chapter does provide case study examples of model setup and specifics of phytoplankton parameterisation in order to describe some of the variability in phytoplankton-climate responses, the wider aim is to target observational capacity at reducing model uncertainty. A key conclusion from this chapter is that while increasing the number of observations and model parameters may help to a degree, we still lack a fundamental understanding of many of the processes which link the physiological response of phytoplankton to a changing environment. Therefore, steps are proposed to target additional observations to regions with the largest projected changes or variability in productivity parameters. This approach could help to constrain extreme values of phytoplankton growth and growth limitation in ecological niches and further our mechanistic understanding of phytoplankton productivity under environmental stress, contributing to reducing overall uncertainty in Southern Ocean scale productivity projections.

Subsequently, Chapters 3 and 4 examine biogeochemical processes linking Southern Ocean phytoplankton to the carbon and nitrogen cycle respectively. Chapter 3 explores aim 2 with a regional focus on the rapidly warming WAP, and presents results describing the relationship between phytoplankton and DOM cycling. This chapter includes the most detailed assessment of DOM currently available for the WAP region, providing stoichiometric, isotopic and high-resolution mass spectrometry data describing the molecular composition of individual organic compounds. DOM is linked to phytoplankton communities from a novel overview of phytoplankton biogeography across the WAP in the record low sea ice year (2023) established using machine learning of Imaging Flow Cytobot data. This chapter

concludes that the smaller size classes of phytoplankton, which are projected to become more abundant in a future Southern Ocean, play a greater role in producing fresh DOM relative to larger diatoms. Consequently, this could have significant implications for the efficiency of biological carbon export if partitioning to the particulate phase is reduced and could liberate more nutrients from organic matter in the surface layer, with a subsequent impact on export of excess nutrients to the global ocean.

Focusing in on the utilisation of nutrients by phytoplankton, Chapter 4 approaches aim 3 with a laboratory-based study using cultures of Southern Ocean phytoplankton species to investigate their uptake of nitrogen from different sources. This experiment employed five different phytoplankton species representing the major functional types (pennate diatoms, centric diatoms, sea ice diatoms, cryptophytes, haptophytes) and measured their uptake of ^{15}N- labelled nitrate, urea and ammonium. This study confirmed the preference of all species for the energetically favourable uptake of ammonium, but also showed a high degree of urea uptake. Advancing on previous measurements using this well-established ^{15}N tracer technique, this chapter also makes a methodological contribution through the development of a correction for isotope dilution (as outlined in 1.3.2). Whereas other studies have typically caveated their ammonium uptake rates to be an underestimate because of dilution, this chapter uses a new titanium mediated chemical technique for the conversion of $^{15}NH_4^+$ to $^{15}N_2O$ in order to measure the change in the ^{15}N source throughout an experiment. Subsequently, this allows for true measurements of NH_4^+ uptake rates in culture, accounting for NH_4^+ regeneration. This could allow future work to examine diel changes in the uptake of NH_4^+ and simultaneous measurement of carbon and nitrogen uptake over a 24-hour period

Collectively, this thesis synthesises our current understanding of how the growth and composition of Southern Ocean primary producers will change in response to modelled climate scenarios, revealing gaps in our mechanistic understanding of the relationship between community composition and biogeochemical cycling. Two aspects of carbon and nitrogen cycling are explored through fieldwork and laboratory experiments, contributing to reducing the knowledge gaps in the interaction between species composition and DOM production and nitrogen dynamics. The species-dependent relationships deduced from these chapters provides evidence that ongoing climate driven changes in phytoplankton communities will likely impact biogeochemical cycles through altering carbon export

efficiency and nutrient budgets of the Southern Ocean; with downstream implications for global scale productivity, carbon cycling and wider ecosystems.

2. Biogeochemistry of climate driven shifts in Southern Ocean primary producers

Abstract

As a net source of nutrients fuelling global primary production, changes in Southern Ocean productivity are expected to influence biological carbon storage across the global ocean. Following a high emission, low mitigation pathway (SSP5-8.5), we show that primary productivity in the Southern Ocean is predicted to increase by up to 30% over the 21st century. The ecophysiological response of marine phytoplankton experiencing climate change will be a key determinant in understanding the impact of Southern Ocean productivity shifts on the carbon cycle. Yet, phytoplankton ecophysiology is poorly represented in Coupled Model Intercomparison 6 (CMIP6) climate models, leading to substantial uncertainty in the representation of their role in carbon sequestration. Here we synthesise the existing spatial and temporal projections of Southern Ocean productivity from CMIP6 models, separated by phytoplankton functional type, and identify key processes where greater observational data coverage can help to improve future model performance. We find substantial variability between models in projections of light concentration (>15000 ($\mu E\ m^2\ s^{-1}$)^2) across much of the iron and light limited Antarctic zone. Projections of iron and light limitation of phytoplankton vary by up to 10 % across latitudinal zones, while the greatest increases in productivity occurs close to the coast. Temperature, pH and nutrients are less spatially variable, projections for 2090-2100 under SSP5-8.5 show zonally averaged changes of +1.6 °C, -0.45 pH units and Si* ($[Si(OH)_4]–[NO_3^-]$) (decreases by 8.5 $\mu mol\ L^{-1}$. Diatoms and pico/misc phytoplankton are equally responsible for driving productivity increases across the Subantarctic and Transitional zones, but pico and misc phytoplankton increase at a greater rate than diatoms in the Antarctic zone. Despite the variability in productivity with different phytoplankton types, we show that the most advanced models disagree on the ecological mechanisms behind these productivity changes. Here we propose an observational sampling approach which targets the regions with the greatest projected rates of climate-driven change in ocean biogeochemistry and community assemblages. This could be a step change towards resolving the empirical principles underlying phytoplankton community structure in the Southern Ocean, substantially improving our ability to model the impact of climate change on Southern Ocean ecosystems.

2.1 Introduction

The biological uptake of carbon by marine phytoplankton represents an important process in the Earth system (Deppeler and Davidson, 2017), with ocean carbon storage mediating atmospheric CO_2 concentrations, including CO_2 of anthropogenic origin (Riebesell et al., 2007). Across the global ocean, uptake of carbon accounts for ~25% of CO_2 released by human activities (Friedlingstein et al., 2022a). The Southern Ocean is a disproportionately large carbon and heat sink relative to its size (Frölicher et al., 2015), accounting for 30-40% of this global anthropogenic CO_2 uptake (e.g. Caldeira and Duffy, 2000, DeVries, 2014), predominantly due to enhanced atmosphere-ocean exchange at increased atmospheric CO_2 concentrations (Friedlingstein et al., 2022a). While biological uptake is considered to play a minor role in total CO_2 uptake (Landschutzer et al., 2015, Gruber et al., 2019), variability in pCO_2 has been associated with summertime blooms in the Southern Ocean (Gregor et al., 2018, Coggins et al., 2023). Under a future climate scenario with longer growth seasons (Moreau et al., 2015), increased seasonal productivity (Leung et al., 2015, Fu et al., 2016) and a reduction in ocean CO_2 absorption efficiency (higher Revelle factor) (Hauck et al., 2015); biological and physical drivers of carbon exchange across the air-sea interface are likely to undergo substantial changes. As the Southern Ocean's ability to buffer increased concentrations of atmospheric CO_2 weakens, the role of pelagic ecosystems, are expected to become increasingly important in Southern Ocean carbon uptake (Henley et al., 2020).

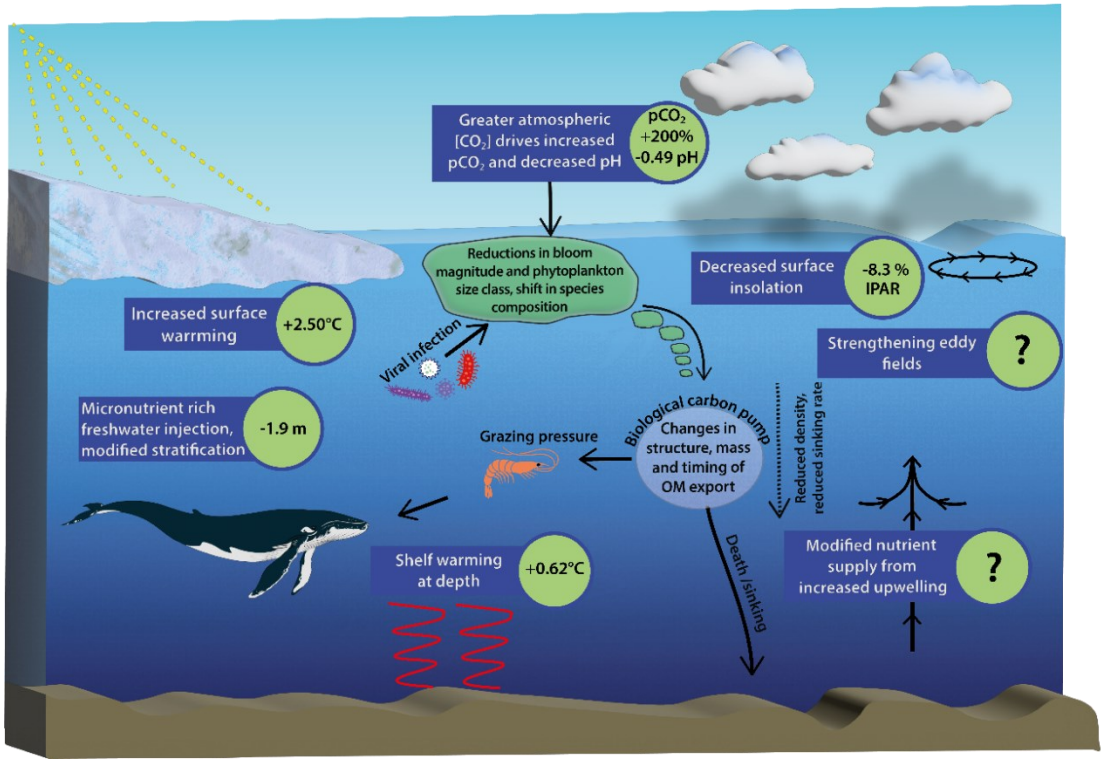

Figure 2.1: Schematic diagram of Southern Ocean pressures associated with climate change and the downstream biogeochemical consequences for ecosystem productivity. Values shown are 100 year mean changes to 2100 under the SSP5-8.5 scenario south of 65°S and are taken from CMIP6 models and existing literature (McNeil and Matear, 2008, Purich and England, 2021) (see **Table 2.1** for a full description). Question marks indicate processes where estimations of change do not currently exist.

Table 2.1: Data descriptors for **Figure 2.1**

Variable	Value	Detail	Reference
Warming at depth	+0.62 °C	Expected warming of Antarctic shelf bottom waters by 2100 across SSP5-8.5 in a CMIP6 multi-ensemble mean.	Purich and England (2021)
Changes in stratification.	CMIP6: -1.9 m/ -7.8% Uncertain, sign change within standard deviation.	Changes in mixed layer depth are highly spatially variable. In the coastal Southern Ocean (south of 60°S) CMIP5 models disagree on the direction of MLD change due to the competing effects of freshwater input with increased upwelling and wind driven mixing (Hauck et al., 2015). CMIP6 models similarly disagree	Hauck et al. (2015)

		but give an overall mean of -1.9 m. Melting of the Antarctic ice sheet is not a process considered within CMIP models.	
pCO_2	+200%	Increase from ~500 µatm (GLODAP) to ~1000 µatm under RCP8.5.	Kawaguchi et al. (2013)
pH	-0.3 pH units	Decrease in Southern Ocean pH from 8.09 to 7.79 calculated using the CSIRO ocean carbon model from CC IS92a atmospheric CO_2 scenario.	McNeil and Matear (2008)
Increased surface warming	+2.50°C	Spatial average taken from the temperature anomaly data shown in **Figure 2.8**. Representative of a CMIP6 multi-model ensemble anomaly between 2100 and (1985-2015) under SSP5-8.5.	This study

Small celled marine phytoplankton (0.002-0.2 mm) are responsible for the production of biological carbon, fuelling ecosystems across the Southern Ocean, but are vulnerable to environmental change because of their specific requirements for light and iron, which are the primary factors limiting their growth in high nutrient low chlorophyll (HNLC) zones of the Southern Ocean (Moore et al., 2013). Following a "middle of the road" SSP2-4.5 pathway, between 2015 and 2023 Southern Ocean phytoplankton (defined as those south of 30°S per Gregg et al. (2003)) represented 36.31% of marine net primary productivity globally, equivalent to 15.5 Pg C yr^{-1} (**Figure 2.2**). Climate impacts on Southern Ocean phytoplankton are likely to manifest in ecological shifts towards smaller cell sizes (Venables et al., 2013, Saba et al., 2014, Schofield et al., 2018, Biggs et al., 2019, Mascioni et al., 2019) and changes in seasonal phenology (Moreau et al., 2015). Increases in overall productivity can be most closely associated with a reduced duration and extent of sea ice coverage, allowing for a greater supply of irradiance to surface waters of this light and iron co-limited productivity system. Strengthened upwelling is also likely to increase the flux of existing iron supplies to the coastal (Annett et al., 2015) and open ocean (Moreau et al., 2023) from sedimentary or hydrothermal sources, however, the extent to which changes in ocean mixing can be expected to impact nutrient supplies remains largely unknown (**Figure 2.1**).

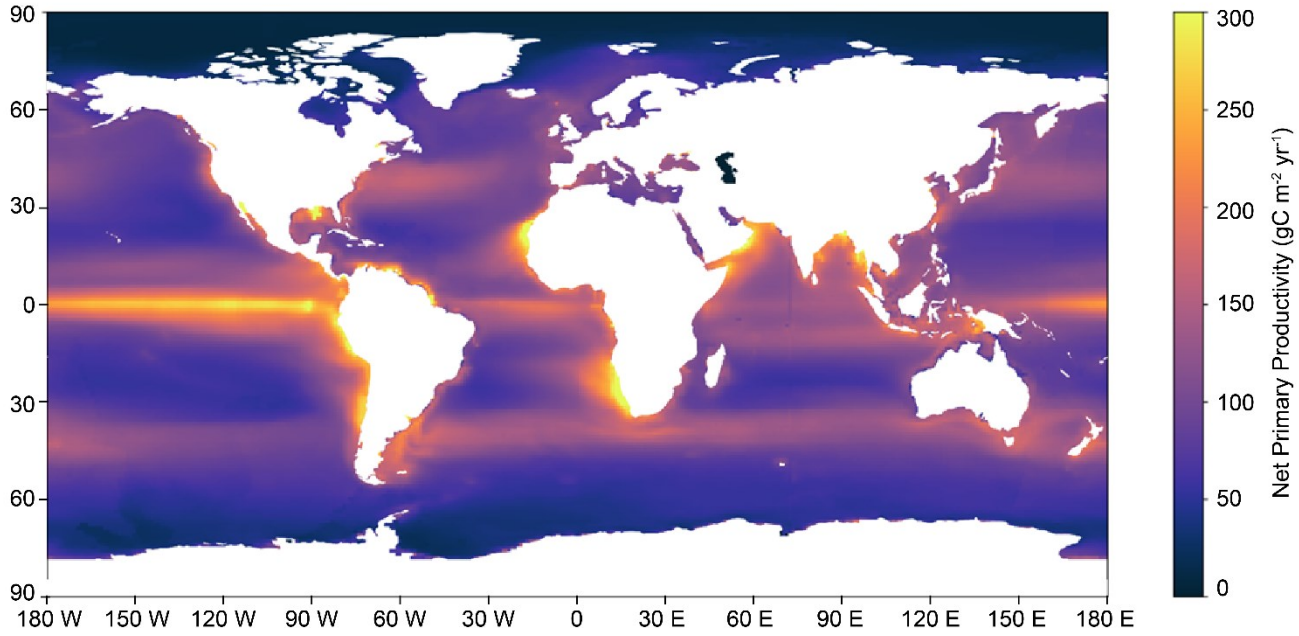

Figure 2.2: Global Net Primary Productivity (2015-2023) under a middle of the road, SSP2-4.5 pathway, from a multi-model CMIP6 ensemble. Models included are listed in **Table 2.2**. For the purpose of determining Southern Ocean productivity, the ocean area is defined as that south of 30°S, per Gregg et al. (2003).

Shifts in community composition from diatoms to smaller cryptophytes have already been documented along the West Antarctic Peninsula from as early as 1997 (Moline et al., 2004, Ducklow et al., 2007, Moline et al., 2008, Montes-Hugo et al., 2008, Rozema et al., 2017b), and are thought to be due to tolerance of cryptophytes to the low-salinity waters induced by increased sea ice melt (Moline et al., 2004), or the tolerance of cryptophytes for high and variable light conditions in well stratified surface layers (Mendes et al., 2023). Conversely, in culture-based competition experiments, diatoms are more successful in simulated future ocean conditions over prevalent haptophytes such as *Phaeocystis antarctica,* albeit with reduced diatom cell sizes (Xu et al., 2014). This difference is potentially driven by reduced iron limitation of diatoms and their greater tolerance to temperature change (Zhu et al., 2016). These varied responses between manipulation experiments and *in situ* observations suggest that physiological, as well as ecological, changes are important in understanding the net biogeochemical implications of phytoplankton community change.

In the sea-ice zone, grazing by zooplankton accounts for ~90% of phytoplankton losses (Moreau et al., 2020). Shifts in phytoplankton size class could rapidly cascade through the ecosystem as the dominant Southern Ocean zooplankton, Antarctic krill (*Euphausia superba*,

hereafter krill), are unable to graze small cryptophytes (Haberman et al., 2003), instead promoting the dominance of carbon-poor salps (*Salpa thompsoni*), which reduces the overall efficiency of the marine food web (Ballerini et al., 2014) and potentially weakens the biological carbon pump (Quéguiner, 2013, Biggs et al., 2021). Additionally, water temperature, alongside changes to zooplankton abundance and diversity, has been shown to increase zooplankton metabolism (Lopez-Urrutia et al., 2006, Mayzaud and Pakhomov, 2014), which can in turn be expected to modulate the grazing pressure and phytoplankton biomass (Lewandowska et al., 2014).

Projections of productivity in the Southern Ocean under future climate scenarios from the Coupled Model Intercomparison Project Phase 6 (CMIP6) class Earth System Models (ESMs) are actively informing research directions, International Panel on Climate Change (IPCC) reports (Masson-Delmotte et al., 2021), and governmental policy (Touzé-Peiffer et al., 2020). Yet, between CMIP5 and CMIP6 the spread of model projections with respect to vertical and horizontal physics as well as the number of phytoplankton functional types included has increased as different models incorporate more complexity and additional processes (e.g., varying elemental stoichiometry, phytoplankton diversity, complex elemental cycling) (Seferian et al., 2020). While representation of ocean physical drivers and nutrient fields compared to observations has improved between CMIP5 and CMIP6, surface chlorophyll is one of three key parameters that did not show improvement in benchmarking of CMIP6 performance over the global ocean (Canadell et al., 2021, Fu et al., 2022). Variance in model projections of phytoplankton and ocean biogeochemistry have been linked to the use of fixed C:N:P elemental stoichiometry (Kwiatkowski et al., 2018), an inability to reflect physiological adaptations, e.g. the ability of diatoms to maintain growth under iron limitation (Person et al., 2018), and complexities in modelling export fluxes, particularly in constraining phytoplankton losses through zooplankton grazing (Henson et al., 2022).

A major difference in the representation of productivity between CMIP6 models is the extent to which they consider different classes of phytoplankton. Diatoms (>20 μm) and pico-/nano-phytoplankton (predominantly cryptophytes and haptophytes) represent the vast majority of productivity across all latitudes of the Southern Ocean. Diatoms are a significant contributor to primary production and carbon export, accounting for ~40% of global marine primary production and POC exported to depth in the ocean (Jin et al., 2006, Tréguer et al.,

2017). Diazotrophs (nitrogen-fixing phytoplankton) are present in small numbers, usually only in subtropical niches, due to the excess supply of nitrogen across the Southern Ocean (Luo et al., 2012). Calcifiers, mostly coccolithophores, inhabit waters north of 60°S where there is a strong supply of light but low Si, high Fe conditions, preventing the growth of diatoms (Charalampopoulou et al., 2016, Nissen et al., 2018). Only 11 CMIP6 models specifically include diatoms under future warming conditions and only three of these additionally consider pico-phytoplankton (CESM2, CESM2-WACCM and GFDL-ESM4).

In recent years, record low sea ice concentrations have been observed in the Southern Ocean (Raphael and Handcock, 2022, Turner et al., 2022). Given the dependence of Southern Ocean productivity on the timing of seasonal sea ice retreat, we consider it possible that this shift in trends of sea ice concentration could cause an abrupt change to sea ice dependent ecosystems in the near future (Swadling et al., 2023). As phytoplankton are the main source of organic carbon in the Southern Ocean, uncertainty in projections of phytoplankton composition compounds existing model uncertainty in the biological carbon flux to the ocean's interior and seafloor (Henson et al., 2022). Within the context of climate change in the Southern Ocean, reducing model uncertainty in ecosystem mediated biogeochemical cycling will be of increased importance in determining the global scale impact of changes in the Southern Ocean productivity regime.

Targeting thesis aim 1, the specific sub-aims of this chapter were to:

- Quantify the degree of uncertainty between models in projections of phytoplankton productivity with a SSP5-8.5 warming scenario, including different phytoplankton functional types.
- Determine mean trends between projected climate driven change in ecosystems, physical processes and biogeochemical cycling across different latitudinal zones of the Southern Ocean.
- Identify regions, timeframes and processes within the Southern Ocean Observing System (SOOS) framework (https://soos.aq), where the greatest projected changes and/or uncertainties occur. Here, we argue that targeting observations to establish phytoplankton-environment response interactions within the regions of the most rapid projected changes is essential to accelerate the improvement of phytoplankton representation in future generations of ESMs.

2.2 Methods

Model and observational data for the Southern Ocean were collected, analysed and visualised to determine a) the physical and biogeochemical changes that force or result from shifts in productivity, and b) the extent of primary productivity shifts over the next century in CMIP6.

2.2.1 CMIP projections

Model output was obtained from the Climate Model Intercomparison Project Phase 6 (CMIP6) data server via pangeo.io using the XMIP package in Python 3.11. Ensemble members for each parameter were chosen based on their availability for historical *(hist)* and SSP5-8.5 *(ssp585)* (ScenarioMIP) data (O'Neill et al., 2016). SSP5-8.5 was chosen as the modelled scenario because it represents the reasonable worst-case scenario, and is useful for discerning the mechanistic trends between different parameters by extrapolating projections to their maximal values. The selected models for each parameter are detailed in **Table 2.2**. Where an analysis type relied on the direct comparison between two or more parameters, only models that contained both parameters were selected. For the analysis presented in section **2.3.5**, annual net primary production (*intpp*) is only included from models which also include diatom-specific annual net primary production (*intppdiat*) parameter. Where the same baseline model is included twice, because of having a low- and high-resolution version, the model is pre-averaged (i.e., both resolutions are assigned a weighting of 0.5 each) to avoid double counting of the same model when calculating the ensemble mean. Examples of models with two resolutions are highlighted in bold in **Table 2.2**. Only a small number of CMIP6 models contain irradiance limitation (*limirr*) and iron limitation (*limfe*) for multiple phytoplankton types, therefore analyses of light and iron limitation of phytoplankton utilise <5 models. All variables were extracted at monthly frequency, except for surface wind speeds where data were initially obtained daily; subsequently, annual weighted means were generated for most parameters per the weighting algorithm by Grover (2021). For mixed layer depth and incidental photosynthetically active radiation (IPAR), austral summertime means were used instead of annual means.

Model data were processed in Python 3.11 to apply the desired analysis (e.g., annual average, annual maximum) and then further averaged over residual variables (e.g., member_id). In most cases, all available member_id's were used; where this was not possible,

any member_id's which could not be aggregated due to differences in array structure were removed. Net primary production (NPP) is provided as a pre-integrated value across the water column; we integrated chlorophyll across the depth dimension between 0 and 500 m, to capture all phytoplankton across different depths, using the integrate function in SciPy (Virtanen et al., 2020). Subsequently, all models were re-gridded to a rectilinear grid via bilinear or nearest neighbour interpolation using XESMF (Zhuang et al., 2018) before being averaged to create multi-model means.

For spatial plotting, data were projected to the Antarctic Polar Stereographic (EPSG:3031) coordinate reference system in ArcGIS pro and visualised in QGIS using the Quantarctica package (Matsuoka et al., 2021), with post processing using SAGA and GDAL tools to remove imperfections in grid alignment through interpolation. All code to extract the CMIP6 data used in this study is available open access.

Table 2.2: Selected models used in analysis of CMIP6 data. Models shown in bold represent multiple resolutions of the same core model. Growth limitation ratio refers to the potential growth of phytoplankton under environmental concentrations of the limiting factor relative to the maximal growth if the limiting factor were replete.

Variable ID	Parameter	Units	Data selection	Models selected
intpp	Primary organic carbon production by all types of phytoplankton / diatoms	gC m^{-2} yr^{-1}	Annual average	ACCESS-ESM1-5, CanESM5, CanESM5-CanOE, CESM2 CESM2-WACCM, CMCC-ESM2, CNRM-ESM2-1, EC-Earth3-CC, GFDL-ESM4, GFDL-CM4, IPSL-CM6A-LR, MIROC-ES2L, **MPI-ESM1-2-HR, MPI-ESM1-2-LR**, MRI-ESM2-0, **NorESM2-LM, NorESM2-MM**, UKESM1-0-LL
intppdiat				CanESM5-CanOE, CESM2-WACCM, CNRM-ESM2-1, GFDL-ESM4, IPSL-CM6A-LR , UKESM1-0-LL
chl	Mass concentration of total phytoplankton expressed as chlorophyll in sea water	kg m^{-3}	Annual average	ACCESS-ESM1-5, CanESM5, CanESM5-CanOE, CESM2, CESM2-WACCM, CMCC-ESM2, GFDL-CM4, GFDL-ESM4, MIROC-ES2L, **MPI-ESM1-2-HR**, **MPI-ESM1-2-LR**, MRI-ESM2-0, **NorESM2-LM**, **NorESM2-MM,** UKESM1-0-LL
limirrpico	Irradiance limitation of pico-phytoplankton / miscellaneous phytoplankton / diatoms/ diazotrophs	Growth limitation ratio	Annual average	CESM2-WACCM, GFDL-ESM4
limirrmisc				CanESM5, CNRM-ESM2-1,GFDL-ESM4, IPSL-CM6A-LR
limirrdiat				CESM2-WACCM, CNRM-ESM2-1, GFDL-ESM4, IPSL-CM6A-LR, UKESM1-0-LL
limirrdiaz				CESM2-WACCM, GFDL-ESM4
limfediat/pico/misc	Iron limitation of diatoms/picophytoplankton/ miscellaneous phytoplankton	Growth limitation ratio	Combined annual average	GFDL-ESM4

rsntds	Net Downward Shortwave Radiation at Sea Water Surface (IPAR)	W m^{-2} (Converted to µE m^{-2} s^{-1})	Summertime (daily) maximum	ACCESS-CM2, CanESM5, CanESM5-CanOE, CESM2-WACCM, CMCC-CM2-SR5, **CNRM-CM6-1**, **CNRM-CM6-1-HR**, CNRM-ESM2-1, EC-Earth3, EC-Earth3-CC, EC-Earth3-Veg, IPSL-CM6A-LR, MIROC-ES2L, **MPI-ESM1-2-HR**, **MPI-ESM1-2-LR**, **NorESM2-LM**, **NorESM2-MM**
sfcWindmax	Daily Maximum Near-Surface Wind Speed	m s^{-1}	Annual average of daily maximum	AWI-CM-1-1-MR, BCC-CSM2-MR, CanESM5, CMCC-CM2-SR5, CMCC-ESM2, **CNRM-CM6-1**, **CNRM-CM6-1-HR**, CNRM-ESM2-1, EC-Earth3, EC-Earth3-CC, **EC-Earth3-Veg**, **EC-Earth3-Veg-LR**, GFDL-CM4, HadGEM3-GC31-MM, INM-CM4-8, INM-CM5-0, IPSL-CM6A-LR, KACE-1-0-G, **MPI-ESM1-2-HR**. **MPI-ESM1-2-LR**, MRI-ESM2-0, UKESM1-0-LL
mlotst	Ocean Mixed Layer Thickness Defined by σ_t	m	Summertime maximum	ACCESS-CM2, BCC-CSM2-MR, CAMS-CSM1-0, CanESM5, CanESM5-CanOE, CESM2, CESM2-WACCM, CNRM-CM6-1, CNRM-ESM2-1, GFDL-ESM4, GISS-E2-1-G, HadGEM3-GC31-LL, IPSL-CM6A-LR, MPI-ESM1-2-HR, MRI-ESM2-0, NESM3, UKESM1-0-LL
phos	Sea surface pH	pH units	Annual average	CanESM5, CanESM5-CanOE, CESM2, CESM2-WACCM, GFDL-ESM4, IPSL-CM6A-LR, MIROC-ES2L, MRI-ESM2-0, NorESM2-LM
sios	Surface concentration of silicic acid	µmol L^{-1}	Annual average	CanESM5-CanOE, GFDL-ESM4, IPSL-CM6A-LR, **MPI-ESM1-2-HR, MPI-ESM1-2-LR**, **NorESM2-LM, NorESM2-MM**, UKESM1-0-LL
no3os	Surface concentration of nitrate	µmol L^{-1}	Annual average	CESM2, CESM2-WACCM, GFDL-ESM4, NorESM2-LM, UKESM1-0-LL
limno3	Nitrate limitation of phytoplankton	Growth limitation ratio	Annual average	GFDL-ESM4

tos	Sea surface temperature	°C	Annual average	ACCESS-CM2, ACCESS-ESM1-5, BCC-CSM2-MR, CAMS-CSM1-0, CanESM5, CanESM5-CanOE, CESM2, CESM2-WACCM, CIESM, CMCC-CM2-SR5, CMCC-ESM2, **CNRM-CM6-1**, **CNRM-CM6-1-HR**, CNRM-ESM2-1, E3SM-1-1, EC-Earth3, EC-Earth3-CC, **EC-Earth3-Veg**, **EC-Earth3-Veg-LR**, FGOALS-f3-L, FGOALS-g3, FIO-ESM-2-0, GFDL-CM4, GFDL-ESM4, **HadGEM3-GC31-LL**, **HadGEM3-GC31-MM**, IITM-ESM, INM-CM4-8, INM-CM5-0, IPSL-CM6A-LR, KACE-1-0-G, KIOST-ESM, MCM-UA-1-0, MIROC6, MIROC-ES2L, **MPI-ESM1-2-HR**, **MPI-ESM1-2-LR**, MRI-ESM2-0, NESM3, **NorESM2-LM**, **NorESM2-MM**, TaiESM1, UKESM1-0-LL

2.2.2 Regional data

Historical concentrations of surface nitrate and silicic acid plus sea surface temperatures were mapped from the World Ocean Atlas 2018 data product (Garcia et al., 2019), representing average values from 1955 to 2017 . For the calculation of Si* ($[Si(OH)_4]$–$[NO_3^-]$), annually averaged data for nitrate and silicic acid were exported at a 1x1 degree resolution and subtracted from one another to produce Si*. To determine Si*, pH and temperature values by SOOS area, SOOS regions south of 55° were drawn as mask layers and subset using the zonal statistics function in QGIS.

2.3 Results and Discussion

2.3.1 Physical climate drives biological changes in Southern Ocean water masses

Climate change is driving substantial changes in Southern Ocean water masses (Bindoff et al., 2019). The widespread strengthening of Southern Ocean winds by up to 0.8 m s^{-1} (**Figure 2.3a**) and increased buoyancy fluxes (including freshwater inputs) act as opposing drivers of stratification, modifying mixed layer depth (**Figure 2.3b**). Mixed layers are projected to deepen across the Subantarctic by up to 10 m, but shoal across much of the rest of the Southern Ocean (**Figure 2.3b**). In light limited regions a shoaling of the mixed layer can be

expected to increase productivity, as phytoplankton become concentrated closer to the surface, while in iron limited regions where iron is supplied by wintertime vertical mixing, deeper mixed layers can benefit depth integrated primary productivity by increasing the productive water volume over which iron concentrations are sufficient to promote growth (Llort et al., 2019) . Subsequently, the changing availability of light and iron across the Southern Ocean determines the abundance and composition of primary producers. Despite the importance of changes in Southern Ocean circulation for global ocean nutrient supply, the cumulative influence of physical processes across different spatial resolutions results in poor overall performance of CMIP-class models in this region when their historical runs are compared with observations (Meredith et al., 2019). A particular weakness of CMIP6 models is in reconstructing the sea ice changes that drive buoyancy forcing (Roach et al., 2020, Shu et al., 2020) which has an important role in determining the flux of heat and CO_2 across the ocean-atmosphere boundary. The uncertainty in sea ice change also results in a high degree of variation in coastal irradiance between models (**Figure 2.4e**), particularly for the Weddell Sea and Ross Sea regions. Recent large and unexpected changes in sea ice around Antarctica emphasise that greater knowledge of the key drivers and controls is required, in order to improve predictive skill in models (Turner and Comiso, 2017).

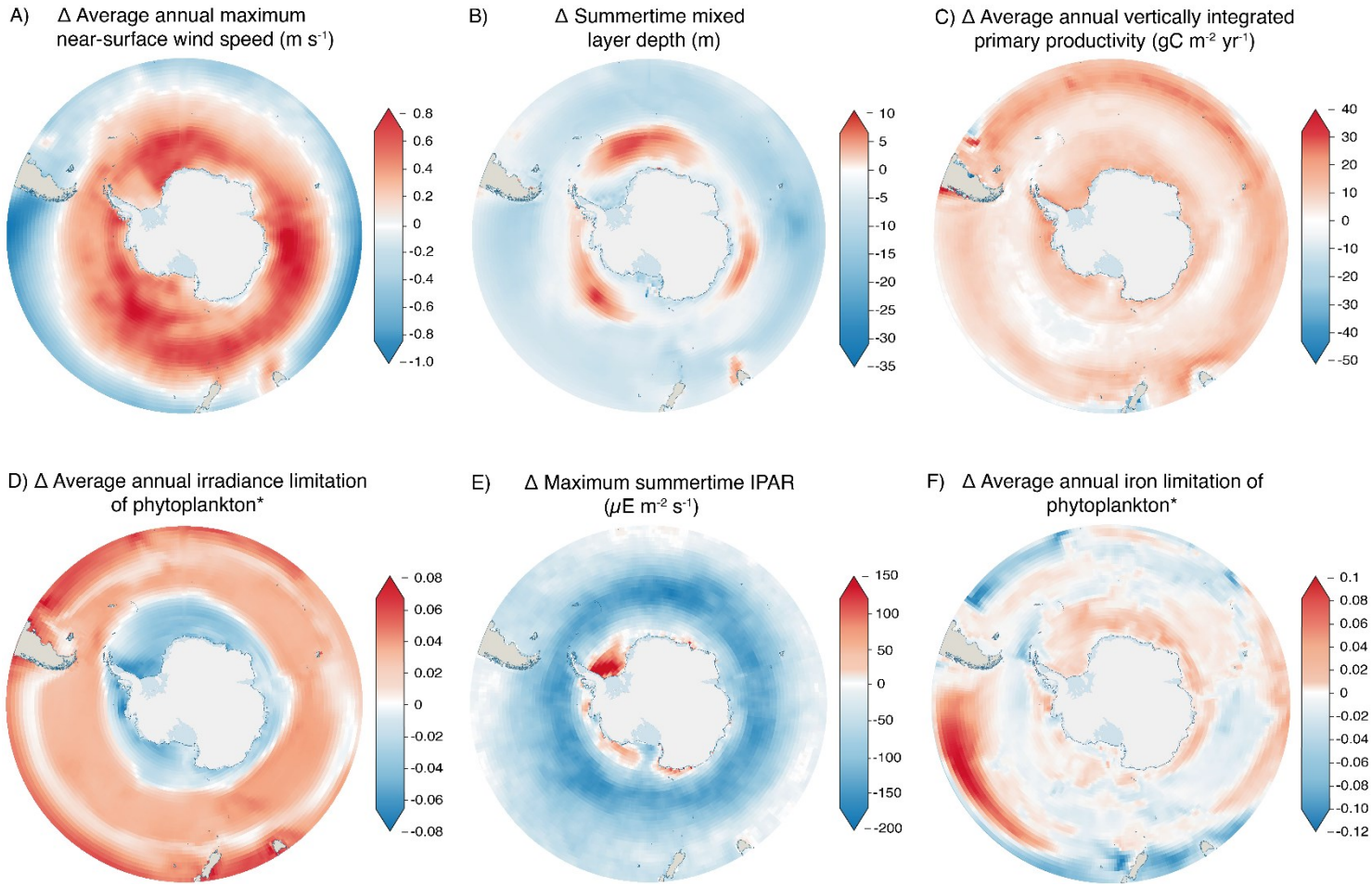

Figure 2.3: CMIP6 anomaly representing change to the end of the century in A) near-surface wind speed, B) mixed layer depth, C) net primary productivity, D) irradiance limitation of phytoplankton, E) incidental photosynthetically active radiation (IPAR) , and F) iron limitation of phytoplankton. Changes are calculated from an ensemble of CMIP6 models, comparing a historical (1985-2015) average against 2090-2100 under the SSP5-8.5 climate scenario. Details of ensemble members are given in **Table 2.2**. *Units in panels D and F are arbitrary ratios of growth under environmental irradiance or iron concentrations against potential growth under unlimited irradiance or iron concentrations. Positive values represent an increase in limitation, while negative values represent a decrease in limitation.

Across the Southern Ocean, the timing of the springtime onset of net primary production and the magnitude of summer biomass accumulation are controlled by light availability, as dictated by sea ice extent, cloud cover and water column structure (Henley et al., 2017). CMIP6 models project the greatest increase in productivity to occur across the coastal zone of the Southern Ocean (65-90°S) (**Figure 2.3c**), where irradiance limitation is reduced (**Figure 2.3d**). Conversely, across the Transitional zone (40-50°S), IPAR reduces (**Figure 2.3e**), irradiance limitation increases (**Figure 2.3d**) and productivity increases are less here compared to the rest of the Southern Ocean (**Figure 2.3c**). Increased iron limitation (**Figure 2.3f**) likely manifests from greater competition for iron driven by increased productivity (**Figure 2.3c**) despite a potential increase in iron supply with a deepening of the mixed layer across parts of the Subantarctic (50-65°S) (**Figure 2.3b**); brought about by reduced upper-ocean stratification from strengthening zonal winds (Carranza and Gille, 2015, Sallee et al., 2021). Iron supply to the surface is subject to changes in the properties and movement of water masses, which lead to variable circulation strengths, depth boundaries, heat content and carbon sequestration resulting from climate-driven perturbations to the ice-ocean-atmosphere system (Bindoff et al., 2019, Meredith et al., 2019). Upwelling of nutrients and light availability for phytoplankton are both strongly influenced by mixed layer depth, which in turn varies seasonally with increased solar warming and ice melt driving deeper Southern Ocean pycnocline stratification through the summer (Sallee et al., 2021). Models generally agree on changes in summertime mixed layer depth across most of the open ocean (**Figure 2.3e**), the greatest source of uncertainty is at the terminus of the Ross and Flicher-Ronne ice shelves, inclusion of freshwater input from ice shelves in future CMIP generations could help to reduce uncertainties in stratification.

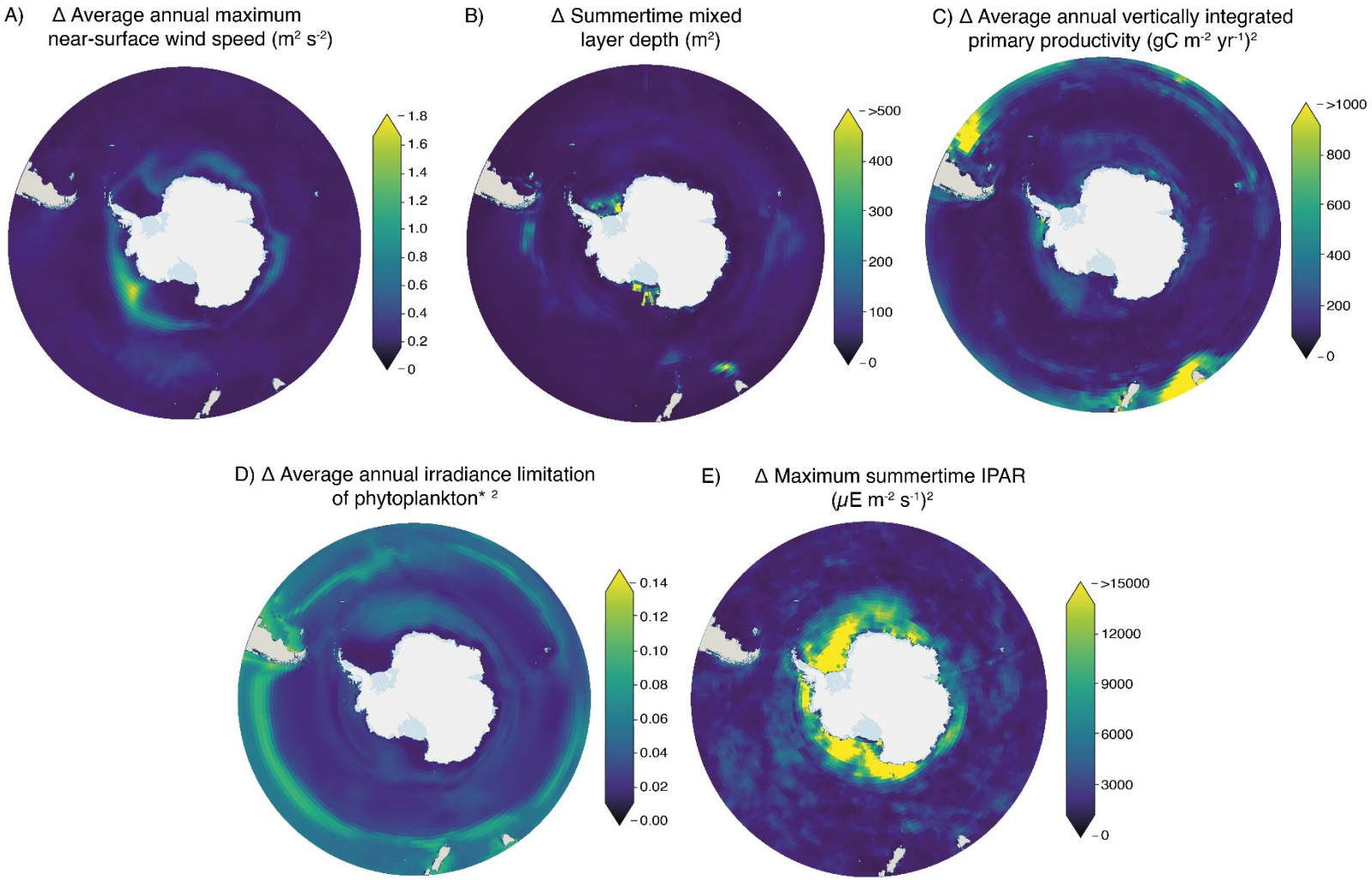

Figure 2.4: Variance in CMIP6 anomalies of the historical (1985-2015) vs end century time period (2090-2100) under the SSP5-8.5 scenario. Panels represent A) near-surface wind speed, B) mixed layer depth, C) net primary productivity, D) irradiance limitation of phytoplankton and E) incidental photosynthetically active radiation (IPAR). Outputs represent multi-model means, with model members listed in **Table 2.2**. No variance is given for iron limitation as only 1 model in our dataset includes the necessary parameters.

2.3.2 Changing biogeochemistry of the Southern Ocean

2.3.2.1 Micronutrient supply and uptake

Iron acts as the primary limiting nutrient across the Southern Ocean (de Baar et al., 1995, Watson et al., 2000), due to supply limitation from low atmospheric inputs and significant distances from terrigenous sources (Boyd and Ellwood, 2010). Around the Antarctic coast, iron concentrations are set by processes including the resuspension of shelf sediments (Blain et al., 2001), melting of sea ice (Lannuzel et al., 2016) and potential transformation of iron into more labile forms by glacial retreat, as seen in the Arctic (Laufer-Meiser et al., 2021). The change in projected iron limitation of phytoplankton appears minimal (between -12 and 10% **Figure 2.3f**). Iron limitation is expected to increase most in the transitional zone between South America and New Zealand, correlating with a reduction in near-surface wind speed (**Figure 2.3a**), suggesting that atmospheric deposition of iron will decline in this region. There is a minor increase in iron limitation around the Antarctic coast, which represents the inverse of the decreasing trend in irradiance limitation (**Figure 2.3d**), indicating a shift towards an increasingly iron limited system, as reductions in sea ice concentrations increase light availability to coastal waters. The co-occurrence of an increase in iron limitation (**Figure 2.3f)** and an increase in total productivity (**Figure 2.3c**) across the coastal zone suggests that this increase in limitation is driven by an increase in the uptake of iron (from a larger productivity sink), as opposed to any substantial changes in supply.

Despite the importance of iron for phytoplankton growth in the Southern Ocean, CMIP series models have historically struggled to resolve the vertical supply of dissolved iron (Tagliabue et al., 2016), which results in widespread uncertainty for modelling primary and export productivity. At the group level, iron limitation could be expected to influence shifts in phytoplankton communities because larger cells have a greater demand for iron compared to smaller cells. In addition, other micronutrients such as manganese have been identified as a control on phytoplankton growth, particularly during seasonal transitions (Browning et al., 2021). For example, manganese has been shown to play an important role in controlling oxidative stress by catalysing antioxidant production in some diatom species (McCain et al., 2021), explaining the observed phenomenon of iron-manganese co-limitation in the Southern Ocean (Pausch et al., 2019, Browning et al., 2021, Balaguer et al., 2022). Yet only

iron is considered in ESMs, due at least partially to the lack of observational data to underpin distribution modelling of other micronutrients. Future work should continue to develop our understanding of the metabolic role of other micronutrients and additionally consider the extent to which diversity exists in micronutrient demand among Southern Ocean phytoplankton species.

2.3.2.2 Macronutrient supply and uptake

Nitrogen species, silicic acid (DSi) and phosphate are all essential for the growth and survival of diatoms, with nitrate and phosphate also being required by all other phytoplankton classes for cellular metabolism. The ratio of utilisation between nitrogen (N) and phosphorus (P) deviates from the Redfield (1958) ratio of 16:1 across the Southern Ocean according to changes in community composition (Weber and Deutsch, 2010, Henley et al., 2020). Unlike much of the global ocean (Moore et al., 2013), high rates of macronutrient supply from the Circumpolar Deep Water (CDW) prevent widespread N or P limitation in the Southern Ocean except in periods of intense summer growth in high-productivity coastal regions (Henley et al., 2017). Although projections indicate an increase in chlorophyll across such regions (**Figure 2.5**), models do not show any increases in nitrate limitation over the remainder of the century (**Figure 2.6**), suggesting that iron and light will continue to be the primary constraints on productivity.

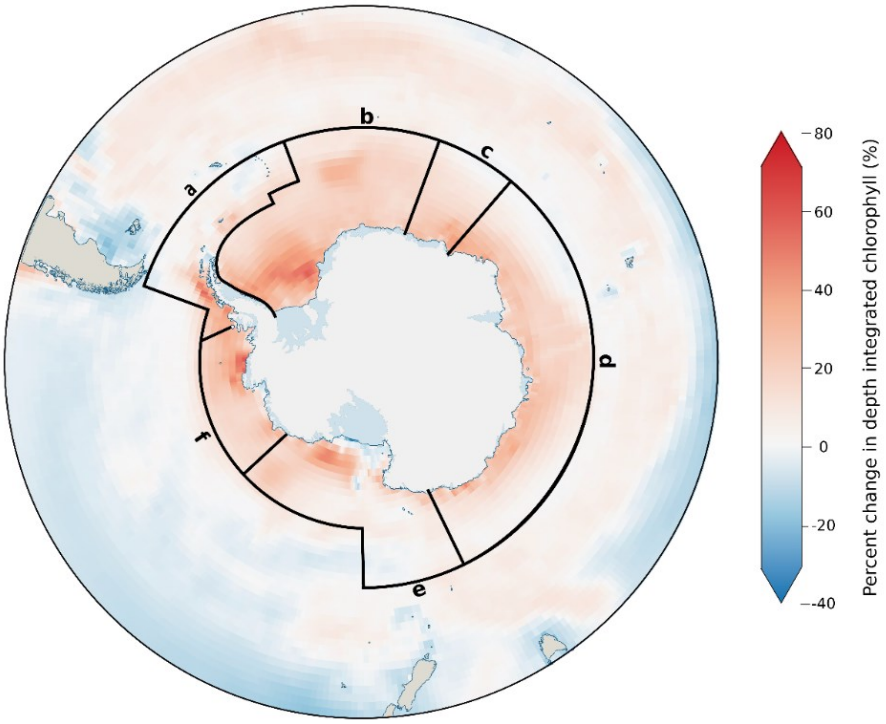

Figure 2.5: Change in depth-integrated chlorophyll (0-500 m) from all phytoplankton, displayed as the percentage change between the annual historical average (1985-2015) and projected values for 2090-2100. Values shown are multi-model means of the models listed in **Table 2.2**. Spatial boundaries show the Southern Ocean Observing System (SOOS) regions south of 55°S, which are defined in **Table 2.3**.

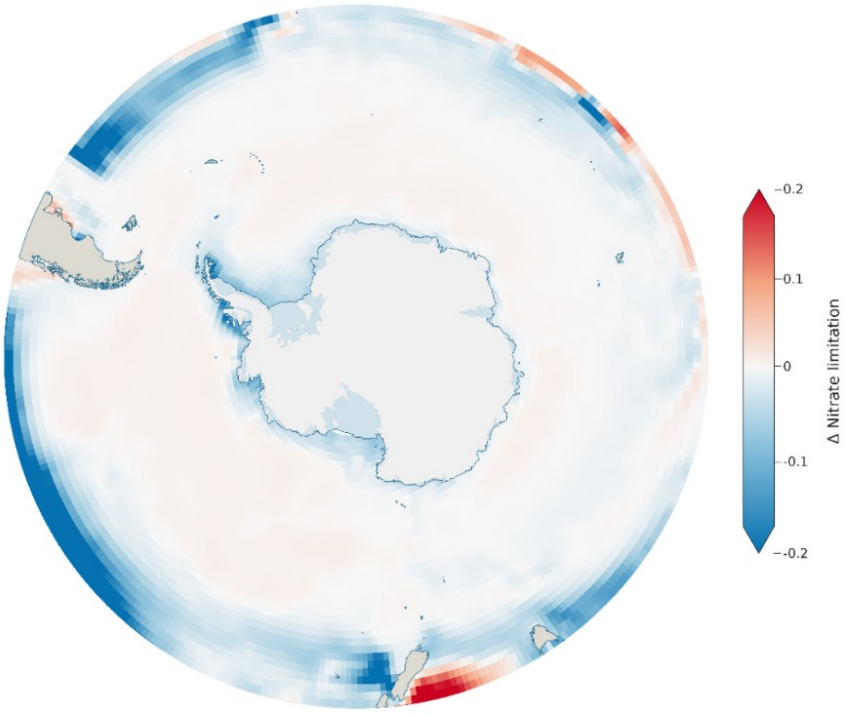

Figure 2.6: Anomaly in nitrate limitation of all groups of phytoplankton across the Southern Ocean for 2090-2100 under SSP5-8.5 compared to a historical mean (1985-2015). Data shown for GFDL-ESM4, being the only CMIP model to include nitrate limitation. Limitation of all groups is derived as the sum of "limndiat","limnpico" and "limnmisc". Units are the anomaly value between a ratio of growth under environmental nitrate concentrations and theoretical growth under unlimited nitrate.

While macronutrients are not usually limiting to Southern Ocean phytoplankton, growth of diatom communities, particularly around high productivity coastal and island zones (supported by lateral iron advection) (Robinson et al., 2016), is likely to place an increased demand on DSi availability (**Table 2.3**). The relative availability of silicate to nitrate is described by Si*, high Si* values (> 25) indicate plentiful DSi availability which supports diatom growth, while low values (< 10) suggest conditions which favour non-silicifying phytoplankton, such as the smaller cryptophytes and haptophytes. Si* is highest in the Antarctic zone (Henley et al., 2020) because of silica input from upwelling of CDW, but remains spatially heterogeneous within this region (**Table 2.3**, **Figure 2.9**). Si* is consistently high in the Weddell Sea, while across the WAP and Ross, Amundsen and Bellingshausen Seas there is a moderate mean Si* with large variability, and the Indian Sector has a substantially lower DSi availability. Si* is projected to decline by 2090-2100 at a zonally averaged value of -8.5 μmol L^{-1}, with the greatest declines being in the Ross and Weddell Seas, as well as the Indian sector (**Table 2.3**).

Changes in Si* correlate with increases in chlorophyll concentration across the same regions (**Figure 2.5**), indicative of increased phytoplankton concentrations resulting in a drawdown of silicic acid. However, increases in chlorophyll appear independent from projected changes in primary productivity (**Figure 2.4c**). For example, the west Antarctic Peninsula and Amundsen Sea regions show the greatest increase in primary productivity, but are among the regions of smallest change for both Si* and chlorophyll. The divergence between chlorophyll and primary productivity indicates variability in Chl:C, with siliceous diatoms typically expressing more chlorophyll per unit of carbon (Sathyendranath et al., 2009). Therefore, the large chlorophyll increase and large Si* decline projected in the Weddell Sea is likely driven by an increase in diatoms, whereas the productivity increase with only small changes in both chlorophyll and Si* seen on the west Antarctic Peninsula probably results from an expansion of non-diatom phytoplankton with a lower Chl:C.

The impact of climate change on DSi supply to the surface is difficult to evaluate because it is dependent on the competing stratification effects from wind driven changes to upwelling and an increase in freshening. Export of DSi from the surface and remineralisation at depth additionally act as important controls on supply; Freeman et al. (2018) showed that increased biological uptake of silicic acid, through increased diatom growth, leads to a poleward shift

in the silicic acid front and a potential decoupling from the Antarctic polar front. Efforts to better define the nutrient budgets, particularly in increasingly common low sea ice years, across different sectors of the Southern Ocean, as well as understanding the changing nutrient demands of phytoplankton will be essential for determining future trends in nutrient limitation (Henley et al., 2019).

2.3.2.3 Ocean acidification

Across all regions of the Southern Ocean, continued uptake of anthropogenic CO_2 is expected to elicit a decrease in surface pH of ~0.45 units south of 55°S (**Table 2.3**) under the high emission scenario (SSP5-8.5). Projected changes in pH do not differ regionally, and shows little variation within regions (low standard deviation) (**Figure 2.7**, **Table 2.3**). This ubiquity in the acidification effect means there no evidence for a direct effect of acidification effect on phytoplankton within our assessment of the Southern Ocean. In the main biogeochemistry modules of CMIP6 members, phytoplankton growth is driven and limited by nutrients and light, while many models are built with complex carbonate systems, these typically only interact with rates of calcification and for the majority of phytoplankton there is no biotic feedback from changes to the carbonate system. Although ocean acidification (OA) is typically considered to have the greatest effect on marine calcifiers through impacts on the production and dissolution of calcium carbonate (Figuerola et al., 2021), OA is also likely to impact diatom (Petrou et al., 2019), pico-phytoplankton (Tortell et al., 2008) and krill (Kawaguchi et al., 2013) populations which form the base of Southern Ocean food webs.

When considering species shifts, unravelling the specific impact of OA on individual phytoplankton types is complex due to the fact that OA often acts on phytoplankton indirectly. For example, Petrou et al. (2019) showed that acidification reduces the rate of silica deposition and therefore the silicification of diatoms (Si:C), likely reducing sinking capacity and increasing rates of remineralisation in the upper ocean, in turn weakening ocean carbon drawdown and acting as a positive feedback on the carbon cycle. Yet in existing CMIP6 biogeochemical modules, silicification is a product of the ambient concentration of either silicic acid (Stock et al., 2020), or silicic acid and iron (Moore et al., 2004), with no interaction from OA. This lack of plasticity might also impact nutrient export rates, Taucher et al., (2022) showed that OA decreases Si dissolution in the surface ocean, resulting in an export flux with a higher Si:N composition. Expanding model setups in CMIP6 to include the impact of OA

and other physiochemical drivers on biogeochemical stoichiometry could help to resolve existing biases in Southern Ocean silicic acid concentrations (Long et al., 2021), which has the potential to cause large uncertainty in global NCP due to the role of the Southern Ocean as a net Si source to the global thermohaline circulation. A key challenge in developing our understanding of OA impacts on phytoplankton at the group level is in resolving the mechanistic influence changing acidity has on different phytoplankton. For example, productivity may increase under OA as a result of shifts towards larger diatom species (Tortell et al., 2008). However, some studies have shown that the growth of smaller size classes (<20 μm) can be more successful at higher pCO_2 values (Hancock et al., 2018) or that total productivity may decrease under OA (Westwood et al., 2018).

Table 2.3: Biogeochemical parameter values calculated for the Southern Ocean Observing System regions. SOOS regional working groups (as defined at: www.soos.aq/activities/rwg) indicated on **Figure 2.5**; section C is an overlap section of sections B and D. Data shown are: Si* ([Si(OH)4]–[NO3–]) values and temperature determined from objectively analysed annual means of World Ocean Atlas 2018 data. pH was determined from a historical run of a multi-model ensemble of CMIP6 models (1985-2015). Delta values are anomalies of multi-model means of pH, temperature and Si* based on comparisons between the mean annual historical value (1985-2015) and projected values for 2090-2100 under SSP5-8.5 for a CMIP6 ensemble (detailed in **Table 2.2**). Values in brackets are standard deviations, representing spatial variation across the region. Anomaly maps for pH, temperature and Si* are shown in **Figures 2.7, 2.8, 2.9** respectively.

Section	SOOS Region	Si* ($\mu mol\ L^{-1}$)	ΔSi* ($\mu mol\ L^{-1}$)	pH	Δ pH	Temperature (°C)	ΔTemperature (°C)
A	West Antarctic Peninsula & Scotia Arc	17.24 (17.82)	-7.06 (3.63)	8.07 (0.15)	-0.43 (0.01)	1.94 (1.87)	1.79 (0.37)
B	Weddell Sea & Dronning Maud Land (WSDML)	37.37 (9.70)	-10.98 (3.77)	8.08 (0.14)	-0.41 (0.01)	-0.07 (0.95)	1.43 (0.49)
C	SOIS/WSDML	23.16 (6.67)	-8.20 (1.59)	8.07 (0.01)	-0.41 (0.01)	1.08 (1.26)	1.89 (0.40)
D	Southern Ocean Indian Sector (SOIS)	4.71 (3.72)	-10.52 (3.67)	8.07 (0.13)	-0.41 (0.01)	1.78 (1.66)	1.78 (0.46)
E	Ross Sea	19.82 (18.49)	-9.13 (5.02)	8.08 (0.13)	-0.40 (0.02)	0.62 (2.22)	1.08 (0.46)
F	Amundsen and Bellingshausen Seas	17.59 (14.02)	-5.27 (4.33)	8.09 (0.16)	-0.43 (0.01)	0.11 (0.83)	1.73 (0.44)

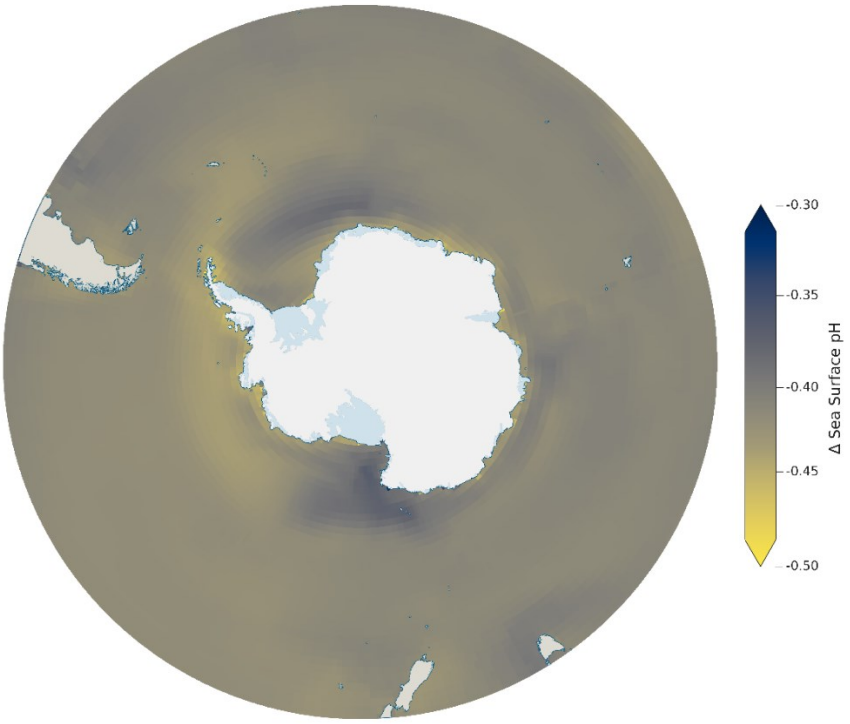

Figure 2.7: Anomaly in sea surface pH between 2100 (SSP5-8.5) and a historical average (1985-2015). Representative of a multi-model ensemble of CMIP6 models; models included are detailed in **Table 2.2**

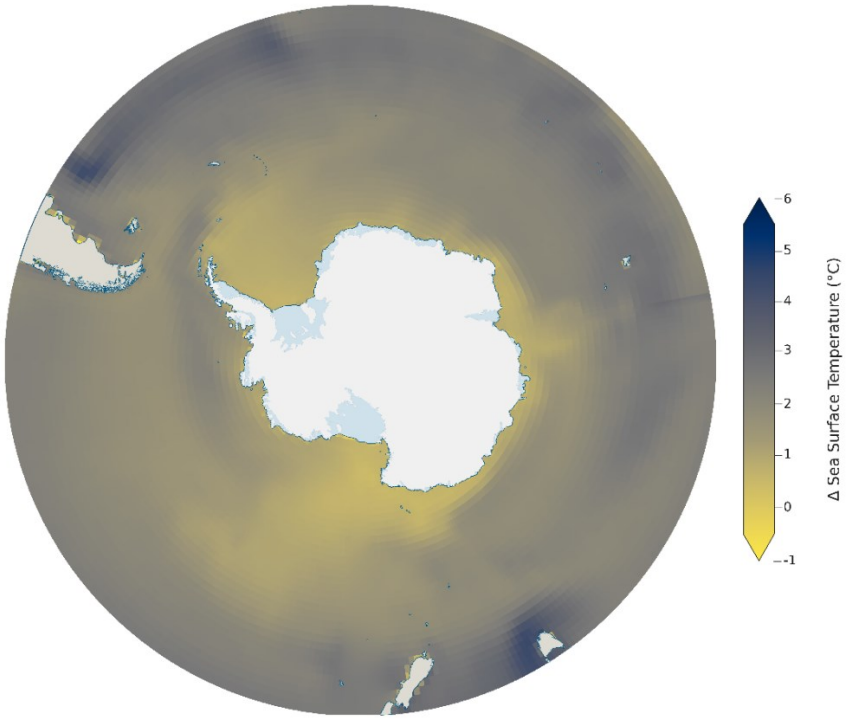

Figure 2.8: Anomaly in sea surface temperature (°C) between 2100 (SSP5-8.5) and a historical average (1985-2015). Representative of a multi-model ensemble of CMIP6 models; models included are detailed in **Table 2.2**

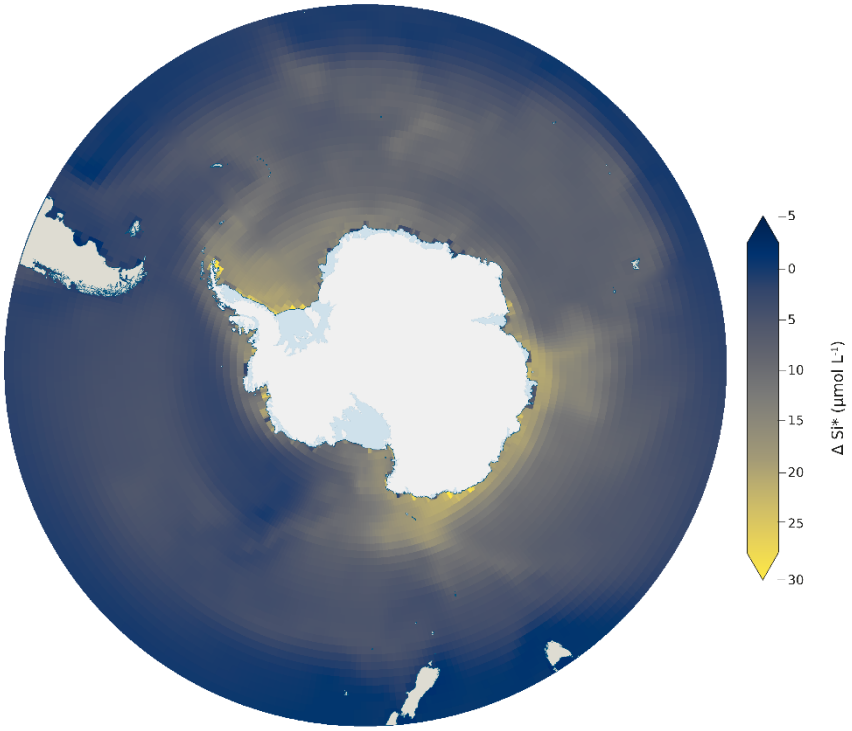

Figure 2.7: Anomaly in Si* ($[Si(OH)_4]$–$[NO_3^-]$ (μmol L^{-1})) between 2100 (SSP5-8.5) and a historical average (1985-2015). Representative of a multi-model ensemble of CMIP6 models; models included are detailed in **Table 2.2**

2.3.3 Primary production and representation in CMIP6

2.3.3.1 Phytoplankton classes

Two CMIP6 models (GFDL-ESM4 and CESM2-WACCM) showed substantial mechanistic differences in productivity projections by phytoplankton type south of 65°S (**Figure 2.10**). While GFDL-ESM4 projects that in this region diatoms account for the majority (55%) of the change in productivity under SSP5-8.5 (**Figure 2.10 a,b**), diatoms represent only 26% of the productivity increase in CESM2-WACCM, with pico-phytoplankton forming the major (74%) phytoplankton group (**Figure 2.10 e,d**). Additionally, the GFDL model indicates that increased productivity is driven by increases in both diatoms and pico-phytoplankton, representing a simultaneous growth scenario while CESM2-WACCM favours a replacement mechanism with diatoms decreasing as pico-phytoplankton populations grow (**Figure 2.10 c,f**). In CESM2-WACCM (MARBL biogeochemistry module) and GFDL-ESM4 (COBALTv2 biogeochemistry module), growth of phytoplankton groups is a product of temperature, nutrient limitation and light availability. In COBALTv2 the iron uptake half saturation constant is greater than in MARBL (0.1 vs 0.03 nmol kg^{-1} for small phytoplankton) and the differential between small and large phytoplankton (diatom) iron requirements is greater (x5 vs x2.3).

Although phytoplankton in MARBL have lower Fe requirements, negative biases towards NO_3^- and PO_4^{-3} in the Southern Ocean by CESM2 suggest that NCP is overestimated, subsequently this could drive the system to iron limitation earlier, resulting in an "insufficient contribution from diatoms" (Long et al., 2021). This could suggest that GFDL-ESM4 presents a more realistic outlook for phytoplankton composition, however fixed nutrient constants which usually represent a global average collected from multiple studies, make no differentiation for changes to nutrient uptake in cold water environments. For example, Timmermans et al. (2004) showed iron uptake half saturation values for Southern Ocean diatoms to vary substantially between 0.19 and 1.14 nmol L^{-1} based on species, compared to a fixed value of 0.5 nmol L^{-1} for COBALTv2 and 0.07 for MARBL, representing diatoms globally (Stock et al., 2020, Long et al., 2021). Experimentally, uptake half saturation constants are determined through the sequential addition of nutrients, yet multiple studies have shown that Southern Ocean diatoms in particular are able to reduce their cellular iron demand through changes to the photosynthetic pathway (e.g. Strzepek and Harrison, 2004, Jabre et al., 2021). Therefore, models based on these fixed constants may be reflecting the maximal iron uptake rather than the low iron acclimated uptake, i.e., this approach towards modelling nutrient limitation does not allow for a molecular adaptation which can, in some cases, achieve the same growth rate under more limiting conditions.

A shift from single species to community-based phytoplankton experiments for the purpose biogeochemical rates would help to improve our understanding of variability within the broad groups that exist for describing phytoplankton in CMIP6 models. For example, dynamic nutrient acquisition rates for different types of diatoms could replace a fixed nutrient half saturation constant for all diatom species if sufficient datasets existed to describe such rates at the species level. Developments of marine ecosystem models may include an expanded range of biological interactions such as group specific phytoplankton-zooplankton predation and bacterially-driven mixotrophic effects, such processes could alter trophic energy transfer and export fluxes through ESM's (Ward and Follows, 2016). Trait-based approaches have been explored as a means of modelling phytoplankton community composition, distinguishing functional groups based on life histories, morphology and physiology (Litchman and Klausmeier, 2008). Ocean biological sampling has some of the lowest coverage in the Southern Ocean (Sunagawa et al., 2020). Expansion of ecosystem

observing at the metagenomics level (e.g., Guidi et al., 2016) offers a promising opportunity to expand our knowledge of traits and trade-offs in Southern Ocean phytoplankton communities, facilitating their integration into climate models.

2.3.3.2 Ecological dynamics and ecophysiology

In a changing ocean, phytoplankton will succeed where they have the greatest biological plasticity, for example the ability to photo-acclimate rapidly (Arrigo et al., 2010) or scavenge and utilise a diverse range of micronutrients. The physiological properties of any individual species ultimately determines their ability to survive in a particular region at a particular time under ever changing climate-driven conditions. Subsequently, species ecology determines the abundance and temporal extent with which a species can exist or compete in a particular region. As the warming of the climate continues to bring about an earlier retreat of sea ice, growth seasons are expected to lengthen, altering the temporal dynamics of species progression (Moreau et al., 2015). In the coastal zone of the Southern Ocean, changes in light appear to be the main influence on productivity with decreased irradiance limitation stimulating pico-phytoplankton growth to a greater extent than diatoms (**Figure 2.10 j,k,m,n**); meanwhile iron limitation shows little correlation with productivity changes in this region (**Figure 2.10 g,h**), likely because of replete iron supplies from coastal upwelling.

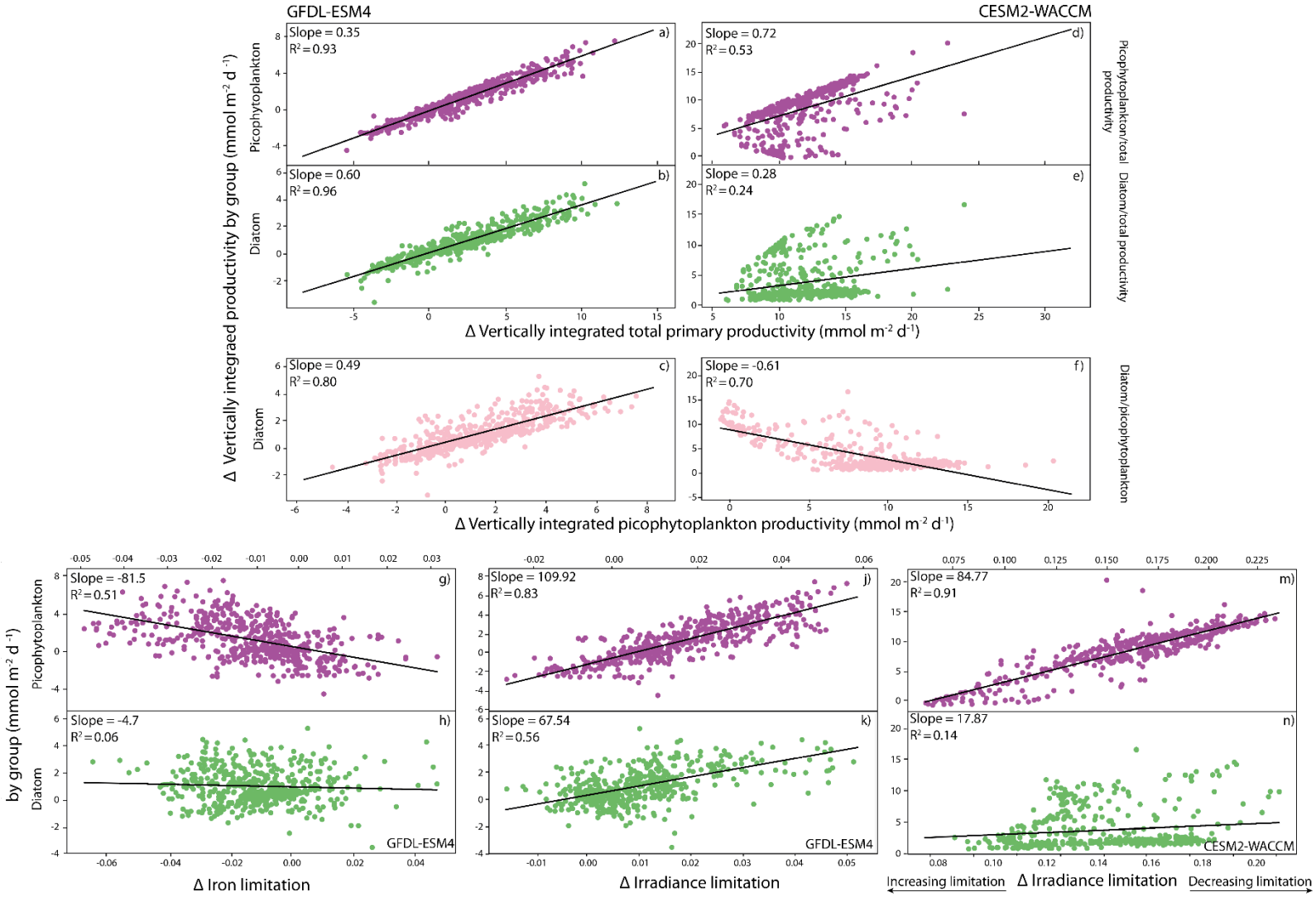

Figure 2.8: Evaluation of GFDL-ESM4 and CESM2-WACCM models using an anomaly between 2090-2100 (SSP5-8.5) and a historical average (1985-2015) for the Antarctic zone (65-90°S). Linear regression between change in total productivity and pico-phytoplankton productivity for GFDL-ESM4 (A) and CESM2-WACCM (D). Linear regression between change in total productivity and diatom productivity for GFDL-ESM4 (B) and CESM2-WACCM (E). Linear regression between change in picophytoplankton productivity and diatom productivity for GFDL-ESM4 (C) and CESM2-WACCM (F). Change in iron limitation with picophytoplankton (G) and diatom (H) productivity for GFDL-ESM4. Change in irradiance limitation with pico-phytoplankton (J) and diatom (K) productivity for GFDL-ESM4. Change in irradiance limitation with pico-phytoplankton (M) and diatom (N) productivity for CESM2-WACCM.3.4 Latitudinal productivity projections in CMIP6.

From those models that do distinguish between at least diatoms and other phytoplankton we are able to examine projected changes in community composition over the 21st century under a continued warming scenario (SSP5-8.5) (**Figure 2.11**). Previous analysis by Laufkötter et al. (2015), using a different set of models (a mix of marine ecosystem models employed in CMIP5 and the Marine Ecosystem Model Intercomparison Project), found substantial disagreement between models in projecting which phytoplankton groups drove NPP changes in the Southern Ocean. In CMIP5, Leung et al. (2015) found a latitudinally banded response of phytoplankton to continued warming, driven by the bottom-up dynamics of nitrate, iron and light limitation. From this analysis, we applied the same latitudinal bands to our analysis of the changes in whole community, diatom and non-diatom productivity across CMIP6. Our whole community projections agree with the trends shown by Leung et al. (2015), of a poleward increase in phytoplankton productivity, increasing average total productivity south of 40°S, with increases in total productivity in the Transitional (40-50°S; **Figure 2.11b**), Subantarctic (50-60°S; **Figure 2.11c**), and Antarctic zones (65-90°S; **Figure 2.11d).** In relative terms, this reflects a ~10% increase in total productivity over the SSP5-8.5 run (2015-2100) for both the Transitional and Subantarctic zones, with a ~30% increase in productivity for the Antarctic zone (**Figure 2.12 b,c,d**). The poleward increases in productivity correlate with a deepening of mixed layers around the Antarctic zone (**Figure 2.3b**) and a reduction in coastal light limitation (**Figure 2.4d**), resulting in greater increases in Antarctic zone productivity compared to the Transitional or Subantarctic. An ensemble mean shows no overall change in productivity across the Subtropics (see also Tagliabue et al., 2021), however individual models show the widest degree of divergence in this region, with some models projecting decreases in the diatom population of over 60% (**Figure 2.12a**), indicating a large amount of uncertainty in the magnitude of productivity changes.

In the Subantarctic (50-65°S), despite a large projected increase in light availability (**Figure 2.3e**), models project only a minor increase in productivity driven by a small amount of diatom growth, suggesting that growth of both diatom and non-diatom species remains largely iron-limited in this region. The coastal zone shows the greatest degree of change in phytoplankton growth, with the largest increases in this region; the majority of the biomass change can be attributed to non-diatoms, however relative changes in both diatom and non-diatom populations are similar (**Figure 2.12d**), suggesting no overall changes to community

composition here. The continued increase in all phytoplankton classes can be attributed to the decreased iron limitation across much of the zone (**Figure 2.3f**), with the success of non-diatoms reflecting the increase in light limitation (**Figure 2.3d**). Large phytoplankton types are more strongly affected by light limitation in CMIP6 because they have a greater requirement for light (as a lower constant for the chlorophyl specific initial slope of the photosynthesis-irradiance curve). In COBALTv2, large phytoplankton require 3x as much light as small phytoplankton to reach the same rate of photosynthesis (Stock et al., 2020). The lower requirements for iron and light by smaller phytoplankton types means that the smaller size fraction is likely to be most responsive to environmental changes in light and iron availability.

While CMIP6 models do not explicitly consider phytoplankton size, the shift from diatoms to, typically smaller, non-diatom species is consistent with more advanced ecological models such as DARWIN which predict a decrease in the slope of the phytoplankton size spectrum, albeit over a greater area of the Southern Ocean than shown in CMIP6 (Henson et al., 2021). Despite the clear differences between latitudinal bands, spatial heterogeneity continues to exist within these zones, particularly for the coastal zone where some of the greatest increases in chlorophyll occur in the WAP and Weddell Sea regions (**Figure 2.5**), reflecting the disproportionately high DSi supply in these regions (**Table 2.3**). Resolving spatial heterogeneity of phytoplankton in global-scale models such as those in CMIP6 is likely to require an increased reliance on, and integration with, regional-scale modelling (Person et al., 2018). The rapid increase of non-diatom species around the coast is in agreement with studies describing declining large diatom (>20 μm) abundances (Kang et al., 2001, Wright et al., 2010, Pearce et al., 2011); however, while it is true that diatoms are projected to decrease as a proportion of the community, diatom-derived carbon production is still projected to increase under continued warming, suggesting that the coastal biological carbon pump may be less threatened by this shift in community composition than previously thought.

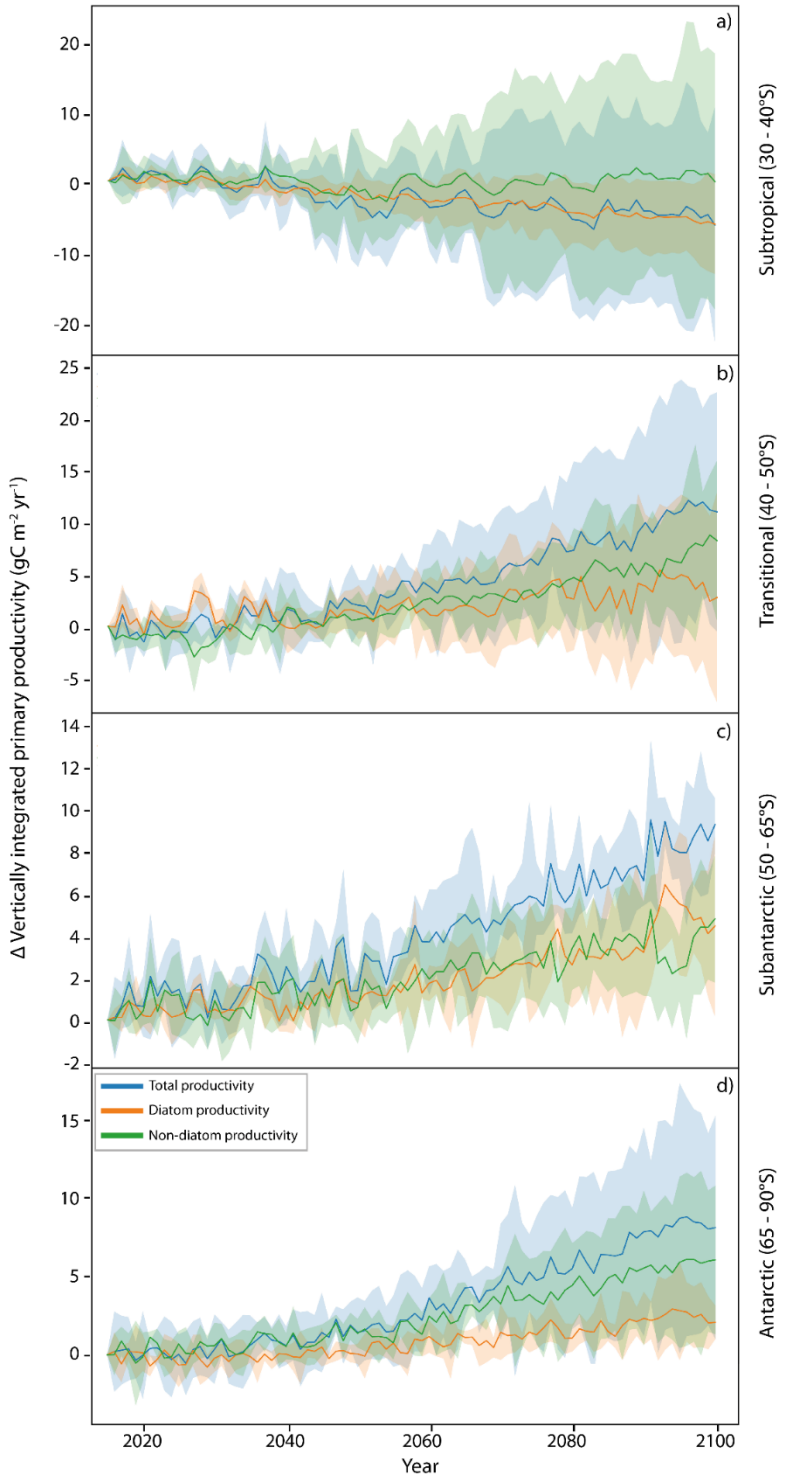

Figure 2.9: Changes in productivity (g C m^{-2} yr^{-1}) and the contribution of different phytoplankton classes to productivity, 2015-2100. The anomaly in CMIP6 model productivity projections (as POC production) compared to 2015 for SSP5-8.5 conditions across 4 latitudinal bands of the Southern Ocean, per Leung et al. (2015). Lines represent multi-model means of total productivity (intpp), diatom productivity (intppdiat) and non-diatom productivity (intpp-intppdiat). Shaded regions represent the spread between models as the interquartile range. Six CMIP6 models were used in this analysis, because only models containing the diatom productivity parameter are included; details of the specific models assessed are given in **Table 2.2**

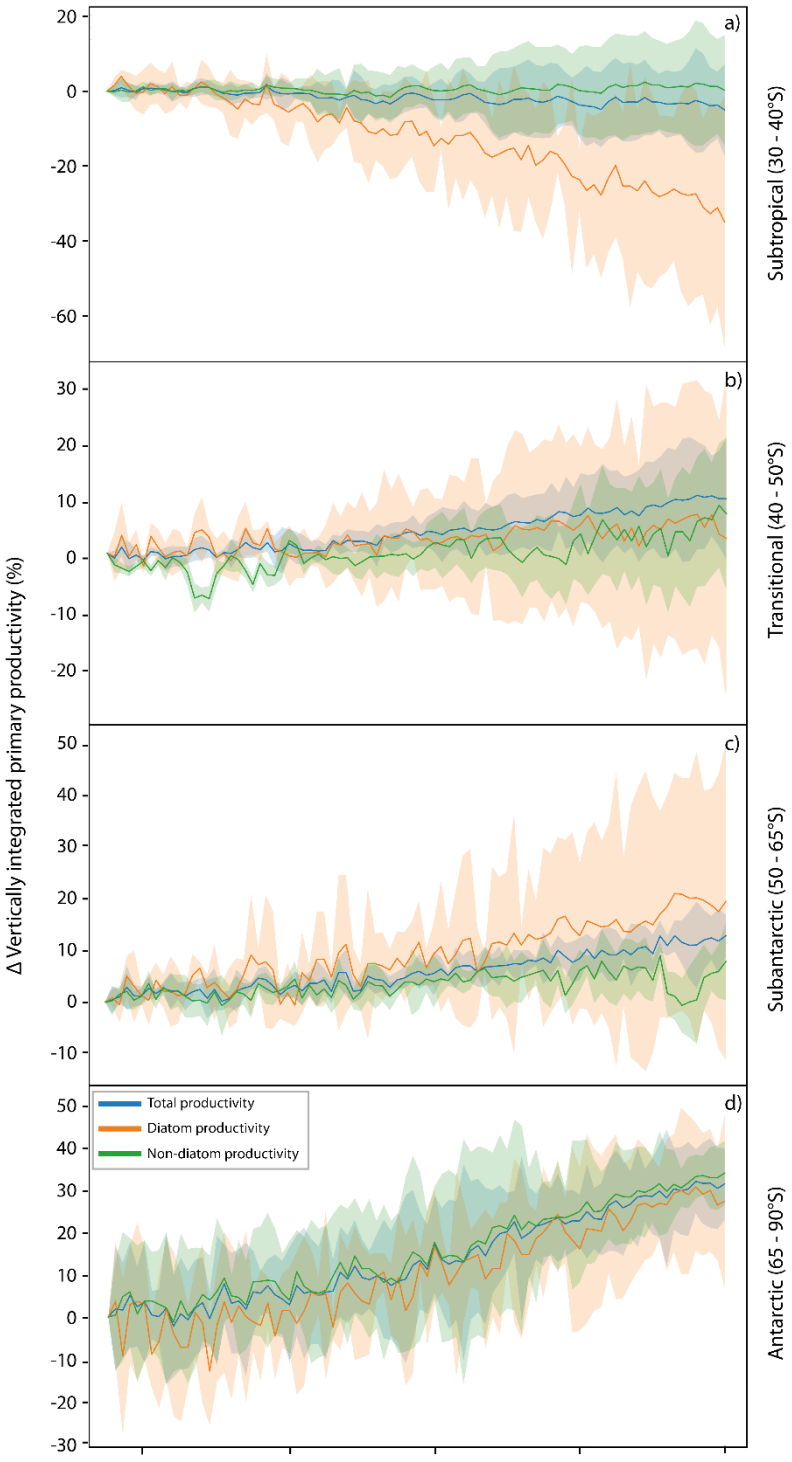

Figure 2.10: Changes in productivity (%) and the contribution of different phytoplankton classes to productivity 2015-2100 in CMIP6. Adapted version of **Figure 2.8** showing the relative change in productivity and phytoplankton group contributions compared to annual productivity at the first time point (2015) in the SSP5-8.5 run. Representative of a multi-model ensemble of CMIP6 models; models included are detailed in **Table 2.2**.

2.4 Conclusions

2.4.1 Implications of Southern Ocean productivity shifts

The cumulative impact of climate change on phytoplankton has the potential to restructure ecosystems of the Southern Ocean, with wider consequences for global ocean productivity and climate. In this study we found that CMIP6 models project a future Southern Ocean with increased levels of productivity, particularly around the Antarctic coastal zone. The major driver of this is reductions in light limitation, brought about by increased light concentrations from reduced sea ice coverage. However, the extent to which light will change is a source of great uncertainty, with the poor performance of models with resepct to sea ice also having additional implications for buoyancy forcing. Resolving freshwater fluxes from the AIS could reduce model uncertainty in coastal mixed layer depth change. The current iteration of CMIP6 models does not suggest any significant shifts in community composition across the Southern Ocean, outside of a decrease in the relative abundance of diatoms in the Subtropics. However, there is a large uncertainty in projected abundance (up to ± 30%) for all phytoplankton classes across all zones of the Southern Ocean, and key processes which will impact phytoplankton (e.g., viral losses, composition of the grazer community) are absent from most models.

In models which do separate productivity by phytoplankton type, the growth of one type of phytoplankton over another is a product of light, temperature and nutrient limitation. Fixed nutrient stoichiometry is a key limitation in projecting phytoplankton composition, in particular the omission of ocean acidification and iron limitation effects on cellular Si:C stoichiometry could be responsible for some of the existing biases in models towards excess silicate in the Southern Ocean. We showed that for two models (GFDL-ESM4 and CESM2-WACCM) the iron requirements of different phytoplankton types can result in either a simultaneous growth of diatoms and picophytoplankton, or a replacement of diatoms with picophytoplankton. Future model generations might consider the acclimation of diatoms to low iron conditions, since models currently use very different uptake half saturation values for iron, which disproportionately impacts community composition in iron limited regions. However, the literature also contains wide divergence in experimentally determined nutrient uptake constants; a more accurate approach towards modelling will first require us to better define what drives this variability in iron requirements. With continued record low sea ice

trends, observation of phytoplankton responses in this multi-stressor environment will be essential in understanding the scale of productivity change occurring and provide a basis to incorporate phytoplankton community change into global scale modelling efforts.

2.4.2 Observational recommendations

Nutrient upwelling, directionality of mixed layer depth change, mutualism and resource competition between phytoplankton classes, and eddy strengthening are key processes largely absent from existing CMIP generation models but could act as step changes towards improved representation of phytoplankton community composition if incorporated in future model generations. In some cases, the absence of these processes is because of lack of monitoring and insufficient data coverage to assess temporal (e.g. seasonal nutrient dynamics) or spatial (e.g. biogeochemical impacts of eddies) variability. While determining the magnitude of MLD change that can be associated with freshwater injection, variability resulting from the relatively recent reversal in Antarctic sea ice trends poses a particular challenge to resolving this process.

The abundance of diatoms between 30°S and 65°S represents one of the greatest sources of uncertainty in phytoplankton community composition. This could be related to poor model representation of diatom species in these regions due to data sparsity, as sampling of open waters is more seasonally limited in comparison to land-based stations in the Antarctic zone, where there is a lower uncertainty for diatom abundance. However, the existence of a single diatom group in models that consider different phytoplankton functional types could also be limiting here, as subtropical diatoms differ in biology (e.g., lack of ice binding proteins) and species composition compared to polar diatoms. Parameterising these distinct species groups in one functional type inevitably means the model will underperform for some groups relative to others. Monitoring of phytoplankton functional group composition, especially in areas of the greatest projected change (WAP and Weddell Sea), ideally capturing temporally-resolved new productivity in the early spring, will be necessary to detect any changes in community composition. We have shown that relationship between chlorophyll, carbon production and Si* can be used as an indicator of community composition, with projected increases in chlorophyll and decreases in Si* in the Weddell Sea indicating a diatom driven increase in productivity. This study shows that proxy variables

such as these are a key way in which data from autonomous platforms could be used to represent community composition at a coarse level without the need for personnel intensive microscopy or genomic methods. Crucially, to then link ecological shifts to global climate, the extent to which different phytoplankton species undergo losses via different pathways, including phytoplankton group specific grazing patterns by zooplankton, represents a substantial target for model development which could substantially improve the predictive skill of ESMs. Finally, to improve the parameterisations (e.g., nutrient half saturation constants and thermal tolerance) of phytoplankton in ESM's there is a need for further process-based studies, specifically those which include a diverse set of phytoplankton species to represent the true extent of functional diversity within broad phytoplankton groups.

3. Southern Ocean phytoplankton communities drive molecular variability in dissolved organic matter composition

Abstract

The West Antarctic Peninsula (WAP) marine ecosystem is a light- and iron-limited region, characterised by summer phytoplankton blooms, varying in timing and magnitude with the retreat of seasonal sea ice cover. The WAP is one of the fastest warming regions on Earth and the associated changes in sea ice have been related to shifts in the phytoplankton community. Phytoplankton are the major energy source to Southern Ocean ecosystems through organic matter production. Labile dissolved organic matter (DOM) is released by phytoplankton in the surface layer, with molecular level transformations over depth resulting in a compositionally distinct deep-water refractory pool of DOM. We sought to determine the extent to which phytoplankton type influences DOM composition during a ship expedition as part of the Palmer Long Term Ecological Research project. Samples were collected over the grid and analyzed using ultrahigh-resolution mass spectrometry (FT-ICR-MS) of solid phase extracted (SPE)-DOM alongside measuring the isotopic ($\delta^{13}C$) and stoichiometric (C,N,P,S) composition of SPE-DOM. Over the euphotic zone (< 50 m), smaller size classes of phytoplankton (≤ ~10 µm) were associated with saturated, fresh DOM, while larger diatoms (>20µm) were associated with aged DOM, indicative of less DOM production. Upper ocean DOM was enriched in phosphorus and sulfur relative to the bulk pool ($C:N:S:P_{SPE}$ =1865:133:15:1), while below the surface layer (> 50 m), DOM was rapidly remineralised and became increasingly homogeneous in composition. The resulting deep-water refractory pool of DOM was more aromatic and unsaturated compared to the upper ocean DOM, and depleted in phosphorus and sulfur, while nitrogen was more stable relative to carbon (2203:147:12:1). The greater presence of fresh DOM with small phytoplankton may indicate a reduced efficiency of carbon export in a future cryptophyte-dominated WAP, while the increased availability of DOM in the surface layer may sustain more diverse and abundant microbial heterotrophs. Additionally, increased DOM release under a future Southern Ocean productivity regime could have important feedback on productivity through increasing nutrient concentrations resulting from remineralization of DOM in the upper ocean. Consequently, changes to the availability of Southern Ocean derived nutrients could

influence productivity at the global scale through modulating leakage and export of excess macronutrients across the global thermohaline circulation.

3.1 Introduction

Marine dissolved organic matter (DOM) represents a substantial carbon stock in the Earth system, comprising 700 PgC globally (Friedlingstein et al., 2022b). DOM can persist in the ocean on time scales from seconds to millennia, with the molecular composition of DOM proposed as a control on longevity (Dittmar et al., 2021). Labile components are released by phytoplankton and the majority are rapidly remineralized in the surface to dissolved inorganic carbon (Osterholz et al., 2014). Some labile compounds avoid remineralization and instead become transformed to semi-labile and then refractory compounds, with the resulting refractory pool of DOM accumulating at depth, with a lifetime of ~16k years (Hansell, 2013). During this transformation, "fresh" DOM becomes more unsaturated over time as hydrogen atoms are lost, with refractory DOM typically being more aromatic and having a greater number of double bonds. In the Southern Ocean, where allochthonous inputs are low, the production of particulate and DOM by marine phytoplankton represents the primary source of energy for heterotrophs. Therefore, any change in the amount or type of DOM release associated with changing community composition has the potential to alter the amount, composition, and fate of organic matter (OM). This has potentially significant impacts for ecosystems and ocean carbon dynamics.

The Southern Ocean is responsible for a disproportionately large amount of anthropogenic CO_2 uptake relative to its size (DeVries, 2014, Frölicher et al., 2015) acting as a global carbon sink. In a future Southern Ocean, transformation of DIC to organic carbon by phytoplankton drives ΔpCO_2 in the surface layer has been associated with an enhanced summertime CO_2 uptake (Hauck et al., 2015), however the community composition of the primary producers, and the associated DOM produced, remains an open question. Understanding the relationship between marine phytoplankton and the composition of DOM will be crucial for determining responses in the global biological carbon dynamics in a changing ocean.

The Southern Ocean is characterized by low surface DOC concentrations (<60 μmol L^{-1}) (e.g. Ogawa et al., 1999, Ksionzek et al., 2016, Dittrich et al., 2022) and low rates of primary productivity (~43 mmol C m^{-2} d^{-1}) (Fisher et al., 2023). Much of the Southern Ocean is a high

nutrient low chlorophyll (HNLC) zone where productivity is limited by a lack of iron and light (Boyd, 2002, Moore et al., 2013). The low overall rates of productivity result in low particulate organic carbon production, leading to a lesser proportion of total organic carbon (TOC) being dissolved in the high latitude Southern (Carlson et al., 2000, Loh and Bauer, 2000) and Arctic Oceans (Mathis et al., 2007) compared to the North Pacific (Loh and Bauer, 2000) or North Atlantic (Carlson et al., 1994, Hansell and Carlson, 2001). Despite the low fraction of DOC in the Southern Ocean, Dittrich et al. (2022) found a correlation between DOC and POC across the West Antarctic Peninsula (WAP), indicative of direct DOC production. The partitioning between dissolved and particulate organic matter has been previously attributed to phytoplankton groups, with *Phaeocystis spp.* being associated with a greater DOC/POC partition compared to cyanobacteria or coccolithophores (DOC/TOC = 27% vs 10-14 %) (Biddanda and Benner, 1997). However, in a Ross Sea *Phaeocystis* bloom, up to 70-99% of the peak seasonal change in TOC was driven by POC (Carlson et al., 2000). Mesocosm experiments suggest that community composition does not alter DOC/POC partitioning (Conan et al., 2007), but instead shows a role for nutrient limitation in shifting the DOC/POC partition, with greater DOC production when nitrate (Walker et al., 1998, Conan et al., 2007) or silicic acid (Poulton et al., 2016) limit cellular biomass growth. A limitation in determining the nature of an organic matter flux based on DOC/POC partitioning is the operational definition of "dissolved" vs. "particulate" based on the size of a compound, since molecular variability also contributes towards determining the fate of an organic compound. Therefore, significant knowledge gaps remain in the interplay between phytoplankton communities and organic matter composition (Thornton, 2014).

As the Southern Ocean continues to undergo rapid environmental change, the corresponding impact on the biogeochemistry is a critical question. Given this understanding the relationship between phytoplankton species and DOM composition will be important. High emission, low mitigation (SSP5-8.5) model scenarios in CMIP project a future Southern Ocean which has strengthened winds, deeper mixed layers, less sea ice, and increased productivity (Leung et al., 2015). Climate-driven change may affect Southern Ocean DOC cycling by increasing the overall production of organic matter due to longer growing seasons due reduced sea ice. This could also result in a reduction in the amount of DOC exported to the deep ocean through a weakening in the subduction of Subantarctic Mode

Water and Antarctic Intermediate Water (Downes et al., 2010, Lønborg et al., 2020). Phytoplankton communities have shown a greater release of DOM at higher temperatures, while on a molecular level, increased temperatures are associated with an increased C/N ratio of DOM production (Engel et al., 2010).

Within the Southern Ocean, the WAP represents one of the fastest warming regions (Turner et al., 2014), where declines in sea ice have led to southward shifts in diatom populations, and northward communities are now dominated by cryptophytes (Brown et al., 2019). The Palmer Antarctica Long Term Ecological Research (LTER) program has studied environmental change throughout the region over the last 30 years, working within a grid which extends across the length of the WAP, to capture the extent of spatial variability in ocean physics and biogeochemistry. This study was conducted within the LTER grid and we compare phytoplankton community composition measurements and FT-ICR-MS for DOM characterization.

Targeting thesis aim 2, the specific sub-aims of this chapter were to:

- Determine how the molecular composition of DOM varies spatially across the WAP region in relation to the species composition and abundance of phytoplankton.
- Examine the extent to which size fractionation of phytoplankton communities drives DOM concentration and the lability of DOM in surface waters.
- Quantify the level of variability in isotopic, stoichiometric and molecular properties of DOM with depth. Subsequently, to deduce how the rate of DOM transformation to more refractory types over depth differ in the presence of different phytoplankton types.

Association of molecular signatures indicative of increased biolability with phytoplankton types which are expected to become more abundant would provide a new perspective on the stability of carbon export in a future Southern Ocean. Determining the fate of carbon in a warming Southern Ocean is the key mechanism by which ecological change in phytoplankton communities can be linked biogeochemical cycling; and therefore contributes towards understanding the importance of phytoplankton communities in large scale climate-carbon feedbacks,

3.2 Materials and Methods

3.2.1 Sampling area and water sampling

Samples were collected across the sampling area defined by the Palmer LTER grid (Waters and Smith, 1992), running the length of the West Antarctic Peninsula, extending up to 200 km off-shore. Selected stations (**Figure 4.1**) of the grid were chosen for DOM sampling, in addition to two off-grid stations (C2 and C3). Phytoplankton community composition was sampled across the euphotic zone (0- ~50 m) at all LTER stations, as well as C2 and C3, while DOM was sampled at 4-5 depths across the full water column (0-3050m). Shelf stations are situated 40 km from coastal stations, with slope stations being 200 km from the corresponding coastal station. Samples were collected between 5th and 28th January 2023 from onboard the ASRV *Laurence M. Gould*.

Water sampling was conducted at each site with the deployment of a stainless-steel rosette equipped with 24 x 10 L Niskin bottles, with a conductivity, temperature, depth (CTD) sensor (SeaBird 911+). The CTD sensors were calibrated pre and post cruise by SeaBird electronics. The CTD was additionally equipped with duplicate sensors for dissolved oxygen (SeaBird 43) and chlorophyll fluorescence (WetLabs ECO Fluorometer) which were calibrated throughout the cruise using Winkler oxygen titrations and independent measurement of chlorophyll fluorescence from pigment analysis of filtered water samples.

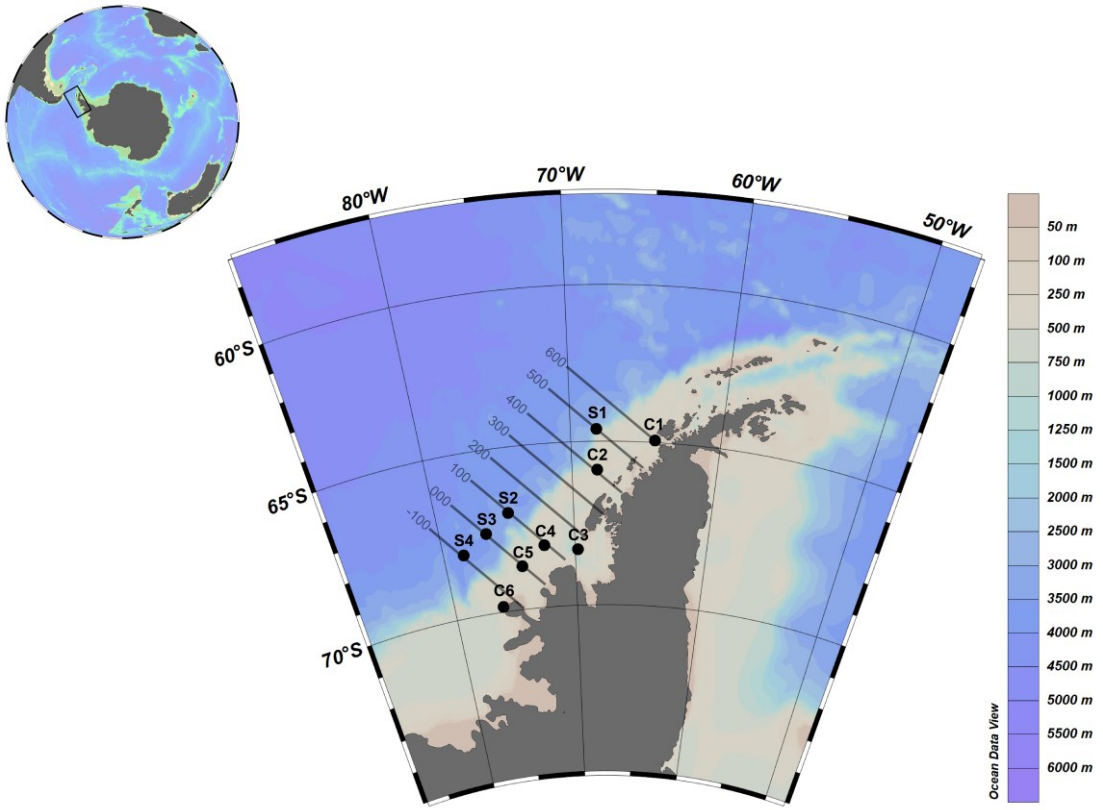

Figure 3.1 Stations sampled for DOM across the Palmer LTER grid on the West Antarctic Peninsula. C# represents coastal stations and S# represents slope stations. S1 corresponds to Palmer LTER grid site 500.200, C1 to 600.040, C2 to 400.040, S2 to 100.200, S3 to 000.200, S4 to -100.200, C4 to 100.040 and C5 to 000.040. Additional stations along the standard LTER grid were sampled for physiochemical properties and community composition, the location of these stations is given in **Figure 3.9**. Bathymetry is obtained from ETOPO1 at 2x2min resolution.

3.2.2 Solid phase extraction of dissolved organic matter

Solid Phase Extractable dissolved organic matter (SPE-DOM) was isolated by pre-filtration of 2 L seawater samples through muffle furnace combusted (4 hours at 450 °C) glass fiber filters (GF/F) (nominal pore size 0.7 µm). The resulting filtrate was acidified to pH 2 through addition of HPLC grade 37% hydrochloric acid (1 mL per L) and loaded on Bond Elute Priority PolLutant (PPL) cartridges (Agilent 1g, 6 mL), prepared according to Dittmar et al. (2008). Cartridges were desalted and dried with N_2 gas, then stored chilled before elution with HPLC grade methanol (99.9%) into muffle furnace combusted amber glass vials (4 hours at 450 °C). Extracts were stored at -20 °C until analysis. Extraction efficiency was determined to be 38 ± 9% by comparing the SPE-DOC concentration to the DOC concentration of seawater (see **3.2.3**), agreeing with previous values for the Southern Ocean (Dittmar et al.,

2008). SPE-DOC samples were prepared by evaporating 100 µL of SPE-DOM extract in a combusted glass vial before resuspending in 10 mL of ultrapure water via ultrasonication.

3.2.3 Dissolved organic carbon and nitrogen analysis

Subsamples of pH 2 acidified seawater were taken prior to SPE for DOC and total dissolved nitrogen (TDN) analysis. Following extraction, aliquots of the SPE-DOM elute were analysed for SPE-DOC and SPE-DON concentrations. SPE-DOC, SPE-DON, DOC and TDN concentrations were determined by high temperature catalytic oxidation using a Shimadzu TOC-V analyzer. Ultrapure water was used as the blank and a deep seawater reference certified reference material (D. Hansell, U. Miami, USA) was used for instrument calibration. Standard deviation on duplicate analyses was < 2 $\mu mol L^{-1}$ for DOC and < 0.5 µmol L^{-1} for DON. The limit of detection was 50 µg L^{-1} for DOC (4.17 $\mu mol L^{-1}$) and 5 µg L^{-1} for DON (0.36 $\mu mol L^{-1}$). The deviation of the average of replicate deep seawater reference standards was <5% from the published value for DOC and <1% for DON.

3.2.4 FT-ICR-MS analysis of SPE-DOM

SPE-DOM methanol extracts were prepared by diluting to a concentration of 2 ppm with MS grade methanol and ultra-pure water (1:1, *v/v*). Samples were run on a 15 Tesla solariX FT-ICR-MS (Bruker Daltonik GmbH, Bremen, Germany) using electrospray ionization in negative mode, with a capillary voltage of 4kV. For each sample, 200 broadband scans across a mass range of 92.14 to 1500 Da were acquired over a period of 0.2 s per scan. Mass spectra were calibrated against an internal list of known compounds which commonly occur for this sample type across the selected mass range, the resulting accuracy was <0.1 ppm. An internal reference standard of deep seawater SPE-DOM was analyzed alongside the samples to account for instrument variability. Molecular formulae were assigned to peaks using the server based tool, ICBM-OCEAN Merder et al. (2020). The method detection limit was applied (Riedel and Dittmar, 2014) with a minimum signal-to-noise ratio of >2.5 and a mass tolerance of <0.5 ppm, the sample junction was set to fast join mode. The minimum signal to method detection limit (MDL) ratio as a backbone was 5 using mean recalibration mode. Formulae were assigned in the stoichiometric ranges: $^{12}C_{1-100}{}^{1}H_{2-200}{}^{16}O_{1-70}{}^{14}N_{0-4}{}^{32}S_{0-2}P_{0-1}$ between m/z ratios of 100 and 1000. Formulae with intensities present in <10% of samples were excluded from the assignment. Molecular formulae assignments which contained isotopes (^{13}C, ^{18}O, ^{15}N, ^{34}S), oxygen to carbon ratios (O/C) ≥1 or hydrogen to carbon ratios

(H/C) ≥ 2.5, were manually excluded. Isotope tolerance was set to 1000 % and isotope ratio mismatches above signal to MDL ratios of isotope formulae >6 were excluded. The formulae assignment was compared against a list of known organic contaminants (e.g., plasticisers and surfactants), with any contaminants removed. Inorganic contaminants which fell outside of the normal distribution were also removed from the dataset. The signal intensities of each peak with an assigned molecular formula were normalised to the sum of all intensities from peaks with assigned molecular formulae in each sample, before being upscaled by a factor of 10,000. Duplicate measurements were averaged where the same mass peaks were present in both samples.

Molecular formulae were assigned to DOM compound groups of differing saturation states after Merder et al. (2020), based on their modified aromaticity index (AI_{mod}) and double bond equivalent (DBE) (Koch and Dittmar, 2006, 2016). Compounds with an AI_{mod} >0.5 suggest an aromatic structure, while a DBE value of 0 indicates a saturated compound. Elemental molar ratios of H/C and O/C were calculated and weighted based on peak intensity, according to Seidel et al. (2014). These ratios are used to differentiate between unsaturated (H/C ≥1.5 & H/C ≤2), and highly unsaturated (AI_{mod} <0.5 & H/C <1.5) compounds, as well as oxygen richness (O/C >0.5) or poorness (O/C ≤0.5). The degradation index (I_{DEG}), indicative of age, was calculated for each sample based on the proportion of compounds present which are known to associate with a high radiocarbon age, following Flerus et al. (2012). The biolability of compounds according to distance from the molecular lability boundary (MLB_L) was calculated according to D'Andrilli et al. (2015) based on the H/C ratio of formulae.

3.2.5 δ^{13}C-SPE-DOM

The stable carbon isotopic composition ($\delta^{13}C$) of SPE-DOM was determined by a stable isotope ratio mass spectrometer (Thermo Electron Delta V Advantage IRMS) and an elemental analyzer (Carlo Erba NA 2500), both are coupled with a Conflo III interface at the Wolfson Isotope Ratio Mass Spectrometry facility, University of Edinburgh. SPE-DOM extracts containing ~20 µg of carbon were pipetted into ultra clean tin capsules (OEA) and the methanol evaporated at 60 °C. Samples were run against an in-house sediment standard IOS (Indian Ocean Sediment) used to calibrate the isotopic value and an acetanilide certified reference material (OEA) used to calibrate the %C content. Duplicates of the in-house IOS

standard (isotope standard) and acetanilide (quality control) were run after every 10 samples; precision was <0.2 ‰. $\delta^{13}C$ values represent the $^{13}C/^{12}C$ ratio relative to the VPDB scale.

3.2.6 SPE-DOP and SPE-DOS

Dissolve organic sulfur (SPE-DOS) and dissolved organic phosphorus (SPE-DOP) concentrations in SPE-DOM extracts were determined by Inductively Coupled Plasma Mass Spectrometry (Agilent 7500ce) at the University of Edinburgh. Samples were prepared by evaporation of 1.5 mL of SPE-DOM extract at 60 °C, before being resolved in 1.5 mL ultrapure water with 1% ultrapure HNO_3 and resuspended by ultrasonication. Sulfur was calibrated between 10-5000 ppb and phosphorus between 1-500 ppb. After every 10 samples, sulfur and phosphorus concentrations were checked against standards (Reagecon) at up to 3 different concentrations. The average deviation from the standard across all concentrations was <4% for sulfur and <2.5% for phosphorus.

3.2.7 Phytoplankton community composition from imaging flow cytobot

Water samples, collected from across the shallowest 5 depths of the CTD cast (0-86 m), covering the euphotic zone, were injected into an Imaging Flow Cytobot (IFCB, McLane labs). Images were acquired for up to 5 mL of sample over 22 minutes, with acquisitions triggered by fluorescence on cells with a size between 5 and ~180 µm (Zheng et al., 2023). Each image was given an index number, with 792,926 indexes assigned over the sampled grid stations. Images were initially classified into 11 groups using the approach by Sosik and Olson (2007), with the IFCB analysis package in MATLAB (9.10.0) (Sosik et al., 2016). Examples images are shown in **Figure 3.2**.

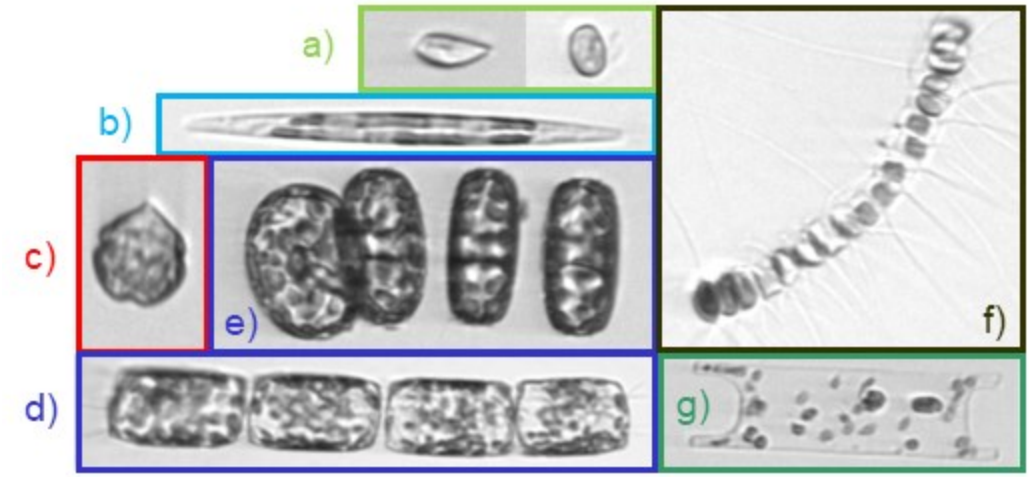

Figure 3.2: Example images of phytoplankton acquired by IFCB. Representing a) cryptophytes, b) pennate diatoms, c) dinoflagellates, d,e,f) centric diatoms chains (here, d&e: *Thalassiosira spp.,* f: Corethon *spp.)* ,g) individual centric diatom *(Eucampia spp.).*

The random forest classifier was trained on >500 manually identified images per group (**Figure 3.3**); where fewer than 500 examples of a group were identified, similar groups were pooled, leaving a total of 5 groups. A group consisted of the different permutations of a phytoplankton type, for example solitary pennate diatoms, solitary centric diatoms, chained pennate diatoms and chained centric diatoms, along with multiple morphologies of dinoflagellates. Chained diatoms were then pooled with the solitary diatoms and all types of dinoflagellate were pooled, this improves the overall accuracy of the model by expanding the sample size, multiple combinations of phytoplankton were pooled until the lowest error rate was achieved relative to the manual classification. The total training data set contained 16,632 images, 97.5% of which were assigned a classification with an error rate of 5.3% relative to manual identification (**Figure 3.4**). After assigning each image to their most likely group, group abundance per sample was normalized according to biovolume, calculated using distance maps per Moberg and Sosik (2012). Images classified as detritus or as having bad focus were excluded from the analysis. An average of 13.3% of images were not classified into the given groups and are shown as 'other'.

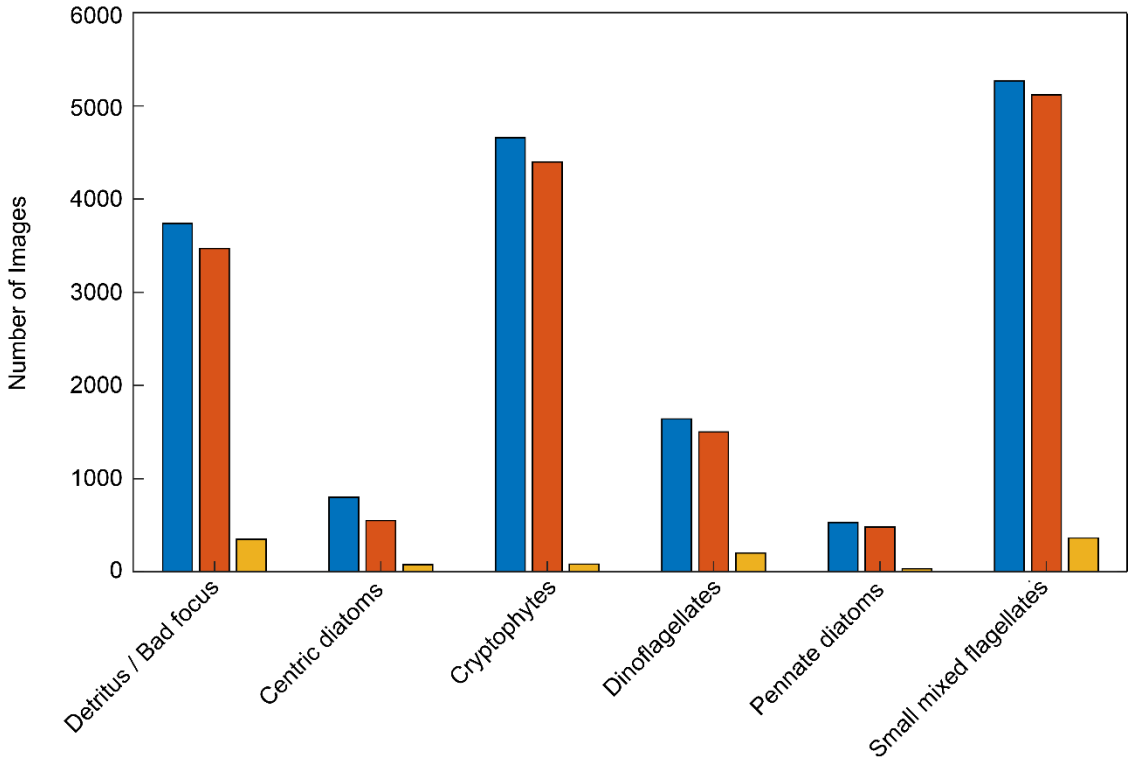

Figure 3.3: Number of images in the random forest classifier training model. The total number of images manually classified (Blue), those where random forest classification matches manual classification (Red) and those where the random forest classification differs from the manual classification (Yellow).

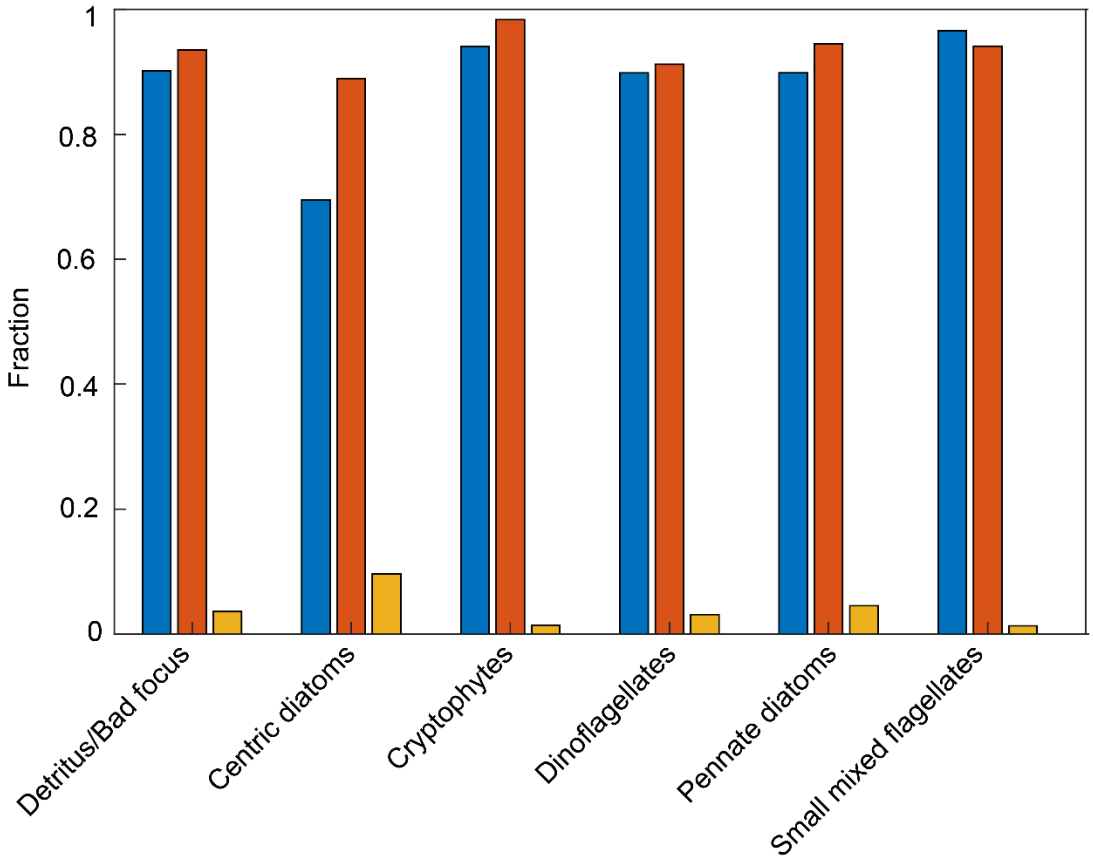

Figure 3.4: Classification evaluation. Performance of the classifier for each group over three metrics. Probability of detection (Blue) is the true positive rate. Precision (Red) represents the accuracy of the positive predictions. Percent missed (Yellow) is the rate at which the classifier misses a true positive.

3.2.8 Statistical analysis

Principal coordinates analysis was conducted on the molecular composition data in R (version 4.3.2) using the *vegan* (2.6-4) package (Oksanen et al., 2007) to calculate the Bray-Curtis dissimilarity metrics between sites. Descriptive variables, including phytoplankton abundance by type, were fitted to the ordination and a p-value calculated based on goodness of fit. Descriptive variables which met the threshold for statistical significance ($P \leq 0.125$) were plotted on top of the molecular data to visualize associations.

3.3 Results

3.3.1 Hydrography

Surface temperatures generally reflected a north to south cooling trend, ranging from 1.93 °C at 63.966 °S to 0.19 °C at 69.303 °S (**Figure 3.5a**). There were two distinct regions of cold water; the northernmost station of the Peninsula, located in the Bransfield Strait, has the lowest recorded temperature at -0.07 °C corresponding with a high salinity water mass

attributed to dense shelf water formed in the Weddell Sea and deposited by the coastal current (Dotto et al., 2016) (**Figure 3.5b,c**). Additionally, cold, low density freshwater (33.3 g kg^{-1}) was observed in Marguerite Bay, where glacial input of freshwater is high (Meredith et al., 2008), and towards the south of the Peninsula where fresh glacial water is postulated to be deposited from Marguerite Bay by the Antarctic Peninsula coastal current (Moffat et al., 2008, Moffat and Meredith, 2018) (**Figure 3.5b,c**). Salinity off the coast remains largely constant across the Peninsula at ~34.0 g kg^{-1}. Maximum chlorophyll fluorescence was variable, with the greatest values being along the shelf break and towards the north of the Peninsula (**Figure 3.5d**). The greatest recorded fluorescence (3.08 RFU) was to the north of Anvers Island; a similarly high fluorescence value (3.00 RFU) was observed abeam Renaud Island. Conversely the lowest fluorescence values were present at slope stations, particularly towards the middle of the Peninsula, and coinciding with the northern dense shelf water mass.

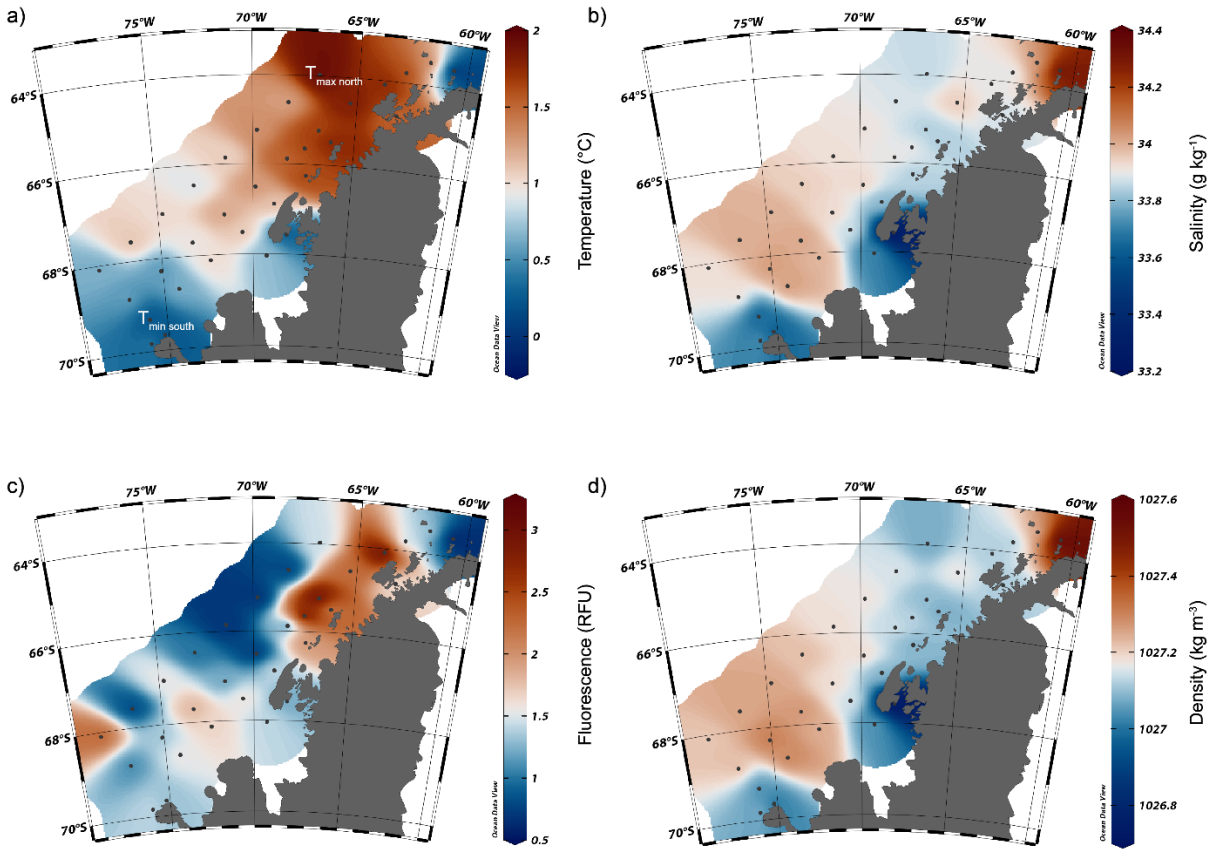

Figure 3.5: Hydrographic surface plots of temperature (a), salinity (b), density (c), and fluorescence (d). All plots show the value for the first depth of the CTD cast except fluorescence where the highest fluorescence value from the cast is shown, maximum fluorescence was achieved at 37.3 ± 23.0 m. Points represent sampling stations.

3.3.2 Solid phase extracted dissolved organic carbon, nitrogen and phosphorus

SPE-DOC had an average concentration of 16.53 (± 2.55 µmol C L^{-1}) compared to 45.70 (± 11.75 µmol L^{-1}) for the bulk DOC. The highest concentrations of SPE-DOC and DOC were typically found in the upper 100 m of the water column where there was a high degree of variability (**Figure 3.7a**, **Figure 3.6d**); however, SPE-DOC did not correlate with depth, with the lowest concentrations (8-11.5 µmol L^{-1}) occurring across 3-1200 m. Concentrations of SPE-DOC were similar between coastal and slope locations. However, DOC was strongly correlated with depth (**Figure 3.6d**); DOC is, being enriched in the surface layer and then rapidly decreasing below 100 m to a background value of ~40 µmol L^{-1}. In surface waters, the highest concentrations of DOC were found at the coastal sites (C4, C5, C3, C1), from across the full length of the WAP (**Figure 3.6d**).

SPE-DON shows a similar distribution to SPE-DOC, with the highest concentrations (up to 1.47 µmol N L^{-1}) occurring in a highly variable layer at the surface and no clear distinction between coastal and slope sites (**Figure 3.7b**). With SPE-DOC and SPE-DON showing similar trends, the SPE-DOC:SPE-DON (hereafter styled as $C:N_{SPE}$) ratio varied between 11.4 and 17.8 in the upper 50 m before converging to 14-15.5 below 800 m (**Figure 3.6a**). SPE-DOS has an average concentration of 111.0 (± 32.8) µmol S L^{-1} in the upper 50 m (**Figure 3.7c**) and variability decreases in the deeper ocean; however, there was no evidence of a decrease in SPE-DOS concentration with depth at most stations across the grid. The $C:S_{SPE}$ ratio was generally greater at depth compared to the surface at most slope stations, suggesting a depletion in sulfur relative to carbon in deeper waters (**Figure 3.6c**). At coastal stations where the maximal depth is shallower, the same trend was not observed. Concentrations of SPE-DOP are greatest in the upper 50 m of the water column (average of 14.3 ± 4.3 µmol S L^{-1}) (**Figure 3.7d**), and the highest concentrations were also observed for coastal sites across the latitudinal range of the grid (C1-C4). There was a general decreasing trend in SPE-DOP with depth, and the lowest concentrations of SPE-DOP are found at slope sites (S1-S3) between 100 and 3050 m. The decreasing trend in SPE-DOP was not observed in the $C:P_{SPE}$ ratio which remains highly variable through the water column (**Figure 3.6b**).

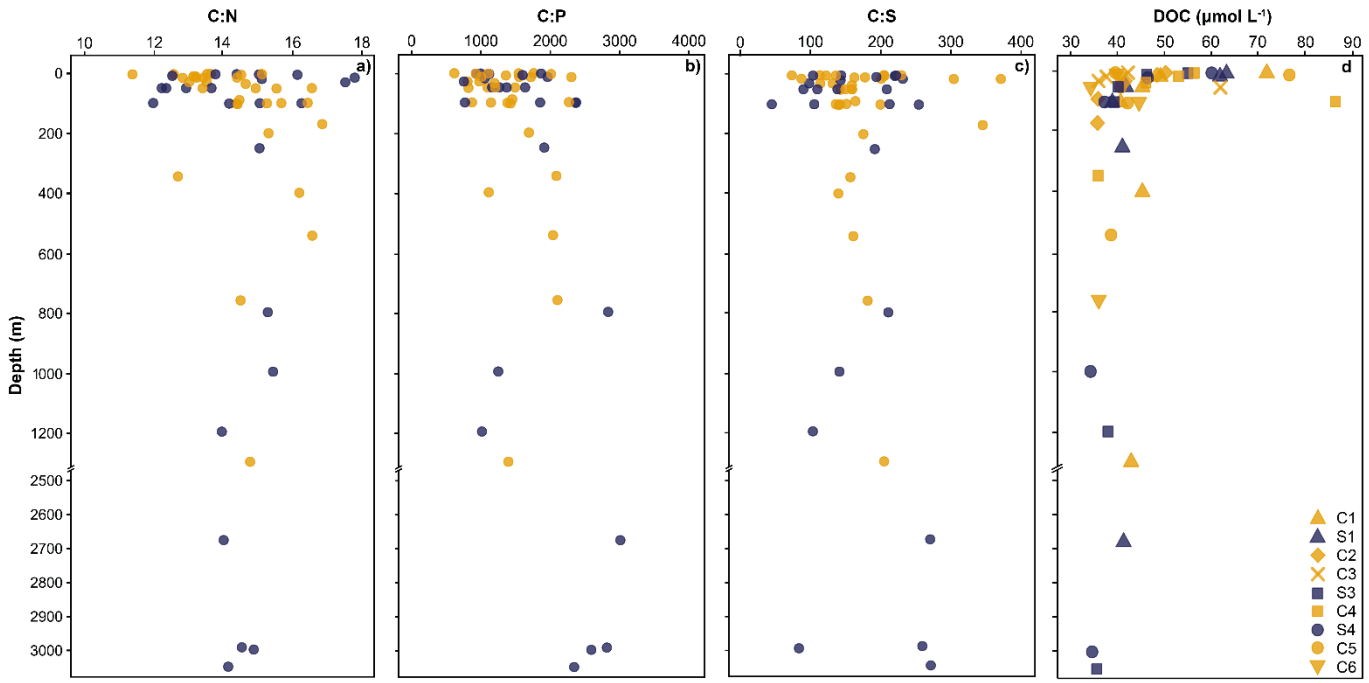

Figure 3.6: Molar ratio between $C:N_{SPE}$ (a), $C:P_{SPE}$ (b) and $C:S_{SPE}$ (c) over depth and DOC concentration by site (d)**.** Coastal sites are shown in orange, shelf sites are shown in blue, for panel d these are represented by different symbols for each site.

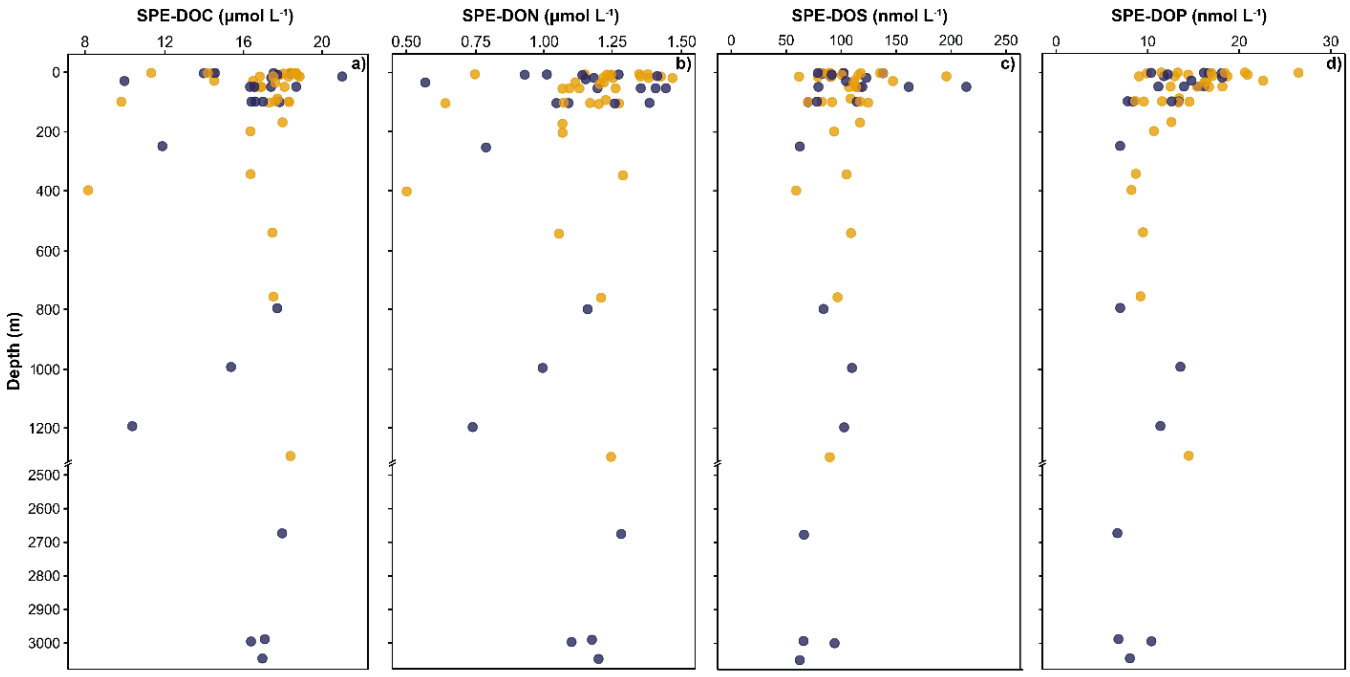

Figure 3.7: Concentrations of dissolved organic carbon (a) and nitrogen (b) (µmol L^{-1}) and sulfur (c) and phosphorus (d) (nmol L^{-1}) in solid phase extracted DOM. Coastal stations are shown in orange and slope stations are shown in blue.

3.3.3 Molecular composition of SPE-DOM

The modified aromaticity index (AI_{Mod}) is an indicative metric for the presence of aromatic structures in DOM (Koch and Dittmar, 2006, 2016). The AI_{Mod} was largely consistent between locations and showed overall low variability with an average value of 0.24 (**Table 3.1**) indicative of a combination of aliphatic and aromatic compounds contributing to the DOM pool. The mean double bond equivalent was marginally greatest at deep and southern stations, indicating a greater degree of unsaturation of compounds in these settings. However, oxygen content and particularly the oxygen to carbon ratio shows no variability, with exclusive formular having a low and consistent O/C at all sites (0.43) representing less oxidised, hydrophobic compounds. Combined with a H/C values of 1.30 this suggests that most compounds within this study are likely to be reduced aliphatic hydrocarbons, poor in oxygen containing functional groups. The results shown for P and S in **Table 3.1** are independent of the concentrations for SPE-DOP and SPE-DOS shown in **Figure 3.7**.

The AI_{mod}, double bond equivalent, and proportion of formulae which are highly unsaturated were at their lowest in the north (**Figure 3.8c, d, g**). In surface waters AI_{mod} increases along the north to south transect (**Figure 3.8c**), with the least aromatic compounds located at C1 and S1 in the north. The lower AI_{mod} values co-occur with lower DBE values at these sites (**Figure 3.8d**), suggesting a decreasing degree of unsaturation, agreeing with a lower proportion of highly unsaturated compounds at the northern sites (**Figure 3.8g**). The northern sites also contain the greatest proportion of unsaturated sites (**Figure 3.8f**), which represents an intermediate between saturated and highly unsaturated compounds. Where highly unsaturated compounds are especially prevalent (e.g., C6), unsaturated compounds were at their lowest. While the northern sites are molecularly similar in many aspects, the coastal site C1 is differentiated from the shelf site S1 by a greater proportion of saturated compounds and a lower SPE-DOC concentration (**Figure 3.8e, h**).

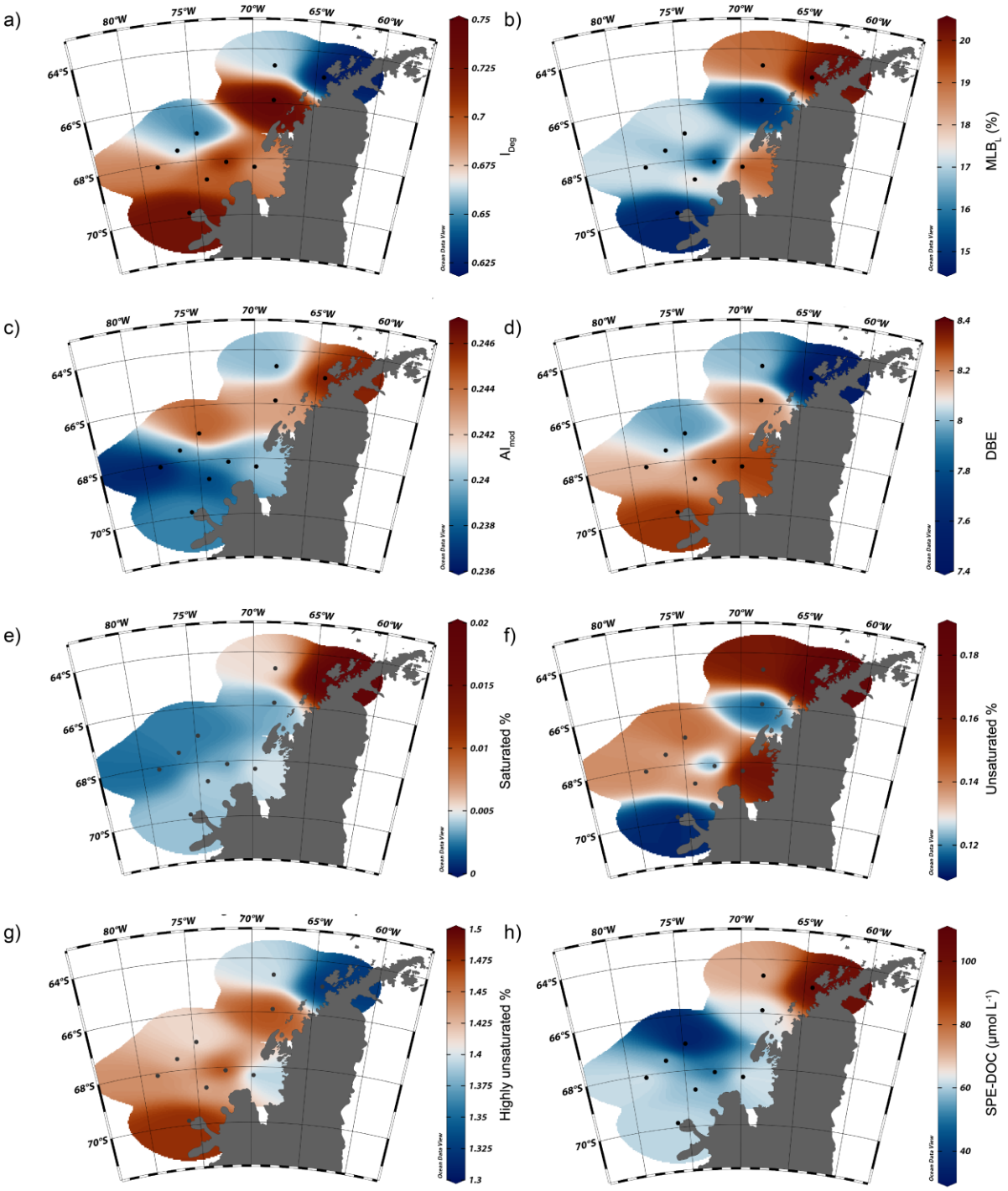

Figure 3.8: Surface plots of DOM molecular composition data. Panels show the calculated degradation index (I_{Deg}) (a), percent biolability (MLB_L) (b), modified aromaticity index (c), and double bond equivalent (d), the intensity-weighted percent average of saturated (e), unsaturated (f) and highly unsaturated (g) compounds and concentration of solid phase extracted dissolved organic carbon (h). Black points indicate the sampled stations (**Figure 3.1**), with values interpolated between these. Surface plots represent data from the first depth of each CTD cast.

Table 3.1: Intensity-weighted average molecular composition of SPE-DOM across different settings for exclusive formulae. Surface sites are defined as <105 m, deep sites are >105 m. North sites are C1, C2, S1; Mid are C3, C4, S2; South are C5, C6, S3 and S4. Values shown are means and bracketed values represent the standard deviation. Formulae represents the number of exclusive molecular formulae in each location group.

Location	Surface n=43	Deep n=15	Coastal n=33	Slope n=24	North n=17	Mid n=18	South n=22
AI_{Mod}	0.24 (±0.004)	0.24 (±0.003)	0.24 (±0.003)	0.24 (±0.004)	0.24 (±0.004)	0.24 (±0.004)	0.24 (±0.003)
DBE	8.11 (±0.18)	8.23 (±0.15)	8.15 (±0.21)	8.13 (±0.14)	8.10 (±0.22)	8.14 (±0.17)	8.18 (±0.15)
O/C	0.43 (±0.01	0.43 (±0.01	0.43 (±0.01)	0.43 (±0.01)	0.43 (±0.01)	0.43 (±0.01)	0.43 (±0.01)
H/C	1.29 (±0.01)	1.29 (±0.01)	1.29 (±0.01)	1.30 (±0.01)	1.30 (±0.01)	1.30 (±0.01)	1.29 (±0.01)
C	19.6 (±0.33	19.8 (±0.38)	1.29 (±0.01)	19.7 (±0.32)	19.6 (±0.40)	19.6 (±0.33)	19.7 (±0.35)
H	25.3 (±0.41	25.6 (±0.52)	25.3 (±0.47)	25.4 (±0.42)	25.3 (±0.45)	25.3 (±0.43)	25.4 (±0.49)
O	8.4 (±0.29)	8.5 (±0.20)	8.5 (±0.29)	8.4 (±0.24)	8.4 (±0.31)	8.4 (±0.31)	8.5 (±0.20)
N	0.32 (±0.02)	0.32 (±0.02)	0.32 (±0.02)	0.32 (±0.02)	0.31 (±0.02)	0.32 (±0.01)	0.32 (±0.01)
P	0.03 (±0.01)	0.03 (±0.01)	0.03 (±0.01)	0.04 (±0.01)	0.03 (±0.01)	0.03 (±0.01)	0.04 (±0.01)
S	0.03 (±0.01)	0.03 (±0.01)	0.03 (±0.01)	0.03 (±0.01)	0.03 (±0.01)	0.03 (±0.01)	0.03 (±0.01)
m/z	400.5 (±8.5)	405.0 (±8.1)	401.8 (±9.4)	401.6 (±7.4)	400.3 (±10.0)	400.7 (±8.4)	403.6 (±7.4)
Formulae	793	139	503	228	142	204	217

3.3.4 $\delta^{13}C$ SPE-DOM

Coastal sites show a general increasing trend in $\delta^{13}C$ SPE-DOM with depth, with an average increase of 0.9 ‰ (± 0.5) from the surface to the deepest sample (**Figure 3.9**). Slope sites differ in having similar surface to deep values, except for the northernmost sample at 65 °S which shows an increase of 1.4 ‰ across the water column. This value matches the northernmost coastal sample (1.4 ‰) and together they represent the largest variation in $\delta^{13}C$ with depth that observed. However, there is no evidence for a latitude-driven effect in $\delta^{13}C$ depth variability when considering all sites. At the deepest point, $\delta^{13}C$ SPE-DOM values generally converge to between -23.0 and -22.0 ‰ (**Figure 3.9**).

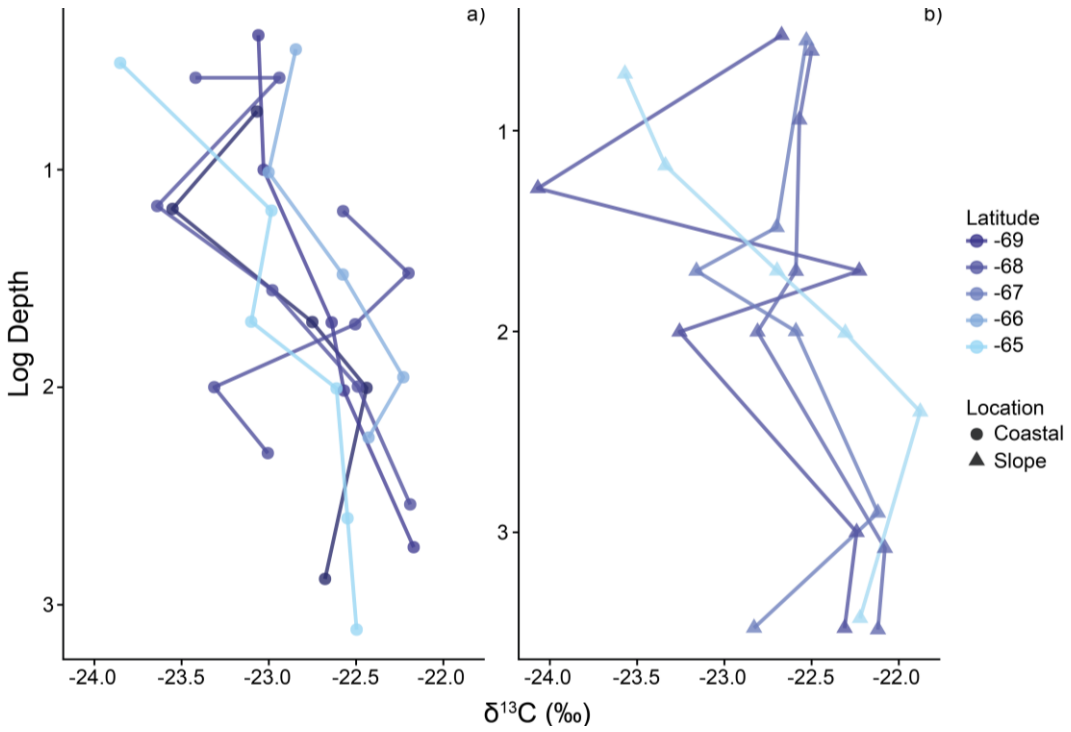

Figure 3.9: $\delta^{13}C$ (‰, VPDB) values for SPE-DOM extracts at coastal (a) and slope (b) sites; colours represent the latitude of sites with the darkest colours representing the most southerly sites.

3.3.5 Phytoplankton community composition

The largest group was the small mixed flagellates, comprising 33.0% of the total images; this group describes numerous small circular cells of ~10 µm diameter which are too small to classify visually. Pennate diatoms were the least abundant group, representing just 3.6% of total biovolume, in part driven by the absence of pennate diatoms from some samples (*n* = 16) (**Figure 3.10**). Across all groups, variability was high between stations, with small mixed flagellates and pennate diatoms being the groups with the largest standard deviations (20.1 and 20.4 %, respectively). Among the sites sampled for DOM (C1-C6, S1-S4) coastal sites generally decreased in the proportion of small mixed flagellates towards the south, from 54.0 (± 7.4) % at the north of the peninsula (C1, C2) to 29.8 (± 11.8) % at the south (C4, C5, C6) (**Figure 3.10**). C3 was further inland than the other sites along the coastal line and was strongly dominated by large centric diatoms (e.g., *Thalassiosira*) with only 0.32% of plankton attributed to small mixed flagellates. Centric diatoms were the major type of diatom observed, forming 14.4% of total biovolume compared to 3.4% for pennate diatoms. Centric diatoms also formed a major group at the northernmost site (45.2 %) and at S1 (27.6 %) (**Figure 3.10**). While IFCB is not a quantitative technique for phytoplankton abundance, the

volume-normalised occurrence of phytoplankton shows that sites with low overall abundance generally have a more diverse population compared to sites with a high overall relative abundance where this is driven primarily by one phytoplankton type (**Figure 3.11**). The relative abundance of phytoplankton was greatest at sites C3 and C1, which could be indicative of phytoplankton blooms at these sites. However, C3 was centric diatom dominated throughout the sampled depth profile (51 m), abundance at C1 was dominated by small mixed flagellates and cryptophytes in the upper 10 m only, with a sharp decline in abundance between 10 and 50 m (**Figure 3.11**).

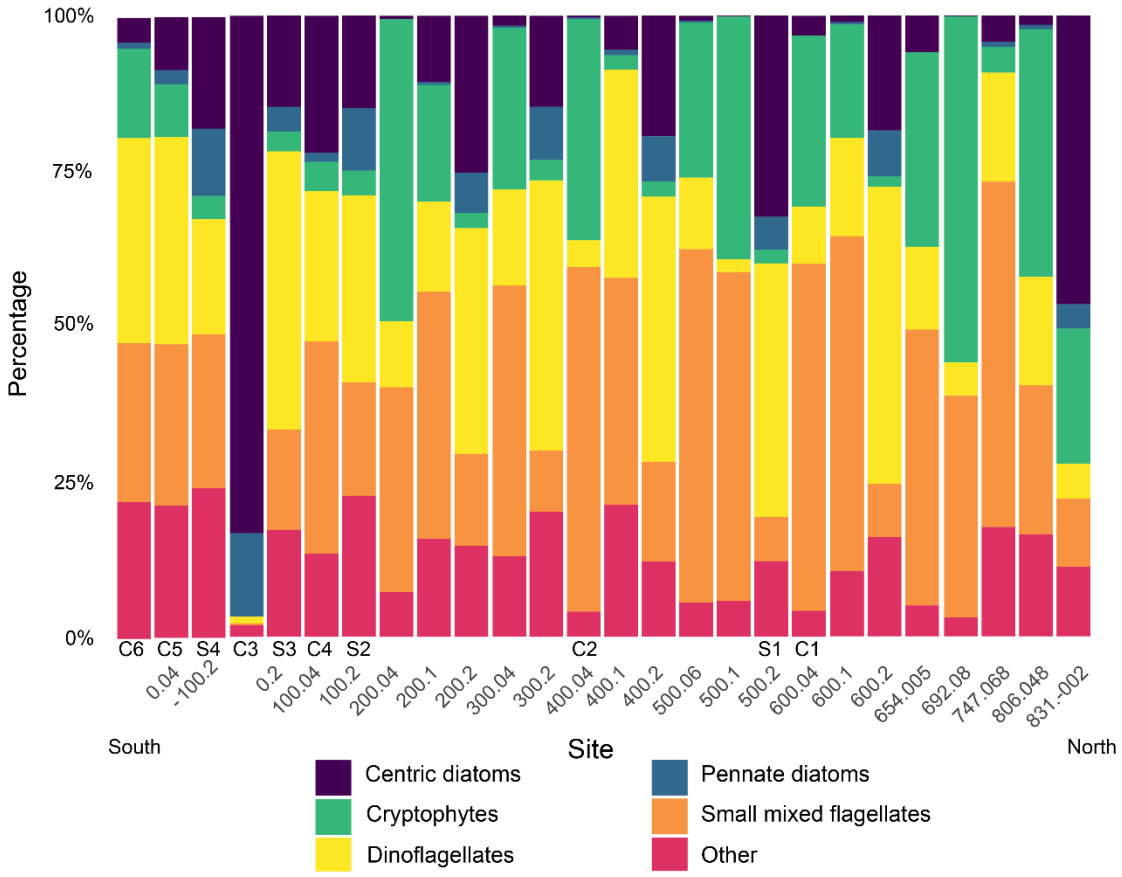

Figure 3.10: Phytoplankton community composition for the Palmer LTER grid, summed for all depths sampled in the euphotic zone, weighted by biovolume. Site numbers represent grid site according to the Palmer LTER site naming convention (where the first number represents northness on the grid and the second number represents distance from the coastline); C/S numbers represent coastal and shelf stations which were also sampled for DOM composition (**Figure 3.1**).

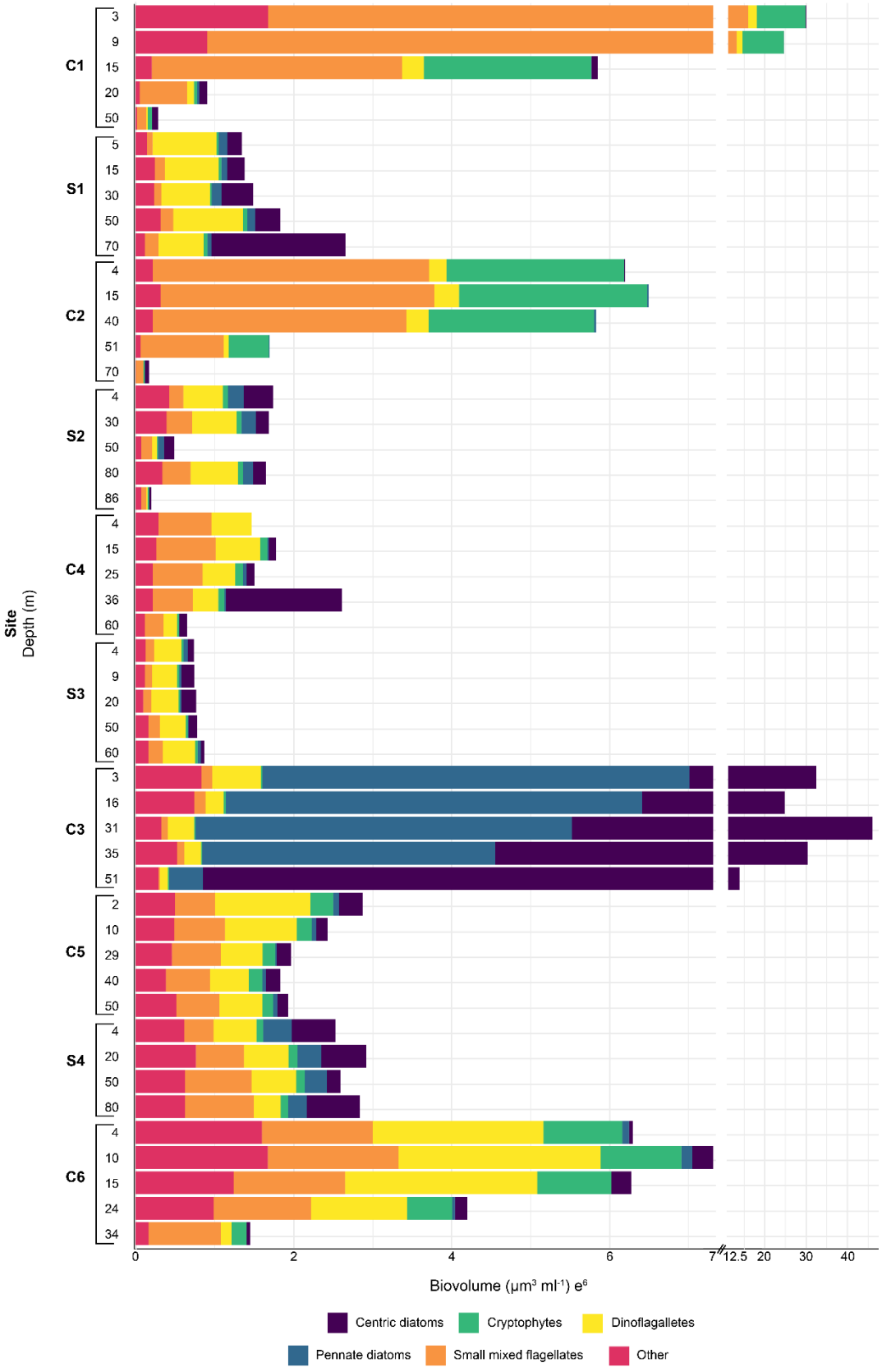

Figure 3.11: Phytoplankton community composition for the Palmer LTER grid scaled by biovolume at each site and depth. C/S numbers represent coastal and shelf stations that were also sampled for DOM composition. Above the x-axis break, data are scaled by a factor of 0.5.

3.4 Discussion

Along the rapidly warming West Antarctic Peninsula, phytoplankton communities have been predicted to undergo shifts favouring smaller cells (Deppeler and Davidson, 2017, Antoni et al., 2020), resulting in a cryptophyte-dominated northern WAP (Moline et al., 2004) while diatoms still dominate further south (Montes-Hugo et al., 2009). These changes in primary producers are important because of their ability to influence ecosystems (Ducklow et al., 2013) and the biological carbon pump through modulating the supply of organic carbon to the ocean, yet the extent to which phytoplankton communities influence DOM is unclear (Thornton, 2014). We found cryptophytes to be more abundant towards the north of the peninsula, and diatoms to have a greater prevalence at coastal sites, particularly in well-stratified fresh water (**Section 3.4.1**). DOM composition was more saturated and less aromatic at northern sites compared to elsewhere (**Section 3.4.2**), but rapidly become more alike in stoichiometry and molecular composition at depth following transformation in the surface layer (**Section 3.4.3**). Statistical analysis of phytoplankton abundance, environmental variables and DOM composition in the surface layer revealed that small cells (cryptophytes, small mixed flagellates, and dinoflagellates) are associated with saturated, fresh DOM, while diatoms correlate with aged DOM (**Section 3.4.4**). Using molecular, isotopic, and stoichiometric properties of DOM we explore the implications of phytoplankton-influenced DOM production for the biological carbon pump in the WAP.

3.4.2 Drivers of phytoplankton community composition

Previous work in the Palmer LTER region has suggested that during periods of increased sea ice, seasonal concentrations of chlorophyll increase, driven primarily by diatoms (Schofield et al., 2017). Conversely, in warmer waters with low sea ice concentrations and deeper mixed layers, the composition of phytoplankton communities is less diverse with fewer diatoms and a greater proportion of cryptophytes (Lin et al., 2021). Ducklow et al. (2015) described gross primary productivity rates of 30 mmol C m^{-2} d^{-1} in low chlorophyll years compared to 100 mmol C m^{-2} d^{-1} in high chlorophyll years, indicating that the magnitude and composition of primary producers has a strong influence on carbon fixation. The 2023 season was characterised by exceptionally low sea ice coverage (**Figure 3.12**), with all stations except the southernmost (C6) being sea ice free, temperatures varied from 2.71 °C to -0.07 °C, and salinity ranged between 33.28 and 34.73 g kg^{-1}.

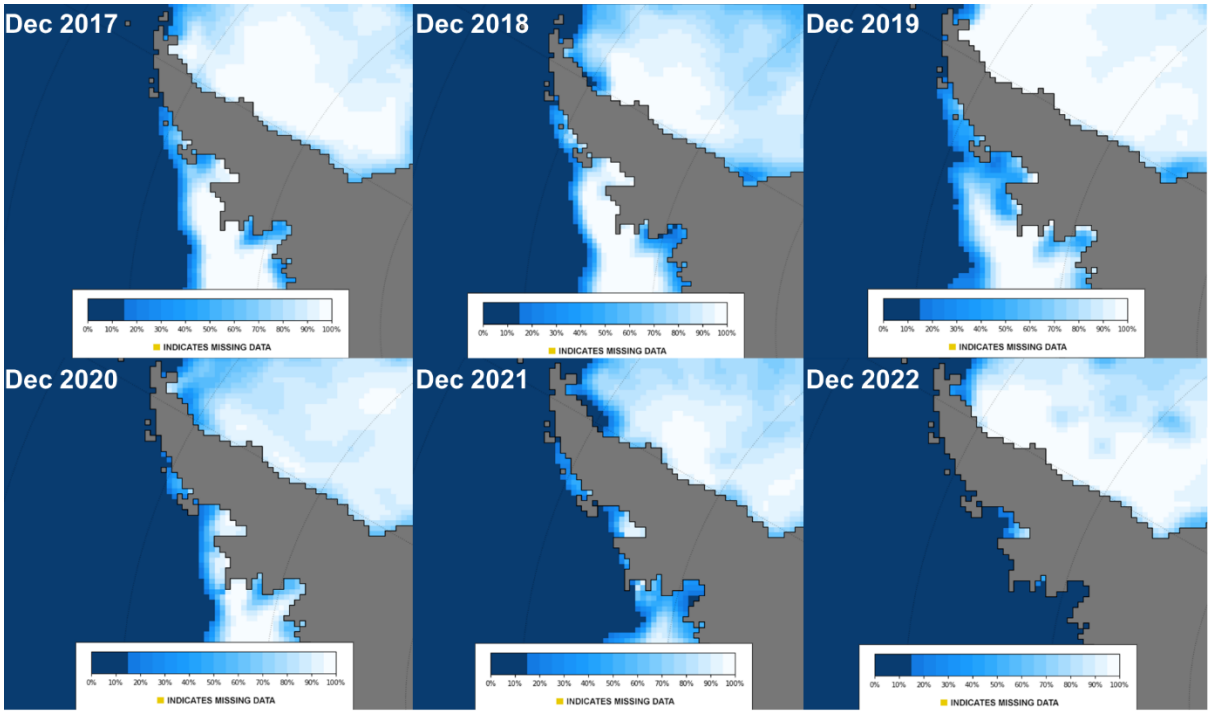

Imagery: © 2023 National Snow and Ice Data Center, University of Colorado Boulder

Figure 3.12: Summer sea ice concentration on the West Antarctic Peninsula for December 2017-2022. Sea ice data is sourced from the NASA MODSI satellite and processed by National Snow and Ice Data Center, University of Colorado Boulder

Across the WAP diatoms have been observed across the full range of temperatures and salinities, while cryptophytes have been seen to inhabit low salinity (32.5-33.75), cold waters (-1 to 1°C) (Schofield et al., 2017). We observed the relative abundance of cryptophytes to be greater towards the north of the peninsula, particularly at stations 692.08 and 806.048 where cryptophytes account for 38.2 and 28.2 % of biovolumes, respectively. At these sites, the temperature was 1.4-1.8°C and the salinity 33.9-34.0 g kg^{-1}, both warmer and more saline than waters previously described for cryptophytes at Palmer Station (Schofield et al., 2017), but within the ranges for cryptophyte presence observed across the wider Peninsula (Henley et al., 2019). In the northern WAP, cryptophyte abundance has been associated with stable, shallow mixed layers resulting from the melting of sea ice (Mendes et al., 2018a, Mendes et al., 2018b). Conversely, we observed phytoplankton communities at multiple sites in the northern WAP with cryptophytes as the major group in the absence of sea ice with warmer and more saline waters than previously recorded. Further south in cooler waters (1.09 °C), cryptophytes were also uniquely prevalent at 200.04 (42% of biovolumes) compared to neighboring sites which had fewer cryptophytes. Genomic analysis between 2013-16 across

the Palmer LTER region found that in all of these years almost 100% of cryptophytes consisted of *Geminigera* species (Brown et al., 2021). In multi-stressor experiments Camoying and Trimborn (2023) found the thermal optimum of *Geminigera cryophila* to be 4°C, with high light at lower temperatures having the greatest negative effect on growth and POC production. Therefore, the relationship between retreating sea ice and abundance of cryptophytes could be a function of light attenuation as sea ice breaks up (e.g., brash ice coverage), rather than a direct result of temperature and salinity. Other light attenuation effects, such as cloud cover or self-shading in the water column, could additionally provide similar optimum light concentrations to cryptophytes as those experienced in sea ice break up, accounting for their continued prevalence under low sea-ice conditions. The type of ice breakup (e.g., rapid reduction in ice vs continued patchy coverage), was previously proposed as a possible control on the abundance of centric diatoms, with fewer centric diatoms after rapid ice breakup (Annett et al., 2010). This suggests there could also be a degree of ecological competition associated with different ice breakup mechanisms which may explain some of the cryptophyte abundance, however few studies have measured community composition during sea ice breakup to date, providing a weak evidence basis from which to deduce the causal factor driving cryptophyte abundance across the WAP.

The sporadic increasing contribution of diatoms towards the south of the LTER grid is consistent with analysis of community composition in previous years (Moreno et al., 2024). In both their data (2018 season) and ours, some stations have a large abundance of diatoms, while neighbouring stations often contain substantially less. In Moreno et al. (2024) the coastal sites 100.04 and 000.04 contained a high proportion of diatoms, while in our analysis these sites contained mixed populations with diatoms forming <30% of the total biovolume. Instead, C3 (a non LTER station in Marguerite Bay, close to 100.04) and 831.-002 (a northern station in the cold dense water mass), contained the greatest proportion of diatoms in 2023 (**Figure 3.10**). While the location of the diatom bloom in the southern region of the WAP moved between 2018 and 2023, in both years proximity to the coast remained a consistent factor. The 2018 season was similar to 2023 in being a low sea ice year, which resulted in low phytoplankton biomass a smaller contribution from diatoms compared to high sea ice years at Palmer Station (Nardelli et al., 2023). With the southern sites being among the last to be sampled in mid to late January, it is likely that this timing excludes most diatom blooms, with

diatoms being substantially less prevalent in the peak summer phase compared to the spring sea ice retreat or late summer (Nardelli et al., 2023). At C3 however, a large diatom bloom resulted in a total biovolume an order of magnitude greater than the neighbouring site at C4, comprised of mostly centric diatoms throughout the euphotic zone. Marguerite Bay is typically a region of high chlorophyll because of the local hydrography, where a large input of melt water results in a stable, well-stratified surface layer, promoting the growth of diatoms (Garibotti et al., 2003a, Garibotti et al., 2005, Annett et al., 2010, Rozema et al., 2017a).

Dinoflagellates and small mixed flagellates represent a consistent and substantial group across most sites (**Figure 3.10**). The high presence of flagellates is in agreement with previous work in the WAP between 2016 and 2017 when dinoflagellates accounted for 58% of biomass and small flagellates were the most prevalent phytoplankton group throughout a summer season, with most dinoflagellates usually being small (<20 μm) and athecate (Mascioni et al., 2019). Similarly, Garzio and Steinberg (2013) showed high abundance of athecate dinoflagellates in 2010 and 2011 across the Palmer LTER region, with an increased presence towards the south of the WAP. Across our sites, dinoflagellates were most abundant in the upper 15 m at C6, the southernmost site, while the largest populations of small flagellates occurred at the northernmost site, C1 (**Figure 3.11**). The increased presence of dinoflagellates towards the south has been associated with higher chlorophyll and POC concentrations in previous years, providing a greater food supply for mixotrophic dinoflagellates (Garzio and Steinberg, 2013). Dinoflagellates have been found to favor lower-salinity fresh waters with a well-stratified shallow upper mixed layer (Moline et al., 2004, Costa et al., 2020). Such conditions correspond with those found at the dinoflagellate-abundant southern site (C6), characterised by low density, low salinity fresh water, contrasting with the saline conditions at the small mixed flagellate-dominated northern site (C1). Some mixotrophic flagellates may have an advantage over other phytoplankton types when iron-limited because of their ability to ingest iron-containing bacteria (Maranger et al., 1998). Under continued warming, lengthened growth seasons are projected to increase the iron stress in coastal areas of the Southern Ocean, which may favor dinoflagellates with diverse iron acquisition mechanisms. This could suggest that mixotrophs will become an increasingly important contributor to the carbon cycle along the WAP, however Stoecker et

al. (2017) notes that the importance of mixotrophic flagellates in HNLC regions remains poorly understood.

3.4.3 Spatial variability in DOM composition

Across the WAP, DOM is produced by primary production and bacterially-mediated decomposition of POM (Dittrich et al., 2022). DOC concentrations were greatest in the surface at the coastal sites C1, C4 and C5 (>70 µmol L^{-1}) (**Figure 3.6d**), appearing to be disconnected from total phytoplankton biovolume (**Figure 3.11**). Below 100 m, DOC concentrations are consistently lower in the range of 35-45 µmol L^{-1}, deep water concentrations of ~40 µmol L^{-1} are consistent with other measured values for the region. Deep water values at the shelf stations S3 and S4 (~35 µmol L^{-1}) are lower than previously reported across the WAP, but are also positioned further south than most prior studies report, only accessible in this year because of the low sea ice conditions. SPE-DOC represented 38 % (± 9 %) of total DOC across our sample set; this low extraction efficiency is to be expected for the Southern Ocean based on previous studies (e.g. 43 ± 5% (Dittmar et al., 2008)) where the major input of DOM is from fresh algal production. Solid phase extraction with PPL is known to be biased against hydrophilic and N rich compounds in the high molecular weight pool, such as those present in fresh labile DOM (Jerusalén-Lleó et al., 2023), therefore SPE-DOM is more representative of the semi-labile and refractory pools. This selection effect is consistent across all samples and represented by low variability in the extraction efficiency. Surface concentrations of the extracted SPE-DOC varied between 11.3 and 18.7 µmol C L^{-1} (**Figure 3.8h**), with the lowest values co-occurring with the large diatom bloom at C3 in Marguerite Bay, and the highest values (>18) being at S1, C2, C5 and C6, which all have markedly different phytoplankton compositions and total biovolumes (**Figure 3.10**, **Figure 3.11**). At sites S1, C5 and C6 the high surface SPE-DOC concentration coincides with a declining trend in phytoplankton biovolumes with depth, with the phytoplankton maximal biovolume typically occurring within the top 15 m at these sites. Conversely, at the low surface SPE-DOC site (C3), total biovolume remains high throughout the sampled water column (3-51 m), with the maximal SPE-DOC concentration reaching 18.9 µmol C L^{-1} at 15 m. The high prevalence of centric diatoms at C3 likely accounts for the depletion of SPE-DOC in surface waters (McDonnell and Buesseler, 2010) as phytoplankton are less concentrated in the surface and diatoms shuttle organic carbon to depth more efficiently compared to

phytoplankton populations consisting of mostly small cells (small mixed flagellates, cryptophytes and dinoflagellates).

Molecular properties of DOM differentiate the northern sites (C1 and S1) from other stations with respect to AI_{mod}, double bond equivalent, O/C, and highly unsaturated compounds, which are all lower at these sites than seen elsewhere (**Figure 3.8b, c, d, g**). Koch and Dittmar (2006, 2016) propose that when considering aromaticity, an AI_{mod} value of >0.5 indicates the presence of aromatic compounds and values ≥ 0.67 indicates condensed aromatic structures. In this study AI_{mod} varies between 0.369 and 0.393. The relatively low aromaticity of compounds in the north (**Figure 3.8c**), lower DBE (**Figure 3.8d**), and lower prevalence of highly unsaturated compounds (**Figure 3.8g**) suggests that surface DOM at the northern sites was generally more saturated and less aromatic, indicative of fresher DOM than seen elsewhere. In contrast, at the southernmost station (C6), highly unsaturated compounds are more abundant and have a relatively higher AI_{mod} and DBE (**Figure 3.8c, g**). These features are characteristic of a more biologically-processed type of DOM of a refractory nature, produced during photo or microbially mediated transformations (Seidel et al., 2015), which is further supported by a lower H/C ratio at C6, associated with aged DOM (Flerus et al., 2012). Conversely, the nearby C3 site – the location of a large diatom bloom, – is postulated to be supplied by the same current (the Antarctic Peninsula Coastal Current) as C5 and C6 but had the highest H/C ratio observed across the grid, perhaps suggesting that the composition or magnitude of phytoplankton communities imparts a control on the molecular characteristics of surface DOM.

The stable carbon isotope composition has been used to identify likely sources of DOM in aquatic environments; uptake of bicarbonate ($\delta^{13}C \approx 0$ ‰) by marine phytoplankton results in a less negative $\delta^{13}C$ value for resulting organic matter, while lighter isotopic values are more indicative of terrestrial endmembers as direct uptake of CO_2 by C3 plants favours the lighter isotope ($\delta^{13}C \approx -29$ ‰) (Descolas-Gros and Fontungne, 2006). Variation in $\delta^{13}C$ has been attributed to both environmental (temperature, freshwater contribution) (Descolas-Gros and Fontungne, 2006) and biological factors (cell size, and by proxy, phytoplankton type) (Trull and Armand, 2001). Typically we would expect a heavier $\delta^{13}C$ signal in phytoplankton influenced surface water, becoming lighter over depth, however an isotopically depleted surface can occur in regions strongly influenced by terrestrial inputs

(e.g. Medeiros et al., 2015). Despite the WAP having a very low terrestrial influence, the most negative $\delta^{13}C$ values are found in surface waters at the northernmost coastal and shelf sites (C1, S1) (**Figure 3.8**). We interpret the trends in $\delta^{13}C$ over depth in this region to be strongly influenced by convection of water masses because of a correlation between salinity and $\delta^{13}C$ (**Figure 3.13**). Therefore, the light $\delta^{13}C$ values observed at the north of the peninsula are consistent with the upwelling of Weddell Sea derived CDW over the north of the peninsula and through the Bransfield Strait, which carries a more depleted $\delta^{13}C$ signal relative to fresher surface waters (**Figure 3.13**). Additionally, the phytoplankton communities at these northern stations are mostly comprised of small mixed flagellates (**Figure 3.10**), as small cells with large surface area-to-volume ratios; such types of phytoplankton have been shown to produce more negative $\delta^{13}C$ compared to large cells undergoing rapid growth (Rau et al., 1997, Trull and Armand, 2001). Differences in the concentration and size fraction of phytoplankton may describe some of the widespread variability in AASW (**Figure 3.13**), however the intrusion of isotopically light CDW over the north of the peninsula remains the dominant control on $\delta^{13}C$ in mid to deep waters. The $\delta^{13}C$ value becomes less variable over depth, ultimately converging on a value of -23.0 ‰ > $\delta^{13}C$ < -22.0 ‰ in bottom waters for all deep stations.

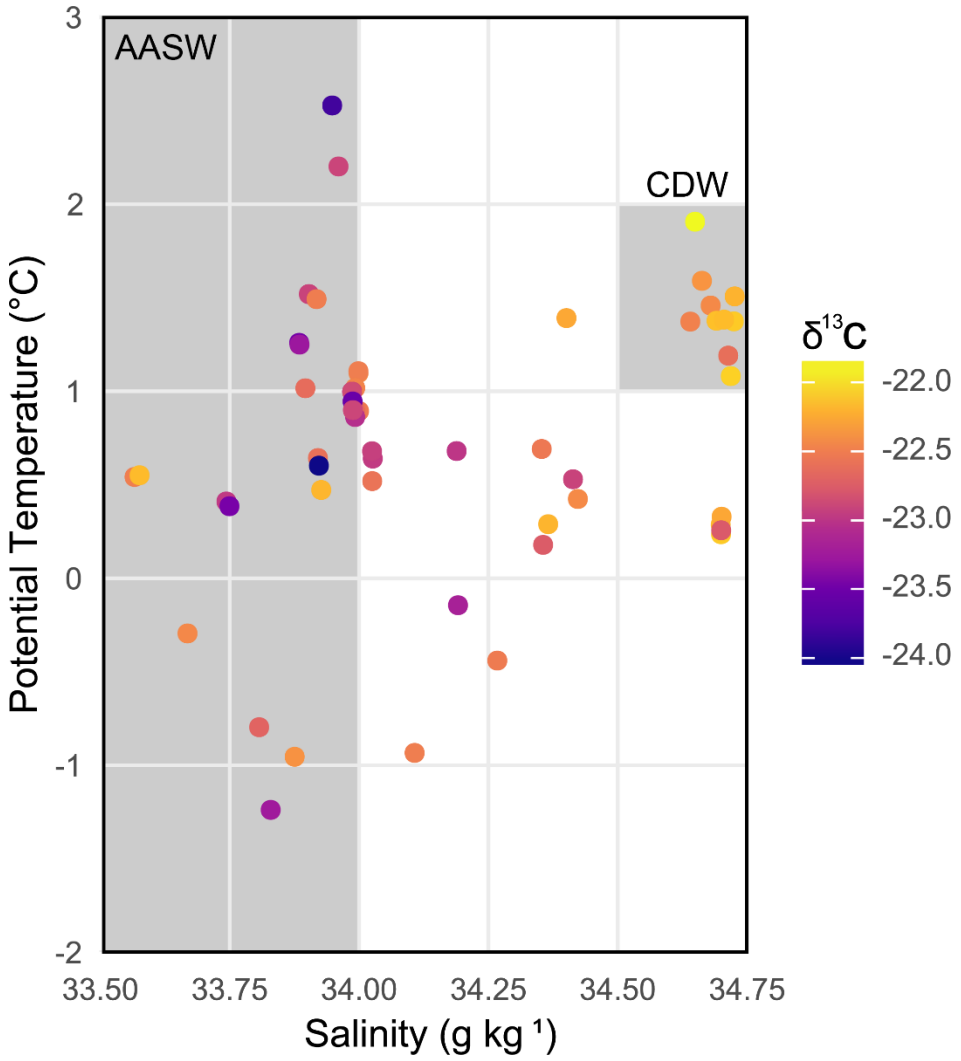

Figure 3.13: Temperature and salinity plot with $\delta^{13}C$ as the z variable. Circumpolar Deep Water (CDW) and Antarctic Surface Water (AASW) boundaries are defined per Dittrich et al. (2022) and references therein.

3.4.4 Fate of DOM

Up to 50% of phytoplankton-derived DOC is rapidly remineralised by heterotrophs in the upper ocean (Hansell et al., 2009). The short residence time of this form of DOM results in a low presence of labile DOM types in the ocean inventory (Davis and Benner, 2007, Hansell et al., 2009). Semi-labile or recalcitrant forms of DOM have a longer residence time, up to millennia, with multiple mechanisms proposed for the formation of recalcitrant fractions (reviewed in Hansell (2013), Dittmar et al. (2021), Cai and Jiao (2023)). The strong role of multiple feedback cycles between DOM and microbial communities is notable as a hitherto underexplored process by which recalcitrant DOM persists in the ocean for extended periods

of time. Forms of recalcitrant DOM, such as carboxyl-rich alicyclic molecules (CRAM) (Hertkorn et al., 2013), have been shown to accumulate at depth in the water column (e.g. Medeiros et al., 2015, Li et al., 2019, Seidel et al., 2022), with vertical gradients existing in molecular properties of DOM over the water column (Cai and Jiao, 2023 and references therein).

In particular, an idealization of AI_{mod} shows an expected increase in aromaticity with depth (Cai and Jiao, 2023), which agrees with the increasing trend in AI_{mod} with depth in our data set (**Figure 3.14**). A greater value of AI_{mod} at depth indicates a relative increase in aromaticity and decrease in bioavailability compared to surface waters. Coinciding with an increased AI_{mod}, we observed an increased representation of highly unsaturated compounds (**Figure 3.14b**) and a decrease in the proportion of unsaturated compounds as these undergo further unsaturation (**Figure 3.14c**) in deeper waters. Saturated compounds are similarly lower in abundance at depth compared to the surface (**Figure 3.14d**). The enrichment of highly unsaturated compounds at depth likely results from the microbial transformation of photosynthetic organic matter and agrees with similar analysis in the North Pacific (Medeiros et al., 2015). Highly unsaturated compounds have been proposed to have photo-resistant properties alongside low bioavailability, which may explain their longevity in the deep ocean, conferring an ability to survive multiple overturning cycles through the surface layer (Stubbins and Dittmar, 2015).

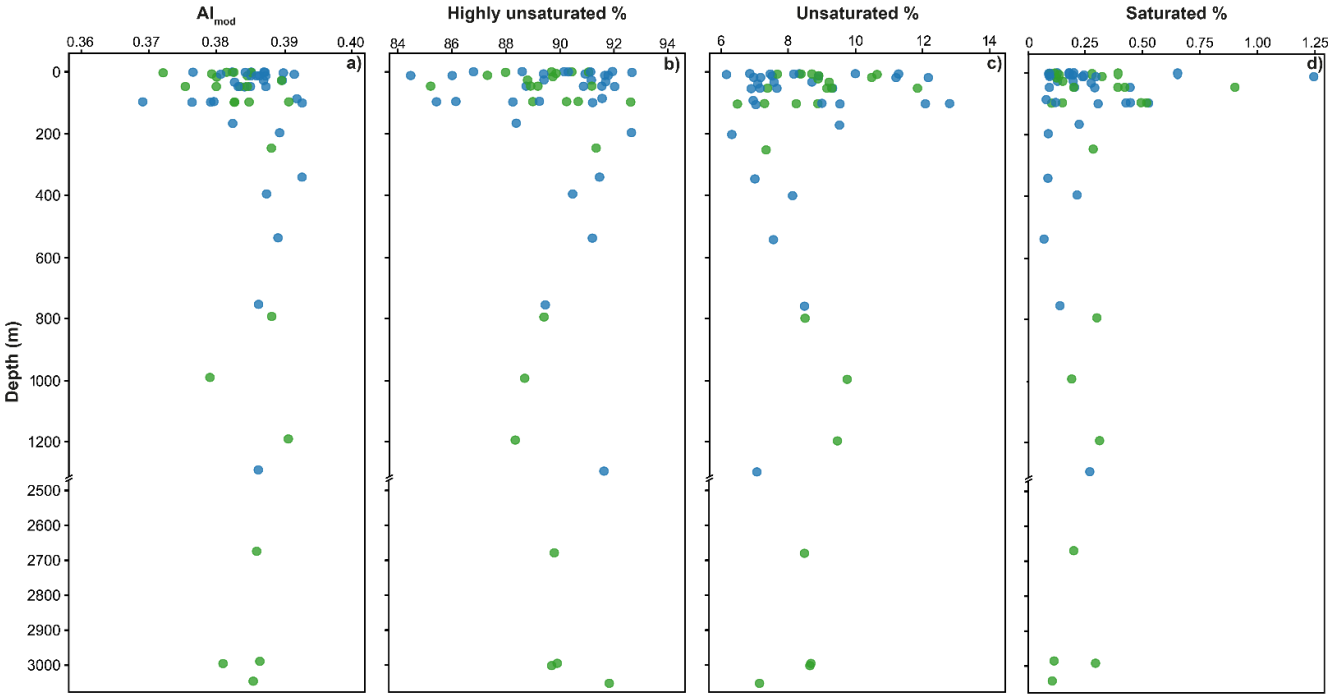

Figure 3.14: Molecular characteristics over depth: modified aromaticity index (a), intensity-weighted average percentage of highly unsaturated (b), unsaturated (c) and saturated (d) compounds. Blue points indicate coastal sites while green represent shelf sites.

Divergence of C, N, P stoichiometry of DOM from the Redfield ratio of 106:16:1 (Redfield et al., 1963) can indicate the extent to which DOM has been degraded, as dissolved organic phosphorus is degraded more rapidly relative to carbon (Letscher and Moore, 2015). In our study, the average C:N:P of SPE-DOM was 1563:108:1 and 1274:92:1 across the upper 50 m. Stoichiometric data of SPE-DOM in the literature is sparse, however Lechtenfeld et al. (2011) separated AASW into fractions based on polarity and found a C_{SPE}:P_{SPE} of 960:1 for the major fraction. C_{SPE}:S_{SPE} for this fraction was 333:1 compared to 163:1 for the samples in the upper 50 m of our study area. Molar ratios of C:N_{SPE} and C:P_{SPE} were most variable in the surface (upper ~100 m) (**Figure 3.6a,b**) with the lowest value of C:N:P_{SPE} (581:38:1) occurring in the surface at C3, the site with the largest observed phytoplankton bloom in our study. The concentration of DOP decreased with depth (**Figure 3.7d**) while the C:P_{SPE} value (**Figure 3.6b**) tended towards higher values in deeper waters with the greatest values of C:N:P (>2300:160:1) located below 100 m. The C:N value of SPE-DOM appears to be more stable over depth than C:S or C:P, showing no overall increase or decrease but instead converging to between 14 and 15.5 (**Figure 3.6a**), this suggests that N-containing compounds are perhaps less bioavailable than P or S containing compounds. The stoichiometric data support previous studies (e.g. Knauer et al., 1979, Karl et al., 1996, Hopkinson and Vallino,

2005) that state that DOP is preferentially remineralised compared to DOC, as our data show depletion of P relative to C in the deep refractory pool. We observed the freshest stoichiometric signal in the surface at C3 with a low C:N:P_{SPE} value, which coincides with the largest diatom bloom detected. This may indicate a small observable signal of fresh DOM production in the surface that has been only partially reworked, remaining enriched in phosphorus relative to the bulk composition.

Sulfur is utilised by phytoplankton for assimilation into organic structures, including amino acids, polypeptides, enzyme cofactors, and as electron donors/acceptors during electron transport processes (Dahl et al., 2008). Sulfurised compounds released by phytoplankton can also contribute towards the removal of toxic divalent trace metals (Brautigam et al., 2009). Phillips et al. (2022) showed that biological assimilation of sulfate forms the major fraction of DOS, with minor contributions from sulfidic porewater. Evidence for a small contribution of protein-derived DOS in the bulk pool has indicated that labile sulfidic organic compounds such as amino acids can be readily remineralised in the surface ocean (Davis and Benner, 2007, Ksionzek et al., 2016), such that DOS compounds that escape remineralization are likely to be more refractory. Across our sample set, the average C:S_{SPE} was 168 ± 64 (**Figure 3.6c**) and the C:N:S:P_{SPE} ratio was 1865:133:15:1. The C:S_{SPE} values were lower and more variable in our sample set compared to the solid phase extracted samples from the Southern Ocean reported by Ksionzek et al. (2016) where C:S_{SPE} was in the range of 217-308. Contrary to Phillips et al. (2022), we do not see an increasing trend in C:S_{SPE} with depth (**Figure 3.6c**), although in agreement with their study, our highest concentrations of DOS also occur within the upper 100 m (**Figure 3.7c**). The lack of a depletion in the C:S_{SPE} ratio suggests that DOS compounds are either remineralised very rapidly in the surface layer, or that DOM in this sample set was less enriched in sulfur during production compared to other studies. This may be due to a species effect, with large interspecies variability in the C:P, S:P and N:P ratios between phytoplankton (Ho et al., 2003). Alternatively, phytoplankton type, alongside sea ice cover, may be associated with large-scale variability in losses of sulfur-containing compounds as volatile DOS species (e.g., dimethyl sulfide, DMS) across the WAP region (Stefels et al., 2018).

3.4.5 A relationship between phytoplankton communities and DOM composition

In a changing climate, biogeochemical and physical changes in the ocean are expected to result in an increase in DOM release from phytoplankton (Wohlers et al., 2009, Engel et al., 2010, Novak et al., 2018). However, the extent to which changes in phytoplankton community structure will affect the biological carbon pump through DOM remains poorly understood (Thornton, 2014). A climate-driven shift towards smaller phytoplankton species under increasingly stratified and nutrient-limited conditions may lead to an increased abundance of smaller phytoplankton types (Finkel et al., 2009), with the larger surface-area-to-volume ratio associated with smaller cells leading to greater DOM exudation (Thornton, 2014). In a warming ocean, an increase in DOM because of a greater abundance of small phytoplankton may lead to increased surface layer remineralisation of DOM, with the potential to reduce the efficiency of carbon export (Lønborg et al., 2020).

We applied a principal coordinate analysis to determine the extent to which phytoplankton type, alongside environmental factors, could describe the variation shown in the molecular composition of DOM across the WAP (**Figure 3.15**). Overall variability in DOM composition was low, with the majority of the variability being described by the first two principal coordinates (56.5%). There was no evidence of clustering based on whether a sample was collected at a coastal or slope site. Fluorescence and potential temperature were significant ($P \leq 0.05$) drivers of variability ($P \leq 0.05$), but no molecular groups were closely associated with these variables. Greater values of $C:S_{SPE}$ and $N:S_{SPE}$ were correlated with the saturated group. Because the contribution of saturated compounds (**Figure 3.14d**) decreases with depth and $C:S_{SPE}$ increases with depth (**Figure 3.6c**), and this analysis only contains sites for which phytoplankton composition is available (i.e., the upper 50m), we do not interpret this correlation to suggest that saturated DOM has a low sulfur content and instead attribute this as a result of the large variability in both saturation and $C:S_{SPE}$ in the surface layer. The saturated group, alongside $C:S_{SPE}$ and $N:S_{SPE}$ both correlate with the abundance of small phytoplankton types (small mixed flagellates and cryptophytes), as well as dinoflagellates to a lesser extent, and anti-correlate with the O/C ratio. Given that the saturated group represents the most oxic, least reworked, type of DOM, and that small phytoplankton exhibit a greater leakage of DOM (Thornton, 2014), this suggests that cryptophytes and small mixed flagellates are the main source of phytoplankton-derived DOM to surface waters along the

WAP. Conversely, pennate diatoms and centric diatoms are closely associated with the H/C ratio and I_{DEG}, indicative of more degraded and aged DOM pool (Flerus et al., 2012). Aged DOM in the locality of diatoms indicates that the diatom population here fails to impress a 'fresh' phytoplankton signal over the background of upwelled refractory DOM. This could be because these diatom populations have a lower partition of organic carbon to the dissolved phase or because supply of the aged DOM pool by upwelling is particularly strong in diatom-abundant regions. The latter could be causal due to diatom growth responding to simultaneous upwelling-driven nutrient supply (Kavanaugh et al., 2015). Overall, these results suggest that phytoplankton type, and particularly size class, was the main driver of the molecular composition of DOM in the surface ocean of the WAP.

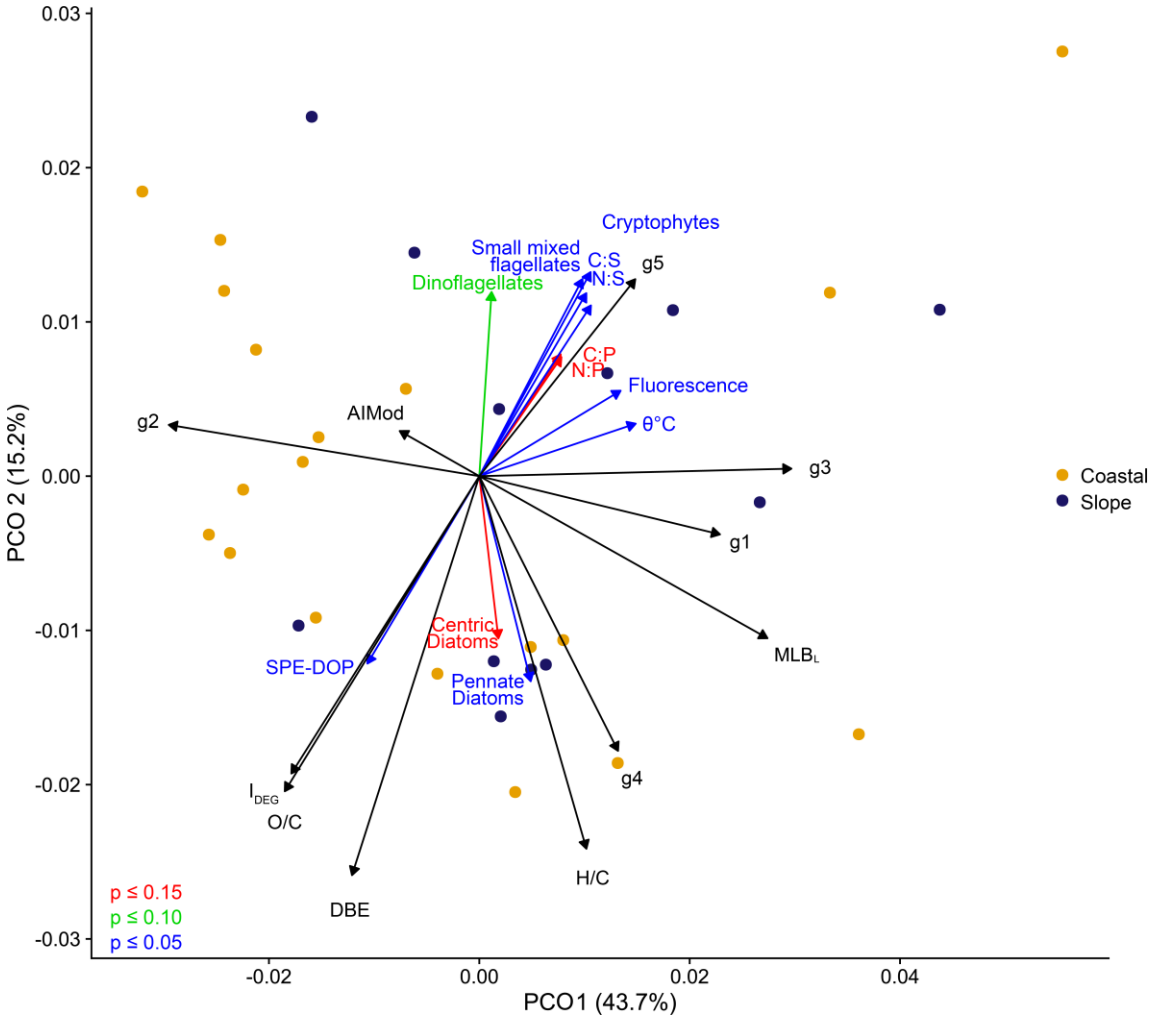

Figure 3.15: Principal coordinate analysis of dissolved organic matter composition in the photic zone from Bray-Curtis dissimilarities. Axes display the percent variability in DOM described by the first 2 principal coordinates. Organic matter types are split into groups, 'g': g1 = aromatic compounds, g2 = highly unsaturated, g3 = unsaturated, g4 = unsaturated with N, g5= saturated. Intensity-weighted averages of O/C and H/C ratios along with the modified aromaticity index (AI_{Mod}), double bond equivalent (DBE), degradation index (I_{DEG}) and biolability index (MLB_L) were fitted to the ordination. Significant environmental and species composition data were also fitted, with statistical significance of $p \leq 0.05$ indicated in blue, $p \leq 0.10$ in green and $p \leq 0.15$ in red.

3.5 Conclusion

During the 2023, low sea ice, spring/summer growing season of 2022/23 we collected phytoplankton community composition data alongside molecular and isotopic characteristics of DOM to determine the extent to which phytoplankton influence DOM, and how ongoing climate-driven shifts in phytoplankton communities may alter the biological carbon pump. With respect to the objectives, we found a dominance of small-celled phytoplankton, such as cryptophytes and small mixed flagellates, in the north of the WAP; these phytoplankton types were then associated with fresh DOM production, having a saturated and more biolabile molecular fingerprint. Additionally, diatom communities, abundant in coastal sites, were co-located with degraded DOM, suggesting of greater partitioning of organic matter to the particulate phase and more efficient export. Over depth however, rapid remineralisation in the surface layer homogenises DOM, converting saturated compounds to highly unsaturated compounds and subsequently leading to an increase in aromaticity with depth.

Collectively, these results indicate that smaller phytoplankton types produce labile DOM in surface waters of the WAP, in contrast to large phytoplankton types which efficiently export their organic content to depth. Therefore, if climate change drives a change in the species composition of Southern Ocean phytoplankton towards smaller types carbon export could become less efficient, with greater concentrations of surface DOM and reduced particulate carbon export. Beyond the Southern Ocean, changes in the amount of DOM production will influence global ocean biogeochemistry by increasing the rate at which nutrients are recycled in the surface layer, reducing global nutrient export in bottom waters. Increased DOM availability in surface waters may provide additional energy to support diverse populations of microbial heterotrophs. This study has shown that despite the low concentrations of DOM in the Southern Ocean, phytoplankton type likely plays a greater role in determining the molecular composition of organic matter than previously realised. Within the context of a changing climate, the release of DOM by emerging phytoplankton types is likely to be an increasingly important process linking climate to the marine carbon cycle. This provides a basis for better integration of phytoplankton carbon release in observational programs and modelling efforts as a means of reducing uncertainty in regional and global marine carbon cycling.

4. Diversity in nitrogen source uptake by a suite of Southern Ocean phytoplankton species

Abstract

Nitrogen is a bio-essential molecule for life, available to marine phytoplankton in inorganic (nitrate (NO_3^-), ammonium (NH_4^+)) and organic (urea) forms. Unlike much of the global ocean, nitrogen does not limit phytoplankton growth in the Southern Ocean, but different types of phytoplankton utilise oxidised (NO_3^-) and reduced (NH_4^+, urea) nitrogen at different rates, dependent on their metabolic pathways and their ability to hydrolyse organic nitrogen or reduce NO_3^-. Therefore, changes in the concentrations and forms of nitrogen resulting from climate driven modulation of sea ice and nutrient upwelling in the Southern Ocean could be expected to modify community composition. Here, we incubated different phytoplankton cultures, broadly representative of Southern Ocean phytoplankton communities, with ^{15}N nutrient tracers and measured the incorporation of nutrients at concentrations representative of the summertime West Antarctic Peninsula. Across all species, NH_4^+ was the major source of nitrogen (>50%), with urea being the secondary source and NO_3^- contributing towards a negligible fraction of uptake. The pennate diatoms *Fragilariopsis. cylindrus* and *Pseduo-nitzschia. subcurvata* had the lowest (0.17 (±0.01) µmol N / µmol C L^{-1} d^{-1}) and highest (1.01 (±0.11) µmol N / µmol C L^{-1} d^{-1}) total nitrogen uptake respectively. The co-occurrence of low nitrogen uptake with a high C:N molar ratio (12.71) in *F. cylindrus* led us to identify growth limitation as being causal of the low uptake rate for this species. We showed that a novel chemical method can be applied for measuring the isotopic enrichment of NH_4^+ in seawater, allowing for the simple calculation of NH_4^+ regeneration rates, a parameter which was previously rarely measured because of methodological limitations.

Subsequently we applied this to NH_4^+ uptake experiments across our phytoplankton cultures and found that NH_4^+ regeneration leads to a 1.34 (±0.8) underestimation factor in NH_4^+ uptake, in agreement with previous estimates. Additionally, we found that inconsistencies in the duration of ^{15}N incubation experiments, aimed at reducing the impact of NH_4^+ regeneration, can lead to significant differences in calculated uptake rates due to the possible impact of diel cycling on nitrogen uptake. This methodological error could therefore be a source of substantial error in our understanding of nutrient acquisition rates by

phytoplankton and lead to further uncertainties in regional nutrient budgets where these are modelled from phytoplankton uptake rates. We recommend that future experiments utilise longer incubations (24 hour) and account for the effects of NH_4^+ regeneration to provide the most accurate rates of nitrogen uptake. The potential for interoperability in measurements where a consistent methodology is applied provides the best opportunity to build a comprehensive understanding of seasonal and spatial variability in nitrogen utilisation rates across the Southern Ocean over the current period of extreme climate driven environmental change.

4.1 Introduction

The Southern Ocean is a region of high macronutrient concentrations, where nitrogen, phosphorus and silicic acid do not limit phytoplankton growth outside of occasional NO_3^- limitation during intense blooms along the shelf (Henley et al., 2017, Henley et al., 2018). Excess macronutrients, those which are not assimilated due to limitation of phytoplankton productivity because of a lack of iron and light, are exported northwards from the Southern Ocean through Subantarctic Mode Waters and are responsible for nutrient supply across the mid to low latitudes (Sarmiento et al., 2004). Some earth system models indicate that projected increases in Southern Ocean productivity under climate change are likely to increase regional macronutrient trapping and reduce primary productivity globally (Steinacher et al., 2010, Laufkötter et al., 2015). Therefore, determining the rates and causes of variability in nutrient uptake and regeneration across the Southern Ocean is important for our understanding of productivity at the global scale.

Nitrate (NO_3^-) and ammonium (NH_4^+) are the major sources of nitrogen to phytoplankton in the Southern Ocean, with dissolved organic nitrogen (e.g., urea) constituting a minor fraction of total nitrogen supply (Cochlan and Bronk, 2001). Concentrations of nitrogenous nutrients follow a seasonal cycle, with NO_3^- being supplied to the surface through wintertime mixing of nutrient-rich circumpolar deep water fuelling 'new' productivity (Henley et al., 2017), and subsequent drawdown of NO_3^- through the summer bloom, largely due to the preference of diatoms for NO_3^- (Litchman et al., 2006, Cavagna et al., 2015, Glibert et al., 2016). Subsequently, microbial remineralisation of phytoplankton derived organic matter generates NH_4^+, approximately half of which then returns to phytoplankton via direct uptake (Bianchi et al., 1997), fuelling the 'regenerated' productivity of phytoplankton communities comprised of

smaller taxa (Karsh et al., 2003). Compared to NO_3^- and NH_4^+, relatively little is known about the spatially or seasonally resolved concentrations and uptake rates of urea in the Southern Ocean. Urea is generally considered to be present in low concentrations across surface waters of the Southern Ocean <1 µ µmol-N L^{-1} in the Pacific and Bellingshausen regions, <0.1 µmol-N L^{-1} in the Ross Sea (Cochlan, 2008). However, much higher concentrations of urea have been measured within and proximal to sea ice (up to 18 µmol-N L^{-1}) (Bury et al., 1995). In the Arctic, high concentrations of urea in landfast sea ice have been linked to the excretion of urea by zooplankton (Conover and Gustavson, 1999) and microbial oxidation of dissolved organic nitrogen (DON) compounds within ice (Conover et al., 1999). Uptake rates of urea are generally low in the open ocean where concentrations are low, with urea being a 'last choice' for Southern Ocean phytoplankton nitrogen acquisition across summer and winter (1996-1997) in all areas except a pack ice dominated station where urea concentrations were greater (Cochlan and Bronk, 2001). Urea uptake had been shown to. With climate driven reductions in sea ice over recent years potentially leading to a redistribution of nutrients concentrated within ice, urea could become more abundant across regions of the open ocean. Prolonged growth seasons resulting from an increased time period of sea ice free open ocean conditions could be expected to increase macronutrient demands and may accordingly impact the utilisation of urea in a future Southern Ocean. Therefore, we sought to determine the capacity of different phytoplankton for urea uptake.

Climate driven changes in the Southern Ocean could impact nitrogen cycling through decreasing wintertime NO_3^- resupply to the surface of the coastal ocean because of reductions in the mixed layer depth as increased freshwater input increases stratification (Chapter 2). Changes in the supply of upwelled iron through increased variability in the MLD can also influence nitrogen utilisation, with iron limitation driving diatoms to NH_4^+ and urea uptake over NO_3^- assimilation (Marchetti et al., 2012). Under iron enrichment, specific uptake rates of NO_3^- have been shown to increase several fold (e.g. Van Leeuwe et al., 1997, Timmermans et al., 1998, Franck et al., 2000, Cochlan et al., 2002), while iron enrichment has a smaller relative impact on NH_4^+ or urea uptake (Cochlan, 2008 and references therein). Thus, projected increases in iron limitation (Chapter 2) could alter nutrient preferences and uptake rates among the diatom community. This effect could be further increased by simultaneous shifts in the phytoplankton community composition from diatom dominated

communities to those composed of smaller cell types (Deppeler and Davidson, 2017), since reduced forms of nitrogen (mostly NH_4^+) are the dominant source to smaller taxa (Karsh et al., 2003).

The ^{15}N tracer method is the main approach by which we can obtain the rates at which phytoplankton utilise different forms of nitrogen (Dugdale and Goering, 2003). Briefly, by incubating a phytoplankton sample with a known spike of isotopically (^{15}N) enriched NO_3^-, NH_4^+ or urea, we can measure the rate of spike (e.g., ^{15}N-NO_3^-) transfer from the aqueous phase to the particulate organic material and use the nutrient concentration to deduce the nutrient uptake rate from this. Applications of this method are highly inconsistent, with many studies differing in their inclusion of source nutrients (e.g., just NO_3^- or NO_3^- and NH_4^+), and duration of incubations varying between 3 and 24 hours (see Table 2 in Mdutyana et al., 2020). Additionally, studies commonly acknowledge that uptake rates of ^{15}N-NH_4^+ are likely to be underestimates due to the effect of isotope dilution (Cavagna et al., 2015, Moschonas et al., 2017), which can similarly impact ^{15}N tracer measurements of NH_4^+ oxidation (Mdutyana et al., 2022). Isotope dilution describes the process by which the release of $^{14}NH_4^+$ due to remineralisation of DON occurring during the incubation dilutes isotopic enrichment of the source pool relative to that calculated based on the NH_4^+ concentration at the start of the incubation (Kanda et al., 1987, Dugdale and Wilkerson, 2003, Gilbert et al., 2003). Subsequently, NH_4^+ uptake is systematically underestimated by a factor of 1.2-2.0 across most experiments which negate to measure NH_4^+ regeneration (Cavagna et al., 2015 and references therein). NH_4^+ regeneration can be corrected for using the equations provided in Gilbert et al. (2003), which replaces a fixed $^{15}N/^{14}N$ enrichment with an exponential decay function. However, this requires knowledge of the ^{15}N-NH_4^+ enrichment at the end of the incubation. Measuring ^{15}N-$NH_4^+{}_{(aq)}$ poses several problems leading to the exclusion of NH_4^+ regeneration in most studies. Firstly, the isotopic enrichment dissuades most laboratories from attempting measurements due to the potential for contamination of natural abundance samples. Additionally, NH_4^+ is present in a seawater matrix, which few extraction methods are designed for. A common method for measuring ^{15}N-$NH_4^+{}_{(aq)}$ in seawater involves diffusion of NH_4^+ under basic conditions to produced NH_3 gas, and collection of this on an acidified filter (Holmes et al., 1998). However, this method requires large volumes (up to 4 L) for low concentration oceanic samples, often results in less than 100% recovery, which itself carries a

fractionation bias in favour of the lighter isotope, and completion of the diffusion takes up to 2 weeks. Liu et al. (2014) propose a chemical method for the quantification of $^{15}N\text{-}NH_4^+$ at natural abundance in freshwaters involving the two-step conversion of NH_4^+ to NO_2^- by hypobromite, followed by the hypobromite mediated reduction of NO_2^- to N_2O. Here, we test this approach for the measurement of enriched isotopes in a seawater matrix, and assess its potential as a fast, simple and accurate method for determining $^{15}N\text{-}NH_4^+{}_{(aq)}$ and NH_4^+ regeneration rates in culture experiments.

Collectively, this chapter aims to further our understanding of nitrogen uptake and regeneration rates by conducting a series of ^{15}N uptake experiments using a suite of species representative of the Southern Ocean phytoplankton community in culture.

Exploring thesis aim 3, the specific sub-aims of this chapter are to:

- Determine how the uptake of NO_3^-, NH_4^+ and urea differ between different phytoplankton types (diatoms, cryptophytes, haptophytes).
- Understand whether the chemical conversion method of Liu et al. (2014) is effective in measuring enriched $^{15}N\text{-}NH_4^+$ in seawater, to determine rates of NH_4^+ regeneration by phytoplankton.
- Calculate the rates of NH_4^+ regeneration in $^{15}NH_4^+$ uptake experiments to understand the extent of species dependent variability in NH_4^+ regeneration.
- Compare differences in uptake rates over long (24 hour) and short (6 hour) incubations, to determine whether rates resulting from different incubation durations are comparable.

Applied to the overall aims of the thesis, this chapter contributes towards understanding how changes in phytoplankton communities associated with a warming climate are likely to impact nutrient budgets at the regional and global level through modulating the availability of nutrients for global export. The dependence of phytoplankton on nutrients for growth means that any change in nutrient uptake because of species specific selection effects could have a feedback on community composition, with downstream implications for carbon export and biogeocheical cycling.

4.2 Methods

4.2.1 Cultures and maintenance conditions

We acquired a suite of five species of marine phytoplankton isolated from the Southern Ocean (**Figure 4.1**) and stored in national culture collections. *Fragilariopsis cylindrus* (CCAP 1023/1) and *Porosira glacialis* (CCAP 1060/9) were purchased from the Scottish Association for Marine Sciences' Culture Collection of Algae and Protozoa. *Geminigera cryophila* (CCMP2564), *Phaeocystis antarctica* (colony forming) (CCMP 1871) and *Pseudonitszchia subcurvata* (CCMP3560) were purchased from the National Centre for Marine Algae, USA. These species were chosen because collectively they represented a variety of the most abundant phytoplankton groups, morphologies and sizes present in the Southern Ocean (**Table 4.1**). Cultures were maintained in artificial seawater (following Harrison et al., 2008) with nutrients, vitamins and minerals added to produce F/2 + Si media, based on the original F/2 recipe by Guillard (1975) plus $Na_2SiO_3.9H_2O$ at a concentration of 49 µmol L^{-1}. An 18:6 light to dark cycle was established at an intensity of ~150 µmol m^{-2} s^{-1} of full spectrum light. All incubations were conducted in a Panasonic MIR-154 temperature-controlled incubator held at 2°C (± 2°C). Cultures were acclimated to these conditions for at least 3 months and held in a growth phase through serial dilution with F/2 + Si media.

Table 4.1: Description of selected phytoplankton species by morphotype, region of isolation and size

Species	Description	Isolation region	Size
Fragilariopsis cylindrus	Pennate sea ice diatom	Palmer Station	10-50 µm
Pseudonitzschia subcurvata	Pennate diatom	Ross Sea	50-150 µm
Geminigera cryophila	Cryptophyte	Ross Sea	10-20 µm
Phaeocystis antarctica	Colony forming haptophyte	Rothera Station	Individual: 2-6 µm Colony: <2 mm
Porosira glacialis	Centric diatom	Palmer Station	40-80 µm

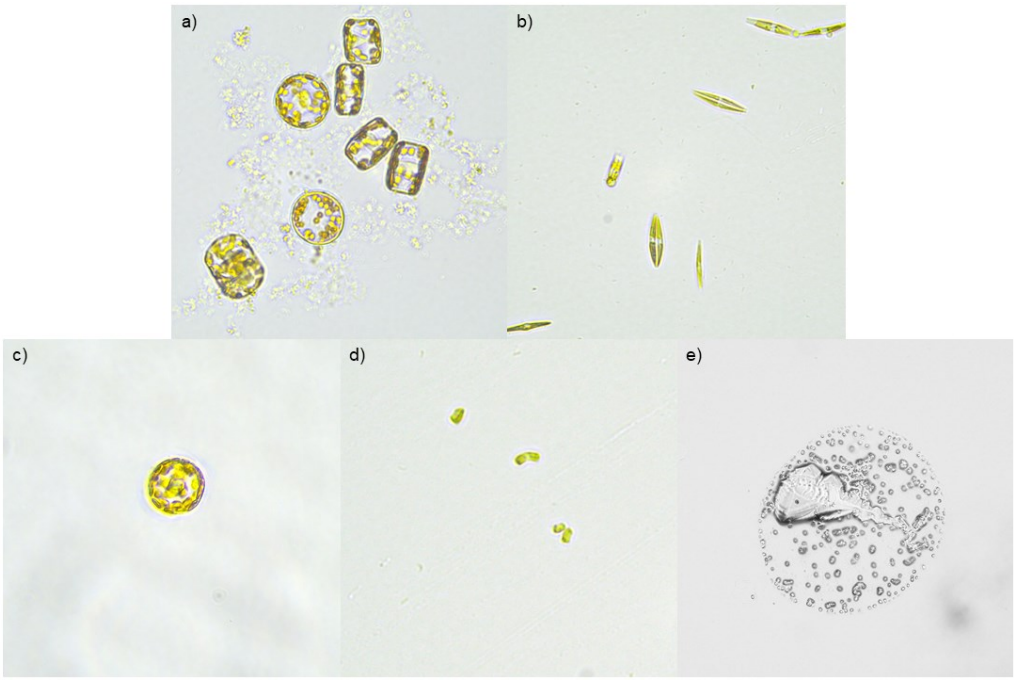

Figure 4.1: Morphology of selected phytoplankton species, *Porosira glacialis* (a), *Pseudonitszchia subcurvata* (b), *Geminigera cryophila* (c), *Fragilariopsis cylindrus* (d), and *Phaeocystis antarctica* (e). Images taken on a LEICA DMI1 inverted microscope with a Flexacam C1. This microscope is not calibrated for scale and therefore images do not represent relative size between species, refer to **Table 4.1** for sizes.

4.2.2 Experimental conditions

To investigate differences in the uptake of nitrogen by phytoplankton based on the presence of different nitrogen sources, multiple experiments were established under a single nitrogenous nutrient regime (either NO_3^- or NH_4^+ or urea). The purpose of these experiments is not to induce nutrient limitation on cultures, but instead to establish how different phytoplankton utilise different nitrogen sources over a typical growth period. Experimental media was produced by the synthesis of sterile artificial seawater (following Harrison et al., 2008). To this, a matrix of nutrients was added at a concentration matched to coastal Southern Ocean summertime averages from Henley et al. (2017) (**Table 4.2**). Since trace metal limitation was not a factor in this experiment, trace metals and vitamins were maintained at the concentrations required for F/2 media (per Guillard, 1975). Experimental cultures were inoculated with the starter cultures to a target concentration of 10^6 cells L^{-1}, in to 10 L of experimental media in a clear polycarbonate biotainer and left to acclimate for at least 7 days before commencement of nutrient uptake experiments. The experimental media contained nitrate, silicate, phosphate at the concentrations given in **Table 4.2**, no additions to this were made throughout the acclimation period.

Table 4.2: Nutrient concentrations in F/2 + Si and experimental media (molar).

Reagent	[F/2 +Si]	[Experimental]
$NaNO_3$	8.82×10^{-4} M	1.765×10^{-5} M
$NaH_2PO_4.2H_2O$	3.62×10^{-5} M	1.3×10^{-6} M
$Na_2SiO_3.9H_2O$	1.06×10^{-4} M	6.0×10^{-5} M

4.2.3 ^{15}N Incubations

Following the acclimation period, 500ml aliquots of the experimental culture were siphoned from the mid depth of the large biotainer to clear polycarbonate bottles. To determine the rates of NO_3^-, NH_4^+ and urea uptake, bottles were enriched with ^{15}N labelled $NaNO_3$, NH_4Cl and urea at concentrations of 10% relative to the existing nutrient concentration (Dugdale and Goering, 2003) in triplicate (3 independent bottles per nitrogen source). For the NO_3^- spike this was 1 µmol L^{-1}, NH_4^+ was 0.2 µmol L^{-1} and urea was 0.05 µmol L^{-1}. NO_3^- had been added at the start of the experiment, NH_4^+ had been regenerated from NO_3^- throughout the growth period, urea was not already present so was added at a concentration of 0.5 µmol L^{-1} immediately prior to addition of ^{15}N labelled urea. Incubations with ^{15}N were conducted over a period of 24 hours rather than a typical ≤6-hour experiment to incubation account for any possible influence of diel cycling on N uptake. One experiment (for *F. cylindrus*) was replicated as a 6-hour incubation to establish the extent to which incubation duration impacted uptake rates.

To account for the greater rate of NH_4^+ regeneration over 24 hours, samples for dissolved ^{15}N NH_4^+ were taken at the end of each NH_4^+ incubation by syringe filtering 50 ml of culture through a 0.8/0.2 um supor acrodisc. These dissolved samples were then immediately frozen in acid washed 60 ml HDPE bottles for later analysis. To terminate the incubation, the remaining culture was filtered on to ashed (4 hours at 450°C) GF/F filters and immediately frozen at -20 °C and stored until analysis.

To determine the ^{15}N concentration of the particulate component samples, filters were prepared by thawing and drying (60 °C), before being wrapped in tin cups (Sercon) and weighed. Samples were analysed for %C, %N and δ^{15}N using a PDZ Europa 20-20 Stable Isotope Ratio Mass Spectrometer coupled to an automated nitrogen carbon analyser (ANCA-

NT) at the Scottish Association for Marine Science. The IRMS was calibrated between 5-300 µg N using variable masses of L-isoleucine standards (Sigma Aldrich). Certified reference materials of ammonium sulphate (IAEA 305B and N-2) were run at the start and end of each sample set; across all reference materials the external precision standard error of $\delta^{15}N$ measurements was <0.45 ‰. The limits of detection were 5.6 µg for nitrogen and 35.3 µg for carbon.

4.2.4 Models of nitrogen uptake

Absolute nitrogen uptake rates were initially calculated based on the model by Dugdale and Wilkerson (2003) (Equation 1). Where ρ is the absolute uptake rate of N (µmol N L^{-1} d^{-1}), ${}^{15}N_{sink}\ (t_1)$ is the ^{15}N value determined from analysis of the filter at the end of the experiment in atom, ${}^{15}N_{sink}\ (t_0)$ is the natural abundance of ^{15}N, ${}^{15}N_{source}\ (t_o)$ is the enrichment (atom %), T is the duration of the experiment in days and $PON(t_1)$ is the concentration of particulate nitrogen at the end of the experiment (µmol N L^{-1}).

$$\rho = \frac{{}^{15}N_{sink}\ (t_1) - {}^{15}N_{sink}\ (t_o)}{{}^{15}N_{source}\ (t_o) - {}^{15}N_{sink}\ (t_o) \times T} \times PON(t_1) \text{ (Eqn. 1)}$$

This equation does not account for the effect of isotope dilution, whereby regeneration of $^{14}NH_4^+$ from organic matter during the course of the incubation dilutes the $^{15}N/^{14}N$ isotopic ratio, resulting in potential underestimates of ρ for NH_4^+ (Kanda et al., 1987, Gilbert et al., 2003).

To account for isotope dilution, we applied the model of Gilbert et al. (2003), which replaces the fixed value of ${}^{15}N_{source}\ (t_o)$ with an exponential decay constant of the source pool (denoted by $\bar{R}$) such that P, representing the isotope dilution corrected value for NH_4^+ uptake, becomes:

$$P = \frac{{}^{15}N_{sink}\ (t_1) - {}^{15}N_{sink}\ (t_o)}{\bar{R} \times T} \times PON(t_1) \text{ (Eqn.2)}$$

Where:

$$\bar{R} = \frac{{}^{15}N_{source}\ (t_o)}{k \times \Delta t} \times (1 - e^{-kt}) \text{ (Eqn. 3)}$$

And:

$$k = \frac{\ln\left({}^{15}N_{source}\,(t_1) / {}^{15}N_{source}\,(t_o)\right)}{\Delta t} \text{ (Eqn. 4)}$$

This equation requires the determination of ${}^{15}N_{source}\,(t_1)$, the isotopic composition of the source pool at the end of the incubation time, to calculate the rate of decay. We achieved this through IRMS analysis of the dissolved phase (see **4.2.5**). $\bar{R}$ represents the enrichment in the source pool at time *t* given a logarithmic decay in atom % enrichment between t_0 and t_1, (constant *k)*. Modelling $\bar{R}$ for increasing values of *k* increases the rate of decay and the extent to which the t_0 enrichment is diluted (**Figure 4.2**). For all modelled values of *k*, the isotopic enrichment at t_1 is lower than at t_0, diverging from the fixed enrichment value used in most studies (dotted line in **Figure 4.2**).

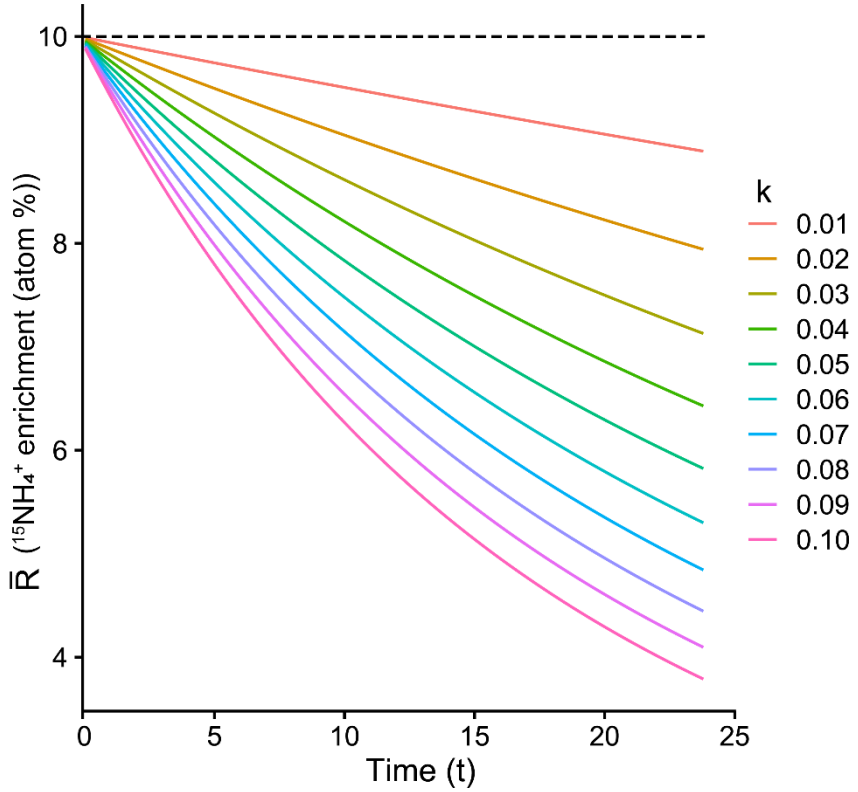

Figure 4.2: Modelled exponential decay of the $^{15}NH_4^+$ enriched pool over time (between 0 and 24 hours) given by Eqn. 2 for increasing values of *k* (see Eqn. 3). The black dotted line represents the fixed isotopic enrichment assumption given by Eqn. 1. Isotopic enrichment begins at 10 atom % per the method by Dugdale and Goering (2003).

4.2.5 Dissolved ^{15}N analysis

The ^{15}N enrichment of the NH_4^+ pool at the end of the incubation was determined to calculate the rate of regeneration (and therefore ^{15}N dilution) over the course of the incubation. Atom % of ^{15}N-NH_4^+ in the dissolved pool was determined by conversion to N_2O;

additionally natural abundance $^{15}N\text{-}NO_3^-$ and $^{15}N\text{-}NH_4^+$ in the dissolved pool were determined in the same manner to check for any contamination and for balancing of the $^{15}N_{sink}\ (t_0)$ value in Eqn. 1. Following chemical conversion of $^{15}N\text{-}NO_3^-$ and $^{15}N\text{-}NH_4^+$ to N_2O, the $^{15}N/^{14}N$ ratio of N_2O was measured using a Sercon HS2002 with CyroGas preparation module at the British Geological Survey, UK.

4.2.5.1 NO_3^- to N_2O conversion

The $^{15}N/^{14}N$ ratio of NO_3^- was determined using a $TiCl_3$ mediated conversion to N_2O following Altabet et al. (2019), shown in equation 5.

$$2NO_{3\ (aq)}^{-} + 8Ti^{+3} + 10H^+ \rightarrow N_2O_{(g)} + 8Ti^{+4} + 5H_2O \text{ (Eqn. 5)}$$

Firstly, the Ti(III) chloride reducing agent was pre-conditioned by adding 1g of Zn powder to 10 ml of Ti(III) chloride in 30% HCl. Zinc complexes with Ti(IV), removing any contamination from the presence of unwanted titanium species, leaving just Ti(III). This working solution was flushed with N_2 and sealed prior to storage to avoid the oxidation of Ti(III).

Due to the relatively low concentrations of NO_3^- in this experiment (**Table 4.3**) compared to freshwater systems, samples were not diluted, and added as 2 ml of sample to a 12 ml exetainer vial. However, the method does recommend dilution of samples with high NO_3^- concentrations to ~14.3 µmol L^{-1} with degassed DI water.

After addition of the sample, the headspace of the vial was evacuated and the Ti(III) solution was added at a ratio of 1:20 (*v/v)* using a gas tight syringe. The resulting sample-reagent mix was left to react for 24 hours to allow for the complete conversion of NO_3^- to N_2O before IRMS analysis of the resulting gaseous phase.

4.2.5.2 NH_4^+ to N_2O conversion

NH_4^+ was first oxidised to NO_2^- according to Liu et al. (2014) by reaction with BrO^-. Firstly, a bromate/bromide stock was prepared by addition of 0.6 g sodium bromate and 5g of sodium bromide to 250 ml of MilliQ. A working solution is then formed from dilution of 1 ml of stock in 50 ml of MilliQ and 3 ml of 12 N HCl. This solution is left in the dark for 5 minutes to produce Br_2 which is then converted to BrO^- by the rapid addition of 50 ml of 10 M NaOH. BrO^- was added to the sample in a 1:10 ratio (*v/v*) in a 12 ml exetainer vial. The oxidation of NH_4^+ was allowed to occur over 30 minutes before termination with the addition of 0.05 ml

of 0.384 mM sodium arsenite. NO_2^- was then reduced to N_2O by addition of $NH_2OH{\cdot}HCl$. A stock solution was made from dissolving 0.2778g of $NH_2OH.HCl$ in 100 ml of MilliQ. Prior to analysis, 3 ml of stock solution was dissolved in 500 ml of MilliQ, leaving a 0.24 µmol L^{-1} solution. For the reduction, 0.5 ml of $NH_2OH.HCl$ solution was added to the sample, the reaction vial heated to 37°C in a water bath and pH adjusted to 0.42 through addition of HCl. After 16 hours the reaction was terminated through addition of 0.5 ml of 5M NaOH.

4.2.5.3 N_2O IRMS

Measurement of the isotopic enrichment of both NO_3^- and NH_4^+ was conducted by GC/IRMS analysis of N_2O resulting from the chemical conversion of both nutrients to the gaseous phase. A common concern with the measurement of enriched isotopes is the potential for contamination of natural abundance samples. Analysis was performed using a Sercon CryoGas preparation module coupled to a 20-22 isotope ratio mass spectrometer (GC-2022) at the British Geological Survey, Keyworth, UK. The primary use of this instrument is for the analysis of $\delta^{13}C$ and $\delta^{2}H$ in methane, so the measurement of enriched ^{15}N would not risk contamination of other samples analysed by this IRMS. The system automates gas chromatography, cryogenic trapping, pyrolysis and continuous flow IRMS, the detailed setup of the instrument is described in Smith et al. (2021a). United States Geological Survey (USGS) and International Atomic Energy Agency (IAEA) standards were run across the ^{15}N enrichment range, resulting values are given in **Table 4.4**.

4.2.6 Cell counts

Cell counts of starter cultures were taken to calculate inoculation volumes for experimental batches, targeting an initial concentration of 1 $x10^5$ cells L^{-1}. Cell counts were determined using a SORP BD LSR Fortessa flow cytometer at the University of Edinburgh. For each sample, 300 µl was collected in triplicate in a 96 well plate and fixed with 1% glutaraldehyde, and measured immediately. From the plate, 100 µl of sample was injected in to the flow cytometer after syringe mixing of the sample. Cell counts were determined by excitation of chlorophyll with red light and measurement of fluorescent emission at 692 nm. A gate was created with thresholds for Fluorescence Intensity Units at 692 nm and a minimum forward scatter requirement (as an indicator of size) to separate viable chlorophyll containing cells from detrital matter (large cells, but low chlorophyll). The exact fluorescence thresholds for

gating varied by species, since larger cells have greater chlorophyll content, however the same gates were maintained for all replicate analyses of each individual species.

4.2.7 Nutrient analysis

Concentrations of NO_3^- and NH_4^+ in the biotainer immediately prior to addition of the enriched isotopes were determined using a SEAL segmented flow autoanalyzer at Plymouth Marine Laboratory. Samples were prepared by filtration of a 50 ml aliquot through a 0.2 µm Supor filter and immediate filtration per the methods of Woodward and Rees (2001). The limit of detection was 0.02 µmol L^{-1} for NO_3^- + nitrite (NO_2^-) and 0.05 µmol L^{-1} for NH_4^+.

4.2.8 Statistical tests

Pairwise t tests were conducted to determine the level of statistical significance in the difference of means between phytoplankton species for their C:N content and experiment duration. Statistical tests were performed using the t.test and pairwise.t.test functions within the base statistics package of R (V3.6.1).

4.3 Results

4.3.1 Absolute nitrogen uptake

Nutrient concentrations of NO_2^-, NO_3^-, and NH_4^+ were determined for each culture immediately prior to addition of the ^{15}N tracers (**Table 4.3**). While the experimental culture only contained 17.65 µmol L^{-1} of NO_3^-, most cultures had a greater final NO_3^- concentration because the inoculation of the experimental culture involved a small carry over of the starter culture which was enriched in NO_3^- due to the F/2 nutrient concentrations (**Table 4.2**). At these concentrations, all the spikes were confirmed to be below 10% of the ambient nutrient concentration, NO_3^- was 5.36 % ± 0.43 and NH_4^+ was 7.97 % ± 5.11. As the urea concentration was fixed, this spike was always at 10% of the ambient concentration.

Table 4.3: Nutrient concentrations prior to spiking with ^{15}N labelled tracers. Nitrite, NO_3^- and NH_4^+ are measured values while urea is the concentration of the natural abundance nutrient added immediately prior to spiking.

Culture	NO_2^- [µmol L^{-1}]	NO_3^- [µmol L^{-1}]	NH_4^+ [µmol L^{-1}]	Urea [µmol L^{-1}]
F. cylindrus	0.08	20.89	5.62	0.5
G. cryophila	0.10	17.08	1.17	0.5
P. antarctica	0.05	17.67	1.89	0.5
P. glacialis	0.14	19.57	2.37	0.5
P. subcurvata	0.15	18.06	1.49	0.5

As each culture contained a different amount of biomass, nitrogen uptake was normalised to particulate organic carbon concentrations (µmol N/ µmol C L^{-1}) . There was a wide range in total uptake of nitrogen by the different phytoplankton species, with *P. subcurvata* having the greatest rate at 1.01 (±0.11) µmol N / µmol C L^{-1} d^{-1} compared to the fellow diatom *F. cylindrus* which had the lowest uptake at 0.17 (±0.01) µmol N / µmol C L^{-1} d^{-1} (**Figure 4.3**). The remaining three species all had similar mean values for total nitrogen uptake between 0.236 and 0.295 µmol N / µmol C L^{-1} d^{-1}. For all species, NH_4^+ and urea were the main sources of nitrogen, with the contribution of the two being roughly equal for *G. cryophila, P. antarctica and P. glacialis*. For *P. subcurvata* and *F. cylindrus*, NH_4^+ was a greater source relative to urea, representing 70.6% and 66.8% of total nitrogen uptake, with urea contributing 25.7% and 19.0% respectively. NO_3^- played a minimal role as a source of nitrogen across all species, representing <5% of total uptake for all species except *F. cylindrus* (which had the lowest overall uptake) where NO_3^- accounted for 14.2%. However, because the overall uptake is so low in this species, the NO_3^- contribution has a relatively large amount of error (0.029 ± 0.016 µmol N / µmol C L^{-1} d^{-1}), so the apparent high percentage contribution of NO_3^- to *F. cylindrus* nitrogen uptake should be considered within the context of these low uptake values. For *P. subcurvata* and *P. antarctica*, an instrumental failure destroyed two of the three triplicate samples for NO_3^- uptake, so these values represent one measurement, however given the consistency with low rates of NO_3^- uptake across all species, this is unlikely to impact interpretation of the results.

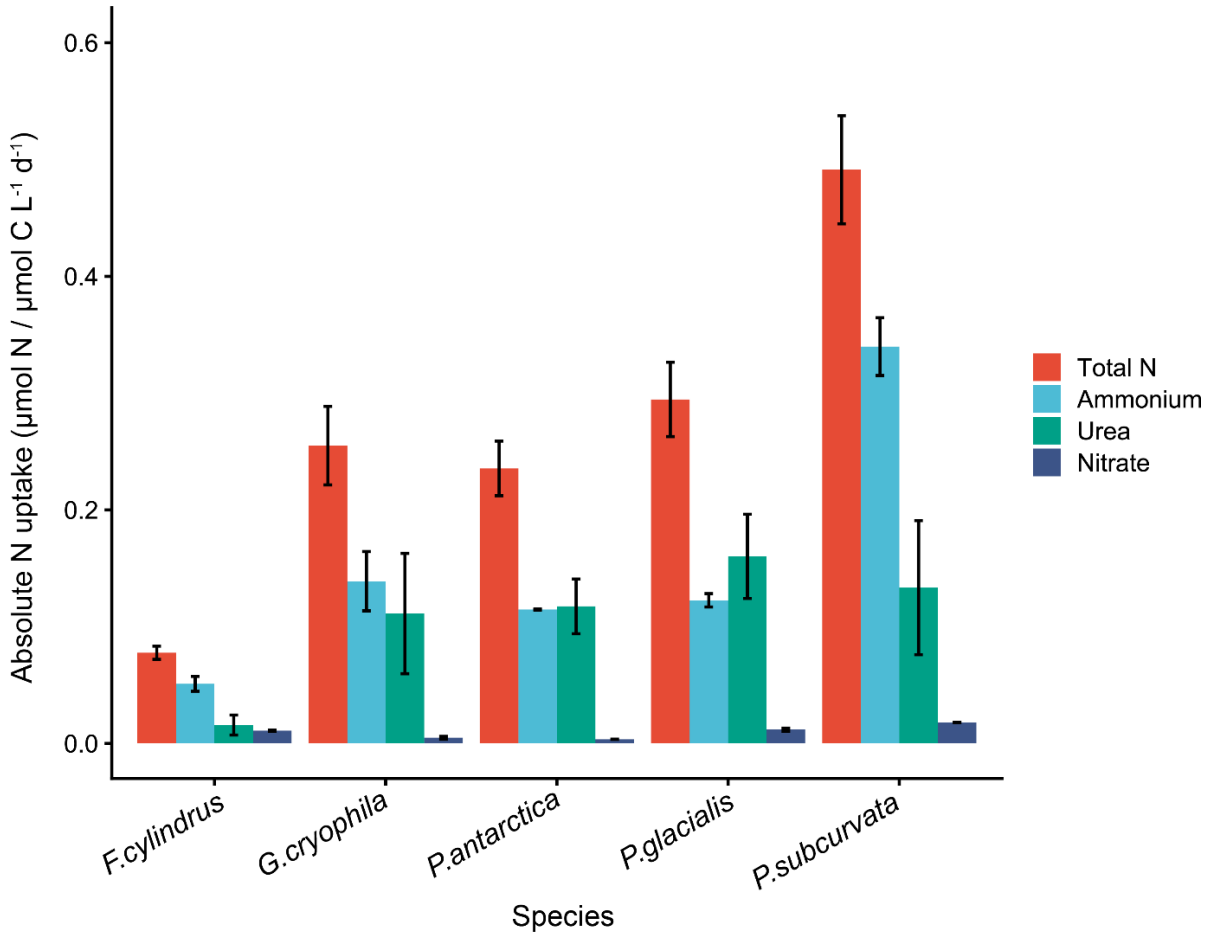

Figure 4.3: Absolute nitrogen uptake from NH_4^+, urea and NO_3^- normalised to carbon content for each phytoplankton culture. Total N is the sum of the three nitrogen sources. NH_4^+ is uncorrected for the isotope dilution effect here, all values represent daily uptake rates resulting from 24-hour incubations. Error bars indicate ±1 standard error of the mean.

4.3.2 Molar C:N

The molar ratio of carbon to nitrogen (C:N) for each species was averaged across all experiments (n=11-15) (**Figure 4.4**). *F. cylindrus* had the greatest C:N value at 12.71 (± 0.58) while *P. subcurvata* the lowest at 5.86 (± 0.21). Variability was generally low within each species group, with the C:N ratio of each species pair being statistically different from each other ($p<0.05$) with pairwise t-tests except for *P. glacialis* and *G. cryophila*.

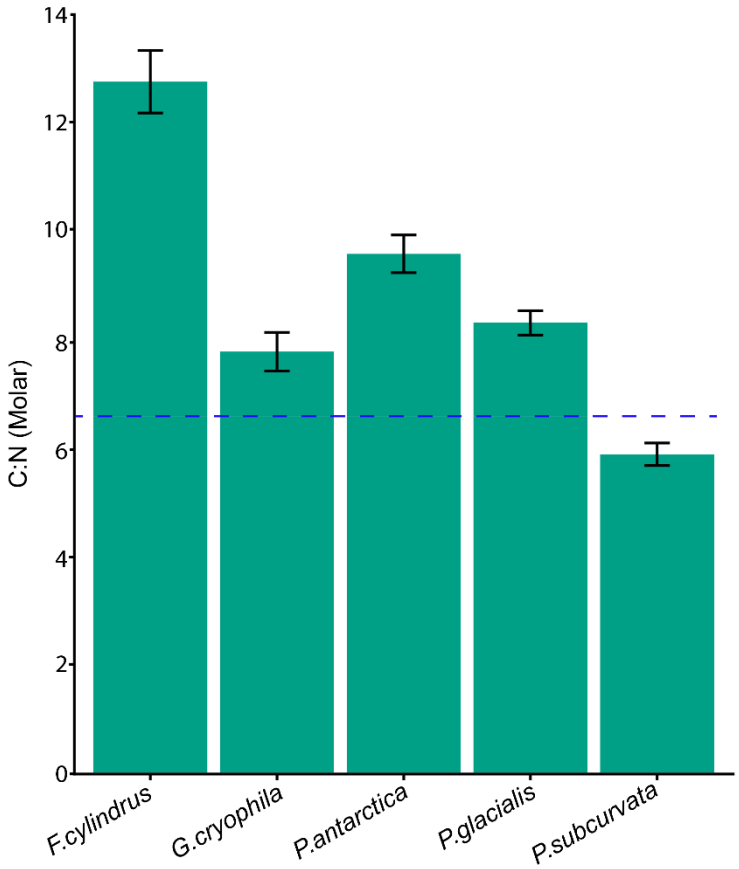

Figure 4.4: Molar ratio of carbon to nitrogen for the five species, error bars represent ±1 standard error of the mean. The dashed blue line represents the Redfield ratio of C:N (6.625:1).

4.3.3 Dissolved $^{15}NH_4^+$

The isotopic composition of aqueous $^{15}NH_4^+$ at the end of the incubation is presented as ^{15}N measured in air, targeting the N_2O produced following the two-stage chemical conversion described in **4.2.5.2**. A suite of matrix matched certified reference materials for $^{15}NH_4^+$ were first analysed to ensure complete conversion of NH_4^+ to NO_2^- and N_2O. The majority of the available reference materials are certified for lower values (-30 to 375 ‰), where natural abundance samples would exist, however IAEA 311 is included as the most enriched commercially available material (**Table 4.4**). With a ^{15}N content of 2.1 atom % IAEA 311 is most representative of our ^{15}N enriched samples; calibrating against this standard resulted in a precision of <0.02% at the top end. Although some CRMs in the natural abundance range (particularly IAEA N1) had greater relative drift from the certified values, this is not concerning because these CRMs represent values several orders of magnitude below any

samples measured, the regression line between CRMs used to deduce the isotopic value had an excellent fit with an R^2 of 1.

Table 4.4: Performance of five IAEA and USGS certified reference materials undergoing the two-stage chemical conversion from NH_4^+ to N_2O. Values are reported in ‰.

CRM	Known value ($\delta^{15}N$)	Average ($\delta^{15}N$)	S.D ($\delta^{15}N$)
USGS 25	-30.41	-25.6	0.2
IAEA N1	0.43	3.5	0.0
USGS 26	53.75	55.0	0.5
IAEA 305b	375.3	365.5	0.5
IAEA 311	4590.9	4591.7	6.9

Isotopically enriched samples produced $^{15}NH_4^+$ values between 1.1 and 5.6 atom % (~2000-14250 ‰) **(Table 4.5**). Each sample was analysed in duplicate and isotopically enriched samples had an average standard deviation between duplicates of 1.4 %. NH_4^+ regeneration was not determined for *G. cryophila*.

Table 4.5: Isotopic composition of NH_4^+ in the dissolved phase at the end of the incubation experiments. For *F. cylindrus* results from the 24- and 6-hour experiments are indicated with a suffix, for all other species a 24-hour incubation was performed. $\delta^{15}N$ (‰) A/B refer to the duplicate analytical repeats while sample replicates refer to the experimental replications. Analytical replicates for *F. cylindrus*- 24h (3) and *P. subcurvata* (4) were removed because the peak height in the replicate was substantially lower for one value compared to the other, suggesting incomplete conversion to of NH_4^+ to N_2O in these samples.

Species	Rep	$\delta^{15}N$ (‰) A	$\delta^{15}N$ (‰) B	Average (‰)	S.D (‰)	Atom %
F. cylindrus- 24h	1	5160.4	5259.2	5209.8	69.9	2.27464
	2	5011.9	4937.3	4974.6	52.7	2.18849
	3	4009.6	N.D	4009.6	N.D	1.83503
	4	3675.5	3861.8	3768.7	131.7	1.74676
F. cylindrus - 6h	1	5554.2	5476.5	5515.3	55.0	2.38657
	2	4233.2	4198.5	4215.9	24.5	1.91057
	3	5195.7	5238.4	5217.0	30.1	2.2773
P. antarctica	1	7834.6	7815.3	7824.9	13.7	3.23258
	2	9923.1	11769.5	10846.3	1305.6	4.3393
	3	9630.1	9436.5	9533.3	136.9	3.85834
P. glacialis	1	7884.9	8003.9	7944.4	84.2	3.27634
	2	6839.1	6573.6	6706.4	187.8	2.82284
	3	7905.5	7754.5	7830.0	106.8	3.23442
	4	1975.1	2064.2	2019.7	63.0	1.1061
P. subcurvata	1	14356.6	14173.3	14265.0	129.7	5.59156
	2	4853.6	4760.7	4807.1	65.7	2.12715
	3	9521.0	9438.2	9479.6	58.5	3.83868
	4	6455.1	N.D	6455.1	N.D	2.73082

4.3.4 NH_4^+ regeneration rates

The $^{15}NH_4^+$ value of the dissolved phase at the end of the incubation was used to correct NH_4^+ uptake rates per Eqn. 2. For all species the dilution corrected values (P) were greater than the uncorrected uptake rates (*p*) (**Figure 4.5**). The ratio between the uncorrected and corrected values is given by *p*:P per Gilbert et al. (2003), we found this value to differs within replicates of the same species (e.g. *P. subcurvata* 1.52 – 2.26) (**Table 4.6**).

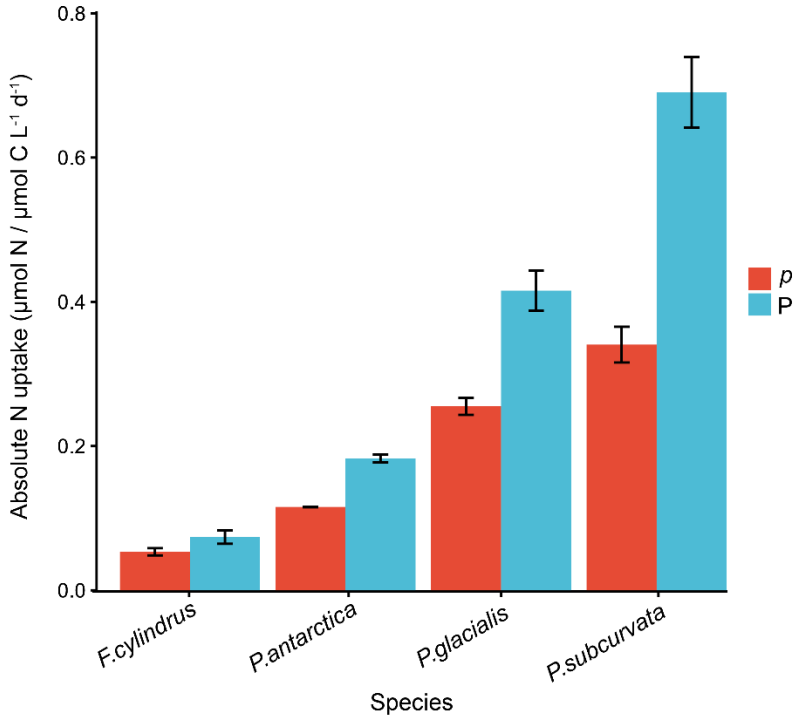

Figure 4.5: Uncorrected (*p*) and isotope dilution corrected (P) NH_4^+ uptake rates for four model species. Error bars represent ±1 standard error of the mean.

The extent of variability in *p*:P increases as the absolute uptake increases, the value of *p*:P across replicates is consistent for *P. antarctica* and *F. cylindrus*. However, both *P. subcurvata* and *P. glacialis* had individual replicates with *p*:P > 2. These higher values of *p*:P occur when the $^{15}NH_4^+$ value of the aqueous pool becomes more depleted during the course of the incubation but this depletion is not proportionally matched by an increased value of $^{15}NH_4^+$ in the particulate phase. Excluding these anomalously high *p*:P values, there is no significant difference between the ratio of corrected to uncorrected NH_4^+ uptake between species. Exclusive of anomalous values, over a 24-hour incubation period across the measured species, inclusion of the isotope dilution effect increases pNH_4^+ by 52 % (±16 %). Therefore, across our experiments, exclusion of NH_4^+ regeneration would lead to an underestimation in pNH_4^+ by 34 % (±8 %).

Table 4.6: Uncorrected (p_c) and isotope dilution corrected (P_c) uptake of NH_4^+ by different marine phytoplankton cultures. R_0 and R_t represent the atom percent $^{15}NH_4^+$ enrichment of the source pool (aqueous phase) at the start and end of the incubation, per Eqn 3. *k* represents the relationship between R_t and R_0 per Eqn 4. Atom excess is the enrichment of the particulate phase at the end of the experiment. Particulate Nitrogen (PN) and Particulate Organic Carbon (POC) are given in µg L^{-1}, the units for p_c and P_c are µmol N / µmol C L^{-1} h^{-1}.

Species	Rep	R_0	R_t	Atom excess (%)	k	PN	POC	p_c	P_c	p_c:P_c
	1	13.42	5.59	1.17	0.04	55.49	274.53	0.006	0.009	1.52
	2	13.42	2.13	2.38	0.08	66.31	357.85	0.014	0.032	2.26
P. subcurvata	3	13.42	3.84	2.32	0.05	50.88	239.76	0.016	0.028	1.79
	1	8.44	2.82	1.67	0.05	39.32	275.62	0.012	0.020	1.69
	2	8.44	3.23	1.52	0.04	36.95	268.18	0.010	0.016	1.59
P. glacialis	3	8.44	1.11	2.12	0.08	45.42	316.32	0.016	0.039	2.49
	1	10.58	4.34	1.17	0.04	41.52	344.04	0.005	0.007	1.54
P. antarctica	2	10.58	3.86	1.19	0.04	38.89	326.34	0.005	0.008	1.62
	1	3.56	2.27	0.50	0.02	22.58	288.64	0.002	0.002	1.28
	2	3.56	2.19	0.52	0.02	20.96	248.13	0.002	0.003	1.30
F. cylindrus	3	3.56	1.84	0.55	0.03	23.70	258.23	0.003	0.004	1.43
	4	3.56	1.75	0.53	0.03	25.20	265.10	0.003	0.004	1.46

4.3.5 6 vs 24-hour uptake rates

To date, most NH_4^+ uptake experiments aim to mitigate against the effect of isotope dilution by using a short (< 6 hour) incubation, supposedly terminating before any substantial amount of $^{14}NH_4^+$ can be regenerated. Using cultures of *F. cylindrus* we found that 4 times multiplication of the 6-hour incubation resulted in values which were statistically significantly greater than the measured 24-hour NH_4^+ uptake for both the uncorrected ($p<0.005$) and corrected ($p<0.01$) rates. However, there was no statistically significant difference between the most common (6-hour, dilution uncorrected) approach and the ideal (24-hour, dilution corrected) approach.

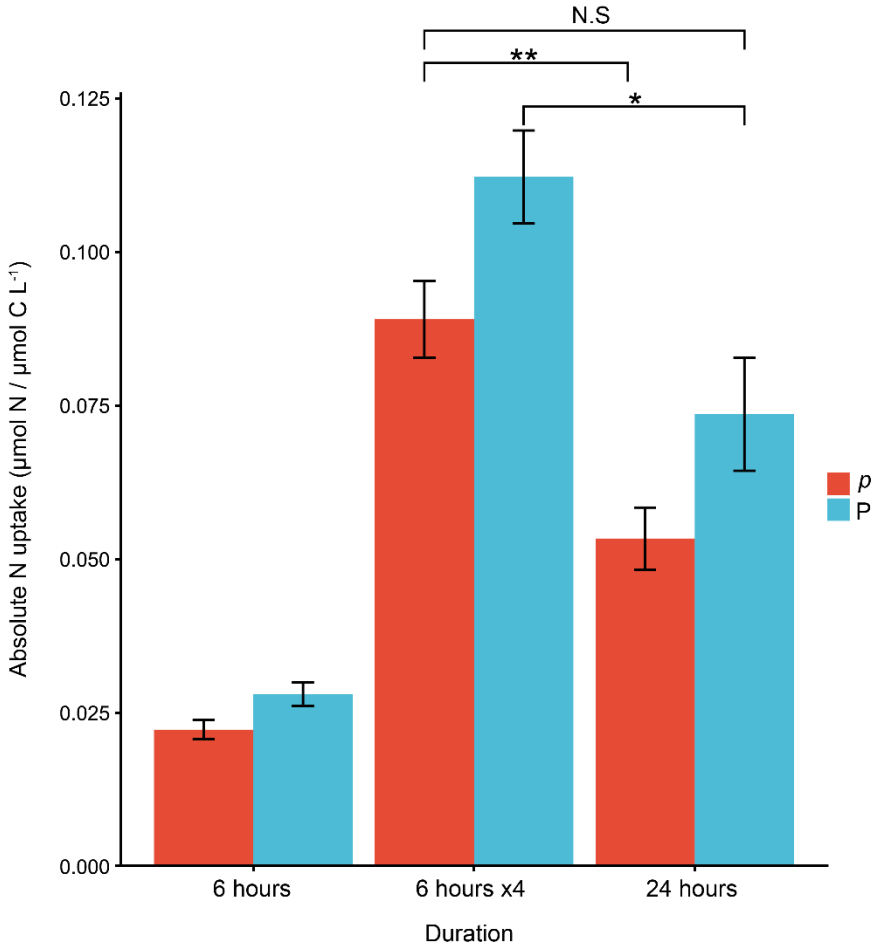

Figure 4.6: Uncorrected (*p*) and isotope dilution corrected (P) NH_4^+ uptake rates for *F. cylindrus* under 6, 6 x 4- and 24-hour incubations. The significance of differences between conditions was assessed by pairwise t-tests and is represented between linked pairs by * notation, with * indicating $p<0.01$ and ** indicating $p<0.005$, no significant difference is shown by N.S Error bars represent ±1 standard error of the mean.

4.3.6 Accounting for isotope dilution in total nitrogen uptake

Applying the isotope dilution corrected values for NH_4^+ regeneration to the total nitrogen uptake (previously uncorrected in **Figure 4.3**) increased both the total nitrogen uptake by each species and the contribution of NH_4^+ to the total nitrogen uptake. NH_4^+ continued to make the greatest contribution to nitrogen uptake in *P. subcurvata* increasing from 69% to 82%. Correcting for isotope dilution had the largest impact on *P. glacialis* where NH_4^+ previously represented only 42% of total nitrogen uptake (**Figure 4.3**) but post correction accounts for 71%. Following dilution correction, NH_4^+ becomes the majority source of nitrogen (>50%) for all phytoplankton species assessed, with urea representing the secondary source (24% ±11%) (**Figure 4.7**).

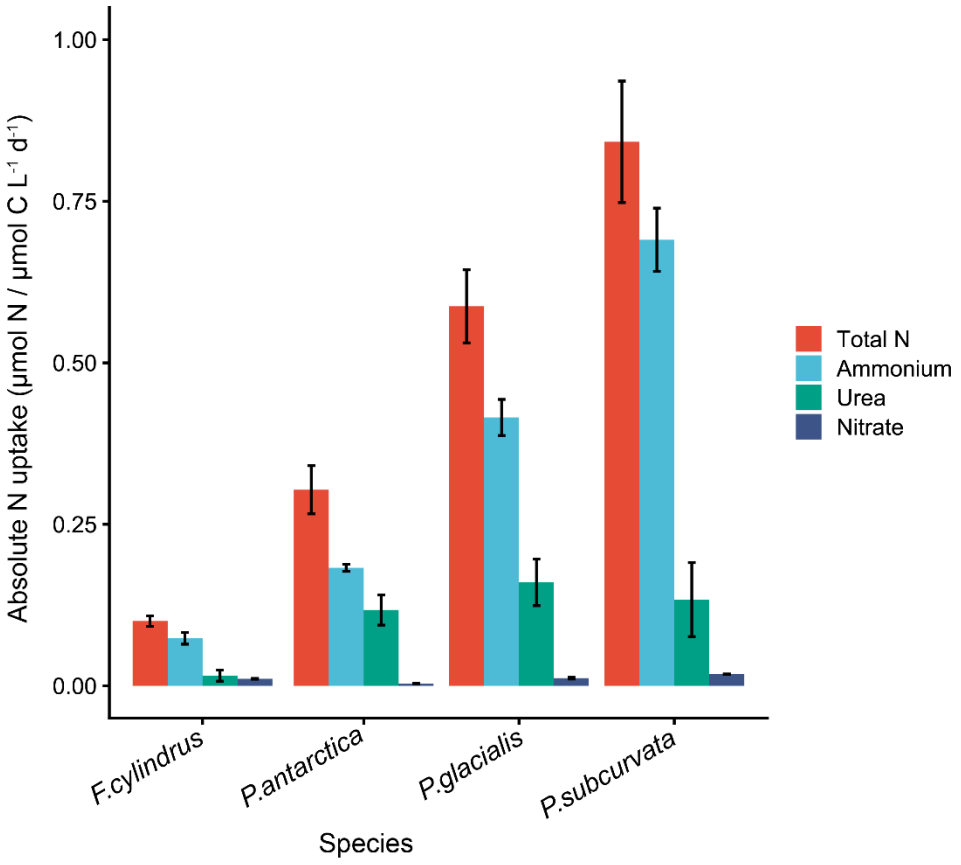

Figure 4.7: Absolute nitrogen uptake from NH_4^+, urea and NO_3^- normalised to carbon content for each phytoplankton culture. Total N is the sum of the three nitrogen sources. The uptake rate for NH_4^+ in all species except *G. cryophila* represents the corrected uptake value, accounting for the measured effect of NH_4^+ isotope dilution (see **Figure 4.3** for uncorrected values). Values represent daily uptake rates resulting from 24-hour incubations. Error bars indicate ±1 standard error of the mean.

4.4 Discussion

4.4.1 Multiple sources contribute towards nitrogen uptake by phytoplankton

Marine phytoplankton can assimilate fixed nitrogen in its oxidised (NO_3^-) and reduced forms (NH_4^+, urea, amino acids) through different uptake pathways (Glibert et al., 2016) with energetic costs varying by substrate. While NH_4^+ can immediately enter the Glutamine Synthetase-Glutamate Synthase (GS/GOGAT) pathway, NO_3^- must be first reduced through a two-step process, forming a NO_2^- intermediate, while urea is transformed to NH_4^+ through a urease mediated reduction (Antia et al., 1991). Consequently, the uptake of NH_4^+ is considered to be energetically favourable over other nitrogenous species (Syrett, 1981), indeed concentrations of NH_4^+ >1 µmol L^{-1} have been described as limiting for NO_3^- uptake

(Dortch, 1990). Under our experimental conditions, the concentration of NH_4^+ at the start of the experiments was 1.2-5.6 µmol L^{-1} (**Table 4.3**), in excess of the NO_3^- limiting threshold. However multiple studies have shown that in contrast to the early literature, NO_3^- limitation when NH_4^+ is available is rarely absolute, and variable by species and environment (Dortch, 1990 and references therein). Biologically, NH_4^+ uptake is related to temperature, under low temperature conditions uptake rates are low and kinetics in the GS/GOGAT pathway occur more slowly. In contrast, NO_3^- reductase favours cooler waters and NO_3^- uptake rates typically exceed an order of magnitude higher than for NH_4^+(Lomas and Glibert, 1999). Therefore, we may have expected to observe NO_3^- uptake at the NH_4^+ concentrations our experiments were performed under, representative of a typical high productivity coastal Southern Ocean environment. However, even without correcting for isotope dilution effects, NH_4^+ represented the largest source of nitrogen to all assessed phytoplankton species, with only a negligible contribution from NO_3^- (**Figure 4.3**).

The ubiquity of dominant NH_4^+ uptake across species suggests that the availability of NH_4^+ in our experimental setup is the key factor explaining the nitrogen source uptake. In the Southern Ocean, NH_4^+ concentrations are seasonally variable, peaking at 2-6 µmol L^{-1} across the highly productive shelf during the winter (Henley et al., 2017), and ~1.5 µmol L^{-1} in the open ocean (Mdutyana et al., 2020). Consequently, NH_4^+ dominates the wintertime uptake north of the sea ice zone while NO_3^- uptake during winter is low (Philibert et al., 2015, Mdutyana et al., 2020). The *f* ratio describes the proportion of 'new' productivity fuelled by NO_3^- compared to total productivity including regenerated productivity utilising NH_4^+or urea; in our study this was highest for *F. cylindrus* at 0.108, but <0.03 for all other species (**Table 4.7**). The relatively higher *f* ratio of *F. cylindrus* is consistent with a transcriptomic study which showed that *F. cylindrus* is less able to biologically adapt at the molecular level in order to utilise NH_4^+ compared to species such as *P. subcurvata* which upregulated of NH_4^+ transporter proteins during periods of increased nitrogen demand (Jabre et al., 2021).

Table 4.7: Absolute nitrogen uptake rates (µmol N/ µmol C L^{-1} d^{-1}) for NO_3^-, NH_4^+ (corrected for isotope dilution), urea and total nitrogen as shown in **Figure 4.7.** The *f* ratio is calculated as the ratio of the specific uptake rate of NO_3^- to the combined specific uptake rate of NO_3^-, urea, and NH_4^+.

Species	ρNO_3^-	ρNH_4^+	ρUrea	ρN	*f* ratio
F. cylindrus	0.01	0.07	0.02	0.10	0.108
G. cryophila	0.00	0.14	0.11	0.26	0.021
P. antarctica	0.00	0.18	0.12	0.30	0.019
P. glacialis	0.01	0.42	0.16	0.59	0.012
P. subcurvata	0.02	0.69	0.13	0.84	0.020

Comparatively, lower *f* ratio values of 0.03 have been measured in the Atlantic sector of the Southern Ocean during winter across the Subantarctic (here: 42-45 °S) (Philibert et al., 2015) and Polar Frontal (50°S) zones (Mdutyana et al., 2020). However, the values of <0.02 (*P. antarctica* and *P. glacialis*) are lower than typically reported for environmental studies, albeit acknowledging that very few measurements of wintertime nitrogen uptake have been made in the Southern Ocean. Several methodological factors could account for the lower *f* ratio values resulting from this experiment. The use of single species cultures minimises the effect of diverse nitrogen source assimilation among different species which are not included in this experiment but would be present in environmental samples. Additionally, although our cultures were not axenic, bacterial abundance remains far lower than in the environment. Therefore, our cultures likely had much lower rates of heterotrophic bacterial nitrogen utilisation, which accounts for a highly variable 5 to >90% of nitrogen uptake across different marine environments (Kirchman, 1994). However, in the Southern Ocean nitrogen uptake rates for heterotrophic bacteria have been shown to be very low (Reay et al., 2001), and fuelled by NH_4^+ (8-25% of total ρNH_4^+) when rates are at their greatest during phytoplankton blooms (Tupas et al., 1994). Consequently, widespread variability in the literature regarding bacterial nitrogen utilisation stemming from methodological limitations in isolating bacterial uptake from phytoplankton uptake (Cochlan, 2008) makes it difficult to determine to what extent the lack of bacterial nitrogen utilisation impacted the *f* ratio in these experiments.

However, if bacteria display a preference for NH_4^+ then this would serve to further reduce the calculated *f* ratio for our cultures. Correcting *p*NH_4^+ for isotope dilution will have reduced the calculated *f* ratio compared to the documented environmental samples but only marginally (<50%) compared to the several orders of magnitude by which *P. antarctica, P. subcurvata, G. cryophila and P. glacialis* differ from the lowest literature values. A better comparison between the uptake rates of nitrogen under culture and environmental conditions could be made in the future if methodological advancements allowed for species specific uptake rates to be determined in samples with mixed populations.

4.4.2 Diversity in carbon and nitrogen stoichiometry between species

Nitrogen uptake by marine phytoplankton drove cellular C:N stoichiometry across the species examined in our experiment, with total nitrogen uptake being inversely correlated to the cellular C:N value (**Figure 4.3,Figure 4.4**). *F. cylindrus* had the greatest C:N at 12.71 (± 0.57) while *P. subcurvata* had the lowest value (5.86 ± 0.21), which was also the closest C:N to the Redfield ratio of 6.625:1 (Redfield et al., 1963). The remaining species were all depleted in nitrogen and enriched in carbon (C:N of 7.75-9.54) relative to the Redfield ratio. The carbon enrichment is a surprising finding because C:N tends towards lower values in the nutrient-rich polar oceans (Martiny et al., 2013). High C:N values typically indicate nitrogen starvation as this leads to a decline in the synthesis of N-rich proteins and cells instead accumulate C-rich carbohydrates and lipids (Liefer et al., 2019). However, concentrations of NO_3^- were replete in our experiments (**Table 4.3**) and nutrient concentrations were similar for all species, therefore it is unlikely that any phytoplankton culture experienced nutrient stress. Iron limitation can reduce nitrogen assimilation, but where this occurs carbon assimilation has been shown to be impacted to the same degree (Maniscalco et al., 2022), and in any case the concentration of trace metals in F/2 media is multiple orders of magnitude greater than oceanic concentrations. In the environment, shifts in phytoplankton community composition from diatoms to coccolithophores are strongly correlated with an increase in C:N from high to lower southern latitudes, with Southern Ocean diatoms predicted to have C:N values lower than the Redfield ratio (~6) (Tanioka et al., 2022). This closely matches the observed C:N for the diatom *P. subcurvata* (5.86 ± 0.21), but contrasts with the much higher ratio for the other diatoms *P. glacialis* (8.28 ± 0.22) and *F. cylindrus* (12.71 ± 0.57). The total uptake of nitrogen for these C:N enriched species is 39.8 % and 91.6 % lower than for *P. subcurvata* respectively.

The larger size of diatoms relative to cryptophytes or haptophytes (**Table 4.1**), allows for greater accumulation of C-rich compounds, with C:N variability in smaller species being smaller, and driven by changes in lipid content (Liefer et al., 2019). Therefore, the larger C:N value in *F. cylindrus* should be considered within the context that variability in C:N is likely larger for *F. cylindrus* than other non-diatom species in this study.

As total nitrogen uptake in *F. cylindrus* is substantially lower than for the other diatoms assessed in this study (**Figure 4.3**, **Figure 4.7**) and C:N is substantially greater, this indicates that growth in this species is impaired (**Figure 4.4**). This is consistent with Finkel et al. (2016) who found a 16 % reduction in nitrogen rich protein content and a 45 % increase in C-rich carbohydrate content among microalgae in the stationary phase compared to when under exponential growth. There is widespread variability in the change in cellular stoichiometry in the stationary vs exponential phase, for example in an experiment where stationary phase was established by nitrogen starvation of the (non-polar) diatoms *Thalassiosira pseudonona* and *T. weissfloggi* the percent change in carbon was 77.5% and 164% respectively while nitrogen changed by -52.1% and -68.8% (Liefer et al., 2019). This reflects differences in macromolecular partitioning and storage within diatoms as a result of variable sizes and metabolisms, yet the agreement in directional changes indicate that large scale increases in C:N relative to the Redfield ratio are a function of growth limitation. From the available measurements it is unclear what led to growth limitation in *F. cylindrus*, as concentrations of macro and micronutrients were sufficient for growth, and salinities and pH's of the synthesised media were well within tolerance (pH: 7.86, salinity: 32.6 g kg^{-1}). One explanation could be that growth limitation was not induced by any one factor for *F. cylindrus* but that the culture was never viable, i.e., that no growth occurred across the duration of the experiment. Cultures can struggle to colonise new media when the dilution factor is too extreme, however biomass at the end of the experiment (given by the mass of POC) was no less for *F. cylindrus* than for species which had values of C:N and *p*N indicative of exponential growth such as *P. glacialis* and *P. subcurvata* (**Table 4.7, Figure 4.4**), indicating that growth must have occurred at some point since inoculation. The trend in growth over the duration of the experiment could have been better defined through daily growth rate measurements as this would have allowed for clear identification of the exponential and stationary phases. This was attempted with flow cytometry but unfortunately performed poorly across

replicates because of the widespread variability in a large volume mesocosm experiment. In >10 L cultures, phytoplankton have a tendency to settle; while agitation of the culture can redistribute phytoplankton homogenously to a degree, this has to be done carefully to avoid physical stress on cells. Salinity gradients within the mesocosm also provide some resistance towards redistribution. Additionally, determining cell counts in a 10 L culture from a 100 µl sample involves a 100,000-x scale factor which contributes substantially to the variability in the resulting normalised cell counts. A daily chlorophyll measurement was considered for this experiment, but it would have required a large sacrifice of experimental volume at the start of the experiment to have enough biomass for chlorophyll extraction (~500 ml), which would have impacted nutrient concentrations. A better approach would be to use an optical density proxy for growth, measuring absorbance of light at the wavelength for chlorophyll *a* (662 nm) (e.g., with a fluorometer), as this represents a good compromise between precision and sample volume (~10 ml).

4.4.3 Diversity in nitrogen uptake between species

Across all species, corrected values show a consistent trend in nitrogen sources, with NH_4^+ being the major (>50%) source, followed by urea and then NO_3^- (**Figure 4.7**); the energetics describing this trend have been previously described (**Section 4.4.1**). Here, we consider the differences in relative uptake by source, particularly the variable contribution of urea compared to NH_4^+ between species. The uptake of urea relative to NH_4^+ is highly variable across species, ranging from 19.3% ($\frac{p\mathrm{Urea}}{pNH_4^+}$ *100) in the diatom *P. subcurvata* to 80.1% in the cryptophyte *G. cryophila*. Interestingly, despite being the most dissimilar pair in terms of NH_4^+ and total nitrogen uptake (**Figure 4.7,Table 4.7**), proportional urea uptake is very similar between the two pennate diatoms *P. subcurvata* (19.3%) and *F. cylindrus* (21.4%). The value for the centric diatom *P. glacialis* is also lower (38.6%) relative to either the cryptophyte (*G. cryophila,* 80.1%) or haptophyte (*P. antarctica,* 64.3%). These divergent patterns in the relative contribution of urea are consistent with a known high level of diversity in the metabolic pathways of urea across different phytoplankton species (Solomon et al., 2010). The greater proportional utilisation of urea by non-diatoms matches with environmental studies showing that urea availability promotes the growth of cryptophytes and dinoflagellates to a greater extent than diatoms (Berg et al., 2003). The uptake of urea by haptophytes appears to be highly variable down to the species level, in communities

dominated by *Phaeocystis pouchetii,* uptake rates of urea have exceeded those of any other nitrogen species by an order of magnitude, accounting for up to 80% of nitrogen supply under NO_3^- depleted conditions (Sanderson et al., 2008). Yet in culture, *P. globosa* colony growth only occurs when NO_3^- is available as the primary nitrogen source (Wang et al., 2011). Wang et al. (2011) propose that solitary cells are responsible for urea drawdown by *Phaeocystis*, with colonies utilising NO_3^-. While no previous studies have measured direct uptake rates for *P. antarctica*, haptophyte blooms in the Ross Sea have been linked to NO_3^- depletion, suggesting that NO_3^- is an important nitrogen source to *P. antarctica* (Smith et al., 1998, Arrigo et al., 1999, Arrigo et al., 2000).

To understand why different phytoplankton types utilise proportionally different amounts of urea, we might consider that different nitrogen sources fulfil different physiological requirements beyond their primary nutritional roles. For example, the apparent preference of diatoms for NO_3^- has been attributed to a mechanism unique in diatoms which allows the excess uptake of negative electrons from NO_3^- to act as an energetic sink during periods between light harvesting and utilisation (Lomas and Glibert, 1999). Differences in urea uptake are usually attributed to physiological divergence in the number of urea transport proteins (Solomon et al., 2010 and references therein), or regulation of active transport processes by nutrient concentrations, particularly downregulation of genes encoding urea uptake proteins when NH_4^+ is replete (e.g. Rees and Syrett, 2006, Jauzein et al., 2008). Some uptake mechanisms may be specialised to specific phytoplankton types, for example a mechanism exists in some non-diatoms for extracellular hydrolysis of DON (here, amino acids), liberating NH_4^+ for cellular uptake (Palenik and Morel, 1990). Since urea can also be produced intracellularly, metabolic pathways linked to the catabolism of generated urea as well as regulatory divergence across the purine catabolic pathway introduce further opportunities for variance in urea utilisation between phytoplankton types. At a high level, possible differences in the urea cycle between phytoplankton groups include the multifunctional use of intermediates in urea catabolism, e.g., ornithine is a product of urease and is the pre-cursor to compounds used in diatom silica precipitation (Armbrust et al., 2004).

Such hypotheses demonstrate that different nitrogen sources play different roles in different phytoplankton types, with variability existing down to the species level. Since these additional roles are often unlinked to basic nutritional metabolism (e.g. excess NO_3^- uptake

acting as an electron sink), we must consider that comparing the uptake rates of different nitrogen sources to one another and between species is not a like for like comparison. Urea, for example could play a different number of roles in one diatom compared to another, and therefore the cellular requirement could be higher leading to a greater uptake, but the absolute concentration of urea partitioned to basic nutritional processes could be the same between these two species. To gain a holistic understanding of differences between species, biogeochemical uptake rates would need to be combined with a biological understanding of the role of nitrogen at the single cell level. This is occasionally possible in culture where some species have well annotated genomes but becomes much more difficult at the community level when applied to environmental studies. In these cases, we should be clear that uptake values describe the bulk utilisation of nitrogen compounds by the phytoplankton and bacterial community present, but provide low specificity regarding what these compounds are used for. Therefore, bulk uptake values should be used with caution when making comparisons at the species level or between the utilisation of different nitrogen sources.

4.4.4 Correcting for NH_4^+ isotope dilution

The 'isotope dilution' problem, describing the cellular release of $^{14}NH_4^+$ diluting the isotopic enrichment after spiking with $^{15}NH_4^+$, has been well known since the early 1980's (Gilbert et al., 2003). Despite this, many subsequent studies which conduct $^{15}NH_4^+$ uptake experiments fail to account for isotope dilution and acknowledge that this likely leads to an underestimation in $p NH_4^+$. Goeyens et al. (1991b) calculated the average rate of NH_4^+ regeneration for the Southern Ocean to be ~50 nmol N L^{-1} d^{-1}, this value has then been used to predict underestimation factors in $p NH_4^+$ (e.g. 1.09-1.24 (Mdutyana et al., 2020)), but as this value relies on one study in one region (Weddell Sea) at one time, it is unclear how robust this factor is to spatial, temporal and biological variation. Indeed, Smith et al. (2022) notes that NH_4^+ regeneration will have a lesser impact on $p NH_4^+$ when NH_4^+ concentrations are higher, suggesting that the importance of the isotope dilution effect itself may be seasonal.

Using a new chemical method for converting NH_4^+ to N_2O, we were able to measure the isotopic enrichment of the ^{15}N source pool at the end of the incubation, allowing us to apply an exponential decay function to the enrichment, accounting for dilution when calculating uptake. We found that a substantial amount of NH_4^+ regeneration occurred in all replicates

of all species in our experiments (*p*:P ≥ 1.28) (**Table 4.6**). Subsequently, the average underestimation factor (*p*:P) across the species in our experiments is ~1.34 (1.26-1.42) **(Section 4.3.4)**, slightly higher than that calculated by Mdutyana et al. (2020) and by Cavagna et al. (2015) (~1.17) for the Southern Ocean, although lower than the range (1.5-2.0) for prior studies (Rees et al., 1995, Elskens et al., 1997, Slawyk et al., 1997) across various global sites synthesised by Cavagna et al. (2015). Additionally, we did not observe any significant differences in *p*:P between species (**Table 4.6**), suggesting that biological variability in isotope dilution is probably low. A key difference between the rates of NH_4^+ regeneration measured in our experiment compared to Goeyens et al. (1991b) is the method for the measurement of $^{15}NH_4^+$ at the end of the experiment. While we perform a chemical method for the complete conversion of NH_4^+ to N_2O, confirmed by use of theoretically excessive concentrations of reagents resulting in low standard deviation between replicate samples **(Section 4.3.4)**, Goeyens et al. (1991b) refer to the isolation of remaining $^{15}NH_4^+$ by an unpublished "adapted diffusion method", likely an early version of (Holmes et al., 1998). Although the reported variance in the subsequent spectrometric analysis is low (<2%), the use of an alternative diffusion-based method makes it difficult to be certain that the measured pools of NH_4^+ between our two methods are consistent. Since this method is unpublished it is not possible to perform comparative experiments.

A contextual difference between the two approaches (culture vs environmental) is the wider biological community. Goeyens et al. (1991b) estimates that bacteria are the source of 11-99% of the total NH_4^+ regenerated through decomposition of organic nitrogen. Since our culture experiments contain substantially fewer bacteria than environmental samples, we might expect our *p*:P values to be lower than previously calculated because of the lack of bacterial remineralisation. Additionally, because NH_4^+ is regenerated from phytoplankton or bacterially derived organic matter, the lack of a viral community in culture experiments likely reduces cell death (and therefore OM release), compared to oceanic studies. A lack of a mesozooplankton community in our culture experiments probably has a minimal effect relative to the differences in microbial communities, since the rate of NH_4^+ production by krill was calculated to be <0.2 nmol L^{-1} h^{-1} (Goeyens et al., 1991b).

Here, culture experiments have demonstrated for the first time that the method of Liu et al. (2014) is effective for the chemical conversion of ^{15}N enriched aqueous NH_4^+ in a seawater

matrix to N_2O. Subsequently, this allows for the determination of isotopic enrichment of the source pool at T_1, fulfilling the requirements to calculate regeneration rates of NH_4^+ per Gilbert et al. (2003). The calculated NH_4^+ regeneration rates for Southern Ocean phytoplankton species in culture are slightly greater when compared to the few studies estimating these rates in the environment (Goeyens et al., 1991b, Cavagna et al., 2015). Differences in the biological community do not explain the greater rates in culture compared to environmental studies, if anything we may expect the reduced bacterial remineralisation in culture-based studies to result in a lower regeneration value than for oceanic samples. Since the methods between our uptake rates and those by Goeyens et al. (1991b) are not comparable, a future research priority will be to implement the reproducible method we deployed in culture experiments for environmental studies. We found that absence of NH_4^+ regeneration rates, which continues to be common practice, could lead to an underestimate in $p NH_4^+$ by 34 (±8) % based on experiments in culture. In environmental studies this could be even greater if bacterially derived NH_4^+ were to be included.

Although regeneration rates did not differ substantially between species as a result of biological variability (**Table 4.6**), the utilisation of resupplied NH_4^+ could depend on phytoplankton community composition in marine settings. For example, taking an average summertime uncorrected value for $p NH_4^+$ in the Southern Ocean of ~0.072 µmol L^{-1} d^{-1} (e.g. Rönner et al., 1983, Koike et al., 1986) ,and applying our calculated 34% underestimation factor, results in 0.037 µmol L^{-1} d^{-1} of NH_4^+ uptake (corrected – uncorrected value) being sourced from regeneration by phytoplankton. Propagating over the summertime season where these, and other comparable uptake rates have been measured (Nov-Jan) (Rönner et al., 1983, Koike et al., 1986, Nelson et al., 1987, Smith Jr and Nelson, 1990, Goeyens et al., 1991a), this would equate to 3.3 µmol L^{-1} of NH_4^+ uptake resulting from resupply by phytoplankton, roughly equivalent to the annual NH_4^+ maximum for the WAP (Henley et al., 2017). This is consistent with our understanding of the NH_4^+ seasonal cycle, whereby NH_4^+ concentrations are initially low in the early summer before reaching a wintertime maximum following accumulation over the summer. Using our value of NH_4^+ regeneration for Southern Ocean phytoplankton species, we can demonstrate that *in situ* regeneration of NH_4^+ by phytoplankton can theoretically account for the vast majority of this summertime accumulation. Since rates of NH_4^+ uptake did not differ substantially between the

investigated phytoplankton species, shifts in community composition may have a minimal impact on net NH_4^+ regeneration. However, considering the properties of different phytoplankton types holistically, increases in the proportion of smaller, more buoyant phytoplankton types around the coastal Antarctic under future climate change could help to maintain regenerated NH_4^+ in surface waters. Conversely, reductions in the proportion of fast sinking diatoms could reduce the flux of diatom associated NH_4^+ subducted to the ACC and subsequently reduce NH_4^+ concentrations in Subantarctic Mode Waters for export to the lower latitude oceans. Projections by CMIP6 models show 25-30% increases in productivity by all phytoplankton types in the coastal Antarctic (**Section 2.3.3.2**). Increases in regional productivity would suggest that rates of NH_4^+ regeneration are also likely to increase under future climatic conditions; the ecological balance between the phytoplankton types which contribute to this productivity increase will be crucial for determining the fate of regenerated NH_4^+.

4.4.5 Importance of incubation length for NH_4^+ uptake

An inconsistency between many experiments using the ^{15}N tracer technique for quantifying nitrogen uptake is the length of the incubation, which varies between 2 (e.g. Moschonas et al., 2017) and 24 hours (e.g. Joubert et al., 2011, Philibert et al., 2015, Mdutyana et al., 2020) across studies. The justification for a short (2-6 hours) incubation often refers to the protocols for the Joint Global Ocean Flux Study (Knap et al., 1996), which suggests that longer uptake experiments could be biased by non-linearity in NH_4^+ uptake over extended time periods. Subsequent studies further explain that a short incubation time prevents the build-up of regenerated NH_4^+, thus minimising the effect of isotope dilution (Gandhi et al., 2012, Smith et al., 2021b). Long incubations (24 hours) can be beneficial in the measurement of slow rates such as during winter (Mdutyana et al., 2020), or for conducting simultaneous measurements of uptake rates alongside ^{14}C, which requires a 24-hour incubation time to measure NPP. Where short incubations are conducted, daily uptake rates are calculated based on a representative 2–6-hour time period. By performing 6- and 24-hour uptake experiments using *F. cylindrus* we aimed to understand how representative a 6-hour incubation period is of the 24-hour cycle, and whether the extent of NH_4^+ regeneration differed between the two time periods. The dilution uncorrected and corrected uptake of NH_4^+ from the 6-hour experiments was compared to the uptake over 24 hours with pairwise

t-tests and in both cases resulted in a daily $p\mathrm{NH_4^+}$ rate which was greater for the 4x 6-hour experiment compared to the 24-hour experiment (**Figure 4.6**).

Therefore, either the 24-hour experiment underestimates $p\mathrm{NH_4^+}$ or the 6-hour experiment leads to an overestimation when converted to a daily rate. Long incubation experiments could lead to underestimations in uptake rates because ^{15}N which becomes incorporated by phytoplankton can be released as ^{15}N-DON before termination of the incubation (Bronk et al., 1994). Therefore, this released ^{15}N is missing from both the particulate phase (sink) and the $^{15}\mathrm{NH_4^+}$ (source) pools at the end of the experiment. Bronk and Glibert (1991) designed a method for measuring ^{15}N-DON release, by extraction of DON using an ion retardation resin, and found that over 30 hours 25% (± 10%) of the $^{15}\mathrm{NH_4^+}$ uptake was released as ^{15}N-DON. However, as they note, sample handling during the filtration process to separate DON from particulate matter can result in accidental release of intracellular DON through mechanical stress. DON directly released by phytoplankton is most likely to be of low molecular weight, isolating the ^{15}N-DON pool to just the low molecular weight fraction substantially reduced the ratio of $p\mathrm{NH_4^+}$ to ^{15}N-DON release to just 2% (± 2%) (Bronk and Glibert, 1991). Consequently, release of ^{15}N-DON may make only a small contribution towards describing the difference between the two experiment durations.

Given we observed statistically significant differences between the 6 and 24-hour experiments, an alternative explanation for higher uptake rate in the 6-hour experiment is that this represents an overestimation of the daily $\mathrm{NH_4^+}$ uptake because uptake rate varies throughout the day. This would be consistent with findings of diel cycling in $\mathrm{NH_4^+}$ and $\mathrm{NO_3^-}$ in other regions, for example Cochlan et al. (1991) showed that rates of $p\mathrm{NH_4^+}$ overnight were only 30-36% of the daytime uptake in the Subarctic Pacific, and that diel cycling in nitrogen uptake resulted in a preferential switch by these phytoplankton communities from $\mathrm{NO_3^-}$ during the day to $\mathrm{NH_4^+}$ overnight. Consequently, extrapolation of daily uptake rates from incubations conducted during 2–6-hour periods of daylight could lead to an overestimation by ignoring reductions in uptake overnight. As our experiments were conducted under an 18:6 light to dark cycle, and all 6-hour incubations were performed during the light period, reduced uptake in the 24-hour experiments during the dark period could account for the discrepancy in $p\mathrm{NH_4^+}$ (**Figure 4.6**).

It could be argued that the impact of diel cycling on nitrogen uptake is less important in the Southern Ocean because most experiments are conducted over summer when the seasonal light cycle dominates over diel cycling in higher latitudes (Tsakalakis et al., 2022). However, multiple studies have sought to investigate the impact of seasonality on nitrogen uptake, or nitrogen uptake in the lower latitudes of the Southern Ocean over winter, where phytoplankton are subject to diel light cycling (e.g. Cota et al., 1992, Kristiansen et al., 1992, Goeyens et al., 1995, Savoye et al., 2004, Philibert et al., 2015, Mdutyana et al., 2020). Use of consistent methodologies which can account for the potential impact of diel cycling, even when this is not anticipated to have an impact on uptake, would subsequently allow for more robust comparisons of nitrogen uptake rates between seasons and regions if methodological variations are reduced.

4.5 Conclusion

The uptake of nitrogen, and particularly NH_4^+, is a key research interest in the Southern Ocean biogeochemical community, particularly as growth seasons lengthen in response to climate induced sea ice losses, placing a greater demand on nitrogen than has previously been observed. The aim of this chapter was to establish how changing phytoplankton species composition could impact nutrient stocks by determining the rate of nutrient acquisition for a suite of Southern Ocean phytoplankton. This chapter represents the first application of a chemical method for the conversion of $^{15}NH_4^+$ to $^{15}N_2O$ in a seawater matrix to measure NH_4^+ regeneration rates in culture experiments, allowing for a more accurate measurement of nitrogenous nutrient uptake than has previously been achieved. Using a suite of Southern Ocean phytoplankton, we conducted a series of experiments which investigated: a) the impact of biological variability between species on nitrogen acquisition and rates of NH_4^+ regeneration, and b) the ability of methodological variation to contribute to uncertainty in nitrogen uptake rates.

Addressing the role of biological variability, we found that the biomass normalised uptake of combined nitrogen sources (*p*N) differed substantially between phytoplankton species, but rates could not be directly attributed to differences in species size or phytoplankton type (e.g., diatoms vs non-scilifying phytoplankton). The pennate diatoms *P. subcurvata* and *F. cylindrus* represented both the highest (0.84) and lowest (0.10) *p*N values across the included species. An elevated C/N ratio in *F. cylindrus* indicated that nitrogen uptake by this species

was impaired due to growth limitation, however no causal factor for growth limitation could be identified. Since the biomass of this culture was similar to other species, it appeared that this culture entered a stationary phase following a period of exponential growth. In future experiments, closer monitoring of growth using bulk proxies (e.g., optical density) would make it easier to ensure consistency in performing uptake experiments during the same part of the growth phase among species.

NH_4^+ was the major source of nitrogen to all species, comprising >50% of total nitrogen uptake following correction for isotope dilution effects. Urea was the secondary source for all species, while NO_3^- made a negligible contribution, following previously established inhibition of NO_3^- uptake in the presence of high concentrations of NH_4^+. While the total uptake of nitrogen differed between the two pennate diatom species, the proportional uptake of urea relative to NH_4^+ was very similar between *F. cylindrus* and *P. subcurvata* (~20%). The proportional uptake of urea did vary with phytoplankton type, being lowest in the diatom species and highest in the cryptophyte (*G.cryophilia,* 80.1 %) and haptophyte *(P. antarctica,* 64.3%). Biologically this trend can be described by catabolic differences between phytoplankton types; in particular the ability of some cells to hydrolyse DON to NH_4^+ extracellularly has been identified in non-diatom species (Palenik and Morel, 1990). Nitrogen is utilised differently by different phytoplankton species, often to fulfil cellular roles which do not relate to the simplistic view of nutrients directly fuelling growth. Consequently, we suggest that species specific uptake rates should be viewed within the context that theoretical catabolic nitrogen demand is highly variable even within phytoplankton groups, making it difficult to make intercomparisons of how well nitrogen uptake matches demand between species.

Secondly, we showed that widespread variability in the incubation duration of $^{15}NH_4^+$ uptake experiments has the potential to introduce statistically significant differences in pNH_4^+ when values are normalised to daily rates. Based on literature from other regions we hypothesise that diel cycling in NH_4^+ uptake could be responsible for the overestimation of pNH_4^+ in short incubations (6 hours) compared to long incubations (24 hours). This is particularly relevant for our culture-based experiments which employed an 18:6 light cycle. While the effects of diel cycling may be less important for experiments in the high latitudes during summer, we suggest that a consistent methodology composed of 24-hour uptake values and

inclusion of isotope dilution corrections will allow for greater interoperability between ^{15}N tracer studies.

Finally, considering the contribution of methodological variability to our uncertainty in Southern Ocean nutrient cycling, we found that across all species, accounting for NH_4^+ regeneration increased pNH_4^+ by an average of 52%. This value was approximately twice that given by the prior estimations of NH_4^+ regeneration in the Southern Ocean based on oceanic samples (Goeyens et al., 1991b, Cavagna et al., 2015). However, undocumented methods were used to isolate the NH_4^+ in these estimations, which prevents direct comparisons against our values. Since modern studies continue to use the regeneration value of Goeyens et al. (1991b) to correct for isotope dilution, we suggest that our work provides the basis for implementing the $^{15}NH_4^+$ chemical conversion method on environmental samples across the Southern Ocean and more widely across marine settings. More values of NH_4^+ regeneration using reproducible methods are required to understand how accurate the values of Goeyens et al. (1991b) are, and how representative the values provided by our culture experiments are of natural populations. Given the ability of NH_4^+ regeneration to substantially alter pNH_4^+, an expansion of the inclusion of accurate NH_4^+ regeneration rates resulting from different phytoplankton types could have wider implications for our understanding of Southern Ocean nitrogen uptake and for budgeting excess nutrient export to the global ocean.

Taking both the role of biological and methodological variability together; as the productivity regime in the Southern Ocean continues to change in response to warming, including projected increases in productivity and potential changes in phytoplankton species composition, we can expect this increased biological variability to alter the net magnitude of nutrient utilisation. Consequently, employing consistent methodologies in measuring nitrogen uptake will improve the collective power of Southern Ocean nitrogen uptake data, providing a clearer understanding of the impact of seasonal transitions and spatial variability on nitrogen uptake for this data sparse region during a period of rapid climate driven environmental change.

5. Synthesis and Conclusions

5.1 Summary and implications of findings

Within the context of ongoing rapid environmental change across most of the Southern Ocean, this thesis sought to determine the extent to which these climate induced changes impact phytoplankton communities, and the subsequent implications for carbon and nitrogen cycles. This thesis first set out to establish the current state of knowledge regarding the physical, chemical and ecological response of the Southern Ocean to projected climatic changes over the current century using an ensemble of CMIP6 models. Subsequently, it then focused on advancing our understanding of the mechanistic relationship between phytoplankton species composition and carbon and nitrogen cycling through a series of *in situ* and laboratory studies. Each of these chapters aimed to investigate in detail a specific component of the ecological-biogeochemical coupling for carbon and nitrogen which were hypothesised to be responsible for a substantial amount of uncertainty in our existing understanding. For carbon, this was the relationship between phytoplankton species composition and DOM production, including the persistence of DOM over depth. For nitrogen, the species dependent variability in uptake of different nitrogen sources and rates of ammonium regeneration were investigated. Through experimentally targeting mechanisms identified as responsible for uncertainty in the assessment of CMIP6 models, namely nutrient half saturation constants, variable carbon production by phytoplankton types, and shifts in community composition, the findings of this thesis can contribute towards an improved representation of the coupling of phytoplankton, carbon and nitrogen cycling in the next generation of earth system models. Continued advancement in the representation of mechanistic ecological-biogeochemical feedbacks could be expected to reduce the discrepancy between observed and projected changes in ocean carbon storage at the Southern Ocean and global scale. This will improve our ability to project the impacts of climate change on the ocean as part of the global scale climate models used to inform policy-making decisions, essential for protecting the fragile environments of the Southern Ocean.

5.1.1 Phytoplankton type as a source of variability in carbon cycling

Projections of ocean carbon uptake using CMIP6 result in underestimates when compared to observation based estimates (Terhaar et al., 2022). Since the Southern Ocean is the largest

marine sink for anthropogenic carbon (Caldeira and Duffy, 2000, Frölicher et al., 2015), it is an obvious target for reducing this discrepancy by improving model estimates. Because the biological uptake of CO_2 is responsible for driving the Southern Ocean from being a wintertime source of carbon to a summertime sink (Hauck and Volker, 2015), understanding changes in the regional phytoplankton community, and coupling to the carbon cycle, provides a basis for improving model estimates of global marine carbon cycling.

To gain a comprehensive view of projected physical, ecological and biogeochemical change, Chapter 2 presents the first regional analysis of multiple variables associated with productivity for the Southern Ocean using CMIP6. From a multi-model mean, an average increase in productivity (as particulate organic carbon production) of 30% was projected across the Southern Ocean by 2100 under a high emission pathway (SSP 5-8.5). Yet across the regions of the Southern Ocean, different phytoplankton types were responsible for driving this increase. While diatoms and pico-/miscellaneous phytoplankton contribute roughly equally to productivity increases across the Subantarctic and Transitional zones (40-65°S), pico-/miscellaneous phytoplankton are projected to increase at rates exceeding those of diatoms in the Antarctic coastal zone. This is important within the context of the carbon cycle because in key regions where pico-/miscellaneous phytoplankton are expected to increase the most, namely the west Antarctic Peninsula and Amundsen Sea, productivity increases but nutrient availability and chlorophyll show relatively little change. Observable variables (e.g., chlorophyll and nitrate concentrations) are often used to deduce productivity, but when phytoplankton types change, the resulting chlorophyll to carbon ratio can also substantially differ (Sathyendranath et al., 2009), which impedes inference of productivity from optical measurements.

One approach towards resolving this inherent variability between phytoplankton groups and carbon production is to determine how the finer scale carbon cycle varies at the functional group level. Within the context of Southern Ocean phytoplankton types, diatoms are seen as efficient exporters of carbon because organic matter becomes incorporated with silica and sinks rapidly. In contrast smaller phytoplankton types remain more buoyant where there is a greater likelihood of remineralisation. Linking back to the discrepancy in carbon uptake, if phytoplankton associated organic matter is rapidly re-released as CO_2 in the surface layer, the net CO_2 uptake is negligible relative to efficient exporters which export carbon below the

mixed layer. Since the microbial remineralisation of organic matter is dependent on the lability of organic molecules, determining the molecular level composition of phytoplankton derived organic matter can provide an insight in to the efficiency of carbon export. While this is not a new method, we have shown that contrary to previous understandings, there is a benefit in conducting such analyses in the Southern Ocean despite the low DOC concentrations, because fresh DOM signals can be detected before they become transformed to the background refractory signal.

Therefore, Chapter 3 presents results from an *in-situ* study examining the composition of dissolved organic matter associated with different phytoplankton types along the West Antarctic Peninsula, one of the regions identified as having a high likelihood of undergoing phytoplankton compositional shifts towards smaller species in Chapter 2. The study presented in Chapter 3 built on previous work in Dittrich et al. (2022), which postulated that phytoplankton may be responsible for a small amount of DOM release during growth because of direct correlations between DOC and POC in the build-up of the bloom phase. This is in contrast to the long-established belief that little to no DOM was directly produced by phytoplankton in the Southern Ocean because of very low measured DOC concentrations (e.g. Ducklow et al., 2012, Rozema et al., 2017a), with the background DOC pool resulting from degradation of particulate organics following cell death. A limitation in these prior studies was in attempting to determine production or DOM source from bulk DOC/DON concentrations, which can only quantify the amount of DOC and DON present, but provides very little analytical power to resolve source or fate. Chapter 3 represents one of the most comprehensive studies of DOM performed globally, resolving solid-phase extracted DOM for molecular, stoichiometric and isotopic properties. After coupling with an image-analysis derived community composition database for the WAP region, this allowed for the identification of a 'fresh' signal of labile DOM in surface waters inhabited by the small cryptophyte and mixed flagellate populations. Conversely, DOM in diatom dominated waters was more refractory in composition, with a greater degradation index, indicative of the aged DOM pool which accumulates at depth but can be routinely overturned in surface waters through upwelling. While the fresh signal can be interpreted as resulting from direct DOM production by smaller phytoplankton communities, the absence of this signal in diatom inhabited waters is in agreement with our understanding of diatoms being efficient

exporters, with greater partitioning of OM to the particulate phase, allowing for rapid export of carbon out of the surface layer.

Consequently, by contextualising the findings from Chapter 2, that the WAP is a region expected to undergo shifts in phytoplankton type towards pico- and miscellaneous phytoplankton, with our new mechanistic evidence that smaller phytoplankton types are associated with *in situ* DOM production, this indicates that the WAP will become a less efficient region for carbon uptake and export in a future Southern Ocean. Additional implications of this change could include reduced trophic transfer efficiency, with the dense krill populations along the WAP shelf being less able to utilise smaller phytoplankton types as an energy source for growth and reproduction. However, greater rates of microbial remineralisation in the surface layer resulting from increased DOM concentrations may liberate increased concentrations of nutrients for global export, with a further feedback on global scale productivity in macronutrient limited regions.

5.1.2 Nutrient utilisation in a future Southern Ocean

Determining the extent to which Southern Ocean nutrients will fuel global productivity in the future is a key research interest because productivity across the macronutrient limited global ocean is projected to decrease in contrast to increases in the Southern Ocean. Nutrient leakage from the Southern Ocean currently accounts for 62 (±5%) of upper ocean nitrate and phosphate supply (Fripiat et al., 2021). Projected increases in productivity could suggest that, despite potential increases in nutrient resupply from DOM remineralisation, phytoplankton nutrient utilisation will increase and therefore leakage will reduce. Earth system models take a broad approach to modelling phytoplankton types, such that the nutrient utilisation, (termed as the half saturation constant) is a fixed value per phytoplankton type included in a model, rarely exceeding 3 functional types (see **2.3.3.1**). This proposes that, for example, all diatoms at all locations in the global ocean have the same requirement for a particular nutrient. Chapter 4 sought to determine to what extent nitrogenous nutrient uptake varies between Southern Ocean phytoplankton types, using ^{15}N isotopic tracers to measure the incorporation rate of ammonium, urea and nitrate in culture experiments.

While the preference for nutrients was consistent between all phytoplankton types (ammonium > urea > nitrate), consistent with energetic favourability for ammonium as a reduced form of nitrogen (Glibert et al., 2016) , the absolute uptake differed substantially

between species. The greatest example of variability was between the two diatoms *Pseudo-nitszchia subcurvata* and *Fragilariopsis cylindrus* which had the greatest and lowest total uptake of nitrogen among the five included species respectively. This result is in contrast to the model assumption that all diatom types utilise nutrients equally and consequently could be a source of uncertainty in regional nutrient utilisation and export towards global productivity. However, these experiments are not without their own uncertainties, and the potential for growth limitation being a contributory factor towards the discrepancy in nitrogen uptake between diatoms is discussed in more detail in section **4.4.2**.

Methodological variability was of particular interest in Chapter 4 because approaches using ^{15}N tracers were found to be highly inconsistent in incubation length and in accounting for isotope dilution resulting from ammonium regeneration. The variability in nitrogen uptake spatially, temporally and by phytoplankton type remains largely unknown for *in situ* studies. Comparing the different methodological approaches for ^{15}N uptake revealed that negating ammonium regeneration led to an average underestimate in ammonium uptake of 34 ±8 %. A new method was adapted for the determination of $^{15}NH_4^+{}_{(aq)}$ in seawater, which could allow for consistent application of a method accounting for ammonium regeneration in future studies. At the larger scale, application of a defined method would improve our ability to build a regional scale understanding of nitrogen uptake by increasing interoperability of results. The widespread differences in nitrogen uptake between similar species in the culture experiments presented here presents a new research priority of measuring nitrogen uptake and ammonium regeneration across different environmental niches to determine the extent to which biological variability drives differences in nutrient uptake. Applying the calculated rate of NH_4^+ regeneration from culture experiments to environmentally measured rates of NH_4^+ uptake in the Southern Ocean showed that regeneration can account for the summertime production of NH_4^+ at concentrations similar to the observed annual maxima. Therefore, biological properties of the phytoplankton species performing NH_4^+ regeneration could be an important determinant of NH_4^+ fate, with smaller buoyant species likely to retain NH_4^+ in surface waters while NH_4^+ associated with fast sinking diatoms is more likely to enter the deep-water circulation and be subsequently exported. Under a regime where Southern Ocean productivity increases, defining the nutrient utilisation expected with changing phytoplankton communities will be essential for resolving excess nutrient availability for

export across the global ocean, and subsequently for improving estimations of global scale productivity.

5.2 Experimental limitations

In Chapter 2, CMIP6 models are used to understand projections of changes in phytoplankton type across the Southern Ocean with climate. Previous studies have addressed this research question at the global scale using more advanced ecological models (e.g. Henson et al. (2021), use a model with 35 phytoplankton types (described in Dutkiewicz et al. (2020)), compared to the two or three types included in the biogeochemical component of CMIP6 models. Since these large-scale ecological models include far more functional types of phytoplankton, they will, by definition, provide a finer scale resolution of ecological change than is possible with CMIP6 series models. Therefore, it could be argued that CMIP6 models are not an appropriate tool to investigate changes in functional type. Other limitations include the lack of explicit size class in phytoplankton types and consistency in the number of types between models, which reduces the power of multi-model means as these can only be generated from models which include the same groups. However, regardless of whether phytoplankton are well or poorly represented in CMIP6, it remains true that these models explicitly include phytoplankton, and phytoplankton do functionally alter biogeochemical variables as nutrient utilisation and carbon content differ by phytoplankton type. Therefore, the purpose of Chapter 2 is not to predict ecological change, but to investigate the way in which variability in the phytoplankton type parameter impacts biogeochemical projections. This remains an important research question because biogeochemistry in CMIP6, particularly nutrient limitation and primary productivity (as POC production), are responsible for driving much of the global marine carbon cycle. Subsequently, projections of oceanic carbon uptake in CMIP6 feed in to policy making decisions at the intergovernmental level. Yet discrepancies between modelled and observed ocean carbon uptake indicate that further development is required to resolve marine carbon dynamics in CMIP6. This chapter aims to strengthen the representation of Southern Ocean biological carbon cycling through identifying spatial and temporal regions where existing models project the largest changes, such that future work by the observational community can target resources towards likely end members of change in the region. Additionally, acknowledging the computational limitations of adding complex ecosystems to global climate models, specific mechanisms which are currently missing from

the existing CMIP6 model suite are identified as targets for future model development. This therefore differentiates Chapter 2 from prior studies which examined ecological change through developing new standalone models. Working within the existing model framework, this chapter sought to strengthen the observational evidence base to improve the representation of Southern Ocean biogeochemistry, as a key driver of the global carbon cycle, in future generations of CMIP.

The *in situ* study conducted within Chapter 3 includes the most comprehensive assessment of DOM composition across the Southern Ocean, but is caveated by multiple methodological and logistical limitations. A key strength of this work is the spatial resolution covered within the study, which allowed for the identification of different phytoplankton communities, and the attribution of phytoplankton types to molecular signatures. However, a compromise in covering such a large area was in the timing of sampling. While early (northern) stations were sampled closer to the summertime productivity peak in early January, later stations were not reached until almost a month later. This effect was further compounded by the record low sea ice concentrations of the 2022/23 season which likely resulted in earlier blooms, with phytoplankton concentrations being consistently low across the majority of sites. Since Southern Ocean productivity is highly seasonal, this time lag probably had a substantial impact on the magnitude and composition of phytoplankton communities. However, as the aim of this study was to link the present phytoplankton types to the present DOM types, the timing lag should not have impacted the phytoplankton-DOM association. This is provable because of the rapid rate of DOM transformation observed, and the short lifetime of labile compounds in the surface (Dittmar et al., 2021), i.e., fresh DOM produced by a community several weeks prior would not still be present in the surface waters of a different community later in the season. Additionally, abundance of different phytoplankton types rather than just composition was used as the input for statistical analysis, such that differences in the magnitude of phytoplankton communities were accounted for when determining significance.

Following the work by Dittrich et al. (2022), which found DOM release to be greatest during the build up to the bloom, the most likely impact of the timing lag was in missing some pulses of DOM release which would have strengthened our ability to associate molecular signatures to phytoplankton by providing more fresh DOM types. We were unable to find

the molecular signature of fresh DOM production co-located with diatom populations in this study, leading us to associate diatoms with a low partitioning of organic matter to the dissolved phase, however it is possible that DOM release from these well-established communities was missed. A methodological limitation to identifying fresh production is the targeting of solid phase extracted DOM. This is necessary for molecular analysis of DOM because of the requirement to both concentrate and de-salt marine derived DOM for FT-ICR-MS analysis. The PPL cartridges used for extraction in this study were judged to have the highest extraction efficiency of the available options in Dittmar et al. (2008), because of its ability to bind a wide range of polarities and a low pore size (150 Å). However, comparable to other studies (Dittmar et al., 2008, Jerusalén-Lleó et al., 2023), there is a low extraction efficiency for SPE-DOM in Antarctic waters, here, 38 % (± 9 %). This is because PPL has a selection bias towards nitrogen poor, low molecular weight and recalcitrant DOM (Jerusalén-Lleó et al., 2023), whereas much of the DOM produced in the Southern Ocean is nitrogen rich (Ogawa et al., 1999), and held in non-SPE extractable forms such as carbohydrates and amino acids. Given that the majority of DOM released by phytoplankton during cell lysis is dominated by carbohydrates and nitrogen rich compounds (Lancelot, 1984), this presents an obvious barrier to identifying fresh DOM production using solid phase extraction. However, the major benefit to this approach is that it provides a consistent reference window between samples, so we are always analysing the same ~38% pool of DOM between samples. This allows for comparisons to be drawn between samples at the molecular level, with the 'fresh' and 'aged' pools identified relative to the range of molecular compositions in the dataset.

The culture-based experiments in Chapter 4, are by definition an analogue to environmental processes. While studying phytoplankton in culture provides a unique benefit in being able to study species individually, removing many of the physical and ecological interactions which would occur naturally is a limitation on the wider application of these results to an environmental context. For example, in Chapter 4, the role of bacterial uptake of nitrogen was discussed as a possible difference in total nitrogen uptake between low bacteria culture experiments and a high bacterial abundance in marine settings. Efforts were taken to make the culture conditions as close as possible to a Southern Ocean summertime environment, matching temperatures, light concentrations, salinities, pH and nutrient concentrations. However, these nutrient concentrations were derived from a time series of nutrients along

the highly productive WAP, where NH_4^+ reaches high (~2 μmol L^{-1}) values during the summer (Henley et al., 2017). Consequently, the majority of nitrogen uptake across all species in culture was fuelled by NH_4^+, which is not representative of the predominantly NO_3^- driven nitrogen uptake across the Southern Ocean, especially in seasons and regions with lower NH_4^+ concentrations. Therefore, conducting these experiments with different nutrient concentrations would likely have yielded different results.

Biological variability is also an important factor to consider; this study only included 5 species out of the >350 identified in the Southern Ocean (Deppeler and Davidson, 2017), so represents a small sample size. Using species which have been isolated in culture is itself a selection bias as many species are not amenable to culture conditions, for example mixotrophs perform poorly in culture but are an integral part of the marine ecosystem, especially in relation to nutrient acquisition having both heterotrophic and autotrophic pathways. The use of a small sample number of species is largely constrained logistically by incubator space, with each species requiring triplicate measurement of the uptake of three nutrients in parallel, with a total volume of ~10 L. Biological variability was accounted for in experimental design by selecting species which represented the main groups of Southern Ocean phytoplankton and including three species of diatoms. The choice to include multiple diatom types revealed the existence of substantial variability in nitrogen uptake within the diatom group, suggesting variability within diatoms should be a key consideration for both these types of experiments and also in model representation of diatom populations.

5.3 Recommendations and future research

In addition to the conclusions drawn by this thesis, opportunities for furthering the work presented here have been identified as a result of developing new methods, defining mechanisms, analysing model deficiencies, and considering limitations of these studies. Considering the *in-situ* study, resolving the temporal variability between sampling sites would be a clear way to expand this work and complement the spatial variability covered in Chapter 3. Temporal variability would be best addressed by remaining within a fixed study area (e.g., the US Palmer Station Time Series or the UK Rothera Time Series), and repeatedly sampling for DOM and phytoplankton over the seasonal transitions. Integrating the work of Dittrich et al. (2022), which indicated that DOM production during bloom build up could be detected by coincident increases in POC and DOC, it would also be recommended to expand

sampling to include POC measurements. This would allow us to address how the dissolved to particulate partitioning of organic matter changes over the duration of a bloom and compare the phytoplankton group specific POM to DOM partitioning trends with the existing literature on this topic from other regions. Given the increasing focus of the scientific community on potential changes to phytoplankton phenology with the ongoing rapid reduction in sea ice concentrations, determining at which times in a phytoplankton growth cycle carbon export is most efficient, and whether this differs by phytoplankton type, would be useful for estimating potential ecological feedbacks of sea ice loss on the carbon cycle.

Noting that fresh production of DOM is likely to be composed largely of compounds which would not be isolated in solid phase extraction, a station-based study may also incorporate additional measurement for carbohydrates and amino acids. Such studies could be limited by biological variability, since most of the biological time series are based along coastal regions of the WAP with high meltwater fluxes and stable water columns which are well suited to dense diatom blooms. However, a network of these time series stations (e.g., including stations in the South Shetland Islands and across the Subantarctic) could encompass enough biological variability to assess seasonally resolved variability in the phytoplankton-DOM relationship.

Learning from the work conducted during this *in situ* study, I would recommend concentrating DOM sampling to the surface ocean (upper 50 m). SPE-DOM analysis and sample acquisition is costly, such that I made a strategic decision to prioritise fewer full depth water column profiles over an increased number of profiles with lower depth resolution. The aim here was to determine the extent to which surface level productivity changes impact carbon storage at depth. However, the results of this indicated a highly homogenous DOM profile in the deep ocean, consistent with the background refractory pool. Therefore, in the future resources could be strategically deployed to focus on increasing spatial or temporal resolution in surface samples over increasing the number of samples per depth profile.

Some prospects for future work in advancing the investigation in to nitrogen uptake measurements (Chapter 4) have been previously alluded to, for example reducing biological variability through increasing the number of species used, changing the ambient nutrient conditions to reflect regional variation, and improving measurements of growth using optical

proxies. However, the most useful output from this project is in the development of the chemical-based method for measuring ^{15}N enriched $NH_4^+{}_{(aq)}$ in seawater. A key limitation in our understanding of nitrogen utilisation is the uncertainty in ^{15}N uptake rates because of the impact of isotope dilution through NH_4^+ release. The carryover of a few literature values of regeneration to correct modern rates of NH_4^+ uptake likely introduces further uncertainty to these rates, which are essential for constraining the Southern Ocean nutrient budget under future conditions with changing phytoplankton communities. Therefore, a key test for this method will be in deploying it to make environmental measurements of NH_4^+ regeneration. The ultimate aim would be to develop a circumpolar database of NH_4^+ uptake rates, allowing the process of NH_4^+ uptake to be linked to biological, physical and temporal variables. To develop the method further, more work could be conducted to further reduce the isotope dilution effect by addressing DON regeneration, requiring a new method to advance the previous approach towards isolating the isotopic composition of urea (4.4.5). The result of these efforts will be to better constrain nitrogenous nutrient utilisation by different types of phytoplankton, both across the Southern Ocean and globally. By applying a consistent methodology producing accurate uptake rates, we can seek to address the question of biological variability within phytoplankton types at the global scale. For example, while most models include just one diatom group, it remains unclear how much uncertainty this introduces when compared to environmental measurements of the sample phytoplankton type in different regions (i.e., does a Southern Ocean diatom have comparable nutrient utilisation rates to a Pacific Ocean diatom?). Generating an evidence base for such questions will be invaluable in determining the least computationally demanding way of increasing ecosystem complexity in large scale earth system models. For example, perhaps models could include phytoplankton groups defined on their biogeochemical rates as opposed to arbitrary ecology-based classifications of groups such as “diatoms” or “picophytoplankton”.

Linking to the initial assessment of CMIP6 models in Chapter 2, this thesis has shown that to truly bridge the gap between observations and models (and laterally policy), observations need to be designed with the existing model architecture in mind. The approach demonstrated here of identifying mechanistic gaps in model representations of biogeochemical processes and then targeting experiments to define the relationship

between biogeochemistry and ecology fundamentally differs from a perspective which produces scientific knowledge first and seeks to apply it to models post-hoc. Chapter 2 demonstrated that they key ways in which phytoplankton influence biogeochemical and carbon dynamics in CMIP6 are through the relationship between phytoplankton type and carbon production, alongside differences in nutrient uptake by different phytoplankton groups. The overarching aim of this thesis has been to work towards defining these mechanisms, both through an experimental perspective on the phytoplankton-carbon relationship and in developing the methods to facilitate future work to precisely measure nutrient acquisition rates. Through wider application of the examples demonstrated here, and collaborative incorporation within the earth system model framework, this provides a way forward towards improving our understanding of the changing biogeochemistry and ecology of the Southern Ocean in an era of rapid environmental change.

6. Appendix: Raw data for Chapter 3 including the physical, stoichometric and molecular data for each SPE-DOM sample.

Sample #	Date	Time (GMT)	Site	Lat	Lon	Vol filtered (L)	Depth(m)	Pressure(dbar)	Potential Temperature (°C)	Salinity(g/kg)	Fluorescence (mg m^{-3})	DOC_avg (µmol L^{-1})	TDN avg (µmol L^{-1})	Empty vial (g)	Full vial (g)	Sample volume (ml)
3	05/01/23	07:06	C1	-64.933	-64.400	2	3.23	3.26	2.53	33.95	5.46	72.78	23.80	8.6421	13.2001	5.760
4	05/01/23	07:06	C1	-64.933	-64.400	2	15.42	15.57	2.20	33.96	3.88	47.73	25.80	8.6196	11.1934	3.253
5	05/01/23	07:06	C1	-64.933	-64.400	2	49.96	50.46	0.68	34.19	0.05	45.36	30.77	8.5846	13.2194	5.857
6	05/01/23	07:06	C1	-64.933	-64.400	2	101.24	102.27	0.69	34.35	-0.01	40.61	33.11	8.6096	12.7585	5.243
7	05/01/23	07:06	C1	-64.933	-64.400	2	400.13	404.48	1.37	34.64	-0.07	45.35	35.90	8.6408	13.1178	5.658
8	05/01/23	07:06	C1	-64.933	-64.400	2	1300.19	1317.21	1.46	34.68	-0.07	41.53	34.98	8.6731	13.3793	5.947
9	09/01/23	13:46	S1	-64.608	-68.293	2	5.21	5.26	1.26	33.88	0.00	63.62	24.32	8.6952	13.3124	5.835
10	09/01/23	13:46	S1	-64.608	-68.293	2	14.92	15.06	1.25	33.88	0.17	62.21	26.54	8.5993	13.2888	5.926
11	09/01/23	13:46	S1	-64.608	-68.293	2	49.81	50.31	1.02	33.90	0.62	41.38	26.38	8.6453	13.2132	5.773
12	09/01/23	13:46	S1	-64.608	-68.293	2	101.60	102.63	1.39	34.40	0.06	38.81	36.42	8.624	13.4461	6.094
13	09/01/23	13:46	S1	-64.608	-68.293	2	250.95	253.58	1.91	34.65	-0.06	40.61	35.88	8.6402	13.2652	5.845
14	09/01/23	13:46	S1	-64.608	-68.293	2	2676.50	2720.41	0.29	34.70	-0.06	41.27	34.07	8.5549	12.9129	5.507
15	11/01/23	14:11	C2	-65.878	-68.286	2	2.80	2.83	1.52	33.90	0.18	50.40	25.27	8.6391	13.1483	5.698
16	11/01/23	14:11	C2	-65.878	-68.286	2	10.28	10.38	1.52	33.90	0.22	48.55	25.63	8.6176	13.3536	5.985
17	11/01/23	14:11	C2	-65.878	-68.286	2	30.33	30.63	1.49	33.92	0.47	41.66	27.11	8.5984	13.6078	6.331
18	11/01/23	14:11	C2	-65.878	-68.286	2	89.92	90.83	0.29	34.37	0.11	35.70	33.17	8.6426	13.1782	5.732
19	11/01/23	14:11	C2	-65.878	-68.286	2	170.28	172.04	1.59	34.66	-0.04	35.61	36.03	8.6139	13.1984	5.794
20	22/01/23	03:15	C3	-68.302	-69.826	2	2.63	2.66	0.54	33.56	5.18	42.23	21.63	8.6205	13.2006	5.788
21	22/01/23	03:15	C3	-68.302	-69.826	2	15.51	15.66	0.54	33.57	4.93	37.50	20.07	8.6204	13.3279	5.949
22	22/01/23	03:15	C3	-68.302	-69.826	2	29.88	30.19	0.55	33.58	3.76	35.81	21.81	8.6123	13.367	6.009
23	22/01/23	03:15	C3	-68.302	-69.826	2	51.34	51.87	-0.29	33.67	0.74	54.12	27.62	8.6105	12.6537	5.110
24	22/01/23	03:15	C3	-68.302	-69.826	2	99.92	100.96	-1.24	33.83	0.00	n.d	n.d	8.6962	13.187	5.675
25	22/01/23	03:15	C3	-68.302	-69.826	2	200.84	202.97	0.53	34.41	-0.02	n.d	35.60	8.6368	13.164	5.721
26	23/01/23	10:02	S4	-68.090	-78.486	2	3.35	3.38	0.64	33.92	0.22	60.40	26.00	8.6185	13.377	6.014
27	23/01/23	10:02	S4	-68.090	-78.486	2	19.38	19.58	0.60	33.92	1.13	46.50	26.51	8.6211	13.0589	5.608

28	23/01/23	10:02	S4	-68.090	-78.486	2	49.88	50.39	0.47	33.93	2.14	40.55	26.10	8.6296	13.2724	5.867
29	23/01/23	10:02	S4	-68.090	-78.486	2	100.34	101.38	-0.14	34.19	0.05	36.61	33.70	8.6922	13.3841	5.929
30	23/01/23	10:02	S4	-68.090	-78.486	2	998.66	1011.21	1.51	34.73	-0.06	34.08	33.60	8.6633	13.3561	5.930
31	23/01/23	10:02	S4	-68.090	-78.486	2	2999.50	3051.76	0.33	34.70	-0.06	34.43	33.37	8.6412	12.8805	5.357
32	24/01/23	21:53	C6	-69.829	-76.084	2	5.40	5.46	0.41	33.74	1.35	39.76	25.33	8.6613	13.2016	5.738
33	24/01/23	21:53	C6	-69.829	-76.084	2	15.14	15.30	0.39	33.75	1.30	40.59	25.21	8.5628	13.3071	5.996
34	24/01/23	21:53	C6	-69.829	-76.084	2	50.15	50.67	-0.80	33.81	0.04	34.11	29.13	8.6087	13.178	5.774
35	24/01/23	21:53	C6	-69.829	-76.084	2	100.67	101.72	-0.95	33.88	-0.02	45.20	29.65	8.7105	10.4456	2.193
36	24/01/23	21:53	C6	-69.829	-76.084	2	760.27	769.46	1.19	34.71	-0.06	35.86	34.27	8.6725	13.2112	5.736
37	26/01/23	22:03	C5	-68.693	-74.195	2	2.41	2.44	0.64	34.03	0.97	39.46	26.52	8.604	13.3656	6.017
38	26/01/23	22:03	C5	-68.693	-74.195	2	10.01	10.11	0.68	34.03	1.06	77.27	25.85	8.6538	13.4418	6.051
39	26/01/23	22:03	C5	-68.693	-74.195	2	50.36	50.88	0.52	34.03	1.56	40.66	27.26	8.6169	13.0504	5.603
40	26/01/23	22:03	C5	-68.693	-74.195	2	103.49	104.57	-0.93	34.11	0.22	42.15	28.81	8.5996	13.2272	5.848
41	26/01/23	22:03	C5	-68.693	-74.195	2	543.46	549.71	1.38	34.69	-0.06	38.54	34.77	8.6033	13.7017	6.443
42	27/01/23	11:35	S3	-67.573	-76.582	2	4.01	4.06	1.10	34.00	0.30	49.97	26.94	8.681	13.3468	5.896
43	27/01/23	11:35	S3	-67.573	-76.582	2	8.82	8.91	1.11	34.00	0.32	46.27	26.28	8.6114	13.508	6.188
44	27/01/23	11:35	S3	-67.573	-76.582	2	50.05	50.56	0.89	34.00	0.59	40.06	26.67	8.6307	13.0968	5.644
45	27/01/23	11:35	S3	-67.573	-76.582	2	100.38	101.41	0.18	34.36	0.05	39.17	34.72	8.6307	13.4519	6.093
46	27/01/23	11:35	S3	-67.573	-76.582	2	1199.23	1214.85	1.08	34.72	-0.06	37.88	33.18	8.6373	13.5158	6.165
47	27/01/23	11:35	S3	-67.573	-76.582	2	3050.24	3103.65	0.24	34.70	-0.06	35.43	33.55	8.627	13.4534	6.099
48	27/01/23	20:51	S2	-67.019	-74.768	2	3.56	3.60	1.02	33.99	0.82	n.d	27.56	8.593	13.195	5.816
49	27/01/23	20:51	S2	-67.019	-74.768	2	30.29	30.60	0.90	33.99	1.31	n.d	26.73	8.69	13.4185	5.976
50	27/01/23	20:51	S2	-67.019	-74.768	2	49.94	50.45	0.86	33.99	1.54	n.d	26.46	8.6274	12.9679	5.485
51	27/01/23	20:51	S2	-67.019	-74.768	2	99.83	100.85	-0.44	34.27	-0.01	n.d	32.46	8.5759	13.1449	5.774
52	27/01/23	20:51	S2	-67.019	-74.768	2	799.63	809.23	1.37	34.72	-0.07	n.d	33.20	8.6429	13.8805	6.619
53	27/01/23	20:51	S2	-67.019	-74.768	2	2992.96	3044.85	0.26	34.70	-0.06	n.d	32.68	8.5994	13.0391	5.611
54	28/01/23	12:04	C4	-68.112	-72.346	2	3.78	3.82	1.00	33.99	0.74	56.60	26.49	8.6524	13.2063	5.755
55	28/01/23	12:04	C4	-68.112	-72.346	2	3.78	3.82	1.00	33.99	0.74	48.43	26.87	8.6227	13.1954	5.779
56	28/01/23	12:04	C4	-68.112	-72.346	2	14.69	14.84	0.95	33.99	1.31	53.24	26.18	8.6133	12.9933	5.535
57	28/01/23	12:04	C4	-68.112	-72.346	2	35.82	36.19	0.90	33.99	1.61	46.09	26.66	8.6391	13.1816	5.741
58	28/01/23	12:04	C4	-68.112	-72.346	2	99.25	100.28	0.42	34.42	-0.01	87.27	36.28	8.5994	13.1998	5.814
59	28/01/23	12:04	C4	-68.112	-72.346	2	345.47	349.26	1.38	34.71	-0.04	35.75	35.83	8.635	13.271	5.859

Sample #	SPE-DOC Extract (µmol L^{-1})	SPE-DON Extract (µmol L^{-1})	Extraction Efficency (%)	$\delta^{13}C$	SPE-DOS (nmol L^{-1})	SPE-DOP (nmol L^{-1})	SPE-DOC Corrected (µmol L^{-1})	SPE-DON Corrected (µmol L^{-1})	C:N	C:S	C:P	N:P	N:S	S:P
3	50.29	3.993	80.10	-23.852	211.32	0.77	14.48	1.15	12.59	68.54	18733.62	1487.44	5.44	273.32
4	103.6	7.701	64.70	-22.985	45.52	10.04	16.85	1.25	13.45	370.14	1678.64	124.78	27.51	4.54
5	61.85	3.734	60.07	-23.101	116.45	17.13	18.11	1.09	16.56	155.54	1057.19	63.82	9.39	6.80
6	69.96	4.861	54.84	-22.612	93.40	13.66	18.34	1.27	14.39	196.37	1342.39	93.27	13.64	6.84
7	28.68	1.77	82.11	-22.549	59.77	7.55	8.11	0.50	16.20	135.75	1074.91	66.34	8.38	7.92
8	61.92	4.187	55.66	-22.497	91.26	13.58	18.41	1.25	14.79	201.77	1356.17	91.70	13.64	6.72
9	63.14	3.91	71.05	-23.57	84.82	17.04	18.42	1.14	16.15	217.17	1081.17	66.95	13.45	4.98
10	71.02	3.991	66.17	-23.338	92.03	10.97	21.04	1.18	17.80	228.67	1918.40	107.81	12.85	8.39
11	64.81	5.005	54.79	-22.698	219.36	15.23	18.71	1.44	12.95	85.27	1228.25	94.85	6.59	14.40
12	58.61	4.131	53.99	-22.307	70.93	7.69	17.86	1.26	14.19	251.79	2323.08	163.74	17.75	9.23
13	40.69	2.702	70.72	-21.8775	63.17	6.36	11.89	0.79	15.06	188.26	1870.96	124.24	12.50	9.94
14	65.32	4.656	56.42	-22.2225	67.08	6.07	17.99	1.28	14.03	268.14	2962.51	211.17	19.11	11.05
15	65.59	4.84	62.92	-22.8455	82.48	12.43	18.69	1.38	13.55	226.57	1503.28	110.93	16.72	6.63
16	62.73	4.767	61.33	-23.0015	118.22	19.78	18.77	1.43	13.16	158.78	949.28	72.14	12.07	5.98
17	52.15	3.851	60.38	-22.5765	150.62	21.43	16.51	1.22	13.54	109.60	770.32	56.88	8.09	7.03
18	61.95	4.278	50.27	-22.2295	110.79	12.57	17.75	1.23	14.48	160.25	1412.02	97.51	11.07	8.81
19	62.17	3.687	49.43	-22.4285	52.34	3.31	18.01	1.07	16.86	344.09	5446.77	323.02	20.41	15.83
20	39.12	2.589	73.19	n.d	103.96	19.50	11.32	0.75	15.11	108.90	580.45	38.41	7.21	5.33
21	63.46	4.938	49.66	-22.5745	62.45	8.35	18.88	1.47	12.85	302.25	2260.20	175.87	23.52	7.48
22	48.36	3.71	59.43	-22.1995	114.03	15.47	14.53	1.11	13.04	127.41	939.28	72.06	9.77	7.37
23	65.02	4.182	69.31	-22.505	119.86	21.22	16.61	1.07	15.55	138.59	782.80	50.35	8.91	5.65
24	64.61	4.119	n.d	-23.313	138.81	21.98	18.33	1.17	15.69	132.08	834.28	53.19	8.42	6.32
25	57.23	3.736	n.d	-23.006	95.33	9.91	16.37	1.07	15.32	171.74	1651.33	107.80	11.21	9.62
26	48.44	3.363	75.89	-22.672	104.27	15.18	14.56	1.01	14.40	139.68	959.23	66.60	9.70	6.87
27	62.17	4.111	62.51	-24.069	125.49	17.11	17.43	1.15	15.12	138.92	1018.96	67.38	9.19	7.33
28	55.75	4.076	59.67	-22.227	121.69	14.55	16.36	1.20	13.68	134.39	1124.03	82.18	9.83	8.36

29	55.41	3.678	55.12	-23.257	162.79	22.40	16.43	1.09	15.07	100.91	733.32	48.68	6.70	7.27
30	51.89	3.359	54.85	-22.242	112.09	12.70	15.39	1.00	15.45	137.27	1211.08	78.40	8.89	8.82
31	61.24	4.112	52.35	-22.311	207.97	6.45	16.40	1.10	14.89	78.88	2545.26	170.90	5.30	32.27
32	62.89	4.328	54.62	-23.068	89.38	9.16	18.04	1.24	14.53	201.87	1969.12	135.51	13.89	9.75
33	61.1	4.612	54.87	-23.552	92.77	12.11	18.32	1.38	13.25	197.44	1512.24	114.15	14.90	7.66
34	58.66	4.37	50.35	-22.751	109.19	11.68	16.94	1.26	13.42	155.11	1450.29	108.04	11.55	9.35
35	89.38	5.852	78.32	-22.440	70.89	8.85	9.80	0.64	15.27	138.24	1106.73	72.46	9.05	8.01
36	61.18	4.215	51.07	-22.678	98.60	8.52	17.55	1.21	14.51	177.96	2060.41	141.95	12.26	11.58
37	61.17	4.479	53.36	-23.06	91.21	10.70	18.40	1.35	13.66	201.77	1719.70	125.92	14.77	8.52
38	59.05	4.469	76.88	-23.03	102.59	13.53	17.86	1.35	13.21	174.13	1320.73	99.96	13.18	7.58
39	60.29	4.033	58.46	-22.64	115.90	14.48	16.89	1.13	14.95	145.73	1166.18	78.01	9.75	8.00
40	59.25	4.107	58.90	-22.57	127.19	12.49	17.32	1.20	14.43	136.21	1386.70	96.12	9.44	10.18
41	54.3	3.276	54.61	-22.17	111.19	8.76	17.49	1.06	16.58	157.32	1996.91	120.48	9.49	12.69
42	47.49	3.157	71.98	-22.50	141.22	15.70	14.00	0.93	15.04	99.14	891.60	59.27	6.59	8.99
43	57.34	4.568	61.66	-22.57	93.10	11.37	17.74	1.41	12.55	190.57	1560.60	124.33	15.18	8.19
44	61.74	4.988	56.51	-22.59	165.30	13.09	17.42	1.41	12.38	105.40	1331.22	107.55	8.52	12.63
45	55.84	3.433	56.57	-22.81	429.34	9.39	17.01	1.05	16.27	39.62	1811.95	111.40	2.44	45.73
46	33.6	2.404	72.66	-22.08	104.73	10.60	10.36	0.74	13.98	98.90	977.09	69.91	7.08	9.88
47	55.69	3.933	52.06	-22.12	63.11	7.38	16.98	1.20	14.16	269.09	2299.77	162.42	19.00	8.55
48	60.36	4.376	n.d	-22.53	80.19	9.62	17.55	1.27	13.79	218.87	1825.40	132.34	15.87	8.34
49	33.33	1.902	n.d	-22.70	106.45	13.87	9.96	0.57	17.52	93.55	718.14	40.98	5.34	7.68
50	60.44	4.934	n.d	-23.16	80.61	10.38	16.58	1.35	12.25	205.63	1596.20	130.31	16.79	7.76
51	57.59	4.798	n.d	-22.59	79.29	7.15	16.63	1.39	12.00	209.69	2325.63	193.76	17.47	11.09
52	53.6	3.504	n.d	-22.12	85.39	6.36	17.74	1.16	15.30	207.75	2787.35	182.22	13.58	13.42
53	60.97	4.19	n.d	-22.83	66.58	6.18	17.10	1.18	14.55	256.89	2768.31	190.24	17.65	10.78
54	64.68	4.275	67.12	-23.42	140.82	17.40	18.61	1.23	15.13	132.17	1069.54	70.69	8.74	8.09
55	49.16	4.31	70.67	-22.94	120.39	15.97	14.20	1.25	11.41	117.98	889.55	77.99	10.34	7.54
56	63.37	4.396	67.06	-23.64	212.68	18.10	17.54	1.22	14.42	82.46	969.11	67.23	5.72	11.75
57	61.49	4.194	61.71	-22.98	113.65	15.24	17.65	1.20	14.66	155.29	1158.28	79.00	10.59	7.46
58	60.67	3.69	79.79	-22.49	119.72	7.93	17.64	1.07	16.44	147.31	2225.14	135.33	8.96	15.10
59	55.92	4.398	54.18	-22.19	106.99	8.01	16.38	1.29	12.71	153.11	2043.89	160.75	12.04	13.35

Sample #	AIMod	OC	HC	C	H	O	N	P	S	DBE	Aromatic	Aromatic O_poor	Aromatic O_rich	Highly unsaturated O_rich	Highly unsaturated O_poor
3	0.0729	0.1524	0.5135	6.8503	9.3786	2.8498	0.2080	0.0378	0.0621	2.6514	0.0201	0.0197	0.0004	0.0594	0.1579
4	0.0670	0.1145	0.4468	5.0486	7.2524	1.8600	0.1246	0.0455	0.0577	1.8140	0.0320	0.0316	0.0004	0.0228	0.1110
5	0.0918	0.1758	0.5259	8.3859	10.8447	3.5903	0.2694	0.0733	0.0548	3.5357	0.0300	0.0298	0.0002	0.0852	0.1944
6	0.0834	0.1659	0.5059	7.9851	10.5406	3.3954	0.2342	0.0745	0.0550	3.2470	0.0276	0.0272	0.0004	0.0714	0.1816
7	0.0804	0.1569	0.4572	7.1338	9.1961	3.1885	0.2181	0.0481	0.0415	3.0187	0.0191	0.0189	0.0001	0.0921	0.1620
8	0.0662	0.1281	0.3665	5.6613	7.2499	2.5660	0.1855	0.0303	0.0312	2.4281	0.0157	0.0157	0.0000	0.0849	0.1308
9	0.0720	0.1590	0.4932	6.8070	9.0646	3.0267	0.1999	0.0319	0.0355	2.7513	0.0166	0.0166	0.0000	0.0861	0.1438
10	0.0954	0.1800	0.5647	8.5318	11.2612	3.5596	0.2756	0.0810	0.0576	3.5015	0.0324	0.0318	0.0005	0.0711	0.2052
11	0.0921	0.1959	0.5924	9.1876	12.1002	4.0375	0.2761	0.0419	0.0945	3.7412	0.0156	0.0152	0.0003	0.1277	0.1892
12	0.0478	0.0976	0.2644	4.1062	5.2142	1.9524	0.1235	0.0211	0.0189	1.7777	0.0103	0.0103	0.0000	0.0748	0.0859
13	0.0932	0.1889	0.5329	8.9168	11.3835	4.0405	0.2801	0.0537	0.0433	3.8058	0.0179	0.0177	0.0001	0.1251	0.2010
14	0.0916	0.1745	0.5219	8.7022	11.2067	3.6804	0.2924	0.0733	0.0539	3.6809	0.0264	0.0261	0.0003	0.0821	0.2073
15	0.0930	0.1910	0.5395	8.6653	11.1430	3.9172	0.2945	0.0606	0.0551	3.6874	0.0240	0.0239	0.0002	0.1121	0.1979
16	0.0922	0.1777	0.5056	7.9940	10.1783	3.5915	0.2876	0.0397	0.0536	3.4628	0.0232	0.0232	0.0000	0.1127	0.1889
17	0.0927	0.1932	0.5292	8.7355	11.1065	4.0129	0.3034	0.0553	0.0525	3.7746	0.0197	0.0193	0.0004	0.1273	0.1932
18	0.0791	0.1467	0.4051	6.2945	7.9204	2.8907	0.2183	0.0288	0.0278	2.7779	0.0225	0.0223	0.0002	0.0981	0.1476
19	0.1019	0.2031	0.5959	10.1710	13.0577	4.3377	0.3217	0.0828	0.0599	4.2985	0.0343	0.0341	0.0002	0.1049	0.2089
20	0.0957	0.1949	0.6022	9.4720	12.5607	4.0765	0.3135	0.0599	0.0593	3.8302	0.0206	0.0205	0.0001	0.0991	0.2219
21	0.1100	0.2015	0.6326	10.6388	13.7303	4.2208	0.3444	0.0952	0.0811	4.4703	0.0458	0.0454	0.0004	0.0782	0.2209
22	0.1067	0.2134	0.6104	9.9624	12.7936	4.4552	0.3296	0.0668	0.0635	4.2351	0.0309	0.0306	0.0002	0.1236	0.2222
23	0.0725	0.1447	0.4161	6.6927	8.5605	2.9952	0.2440	0.0404	0.0336	2.8773	0.0115	0.0115	0.0000	0.0900	0.1685
24	0.0604	0.1290	0.4845	6.1064	8.5379	2.3226	0.1969	0.0447	0.0519	2.2944	0.0077	0.0077	0.0000	0.0385	0.1465
25	0.0737	0.1435	0.3888	6.3150	7.8944	2.9531	0.2113	0.0160	0.0304	2.7905	0.0142	0.0138	0.0004	0.1151	0.1372
26	0.0925	0.1927	0.5595	8.9395	11.6139	3.9801	0.3029	0.0615	0.0618	3.7410	0.0212	0.0209	0.0003	0.1094	0.2037
27	0.0844	0.1739	0.5030	7.9964	10.3688	3.5641	0.2660	0.0664	0.0453	3.3617	0.0211	0.0210	0.0002	0.0916	0.1861
28	0.0630	0.1209	0.3539	5.1307	6.6420	2.2922	0.1883	0.0268	0.0338	2.1881	0.0155	0.0155	0.0000	0.0732	0.1265
29	0.0969	0.1961	0.5729	9.4952	12.2723	4.1197	0.2978	0.0750	0.0662	3.9821	0.0294	0.0292	0.0003	0.1059	0.2025

30	0.0798	0.1556	0.4923	8.1782	10.7006	3.2927	0.2620	0.0742	0.0517	3.3628	0.0233	0.0230	0.0003	0.0585	0.1868
31	0.0902	0.1780	0.5314	9.4638	12.1392	3.9165	0.3136	0.0771	0.0628	3.9953	0.0246	0.0243	0.0003	0.0872	0.2058
32	0.0816	0.1627	0.4195	6.7635	8.3582	3.2781	0.2347	0.0102	0.0335	3.0453	0.0165	0.0161	0.0004	0.1432	0.1400
33	0.0925	0.1972	0.5259	8.6278	10.8789	4.0547	0.2993	0.0432	0.0635	3.7733	0.0158	0.0155	0.0002	0.1502	0.1797
34	0.0827	0.1619	0.4492	7.1800	9.0931	3.2789	0.2449	0.0413	0.0410	3.1290	0.0197	0.0196	0.0001	0.1046	0.1706
35	0.0879	0.1682	0.5581	7.7270	10.3916	3.1618	0.2295	0.0720	0.0495	3.0865	0.0344	0.0343	0.0002	0.0554	0.1748
36	0.1090	0.2151	0.6089	10.9823	13.8717	4.7208	0.3466	0.0843	0.0679	4.7355	0.0356	0.0353	0.0003	0.1251	0.2223
37	0.0749	0.1446	0.4054	6.3572	8.0678	2.9096	0.2260	0.0271	0.0332	2.7677	0.0154	0.0152	0.0002	0.1001	0.1525
38	0.0855	0.1742	0.5070	8.0483	10.4547	3.5463	0.2646	0.0710	0.0499	3.3739	0.0250	0.0248	0.0002	0.0862	0.1860
39	0.0810	0.1682	0.4719	7.4731	9.6092	3.4263	0.2409	0.0389	0.0490	3.1726	0.0169	0.0165	0.0004	0.1153	0.1614
40	0.0797	0.1422	0.4089	6.2864	7.9826	2.8058	0.2168	0.0255	0.0302	2.7369	0.0232	0.0230	0.0002	0.0909	0.1539
41	0.0736	0.1398	0.4089	6.2640	8.0232	2.7852	0.2078	0.0341	0.0284	2.6888	0.0181	0.0179	0.0002	0.0833	0.1513
42	0.0925	0.1930	0.5290	8.6851	11.0589	4.0162	0.2935	0.0487	0.0493	3.7396	0.0202	0.0202	0.0000	0.1283	0.1942
43	0.0722	0.1425	0.4370	6.6946	8.8024	2.8397	0.2272	0.0566	0.0477	2.7641	0.0169	0.0169	0.0000	0.0641	0.1699
44	0.0871	0.1769	0.5190	8.2396	10.7304	3.6030	0.2773	0.0729	0.0523	3.4433	0.0254	0.0251	0.0003	0.0852	0.1945
45	0.0853	0.1636	0.4848	7.8608	10.1326	3.3730	0.2592	0.0615	0.0495	3.3267	0.0232	0.0229	0.0004	0.0818	0.1909
46	0.0972	0.1771	0.5549	8.6600	11.3538	3.5870	0.2588	0.0826	0.0630	3.5719	0.0324	0.0322	0.0003	0.0658	0.2178
47	0.0772	0.1571	0.4400	7.2149	9.2041	3.2684	0.2447	0.0495	0.0421	3.1020	0.0148	0.0148	0.0000	0.0983	0.1710
48	0.0664	0.1282	0.3890	5.6706	7.4443	2.4529	0.2045	0.0384	0.0358	2.3642	0.0153	0.0152	0.0002	0.0629	0.1495
49	0.0836	0.1516	0.4685	6.8810	9.0143	2.9084	0.2185	0.0579	0.0471	2.8668	0.0302	0.0297	0.0005	0.0617	0.1764
50	0.0819	0.1273	0.4729	7.7931	10.3610	2.6145	0.2239	0.0814	0.0652	3.1084	0.0415	0.0403	0.0012	0.0198	0.1598
51	0.0780	0.1398	0.4009	6.1560	7.8355	2.7476	0.2133	0.0308	0.0278	2.6741	0.0251	0.0249	0.0002	0.0864	0.1472
52	0.0866	0.1597	0.4790	7.5083	9.7285	3.2232	0.2305	0.0666	0.0512	3.1580	0.0305	0.0305	0.0000	0.0723	0.1804
53	0.0727	0.1318	0.4181	6.2575	8.1843	2.5942	0.2092	0.0512	0.0388	2.6108	0.0208	0.0207	0.0002	0.0536	0.1641
54	0.0805	0.1563	0.4550	7.0523	9.1336	3.1317	0.2262	0.0510	0.0421	2.9732	0.0227	0.0226	0.0002	0.0826	0.1723
55	0.0927	0.1878	0.5246	8.5808	10.9542	3.9133	0.2905	0.0453	0.0479	3.6806	0.0210	0.0210	0.0000	0.1223	0.1973
56	0.0917	0.1898	0.5139	8.4925	10.7489	3.9678	0.2860	0.0362	0.0453	3.6842	0.0196	0.0192	0.0004	0.1385	0.1884
57	0.0866	0.1854	0.5036	8.3707	10.6455	3.8964	0.2723	0.0488	0.0526	3.6016	0.0158	0.0156	0.0001	0.1303	0.1820
58	0.0938	0.1889	0.5476	9.6537	12.3633	4.1148	0.3008	0.0791	0.0571	4.0811	0.0294	0.0291	0.0003	0.0975	0.1998
59	0.0778	0.1418	0.4022	6.3641	8.0634	2.8530	0.2137	0.0317	0.0303	2.7713	0.0230	0.0229	0.0002	0.0904	0.1525

Sample #	Highly unsaturated	Unsaturated	Unsaturated O_poor	Unsaturated O_rich	Unsaturated with N	Saturated	Saturated O_poor	Saturated O_rich	Number of formulae	m/z
3	0.2173	0.1165	0.0883	0.0282	0.0108	0.0074	0.0069	0.0005	1336	142.9355
4	0.1339	0.1163	0.0810	0.0352	0.0079	0.0137	0.0119	0.0018	745	102.3321
5	0.2796	0.0802	0.0477	0.0325	0.0136	0.0026	0.0010	0.0016	1793	176.3782
6	0.2530	0.0813	0.0450	0.0363	0.0113	0.0056	0.0041	0.0015	1468	167.7174
7	0.2541	0.0681	0.0419	0.0262	0.0071	0.0026	0.0020	0.0006	1406	151.3923
8	0.2156	0.0446	0.0310	0.0136	0.0054	0.0030	0.0025	0.0005	1025	120.5308
9	0.2299	0.1061	0.0849	0.0211	0.0066	0.0030	0.0027	0.0003	1242	143.7898
10	0.2763	0.0994	0.0613	0.0380	0.0135	0.0039	0.0019	0.0020	1888	178.4519
11	0.3169	0.0972	0.0749	0.0224	0.0093	0.0099	0.0094	0.0005	1938	194.7617
12	0.1608	0.0297	0.0215	0.0082	0.0044	0.0008	0.0008	0.0000	614	88.53574
13	0.3261	0.0610	0.0409	0.0201	0.0095	0.0038	0.0026	0.0012	2114	189.6546
14	0.2894	0.0730	0.0422	0.0308	0.0150	0.0027	0.0009	0.0019	1774	182.2728
15	0.3100	0.0734	0.0418	0.0316	0.0139	0.0018	0.0011	0.0007	1994	185.2129
16	0.3016	0.0627	0.0399	0.0228	0.0104	0.0020	0.0015	0.0005	1816	170.2068
17	0.3205	0.0644	0.0381	0.0262	0.0126	0.0020	0.0006	0.0013	2057	187.4307
18	0.2457	0.0461	0.0258	0.0203	0.0071	0.0008	0.0006	0.0002	1255	134.2697
19	0.3138	0.0935	0.0556	0.0380	0.0168	0.0036	0.0007	0.0028	2226	213.1186
20	0.3210	0.0997	0.0748	0.0249	0.0146	0.0029	0.0020	0.0010	2363	199.212
21	0.2991	0.1172	0.0726	0.0446	0.0213	0.0043	0.0018	0.0025	2142	218.8973
22	0.3458	0.0854	0.0525	0.0329	0.0134	0.0025	0.0017	0.0008	2626	211.9419
23	0.2585	0.0466	0.0339	0.0127	0.0088	0.0030	0.0022	0.0008	1235	142.2657
24	0.1850	0.1343	0.1217	0.0127	0.0123	0.0047	0.0044	0.0003	927	124.4947
25	0.2523	0.0380	0.0287	0.0093	0.0057	0.0010	0.0007	0.0003	1124	135.0868
26	0.3131	0.0800	0.0505	0.0295	0.0118	0.0050	0.0036	0.0014	2196	190.3316
27	0.2777	0.0751	0.0441	0.0310	0.0101	0.0019	0.0007	0.0012	1782	170.2553
28	0.1997	0.0454	0.0306	0.0149	0.0066	0.0044	0.0037	0.0007	955	109.1991
29	0.3084	0.0846	0.0500	0.0346	0.0147	0.0061	0.0048	0.0014	2296	200.3735

30	0.2454	0.0866	0.0561	0.0305	0.0164	0.0027	0.0011	0.0016	1503	168.8415
31	0.2930	0.0758	0.0473	0.0284	0.0169	0.0040	0.0030	0.0010	1882	196.8204
32	0.2833	0.0364	0.0235	0.0128	0.0056	0.0015	0.0013	0.0002	1259	146.351
33	0.3300	0.0600	0.0400	0.0200	0.0098	0.0030	0.0024	0.0006	1851	186.4941
34	0.2751	0.0516	0.0316	0.0200	0.0077	0.0010	0.0008	0.0002	1518	153.4358
35	0.2302	0.1257	0.0851	0.0406	0.0099	0.0034	0.0018	0.0016	1517	160.387
36	0.3474	0.0799	0.0432	0.0367	0.0174	0.0025	0.0004	0.0021	2406	230.4361
37	0.2526	0.0431	0.0319	0.0112	0.0062	0.0025	0.0020	0.0005	1209	135.7023
38	0.2723	0.0758	0.0435	0.0323	0.0120	0.0036	0.0015	0.0021	1795	170.9507
39	0.2766	0.0607	0.0411	0.0196	0.0085	0.0052	0.0044	0.0008	1543	159.9434
40	0.2449	0.0447	0.0274	0.0174	0.0072	0.0039	0.0035	0.0005	1252	132.8293
41	0.2346	0.0574	0.0404	0.0170	0.0060	0.0008	0.0005	0.0003	1236	132.3585
42	0.3225	0.0636	0.0384	0.0252	0.0110	0.0017	0.0006	0.0011	2113	186.3847
43	0.2340	0.0687	0.0460	0.0227	0.0106	0.0023	0.0012	0.0011	1270	140.7542
44	0.2797	0.0774	0.0434	0.0340	0.0133	0.0032	0.0010	0.0022	1829	174.7347
45	0.2727	0.0665	0.0403	0.0262	0.0114	0.0022	0.0004	0.0017	1666	165.2335
46	0.2835	0.0881	0.0485	0.0396	0.0128	0.0045	0.0021	0.0023	1942	180.5104
47	0.2693	0.0511	0.0305	0.0205	0.0090	0.0015	0.0003	0.0012	1468	154.0943
48	0.2124	0.0591	0.0399	0.0192	0.0071	0.0016	0.0008	0.0008	1089	119.6829
49	0.2382	0.0772	0.0448	0.0325	0.0086	0.0017	0.0012	0.0005	1424	144.178
50	0.1797	0.1018	0.0627	0.0391	0.0233	0.0061	0.0021	0.0040	914	153.1711
51	0.2335	0.0478	0.0279	0.0200	0.0079	0.0028	0.0026	0.0002	1235	130.2279
52	0.2527	0.0691	0.0347	0.0344	0.0098	0.0038	0.0026	0.0011	1531	158.0216
53	0.2177	0.0685	0.0457	0.0229	0.0090	0.0016	0.0006	0.0011	1263	130.2689
54	0.2550	0.0631	0.0354	0.0277	0.0075	0.0015	0.0007	0.0008	1406	149.6659
55	0.3196	0.0609	0.0395	0.0214	0.0097	0.0026	0.0011	0.0015	2018	183.1931
56	0.3269	0.0544	0.0339	0.0205	0.0088	0.0015	0.0007	0.0008	1912	182.3765
57	0.3123	0.0564	0.0358	0.0206	0.0079	0.0034	0.0022	0.0012	1748	180.1113
58	0.2973	0.0814	0.0432	0.0382	0.0160	0.0019	0.0001	0.0018	1896	202.1865
59	0.2428	0.0446	0.0247	0.0200	0.0074	0.0010	0.0006	0.0004	1268	134.7538

7. References:

Alderkamp, A. C., Mills, M. M., Van Dijken, G. L., Laan, P., Thuróczy, C. E., Gerringa, L. J. A., De Baar, H. J. W., Payne, C. D., Visser, R. J. W., Buma, A. G. J. & Arrigo, K. R. 2012. Iron from melting glaciers fuels phytoplankton blooms in the Amundsen Sea (Southern Ocean): Phytoplankton characteristics and productivity. *Deep-Sea Research Part Ii-Topical Studies in Oceanography,* 71-76**,** 32-48.

Alderkamp, A. C., Van Dijken, G. L., Lowry, K. E., Lewis, K. M., Joy-Warren, H. L., Van De Poll, W., Laan, P., Gerringa, L., Delmont, T. O., Jenkins, B. D. & Arrigo, K. R. 2019. Effects of iron and light availability on phytoplankton photosynthetic properties in the Ross Sea. *Marine Ecology Progress Series,* 621**,** 33-50.

Altabet, M. A., Wassenaar, L. I., Douence, C. & Roy, R. 2019. A Ti(III) reduction method for one-step conversion of seawater and freshwater nitrate into N(2) O for stable isotopic analysis of (15) N/(14) N, (18) O/(16) O and (17) O/(16) O. *Rapid Commun Mass Spectrom,* 33**,** 1227-1239.

Annett, A. L., Carson, D. S., Crosta, X., Clarke, A. & Ganeshram, R. S. 2010. Seasonal progression of diatom assemblages in surface waters of Ryder Bay, Antarctica. *Polar Biology,* 33**,** 13-29.

Annett, A. L., Skiba, M., Henley, S. F., Venables, H. J., Meredith, M. P., Statham, P. J. & Ganeshram, R. S. 2015. Comparative roles of upwelling and glacial iron sources in Ryder Bay, coastal western Antarctic Peninsula. *Marine Chemistry,* 176**,** 21-33.

Antia, N. J., Harrison, P. J. & Oliveira, L. 1991. The Role of Dissolved Organic Nitrogen in Phytoplankton Nutrition, Cell Biology and Ecology. *Phycologia,* 30**,** 1-89.

Antoni, J. S., Almandoz, G. O., Ferrario, M. E., Hernando, M. P., Varela, D. E., Rozema, P. D., Buma, A. G. J., Paparazzo, F. E. & Schloss, I. R. 2020. Response of a natural Antarctic phytoplankton assemblage to changes in temperature and salinity. *Journal of Experimental Marine Biology and Ecology,* 532**,** 151444.

Aoki, S., Yamazaki, K., Hirano, D., Katsumata, K., Shimada, K., Kitade, Y., Sasaki, H. & Murase, H. 2020. Reversal of freshening trend of Antarctic Bottom Water in the Australian-Antarctic Basin during 2010s. *Sci Rep,* 10**,** 14415.

Armbrust, E. V., Berges, J. A., Bowler, C., Green, B. R., Martinez, D., Putnam, N. H., Zhou, S., Allen, A. E., Apt, K. E., Bechner, M., Brzezinski, M. A., Chaal, B. K., Chiovitti, A., Davis, A. K., Demarest, M. S., Detter, J. C., Glavina, T., Goodstein, D., Hadi, M. Z., Hellsten, U., Hildebrand, M., Jenkins, B. D., Jurka, J., Kapitonov, V. V., Kroger, N., Lau, W. W., Lane, T. W., Larimer, F. W., Lippmeier, J. C., Lucas, S., Medina, M., Montsant, A., Obornik, M., Parker, M. S., Palenik, B., Pazour, G. J., Richardson, P. M., Rynearson, T. A., Saito, M. A., Schwartz, D. C., Thamatrakoln, K., Valentin, K., Vardi, A., Wilkerson, F. P. & Rokhsar, D. S. 2004. The genome of the diatom Thalassiosira pseudonana: ecology, evolution, and metabolism. *Science,* 306**,** 79-86.

Arrigo, K. R., Ditullio, G. R., Dunbar, R. B., Robinson, D. H., Vanwoert, M., Worthen, D. L. & Lizotte, M. P. 2000. Phytoplankton taxonomic variability in nutrient utilization and primary production in the Ross Sea. *Journal of Geophysical Research-Oceans,* 105**,** 8827-8845.

Arrigo, K. R., Mills, M. M., Kropuenske, L. R., Van Dijken, G. L., Alderkamp, A. C. & Robinson, D. H. 2010. Photophysiology in two major southern ocean phytoplankton taxa: photosynthesis and growth of Phaeocystis antarctica and Fragilariopsis cylindrus under different irradiance levels. *Integr Comp Biol,* 50**,** 950-66.

Arrigo, K. R., Robinson, D. H., Worthen, D. L., Dunbar, R. B., Ditullio, G. R., Vanwoert, M. & Lizotte, M. P. 1999. Phytoplankton community structure and the drawdown of nutrients and CO2 in the southern ocean. *Science,* 283**,** 365-7.

Arrigo, K. R., Van Dijken, G. L. & Bushinsky, S. 2008. Primary production in the Southern Ocean, 1997-2006. *Journal of Geophysical Research-Oceans,* 113.

Arrigo, K. R., Worthen, D., Schnell, A. & Lizotte, M. P. 1998. Primary production in Southern Ocean waters. *Journal of Geophysical Research-Oceans,* 103**,** 15587-15600.

Arrigo, K. R., Worthen, D. L., Lizotte, M. P., Dixon, P. & Dieckmann, G. 1997. Primary Production in Antarctic Sea Ice. *Science,* 276**,** 394-7.

Arteaga, L. A., Boss, E., Behrenfeld, M. J., Westberry, T. K. & Sarmiento, J. L. 2020. Seasonal modulation of phytoplankton biomass in the Southern Ocean. *Nat Commun,* 11**,** 5364.

Assmy, P., Smetacek, V., Montresor, M., Klaas, C., Henjes, J., Strass, V. H., Arrieta, J. M., Bathmann, U., Berg, G. M. & Breitbarth, E. 2013. Thick-shelled, grazer-protected diatoms decouple ocean carbon and silicon cycles in the iron-limited Antarctic Circumpolar Current. *Proceedings of the National Academy of Sciences,* 110**,** 20633-20638.

Atkinson, A., Siegel, V., Pakhomov, E. & Rothery, P. 2004. Long-term decline in krill stock and increase in salps within the Southern Ocean. *Nature,* 432**,** 100-3.

Bakker, D. C. E., Debaar, H. J. W. & Bathmann, U. V. 1997. Changes of carbon dioxide in surface waters during spring in the Southern Ocean. *Deep-Sea Research Part Ii-Topical Studies in Oceanography,* 44**,** 91-127.

Balaguer, J., Koch, F., Hassler, C. & Trimborn, S. 2022. Iron and manganese co-limit the growth of two phytoplankton groups dominant at two locations of the Drake Passage. *Commun Biol,* 5**,** 207.

Ballerini, T., Hofmann, E. E., Ainley, D. G., Daly, K., Marrari, M., Ribic, C. A., Smith, W. O. & Steele, J. H. 2014. Productivity and linkages of the food web of the southern region of the western Antarctic Peninsula continental shelf. *Progress in Oceanography,* 122**,** 10-29.

Bender, S. J., Moran, D. M., Mcilvin, M. R., Zheng, H., Mccrow, J. P., Badger, J., Ditullio, G. R., Allen, A. E. & Saito, M. A. 2018. Colony formation in Phaeocystis antarctica: connecting molecular mechanisms with iron biogeochemistry. *Biogeosciences,* 15**,** 4923-4942.

Berg, G. M., Balode, M., Purina, I., Bekere, S., Béchemin, C. & Maestrini, S. Y. 2003. Plankton community composition in relation to availability and uptake of oxidized and reduced nitrogen. *Aquatic Microbial Ecology,* 30**,** 263-274.

Bernard, K. S., Steinberg, D. K. & Schofield, O. M. E. 2012. Summertime grazing impact of the dominant macrozooplankton off the Western Antarctic Peninsula. *Deep-Sea Research Part I-Oceanographic Research Papers,* 62**,** 111-122.

Bertrand, E. M., Saito, M. A., Rose, J. M., Riesselman, C. R., Lohan, M. C., Noble, A. E., Lee, P. A. & Ditullio, G. R. 2007. Vitamin B12 and iron colimitation of phytoplankton growth in the Ross Sea. *Limnology and Oceanography,* 52**,** 1079-1093.

Bianchi, M., Feliatra, F., Treguer, P., Vincendeau, M. A. & Morvan, J. 1997. Nitrification rates, ammonium and nitrate distribution in upper layers of the water column and in sediments of the Indian sector of the Southern Ocean. *Deep-Sea Research Part Ii-Topical Studies in Oceanography,* 44**,** 1017-1032.

Biddanda, B. & Benner, R. 1997. Carbon, nitrogen, and carbohydrate fluxes during the production of particulate and dissolved organic matter by marine phytoplankton. *Limnology and Oceanography,* 42**,** 506-518.

Biggs, T. E. G., Alvarez-Fernandez, S., Evans, C., Mojica, K. D. A., Rozema, P. D., Venables, H. J., Pond, D. W. & Brussaard, C. P. D. 2019. Antarctic phytoplankton community composition and size structure: importance of ice type and temperature as regulatory factors. *Polar Biology,* 42**,** 1997-2015.

Biggs, T. E. G., Huisman, J. & Brussaard, C. P. D. 2021. Viral lysis modifies seasonal phytoplankton dynamics and carbon flow in the Southern Ocean. *ISME J,* 15**,** 3615-3622.

Bindoff, N. L., Cheung, W. W., Kairo, J. G., Arístegui, J., Guinder, V. A., Hallberg, R., Hilmi, N. J. M., Jiao, N., Karim, M. S. & Levin, L. 2019. Changing ocean, marine ecosystems, and dependent communities. *IPCC special report on the ocean and cryosphere in a changing climate***,** 477-587.

Blain, S., Tréguer, P., Belviso, S., Bucciarelli, E., Denis, M., Desabre, S., Fiala, M., Jézéquel, V. M., Le Fèvre, J., Mayzaud, P., Marty, J. C. & Razouls, S. 2001. A biogeochemical study of the island mass effect in the context of the iron hypothesis:: Kerguelen Islands, Southern Ocean. *Deep-Sea Research Part I-Oceanographic Research Papers,* 48**,** 163-187.

Böckmann, S., Koch, F., Meyer, B., Pausch, F., Iversen, M., Driscoll, R., Laglera, L. M., Hassler, C. & Trimborn, S. 2021. Salp fecal pellets release more bioavailable iron to Southern Ocean phytoplankton than krill fecal pellets. *Current Biology,* 31**,** 2737-2746.e3.

Boyd, P., Laroche, J., Gall, M., Frew, R. & Mckay, R. M. L. 1999. Role of iron, light, and silicate in controlling algal biomass in subantarctic waters SE of New Zealand. *Journal of Geophysical Research-Oceans,* 104**,** 13395-13408.

Boyd, P. W. 2002. Environmental Factors Controlling Phytoplankton Processes in the Southern Ocean. *Journal of Phycology,* 38**,** 844-861.

Boyd, P. W., Doney, S. C., Strzepek, R., Dusenberry, J., Lindsay, K. & Fung, I. 2008. Climate-mediated changes to mixed-layer properties in the Southern Ocean: assessing the phytoplankton response. *Biogeosciences,* 5**,** 847-864.

Boyd, P. W. & Ellwood, M. J. 2010. The biogeochemical cycle of iron in the ocean. *Nature Geoscience,* 3**,** 675-682.

Boyd, P. W., Watson, A. J., Law, C. S., Abraham, E. R., Trull, T., Murdoch, R., Bakker, D. C., Bowie, A. R., Buesseler, K. O., Chang, H., Charette, M., Croot, P., Downing, K., Frew, R., Gall, M., Hadfield, M., Hall, J., Harvey, M., Jameson, G., Laroche, J., Liddicoat, M., Ling, R., Maldonado, M. T., Mckay, R. M., Nodder, S., Pickmere, S., Pridmore, R., Rintoul, S., Safi, K., Sutton, P., Strzepek, R., Tanneberger, K., Turner, S., Waite, A. & Zeldis, J. 2000. A mesoscale phytoplankton bloom in the polar Southern Ocean stimulated by iron fertilization. *Nature,* 407**,** 695-702.

Brautigam, A., Schaumloffel, D., Krauss, G. J. & Wesenberg, D. 2009. Analytical approach for characterization of cadmium-induced thiol peptides--a case study using Chlamydomonas reinhardtii. *Anal Bioanal Chem,* 395**,** 1737-47.

Bronk, D. A. & Glibert, P. M. 1991. A 15N tracer method for the measurement of dissolved organic nitrogen release by phytoplankton. *Marine Ecology Progress Series,* 77**,** 171-182.

Bronk, D. A., Glibert, P. M. & Ward, B. B. 1994. Nitrogen uptake, dissolved organic nitrogen release, and new production. *Science,* 265**,** 1843-6.

Brown, M. S., Bowman, J. S., Lin, Y. J., Feehan, C. J., Moreno, C. M., Cassar, N., Marchetti, A. & Schofield, O. M. 2021. Low diversity of a key phytoplankton group along the West Antarctic Peninsula. *Limnology and Oceanography,* 66**,** 2470-2480.

Brown, M. S., Munro, D. R., Feehan, C. J., Sweeney, C., Ducklow, H. W. & Schofield, O. M. 2019. Enhanced oceanic CO2 uptake along the rapidly changing West Antarctic Peninsula. *Nature Climate Change,* 9**,** 678-+.

Browning, T. J., Achterberg, E. P., Engel, A. & Mawji, E. 2021. Manganese co-limitation of phytoplankton growth and major nutrient drawdown in the Southern Ocean. *Nat Commun,* 12**,** 884.

Browning, T. J. & Moore, C. M. 2023. Global analysis of ocean phytoplankton nutrient limitation reveals high prevalence of co-limitation. *Nat Commun,* 14**,** 5014.

Bury, S. J., Owen, N. J. P. & Preston, T. 1995. 13C and 15N uptake by phytoplankton in the marginal ice zone of the Bellingshausen Sea. *Deep Sea Research Part II: Topical Studies in Oceanography,* 42**,** 1225-1252.

Bushinsky, S. M. & Cerovecki, I. 2023. Subantarctic Mode Water Biogeochemical Formation Properties and Interannual Variability. *Agu Advances,* 4**,** e2022AV000722.

Bushinsky, S. M., Landschutzer, P., Rodenbeck, C., Gray, A. R., Baker, D., Mazloff, M. R., Resplandy, L., Johnson, K. S. & Sarmiento, J. L. 2019. Reassessing Southern Ocean Air-Sea CO2 Flux Estimates With the Addition of Biogeochemical Float Observations. *Global Biogeochem Cycles,* 33**,** 1370-1388.

Cai, Q. Q., Wang, J., Beletsky, D., Overland, J., Ikeda, M. & Wan, L. Y. 2021. Accelerated decline of summer Arctic sea ice during 1850-2017 and the amplified Arctic warming during the recent decades. *Environmental Research Letters,* 16**,** 034015.

Cai, R. H. & Jiao, N. Z. 2023. Recalcitrant dissolved organic matter and its major production and removal processes in the ocean. *Deep-Sea Research Part I-Oceanographic Research Papers,* 191**,** 103922.

Caldeira, K. & Duffy, P. B. 2000. The role of the southern ocean in uptake and storage of anthropogenic carbon dioxide. *Science,* 287**,** 620-2.

Camoying, M. G., Thoms, S., Geuer, J. K., Koch, B. P., Bischof, K. & Trimborn, S. 2022. In contrast to diatoms, cryptophytes are susceptible to iron limitation, but not to ocean acidification. *Physiol Plant,* 174**,** e13614.

Camoying, M. G. & Trimborn, S. 2023. Physiological response of an Antarctic cryptophyte to increasing temperature, CO2, and irradiance. *Limnology and Oceanography,* 68**,** 1880-1894.

Canadell, J. G., Monteiro, P. M., Costa, M. H., Da Cunha, L. C., Cox, P. M., Alexey, V., Henson, S., Ishii, M., Jaccard, S., Koven, C., Lohila, A., Patra, P. K., Piao, S., Rogelj, J., Syampungani, S., Zaehle, S. & Zickfield, K. 2021. Global carbon and other Biogeochemical Cycles and Feedbacks. *In:* MASSON-DELMOTTE, V., P. ZHAI, A. PIRANI, S.L. CONNORS, C. PÉAN, S. BERGER, N. CAUD, Y. CHEN, L. GOLDFARB, M.I. GOMIS, M. HUANG, K. LEITZELL, E. LONNOY, J.B.R. MATTHEWS, T.K. MAYCOCK, T. WATERFIELD, O. YELEKÇI, R. YU & ZHOU, B. (eds.) *Climate Change 2021: The Physical Science Basis. Contribution of Working Group I to the Sixth Assessment Report of the Intergovernmental Panel on Climate Change* In Press: Cambridge University Press.

Carlson, C. A., Ducklow, H. W. & Michaels, A. F. 1994. Annual Flux of Dissolved Organic-Carbon from the Euphotic Zone in the Northwestern Sargasso Sea. *Nature,* 371**,** 405-408.

Carlson, C. A., Hansell, D. A., Peltzer, E. T. & Smith, W. O. 2000. Stocks and dynamics of dissolved and particulate organic matter in the southern Ross Sea, Antarctica. *Deep-Sea Research Part Ii-Topical Studies in Oceanography,* 47**,** 3201-3225.

Carranza, M. M. & Gille, S. T. 2015. Southern Ocean wind-driven entrainment enhances satellite chlorophyll-a through the summer. *Journal of Geophysical Research-Oceans,* 120**,** 304-323.

Carter, L., Mccave, I. N. & Williams, M. J. M. 2008. Circulation and Water Masses of the Southern Ocean: A Review. *In:* FLORINDO, F. & SIEGERT, M. (eds.) *Antarctic Climate Evolution.* Elsevier.

Cassar, N., Bender, M. L., Barnett, B. A., Fan, S., Moxim, W. J., Levy, H., 2nd & Tilbrook, B. 2007. The Southern Ocean biological response to aeolian iron deposition. *Science,* 317**,** 1067-70.

Castillo, D. J., Dithugoe, C. D., Bezuidt, O. K. & Makhalanyane, T. P. 2022. Microbial ecology of the Southern Ocean. *FEMS Microbiol Ecol,* 98.

Cavagna, A. J., Fripiat, F., Elskens, M., Mangion, P., Chirurgien, L., Closset, I., Lasbleiz, M., Florez-Leiva, L., Cardinal, D., Leblanc, K., Fernandez, C., Lefèvre, D., Oriol, L., Blain, S., Quéguiner, B. & Dehairs, F. 2015. Production regime and associated N cycling in the vicinity of Kerguelen Island, Southern Ocean. *Biogeosciences,* 12**,** 6515-6528.

Charalampopoulou, A., Poulton, A. J., Bakker, D. C. E., Lucas, M. I., Stinchcombe, M. C. & Tyrrell, T. 2016. Environmental drivers of coccolithophore abundance and calcification across Drake Passage (Southern Ocean). *Biogeosciences,* 13**,** 5917-5935.

Chierici, M., Fransson, A., Turner, D. R., Pakhomov, E. A. & Froneman, P. W. 2004. Variability in pH, fCO2, oxygen and flux of CO2 in the surface water along a transect in the Atlantic sector of the Southern Ocean. *Deep Sea Research Part II: Topical Studies in Oceanography,* 51**,** 2773-2787.

Cho, H., Hwang, C. Y., Kim, J. G., Kang, S., Knittel, K., Choi, A., Kim, S. H., Rhee, S. K., Yang, E. J., Lee, S. & Hyun, J. H. 2020. A Unique Benthic Microbial Community Underlying the Phaeocystis antarctica-Dominated Amundsen Sea Polynya, Antarctica: A Proxy for Assessing the Impact of Global Changes. *Frontiers in Marine Science,* 6**,** 797.

Cimino, M. A., Conroy, J. A., Connors, E., Bowman, J., Corso, A., Ducklow, H., Fraser, W., Friedlaender, A., Kim, H. H., Larsen, G. D., Moffat, C., Nichols, R., Pallin, L., Patterson-Fraser, D., Roberts, D., Roberts, M., Steinberg, D. K., Thibodeau, P., Trinh, R., Schofield, O. & Stammerjohn, S. 2023. Long-term patterns in ecosystem phenology near Palmer Station, Antarctica, from the perspective of the Adelie penguin. *Ecosphere,* 14**,** e4417.

Clarke, L. J., Suter, L., King, R., Bissett, A. & Deagle, B. E. 2018. Antarctic Krill Are Reservoirs for Distinct Southern Ocean Microbial Communities. *Front Microbiol,* 9**,** 3226.

Cochlan, W. P. 2008. Nitrogen Uptake in the Southern Ocean. *Nitrogen in the Marine Environment, 2nd Edition***,** 569-596.

Cochlan, W. P. & Bronk, D. A. 2001. Nitrogen uptake kinetics in the Ross Sea, Antarctica. *Deep-Sea Research Part Ii-Topical Studies in Oceanography,* 48**,** 4127-4153.

Cochlan, W. P., Bronk, D. A. & Coale, K. H. 2002. Trace metals and nitrogenous nutrition of Antarctic phytoplankton: experimental observations in the Ross Sea. *Deep-Sea Research Part Ii-Topical Studies in Oceanography,* 49**,** 3365-3390.

Cochlan, W. P., Harrison, P. J. & Denman, K. L. 1991. Diel Periodicity of Nitrogen Uptake by Marine-Phytoplankton in Nitrate-Rich Environments. *Limnology and Oceanography,* 36**,** 1689-1700.

Coggins, A., Watson, A. J., Schuster, U., Mackay, N., King, B., Mcdonagh, E. & Poulton, A. J. 2023. Surface ocean carbon budget in the 2017 south Georgia diatom bloom: Observations and validation of profiling biogeochemical argo floats. *Deep-Sea Research Part Ii-Topical Studies in Oceanography,* 209**,** 105275.

Comiso, J. C. 2010. Variability and trends of the global sea ice cover. *Sea ice,* 2**,** 205-246.

Conan, P., Sondergaard, M., Kragh, T., Thingstad, F., Pujo-Pay, M., Williams, P. J. L. B., Markager, S., Cauwet, G., Borch, N. H., Evans, D. & Riemann, B. 2007. Partitioning of organic production in marine plankton communities: The effects of inorganic nutrient ratios and community composition on new dissolved organic matter. *Limnology and Oceanography,* 52**,** 753-765.

Conover, R. J. & Gustavson, K. R. 1999. Sources of urea in arctic seas: zooplankton metabolism. *Marine Ecology Progress Series,* 179**,** 41-54.

Conover, R. J., Mumm, N., Bruecker, P. & Mackenzie, S. 1999. Sources of urea in arctic seas: seasonal fast ice? *Marine Ecology Progress Series,* 179**,** 55-69.

Cory, R. M. & Kling, G. W. 2018. Interactions between sunlight and microorganisms influence dissolved organic matter degradation along the aquatic continuum. *Limnology and Oceanography Letters,* 3**,** 102-116.

Costa, R. R., Mendes, C. R. B., Tavano, V. M., Dotto, T. S., Kerr, R., Monteiro, T., Odebrecht, C. & Secchi, E. R. 2020. Dynamics of an intense diatom bloom in the Northern Antarctic Peninsula, February 2016. *Limnology and Oceanography,* 65**,** 2056-2075.

Cota, G. F., Smith, W. O., Nelson, D. M., Muench, R. D. & Gordon, L. I. 1992. Nutrient and Biogenic Particulate Distributions, Primary Productivity and Nitrogen Uptake in the Weddell-Scotia Sea Marginal Ice-Zone during Winter. *Journal of Marine Research,* 50**,** 155-181.

Cullen, J. T., Chase, Z., Coale, K. H., Fitzwater, S. E. & Sherrell, R. M. 2003. Effect of iron limitation on the cadmium to phosphorus ratio of natural phytoplankton assemblages from the Southern Ocean. *Limnology and Oceanography,* 48**,** 1079-1087.

D'andrilli, J., Cooper, W. T., Foreman, C. M. & Marshall, A. G. 2015. An ultrahigh-resolution mass spectrometry index to estimate natural organic matter lability. *Rapid Commun Mass Spectrom,* 29**,** 2385-401.

Dahl, C., Hell, R., Leustek, T. & Knaff, D. 2008. Introduction to sulfur metabolism in phototrophic organisms. *Sulfur metabolism in phototrophic organisms***,** 1-14.

Davis, J. & Benner, R. 2007. Quantitative estimates of labile and semi-labile dissolved organic carbon in the western Arctic Ocean: A molecular approach. *Limnology and Oceanography,* 52**,** 2434-2444.

De Baar, H. J. W., De Jong, J. T. M., Bakker, D. C. E., Löscher, B. M., Veth, C., Bathmann, U. & Smetacek, V. 1995. Importance of iron for plankton blooms and carbon dioxide drawdown in the Southern Ocean. *Nature,* 373**,** 412-415.

De Lavergne, C., Madec, G., Roquet, F., Holmes, R. M. & Mcdougall, T. J. 2017. Abyssal ocean overturning shaped by seafloor distribution. *Nature,* 551**,** 181-186.

Delille, B., Jourdain, B., Borges, A. V., Tison, J.-L. & Delille, D. 2007. Biogas (CO2, O2, dimethylsulfide) dynamics in spring Antarctic fast ice. *Limnology and Oceanography,* 52**,** 1367-1379.

Delille, B., Vancoppenolle, M., Geilfus, N. X., Tilbrook, B., Lannuzel, D., Schoemann, V., Becquevort, S., Carnat, G., Delille, D., Lancelot, C., Chou, L., Dieckmann, G. S. & Tison, J. L. 2014. Southern Ocean CO2 sink: The contribution of the sea ice. *Journal of Geophysical Research: Oceans,* 119**,** 6340-6355.

Deppeler, S. L. & Davidson, A. T. 2017. Southern Ocean Phytoplankton in a Changing Climate. *Frontiers in Marine Science,* 4.

Descolas-Gros, C. & Fontungne, M. 2006. Stable carbon isotope fractionation by marine phytoplankton during photosynthesis. *Plant, Cell & Environment,* 13**,** 207-218.

Devries, T. 2014. The oceanic anthropogenic CO2 sink: Storage, air-sea fluxes, and transports over the industrial era. *Global Biogeochemical Cycles,* 28**,** 631-647.

Dierssen, H. M., Smith, R. C. & Vernet, M. 2002. Glacial meltwater dynamics in coastal waters west of the Antarctic peninsula. *Proc Natl Acad Sci U S A,* 99**,** 1790-5.

Dinniman, M. S., St-Laurent, P., Arrigo, K. R., Hofmann, E. E. & Van Dijken, G. L. 2023. Sensitivity of the Relationship Between Antarctic Ice Shelves and Iron Supply to Projected Changes in the Atmospheric Forcing. *Journal of Geophysical Research-Oceans,* 128**,** e2022JC019210.

Dittmar, T., Koch, B., Hertkorn, N. & Kattner, G. 2008. A simple and efficient method for the solid-phase extraction of dissolved organic matter (SPE-DOM) from seawater. *Limnology and Oceanography-Methods,* 6**,** 230-235.

Dittmar, T., Lennartz, S. T., Buck-Wiese, H., Hansel, D. A., Santinelli, C., Vanni, C., Blasius, B. & Hehemann, J. H. 2021. Enigmatic persistence of dissolved organic matter in the ocean. *Nature Reviews Earth & Environment,* 2**,** 570-583.

Dittrich, R., Henley, S. F., Ducklow, H. W. & Meredith, M. P. 2022. Dissolved organic carbon and nitrogen cycling along the west Antarctic Peninsula during summer. *Progress in Oceanography,* 206**,** 102854.

Ditullio, G. R. & Smith, W. O. 1996. Spatial patterns in phytoplankton biomass and pigment distributions in the Ross Sea. *Journal of Geophysical Research-Oceans,* 101**,** 18467-18477.

Dong, S., Sprintall, J., Gille, S. T. & Talley, L. 2008. Southern Ocean mixed-layer depth from Argo float profiles. *Journal of Geophysical Research-Oceans,* 113.

Dortch, Q. 1990. The Interaction between Ammonium and Nitrate Uptake in Phytoplankton. *Marine Ecology Progress Series,* 61**,** 183-201.

Dotto, T. S., Kerr, R., Mata, M. M. & Garcia, C. a. E. 2016. Multidecadal freshening and lightening in the deep waters of the Bransfield Strait, Antarctica. *Journal of Geophysical Research-Oceans,* 121**,** 3741-3756.

Downes, S. M., Bindoff, N. L. & Rintoul, S. R. 2010. Changes in the Subduction of Southern Ocean Water Masses at the End of the Twenty-First Century in Eight IPCC Models. *Journal of Climate,* 23**,** 6526-6541.

Du Plessis, M., Swart, S., Ansorge, I. J. & Mahadevan, A. 2017. Submesoscale processes promote seasonal restratification in the Subantarctic Ocean. *Journal of Geophysical Research: Oceans,* 122**,** 2960-2975.

Ducklow, H., Doney, S. & Sailley, S. 2015. Ecological controls on biogeochemical fluxes in the western Antarctic peninsula studied with an inverse foodweb model. *Advances in Polar Science,* 122.

Ducklow, H. W., Baker, K., Martinson, D. G., Quetin, L. B., Ross, R. M., Smith, R. C., Stammerjohn, S. E., Vernet, M. & Fraser, W. 2007. Marine pelagic ecosystems: the west Antarctic Peninsula. *Philos Trans R Soc Lond B Biol Sci,* 362**,** 67-94.

Ducklow, H. W., Fraser, W. R., Meredith, M. P., Stammerjohn, S. E., Doney, S. C., Martinson, D. G., Sailley, S. F., Schofield, O. M., Steinberg, D. K., Venables, H. J. & Amsler, C. D. 2013. West Antarctic Peninsula An Ice-Dependent Coastal Marine Ecosystem in Transition. *Oceanography,* 26**,** 190-203.

Ducklow, H. W., Schofield, O., Vernet, M., Stammerjohn, S. & Erickson, M. 2012. Multiscale control of bacterial production by phytoplankton dynamics and sea ice along the western Antarctic Peninsula: A regional and decadal investigation. *Journal of Marine Systems,* 98-99**,** 26-39.

Dugdale, R. C. & Goering, J. J. 2003. Uptake of New and Regenerated Forms of Nitrogen in Primary Productivity. *Limnology and Oceanography,* 12**,** 196-206.

Dugdale, R. C. & Wilkerson, F. P. 2003. The use of 15N to measure nitrogen uptake in eutrophic oceans; experimental considerations. *Limnology and Oceanography,* 31**,** 673-689.

Dutkiewicz, S., Cermeno, P., Jahn, O., Follows, M. J., Hickman, A. E., Taniguchi, D. a. A. & Ward, B. 2020. Dimensions of marine phytoplankton diversity. *Biogeosciences,* 17**,** 609-634.

Dutkiewicz, S., Hickman, A. E., Jahn, O., Gregg, W. W., Mouw, C. B. & Follows, M. J. 2015. Capturing optically important constituents and properties in a marine biogeochemical and ecosystem model. *Biogeosciences,* 12**,** 4447-4481.

Ellwood, M. J., Strzepek, R. F., Strutton, P. G., Trull, T. W., Fourquez, M. & Boyd, P. W. 2020. Distinct iron cycling in a Southern Ocean eddy. *Nat Commun,* 11**,** 825.

Elskens, M., Baeyens, W. & Goeyens, L. 1997. Contribution of nitrate to the uptake of nitrogen by phytoplankton in an ocean margin environment. *Hydrobiologia,* 353**,** 139-152.

Engel, A., Handel, N., Wohlers, J., Lunau, M., Grossart, H. P., Sommer, U. & Riebesell, U. 2010. Effects of sea surface warming on the production and composition of dissolved organic matter during phytoplankton blooms: results from a mesocosm study. *Journal of Plankton Research,* 33**,** 357-372.

Eppley, R. W. & Peterson, B. J. 1979. Particulate Organic-Matter Flux and Planktonic New Production in the Deep Ocean. *Nature,* 282**,** 677-680.

Evans, C. & Brussaard, C. P. 2012. Regional variation in lytic and lysogenic viral infection in the Southern Ocean and its contribution to biogeochemical cycling. *Appl Environ Microbiol,* 78**,** 6741-8.

Evans, C., Thomson, P. G., Davidson, A. T., Bowie, A. R., Van Den Enden, R., Witte, H. & Brussaard, C. P. D. 2011. Potential climate change impacts on microbial distribution and carbon cycling in the Australian Southern Ocean. *Deep-Sea Research Part Ii-Topical Studies in Oceanography,* 58**,** 2150-2161.

Evans, D. G., Zika, J. D., Naveira Garabato, A. C. & Nurser, A. J. G. 2018. The Cold Transit of Southern Ocean Upwelling. *Geophysical Research Letters,* 45**,** 13386-13395.

Fernández I, C., Raimbault, P., Garcia, N., Rimmelin, P. & Caniaux, G. 2005. An estimation of annual new production and carbon fluxes in the northeast Atlantic Ocean during 2001. *Journal of Geophysical Research: Oceans,* 110.

Figuerola, B., Hancock, A. M., Bax, N., Cummings, V. J., Downey, R., Griffiths, H. J., Smith, J. & Stark, J. S. 2021. A Review and Meta-Analysis of Potential Impacts of Ocean Acidification on Marine Calcifiers From the Southern Ocean. *Frontiers in Marine Science,* 8.

Finkel, Z. V., Beardall, J., Flynn, K. J., Quigg, A., Rees, T. a. V. & Raven, J. A. 2009. Phytoplankton in a changing world: cell size and elemental stoichiometry. *Journal of Plankton Research,* 32**,** 119-137.

Finkel, Z. V., Follows, M. J., Liefer, J. D., Brown, C. M., Benner, I. & Irwin, A. J. 2016. Phylogenetic Diversity in the Macromolecular Composition of Microalgae. *PLoS One,* 11**,** e0155977.

Fisher, B. J., Poulton, A. J., Meredith, M. P., Baldry, K., Schofield, O. & Henley, S. F. 2023. Biogeochemistry of climate driven shifts in Southern Ocean primary producers. *Biogeosciences Discuss.,* 2023**,** 1-29.

Flerus, R., Lechtenfeld, O. J., Koch, B. P., Mccallister, S. L., Schmitt-Kopplin, P., Benner, R., Kaiser, K. & Kattner, G. 2012. A molecular perspective on the ageing of marine dissolved organic matter. *Biogeosciences,* 9**,** 1935-1955.

Flynn, R. F., Haraguchi, L., Mcquaid, J., Burger, J. M., Mutseka Lunga, P., Stirnimann, L., Samanta, S., Roychoudhury, A. N. & Fawcett, S. E. 2023. Nanoplankton: The dominant vector for carbon export across the Atlantic Southern Ocean in spring. *Sci Adv,* 9**,** eadi3059.

Fourquez, M., Janssen, D. J., Conway, T. M., Cabanes, D., Ellwood, M. J., Sieber, M., Trimborn, S. & Hassler, C. 2023. Chasing iron bioavailability in the Southern Ocean: Insights from Phaeocystis antarctica and iron speciation. *Sci Adv,* 9**,** eadf9696.

Franck, V. M., Brzezinski, M. A., Coale, K. H. & Nelson, D. M. 2000. Iron and silicic acid concentrations regulate Si uptake north and south of the Polar Frontal Zone in the Pacific Sector of the Southern Ocean. *Deep Sea Research Part II: Topical Studies in Oceanography,* 47**,** 3315-3338.

Fransson, A., Chierici, M., Anderson, L. G. & David, R. 2004. Transformation of carbon and oxygen in the surface layer of the eastern Atlantic sector of the Southern Ocean. *Deep-Sea Research Part Ii-Topical Studies in Oceanography,* 51**,** 2757-2772.

Freeman, N. M., Lovenduski, N. S., Munro, D. R., Krumhardt, K. M., Lindsay, K., Long, M. C. & Maclennan, M. 2018. The Variable and Changing Southern Ocean Silicate Front: Insights From the CESM Large Ensemble. *Global Biogeochemical Cycles,* 32**,** 752-768.

Friedlingstein, P., Jones, M. W., O'sullivan, M., Andrew, R. M., Bakker, D. C. E., Hauck, J., Le Quéré, C., Peters, G. P., Peters, W., Pongratz, J., Sitch, S., Canadell, J. G., Ciais, P., Jackson, R. B., Alin, S. R., Anthoni, P., Bates, N. R., Becker, M., Bellouin, N., Bopp, L., Chau, T. T. T., Chevallier, F., Chini, L. P., Cronin, M., Currie, K. I., Decharme, B., Djeutchouang, L. M., Dou, X. Y., Evans, W., Feely, R. A., Feng, L., Gasser, T., Gilfillan, D., Gkritzalis, T., Grassi, G., Gregor, L., Gruber, N., Gürses, Ö., Harris, I., Houghton, R. A., Hurtt, G. C., Iida, Y., Ilyina, T., Luijkx, I. T., Jain, A., Jones, S. D., Kato, E., Kennedy, D., Goldewijk, K. K., Knauer, J., Korsbakken, J. I., Körtzinger, A., Landschützer, P., Lauvset, S. K., Lefèvre, N., Lienert, S., Liu, J. J., Marland, G., Mcguire, P. C., Melton, J. R., Munro, D. R., Nabel, J. E. M. S., Nakaoka, S. I., Niwa, Y., Ono, T., Pierrot, D., Poulter, B., Rehder, G., Resplandy, L., Robertson, E., Rödenbeck, C., Rosan, T. M., Schwinger, J., Schwingshackl, C., Séférian, R., Sutton, A. J., Sweeney, C., Tanhua, T., Tans, P. P., Tian, H. Q., Tilbrook, B., Tubiello, F., Van Der Werf, G. R., Vuichard, N., Wada, C., Wanninkhof, R., Watson, A. J., Willis, D., Wiltshire, A. J., Yuan, W. P., Yue, C., Yue, X., Zaehle, S. & Zeng, J. Y. 2022a. Global Carbon Budget 2021. *Earth System Science Data,* 14**,** 1917-2005.

Friedlingstein, P., O'sullivan, M., Jones, M. W., Andrew, R. M., Gregor, L., Hauck, J., Le Quéré, C., Luijkx, I. T., Olsen, A., Peters, G. P., Peters, W., Pongratz, J., Schwingshackl, C., Sitch, S., Canadell, J. G., Ciais, P., Jackson, R. B., Alin, S. R., Alkama, R., Arneth, A., Arora, V. K., Bates, N. R., Becker, M., Bellouin, N., Bittig, H. C., Bopp, L., Chevallier, F., Chini, L. P., Cronin, M., Evans, W., Falk, S., Feely, R. A., Gasser, T., Gehlen, M., Gkritzalis, T., Gloege, L., Grassi, G., Gruber, N., Gürses, Ö., Harris, I., Hefner, M., Houghton, R. A., Hurtt, G. C., Iida, Y., Ilyina, T., Jain, A. K., Jersild, A., Kadono, K., Kato, E., Kennedy, D., Goldewijk, K. K., Knauer, J., Korsbakken, J. I., Landschützer, P., Lefèvre, N., Lindsay, K., Liu, J. J., Liu, Z.,

Marland, G., Mayot, N., Mcgrath, M. J., Metzl, N., Monacci, N. M., Munro, D. R., Nakaoka, S. I., Niwa, Y., O'brien, K., Ono, T., Palmer, P. I., Pan, N. Q., Pierrot, D., Pocock, K., Poulter, B., Resplandy, L., Robertson, E., Rödenbeck, C., Rodriguez, C., Rosan, T. M., Schwinger, J., Séférian, R., Shutler, J. D., Skjelvan, I., Steinhoff, T., Sun, Q., Sutton, A. J., Sweeney, C., Takao, S., Tanhua, T., Tans, P. P., Tian, X. J., Tian, H. Q., Tilbrook, B., Tsujino, H., Tubiello, F., Van Der Werf, G. R., Walker, A. P., Wanninkhof, R., Whitehead, C., Wranne, A. W., Wright, R., et al. 2022b. Global Carbon Budget 2022. *Earth System Science Data,* 14**,** 4811-4900.

Fripiat, F., Martínez-García, A., Marconi, D., Fawcett, S. E., Kopf, S. H., Luu, V. H., Rafter, P. A., Zhang, R., Sigman, D. M. & Haug, G. H. 2021. Nitrogen isotopic constraints on nutrient transport to the upper ocean. *Nature Geoscience,* 14**,** 855-+.

Frölicher, T. L., Sarmiento, J. L., Paynter, D. J., Dunne, J. P., Krasting, J. P. & Winton, M. 2015. Dominance of the Southern Ocean in Anthropogenic Carbon and Heat Uptake in CMIP5 Models. *Journal of Climate,* 28**,** 862-886.

Froneman, P. W. & Perissinotto, R. 1996. Microzooplankton grazing and protozooplankton community structure in the South Atlantic and in the Atlantic sector of the Southern Ocean. *Deep-Sea Research Part I-Oceanographic Research Papers,* 43**,** 703-721.

Fu, W., Moore, J. K., Primeau, F., Collier, N., Ogunro, O. O., Hoffman, F. M. & Randerson, J. T. 2022. Evaluation of Ocean Biogeochemistry and Carbon Cycling in CMIP Earth System Models With the International Ocean Model Benchmarking (IOMB) Software System. *Journal of Geophysical Research: Oceans,* 127.

Fu, W. W., Randerson, J. T. & Moore, J. K. 2016. Climate change impacts on net primary production (NPP) and export production (EP) regulated by increasing stratification and phytoplankton community structure in the CMIP5 models. *Biogeosciences,* 13**,** 5151-5170.

Fuhrman, J. A. 1999. Marine viruses and their biogeochemical and ecological effects. *Nature,* 399**,** 541-8.

Gall, M. P., Boyd, P. W., Hall, J., Safi, K. A. & Chang, H. 2001. Phytoplankton processes. Part 1: Community structure during the Southern Ocean Iron RElease Experiment (SOIREE). *Deep-Sea Research Part Ii-Topical Studies in Oceanography,* 48**,** 2551-2570.

Gandhi, N., Ramesh, R., Laskar, A. H., Sheshshayee, M. S., Shetye, S., Anilkumar, N., Patil, S. M. & Mohan, R. 2012. Zonal variability in primary production and nitrogen uptake rates in the southwestern Indian Ocean and the Southern Ocean. *Deep-Sea Research Part I-Oceanographic Research Papers,* 67**,** 32-43.

Garcia, H., Weathers, K., Paver, C., Smolyar, I., Boyer, T., Locarnini, M., Zweng, M., Mishonov, A., Baranova, O. & Seidov, D. 2019. World ocean atlas 2018. Vol. 4: Dissolved inorganic nutrients (phosphate, nitrate and nitrate+ nitrite, silicate).

Garcia, N. S., Sedwick, P. N. & Ditullio, G. R. 2009. Influence of irradiance and iron on the growth of colonial Phaeocystis antarctica: implications for seasonal bloom dynamics in the Ross Sea, Antarctica. *Aquatic Microbial Ecology,* 57**,** 203-220.

Garibotti, I. A., Vernet, M. & Ferrario, M. E. 2005. Annually recurrent phytoplanktonic assemblages during summer in the seasonal ice zone west of the Antarctic Peninsula (Southern Ocean). *Deep-Sea Research Part I-Oceanographic Research Papers,* 52**,** 1823-1841.

Garibotti, I. A., Vernet, M., Ferrario, M. E., Smith, R. C., Ross, R. M. & Quetin, L. B. 2003a. Phytoplankton spatial distribution patterns along the western Antarctic Peninsula (Southern Ocean). *Marine Ecology Progress Series,* 261**,** 21-39.

Garibotti, I. A., Vernet, M., Kozlowski, W. A. & Ferrario, M. E. 2003b. Composition and biomass of phytoplankton assemblages in coastal Antarctic waters: a comparison of chemotaxonomic and microscopic analyses. *Marine Ecology Progress Series,* 247**,** 27-42.

Garzio, L. M. & Steinberg, D. K. 2013. Microzooplankton community composition along the Western Antarctic Peninsula. *Deep-Sea Research Part I-Oceanographic Research Papers,* 77**,** 36-49.

Gilbert, P. M., Lipschultz, F., Mccarthy, J. J. & Altabet, M. A. 2003. Isotope dilution models of uptake and remineralization of ammonium by marine plankton. *Limnology and Oceanography,* 27**,** 639-650.

Glibert, P. M., Wilkerson, F. P., Dugdale, R. C., Raven, J. A., Dupont, C. L., Leavitt, P. R., Parker, A. E., Burkholder, J. M. & Kana, T. M. 2016. Pluses and minuses of ammonium and nitrate uptake and assimilation by phytoplankton and implications for productivity and community composition, with emphasis on nitrogen-enriched conditions. *Limnology and Oceanography,* 61**,** 165-197.

Goeyens, L., Sörensson, F., Tréguer, P., Morvan, J., Panouse, M. & Dehairs, F. 1991a. Spatiotemporal variability of inorganic nitrogen stocks and uptake fluxes in the Scotia-Weddell Confluence area during November and December 1988. *Marine Ecology Progress Series,* 77**,** 7-19.

Goeyens, L., Treguer, P., Baumann, M. E. M., Baeyens, W. & Dehairs, F. 1995. The Leading Role of Ammonium in the Nitrogen Uptake Regime of Southern-Ocean Marginal Ice Zones. *Journal of Marine Systems,* 6**,** 345-361.

Goeyens, L., Treguer, P., Lancelot, C., Mathot, S., Becquevort, S., Morvan, J., Dehairs, F. & Baeyens, W. 1991b. Ammonium Regeneration in the Scotia-Weddell Confluence Area during Spring 1988. *Marine Ecology Progress Series,* 78**,** 241-252.

Gordon, A. L. 1991. Two stable modes of Southern Ocean winter stratification. *Elsevier Oceanography Series.* Elsevier.

Gordon, A. L. & Huber, B. A. 2012. Southern ocean winter mixed layer. *Journal of Geophysical Research: Oceans,* 95**,** 11655-11672.

Gowing, M. M., Garrison, D. L., Gibson, A. H., Krupp, J. M., Jeffries, M. O. & Fritsen, C. H. 2004. Bacterial and viral abundance in Ross Sea summer pack ice communities. *Marine Ecology Progress Series,* 279**,** 3-12.

Gray, A. R. 2024. The Four-Dimensional Carbon Cycle of the Southern Ocean. *Ann Rev Mar Sci,* 16**,** 163-190.

Gregg, W. W., Conkright, M. E., Ginoux, P., O'reilly, J. E. & Casey, N. W. 2003. Ocean primary production and climate: Global decadal changes. *Geophysical Research Letters,* 30.

Gregor, L., Kok, S. & Monteiro, P. M. S. 2018. Interannual drivers of the seasonal cycle of CO2 in the Southern Ocean. *Biogeosciences,* 15**,** 2361-2378.

Grover, M. 2021. *Correctly calculating annual averages with Xarray* [Online]. Available: https://ncar.github.io/esds/posts/2021/yearly-averages-xarray/ [Accessed 20/01/2024 2024].

Gruber, N., Landschutzer, P. & Lovenduski, N. S. 2019. The Variable Southern Ocean Carbon Sink. *Ann Rev Mar Sci,* 11**,** 159-186.

Guidi, L., Chaffron, S., Bittner, L., Eveillard, D., Larhlimi, A., Roux, S., Darzi, Y., Audic, S., Berline, L., Brum, J., Coelho, L. P., Espinoza, J. C. I., Malviya, S., Sunagawa, S., Dimier, C., Kandels-Lewis, S., Picheral, M., Poulain, J., Searson, S., Tara Oceans, C., Stemmann, L., Not, F., Hingamp, P., Speich, S., Follows, M., Karp-Boss, L., Boss, E., Ogata, H., Pesant,

S., Weissenbach, J., Wincker, P., Acinas, S. G., Bork, P., De Vargas, C., Iudicone, D., Sullivan, M. B., Raes, J., Karsenti, E., Bowler, C. & Gorsky, G. 2016. Plankton networks driving carbon export in the oligotrophic ocean. *Nature,* 532**,** 465-470.

Guillard, R. R. Culture of phytoplankton for feeding marine invertebrates. Culture of marine invertebrate animals: proceedings—1st conference on culture of marine invertebrate animals greenport, 1975. Springer, 29-60.

Haberman, K. L., Ross, R. M. & Quetin, L. B. 2003. Diet of the Antarctic krill (Euphausia superba Dana): II.: Selective grazing in mixed phytoplankton assemblages. *Journal of Experimental Marine Biology and Ecology,* 283**,** 97-113.

Hancock, A. M., Davidson, A. T., Mckinlay, J., Mcminn, A., Schulz, K. G. & Van Den Enden, R. L. 2018. Ocean acidification changes the structure of an Antarctic coastal protistan community. *Biogeosciences,* 15**,** 2393-2410.

Hansell, D. A. 2013. Recalcitrant dissolved organic carbon fractions. *Ann Rev Mar Sci,* 5**,** 421-45.

Hansell, D. A. & Carlson, C. A. 2001. Biogeochemistry of total organic carbon and nitrogen in the Sargasso Sea: control by convective overturn. *Deep-Sea Research Part Ii-Topical Studies in Oceanography,* 48**,** 1649-1667.

Hansell, D. A., Carlson, C. A., Repeta, D. J. & Schlitzer, R. 2009. Dissolved Organic Matter in the Ocean a Controversy Stimulates New Insights. *Oceanography,* 22**,** 202-211.

Harrison, P. J., Waters, R. E. & Taylor, F. J. R. 2008. A Broad Spectrum Artificial Sea Water Medium for Coastal and Open Ocean Phytoplankton. *Journal of Phycology,* 16**,** 28-35.

Hauck, J. & Volker, C. 2015. Rising atmospheric CO2 leads to large impact of biology on Southern Ocean CO2 uptake via changes of the Revelle factor. *Geophys Res Lett,* 42**,** 1459-1464.

Hauck, J., Völker, C., Wolf-Gladrow, D. A., Laufkötter, C., Vogt, M., Aumont, O., Bopp, L., Buitenhuis, E. T., Doney, S. C., Dunne, J., Gruber, N., Hashioka, T., John, J., Le Quéré, C., Lima, I. D., Nakano, H., Séférian, R. & Totterdell, I. 2015. On the Southern Ocean CO2 uptake and the role of the biological carbon pump in the 21st century. *Global Biogeochemical Cycles,* 29**,** 1451-1470.

Haumann, F. A., Gruber, N., Munnich, M., Frenger, I. & Kern, S. 2016. Sea-ice transport driving Southern Ocean salinity and its recent trends. *Nature,* 537**,** 89-92.

Hauri, C., Doney, S. C., Takahashi, T., Erickson, M., Jiang, G. & Ducklow, H. W. 2015. Two decades of inorganic carbon dynamics along the West Antarctic Peninsula. *Biogeosciences,* 12**,** 6761-6779.

Hayward, A., Pinkerton, M. H. & Gutierrez-Rodriguez, A. 2023. Phytoclass: A pigment-based chemotaxonomic method to determine the biomass of phytoplankton classes. *Limnology and Oceanography-Methods,* 21**,** 220-241.

Hayward, A., Pinkerton, M. H., Wright, S. W., Gutiérrez-Rodriguez, A. & Law, C. S. 2024. Twenty-six years of phytoplankton pigments reveal a circumpolar Class Divide around the Southern Ocean. *Communications Earth & Environment,* 5**,** 92.

Hendry, K. R., Rickaby, R. E. M., De Hoog, J. C. M., Weston, K. & Rehkämper, M. 2008. Cadmium and phosphate in coastal Antarctic seawater: Implications for Southern Ocean nutrient cycling. *Marine Chemistry,* 112**,** 149-157.

Henley, S. F., Cavan, E. L., Fawcett, S. E., Kerr, R., Monteiro, T., Sherrell, R. M., Bowie, A. R., Boyd, P. W., Barnes, D. K. A., Schloss, I. R., Marshall, T., Flynn, R. & Smith, S. 2020. Changing Biogeochemistry of the Southern Ocean and Its Ecosystem Implications. *Frontiers in Marine Science,* 7.

Henley, S. F., Cozzi, S., Fripiat, F., Lannuzel, D., Nomura, D., Thomas, D. N., Meinersg, K. M., Vancoppenollej, M., Arrigo, K., Stefels, J., Van Leeuwe, M., Moreau, S., Jones, E. M., Fransson, A., Chierici, M. & Delilleo, B. 2023. Macronutrient biogeochemistry in Antarctic land-fast sea ice: Insights from a circumpolar data compilation. *Marine Chemistry,* 257**,** 104324.

Henley, S. F., Jones, E. M., Venables, H. J., Meredith, M. P., Firing, Y. L., Dittrich, R., Heiser, S., Stefels, J. & Dougans, J. 2018. Macronutrient and carbon supply, uptake and cycling across the Antarctic Peninsula shelf during summer. *Philos Trans A Math Phys Eng Sci,* 376**,** 20170168.

Henley, S. F., Schofield, O. M., Hendry, K. R., Schloss, I. R., Steinberg, D. K., Moffat, C., Peck, L. S., Costa, D. P., Bakker, D. C. E., Hughes, C., Rozema, P. D., Ducklow, H. W., Abele, D., Stefels, J., Van Leeuwe, M. A., Brussaard, C. P. D., Buma, A. G. J., Kohut, J., Sahade, R., Friedlaender, A. S., Stammerjohn, S. E., Venables, H. J. & Meredith, M. P. 2019. Variability and change in the west Antarctic Peninsula marine system: Research priorities and opportunities. *Progress in Oceanography,* 173**,** 208-237.

Henley, S. F., Tuerena, R. E., Annett, A. L., Fallick, A. E., Meredith, M. P., Venables, H. J., Clarke, A. & Ganeshram, R. S. 2017. Macronutrient supply, uptake and recycling in the coastal ocean of the west Antarctic Peninsula. *Deep-Sea Research Part Ii-Topical Studies in Oceanography,* 139**,** 58-76.

Henson, S., Bisson, K., Hammond, M. L., Martin, A., Mouw, C. & Yool, A. 2024. Effect of sampling bias on global estimates of ocean carbon export. *Environmental Research Letters,* 19**,** 024009.

Henson, S. A., Cael, B. B., Allen, S. R. & Dutkiewicz, S. 2021. Future phytoplankton diversity in a changing climate. *Nat Commun,* 12**,** 5372.

Henson, S. A., Laufkötter, C., Leung, S., Giering, S. L. C., Palevsky, H. I. & Cavan, E. L. 2022. Uncertain response of ocean biological carbon export in a changing world. *Nature Geoscience,* 15**,** 248-254.

Hertkorn, N., Harir, M., Koch, B. P., Michalke, B. & Schmitt-Kopplin, P. 2013. High-field NMR spectroscopy and FTICR mass spectrometry: powerful discovery tools for the molecular level characterization of marine dissolved organic matter. *Biogeosciences,* 10**,** 1583-1624.

Ho, T. Y., Quigg, A., Finkel, Z. V., Milligan, A. J., Wyman, K., Falkowski, P. G. & Morel, F. M. M. 2003. The Elemental Composition of Some Marine Phytoplankton. *Journal of Phycology,* 39**,** 1145-1159.

Hogg, A. M., Meredith, M. P., Chambers, D. P., Abrahamsen, E. P., Hughes, C. W. & Morrison, A. K. 2015. Recent trends in the Southern Ocean eddy field. *Journal of Geophysical Research-Oceans,* 120**,** 257-267.

Hogg, A. M. & Munday, D. R. 2014. Does the sensitivity of Southern Ocean circulation depend upon bathymetric details? *Philos Trans A Math Phys Eng Sci,* 372**,** 20130050.

Holmes, R. M., Mcclelland, J. W., Sigman, D. M., Fry, B. & Peterson, B. J. 1998. Measuring – NH4+ in marine, estuarine and fresh waters: An adaptation of the ammonia diffusion method for samples with low ammonium concentrations. *Marine Chemistry,* 60**,** 235-243.

Hopkinson, C. S., Jr. & Vallino, J. J. 2005. Efficient export of carbon to the deep ocean through dissolved organic matter. *Nature,* 433**,** 142-5.

Hopwood, M. J., Carroll, D., Hofer, J., Achterberg, E. P., Meire, L., Le Moigne, F. a. C., Bach, L. T., Eich, C., Sutherland, D. A. & Gonzalez, H. E. 2019. Highly variable iron content

modulates iceberg-ocean fertilisation and potential carbon export. *Nat Commun,* 10**,** 5261.

Hutchins, D. A. & Bruland, K. W. 1998. Iron-limited diatom growth and Si:N uptake ratios in a coastal upwelling regime. *Nature,* 393**,** 561-564.

Hutchins, D. A., Sedwick, P. N., Ditullio, G. R., Boyd, P. W., Quéguiner, B., Griffiths, F. B. & Crossley, C. 2001. Control of phytoplankton growth by iron and silicic acid availability in the subantarctic Southern Ocean:: Experimental results from the SAZ Project. *Journal of Geophysical Research-Oceans,* 106**,** 31559-31572.

Ito, T. & Follows, M. J. 2013. Air-sea disequilibrium of carbon dioxide enhances the biological carbon sequestration in the Southern Ocean. *Global Biogeochemical Cycles,* 27**,** 1129-1138.

Jabaud-Jan, A., Metzl, N., Brunet, C., Poisson, A. & Schauer, B. 2004. Interannual variability of the carbon dioxide system in the southern Indian Ocean (20 S–60 S): The impact of a warm anomaly in austral summer 1998. *Global Biogeochemical Cycles,* 18.

Jabre, L. J., Allen, A. E., Mccain, J. S. P., Mccrow, J. P., Tenenbaum, N., Spackeen, J. L., Sipler, R. E., Green, B. R., Bronk, D. A., Hutchins, D. A. & Bertrand, E. M. 2021. Molecular underpinnings and biogeochemical consequences of enhanced diatom growth in a warming Southern Ocean. *Proc Natl Acad Sci U S A,* 118**,** e2107238118.

Jauzein, C., Collos, Y., Garces, E., Vila, M. & Maso, M. 2008. Short-Term Temporal Variability of Ammonium and Urea Uptake by Alexandrium Catenella (Dinophyta) in Cultures. *J Phycol,* 44**,** 1136-45.

Jerusalén-Lleó, E., Nieto-Cid, M., Fuentes-Santos, I., Dittmar, T. & Álvarez-Salgado, X. A. 2023. Solid phase extraction of ocean dissolved organic matter with PPL cartridges: efficiency and selectivity. *Frontiers in Marine Science,* 10.

Jickells, T. D., An, Z. S., Andersen, K. K., Baker, A. R., Bergametti, G., Brooks, N., Cao, J. J., Boyd, P. W., Duce, R. A., Hunter, K. A., Kawahata, H., Kubilay, N., Laroche, J., Liss, P. S., Mahowald, N., Prospero, J. M., Ridgwell, A. J., Tegen, I. & Torres, R. 2005. Global iron connections between desert dust, ocean biogeochemistry, and climate. *Science,* 308**,** 67-71.

Jin, X., Gruber, N., Dunne, J. P., Sarmiento, J. L. & Armstrong, R. A. 2006. Diagnosing the contribution of phytoplankton functional groups to the production and export of particulate organic carbon, CaCO3, and opal from global nutrient and alkalinity distributions. *Global Biogeochemical Cycles,* 20.

Jochem, F. J., Mathot, S. & Queguiner, B. 1995. Size-Fractionated Primary Production in the Open Southern-Ocean in Austral Spring. *Polar Biology,* 15**,** 381-392.

Joubert, W. R., Thomalla, S. J., Waldron, H. N., Lucas, M. I., Boye, M., Le Moigne, F. a. C., Planchon, F. & Speich, S. 2011. Nitrogen uptake by phytoplankton in the Atlantic sector of the Southern Ocean during late austral summer. *Biogeosciences,* 8**,** 2947-2959.

Kahru, M., Mitchell, B. G., Gille, S. T., Hewes, C. D. & Holm-Hansen, O. 2007. Eddies enhance biological production in the Weddell-Scotia confluence of the southern ocean. *Geophysical Research Letters,* 34.

Kanda, J., Laws, E. A., Saino, T. & Hattori, A. 1987. An evaluation of isotope dilution effect from conventional data sets of 15N uptake experiments. *Journal of Plankton Research,* 9**,** 79-90.

Kang, S. H., Kang, J. S., Lee, S., Chung, K. H., Kim, D. & Park, M. G. 2001. Antarctic phytoplankton assemblages in the marginal ice zone of the northwestern Weddell Sea. *Journal of Plankton Research,* 23**,** 333-352.

Karl, D. M., Christian, J. R., Dore, J. E., Hebel, D. V., Letelier, R. M., Tupas, L. M. & Winn, C. D. 1996. Seasonal and interannual variability in primary production and particle flux at Station ALOHA. *Deep-Sea Research Part Ii-Topical Studies in Oceanography,* 43**,** 539-568.

Karsh, K. L., Trull, T. W., Lourey, A. J. & Sigman, D. M. 2003. Relationship of nitrogen isotope fractionation to phytoplankton size and iron availability during the Southern Ocean Iron RElease Experiment (SOIREE). *Limnology and Oceanography,* 48**,** 1058-1068.

Kavanaugh, M. T., Abdala, F., Ducklow, H., Glover, D., Fraser, W., Martinson, D., Stammerjohn, S., Schofield, O. & Doney, S. C. 2015. Effect of continental shelf canyons on phytoplankton biomass and community composition along the western Antarctic Peninsula. *Marine Ecology Progress Series,* 524**,** 11-26.

Kawaguchi, S., Ishida, A., King, R., Raymond, B., Waller, N., Constable, A., Nicol, S., Wakita, M. & Ishimatsu, A. 2013. Risk maps for Antarctic krill under projected Southern Ocean acidification. *Nature Climate Change,* 3**,** 843-847.

Keppler, L. & Landschutzer, P. 2019. Regional Wind Variability Modulates the Southern Ocean Carbon Sink. *Sci Rep,* 9**,** 7384.

Kirchman, D. L. 1994. The uptake of inorganic nutrients by heterotrophic bacteria. *Microb Ecol,* 28**,** 255-71.

Kiuchi, M., Nomura, D., Hirano, D., Tamura, T., Hashida, G., Ushio, S., Simizu, D., Ono, K. & Aoki, S. 2021. The Effect of Basal Melting of the Shirase Glacier Tongue on the CO2 System in Lutzow-Holm Bay, East Antarctica. *Journal of Geophysical Research-Biogeosciences,* 126**,** e2020JG005762.

Knap, A., Michaels, A., Close, A., Ducklow, H. & Dickson, A. 1996. Protocols for the joint global ocean flux study (JGOFS) core measurements. *JGOFS, Reprint of the IOC Manuals and Guides No. 29, UNESCO 1994,* 19.

Knauer, G. A., Martin, J. H. & Bruland, K. W. 1979. Fluxes of Particulate Carbon, Nitrogen, and Phosphorus in the Upper Water Column of the Northeast Pacific. *Deep-Sea Research,* 26**,** 97-108.

Koch, B. P. & Dittmar, T. 2006. From mass to structure: an aromaticity index for high-resolution mass data of natural organic matter. *Rapid Communications in Mass Spectrometry,* 20**,** 926-932.

Koch, B. P. & Dittmar, T. 2016. From mass to structure: an aromaticity index for high-resolution mass data of natural organic matter. *Rapid Communications in Mass Spectrometry,* 30**,** 250-250.

Koch, F., Beszteri, S., Harms, L. & Trimborn, S. 2018. The impacts of iron limitation and ocean acidification on the cellular stoichiometry, photophysiology, and transcriptome of Phaeocystis antarctica. *Limnology and Oceanography,* 64**,** 357-375.

Koike, I., Holmhansen, O. & Biggs, D. C. 1986. Inorganic Nitrogen-Metabolism by Antarctic Phytoplankton with Special Reference to Ammonium Cycling. *Marine Ecology Progress Series,* 30**,** 105-116.

Kristiansen, S., Syvertsen, E. E. & Farbrot, T. 1992. Nitrogen Uptake in the Weddell Sea during Late Winter and Spring. *Polar Biology,* 12**,** 245-251.

Kropuenske, L. R., Mills, M. M., Van Dijken, G. L., Alderkamp, A. C., Mine Berg, G., Robinson, D. H., Welschmeyer, N. A. & Arrigo, K. R. 2010. Strategies And Rates Of Photoacclimation

In Two Major Southern Ocean Phytoplankton Taxa: Phaeocystis Antarctica (Haptophyta) And Fragilariopsis Cylindrus (Bacillariophyceae). *Journal of Phycology,* 46**,** 1138-1151.

Kropuenske, L. R., Mills, M. M., Van Dijken, G. L., Bailey, S., Robinson, D. H., Welschmeyer, N. A. & Arrigo, K. R. 2009. Photophysiology in two major Southern Ocean phytoplankton taxa: Photoprotection in Phaeocystis antarctica and Fragilariopsis cylindrus. *Limnology and Oceanography,* 54**,** 1176-1196.

Ksionzek, K. B., Lechtenfeld, O. J., Mccallister, S. L., Schmitt-Kopplin, P., Geuer, J. K., Geibert, W. & Koch, B. P. 2016. Dissolved organic sulfur in the ocean: Biogeochemistry of a petagram inventory. *Science,* 354**,** 456-459.

Kwiatkowski, L., Aumont, O., Bopp, L. & Ciais, P. 2018. The Impact of Variable Phytoplankton Stoichiometry on Projections of Primary Production, Food Quality, and Carbon Uptake in the Global Ocean. *Global Biogeochemical Cycles,* 32**,** 516-528.

Lam, P. J. & Bishop, J. K. B. 2007. High biomass, low export regimes in the Southern Ocean. *Deep-Sea Research Part Ii-Topical Studies in Oceanography,* 54**,** 601-638.

Lam, P. J., Bishop, J. K. B., Henning, C. C., Marcus, M. A., Waychunas, G. A. & Fung, I. Y. 2006. Wintertime phytoplankton bloom in the subarctic Pacific supported by continental margin iron. *Global Biogeochemical Cycles,* 20.

Lancelot, C. 1984. Extracellular release of small and large molecules by phytoplankton in the Southern Bight of the North Sea. *Estuarine, Coastal and Shelf Science,* 18**,** 65-77.

Lancelot, C., De Montety, A., Goosse, H., Becquevort, S., Schoemann, V., Pasquer, B. & Vancoppenolle, M. 2009. Spatial distribution of the iron supply to phytoplankton in the Southern Ocean: a model study. *Biogeosciences,* 6**,** 2861-2878.

Lancelot, C., Hannon, E., Becquevort, S., Veth, C. & De Baar, H. J. W. 2000. Modeling phytoplankton blooms and carbon export production in the Southern Ocean: dominant controls by light and iron in the Atlantic sector in Austral spring 1992. *Deep-Sea Research Part I-Oceanographic Research Papers,* 47**,** 1621-1662.

Landschutzer, P., Gruber, N., Haumann, F. A., Rodenbeck, C., Bakker, D. C., Van Heuven, S., Hoppema, M., Metzl, N., Sweeney, C., Takahashi, T., Tilbrook, B. & Wanninkhof, R. 2015. The reinvigoration of the Southern Ocean carbon sink. *Science,* 349**,** 1221-4.

Lannuzel, D., Chever, F., Van Der Merwe, P. C., Janssens, J., Roukaerts, A., Cavagna, A. J., Townsend, A. T., Bowie, A. R. & Meiners, K. M. 2016. Iron biogeochemistry in Antarctic pack ice during SIPEX-2. *Deep-Sea Research Part Ii-Topical Studies in Oceanography,* 131**,** 111-122.

Laubscher, R. K., Perissinotto, R. & Mcquaid, C. D. 1993. Phytoplankton Production and Biomass at Frontal Zones in the Atlantic Sector of the Southern-Ocean. *Polar Biology,* 13**,** 471-481.

Laufer-Meiser, K., Michaud, A. B., Maisch, M., Byrne, J. M., Kappler, A., Patterson, M. O., Roy, H. & Jorgensen, B. B. 2021. Potentially bioavailable iron produced through benthic cycling in glaciated Arctic fjords of Svalbard. *Nat Commun,* 12**,** 1349.

Laufkötter, C., Vogt, M., Gruber, N., Aita-Noguchi, M., Aumont, O., Bopp, L., Buitenhuis, E., Doney, S. C., Dunne, J. & Hashioka, T. 2015. Drivers and uncertainties of future global marine primary production in marine ecosystem models. *Biogeosciences,* 12**,** 6955-6984.

Lavaud, J., Strzepek, R. F. & Kroth, P. G. 2007. Photoprotection capacity differs among diatoms: Possible consequences on the spatial distribution of diatoms related to

fluctuations in the underwater light climate. *Limnology and Oceanography,* 52**,** 1188-1194.
Lavery, T. J., Roudnew, B., Gill, P., Seymour, J., Seuront, L., Johnson, G., Mitchell, J. G. & Smetacek, V. 2010. Iron defecation by sperm whales stimulates carbon export in the Southern Ocean. *Proc Biol Sci,* 277**,** 3527-31.
Lechtenfeld, O. J., Koch, B. P., Geibert, W., Ludwichowski, K. U. & Kattner, G. 2011. Inorganics in organics: quantification of organic phosphorus and sulfur and trace element speciation in natural organic matter using HPLC-ICPMS. *Anal Chem,* 83**,** 8968-74.
Legge, O. J., Bakker, D. C. E., Meredith, M. P., Venables, H. J., Brown, P. J., Jones, E. M. & Johnson, M. T. 2017. The seasonal cycle of carbonate system processes in Ryder Bay, West Antarctic Peninsula. *Deep-Sea Research Part Ii-Topical Studies in Oceanography,* 139**,** 167-180.
Lenton, A., Tilbrook, B., Law, R. M., Bakker, D., Doney, S. C., Gruber, N., Ishii, M., Hoppema, M., Lovenduski, N. S., Matear, R. J., Mcneil, B. I., Metzl, N., Mikaloff Fletcher, S. E., Monteiro, P. M. S., Rödenbeck, C., Sweeney, C. & Takahashi, T. 2013. Sea–air CO2 fluxes in the Southern Ocean for the period 1990–2009. *Biogeosciences,* 10**,** 4037-4054.
Letscher, R. T. & Moore, J. K. 2015. Preferential remineralization of dissolved organic phosphorus and non-Redfield DOM dynamics in the global ocean: Impacts on marine productivity, nitrogen fixation, and carbon export. *Global Biogeochemical Cycles,* 29**,** 325-340.
Leung, S., Cabré, A. & Marinov, I. 2015. A latitudinally banded phytoplankton response to 21st century climate change in the Southern Ocean across the CMIP5 model suite. *Biogeosciences,* 12**,** 5715-5734.
Levermann, A., Winkelmann, R., Nowicki, S., Fastook, J. L., Frieler, K., Greve, R., Hellmer, H. H., Martin, M. A., Meinshausen, M., Mengel, M., Payne, A. J., Pollard, D., Sato, T., Timmermann, R., Wang, W. L. & Bindschadler, R. A. 2014. Projecting Antarctic ice discharge using response functions from SeaRISE ice-sheet models. *Earth System Dynamics,* 5**,** 271-293.
Lewandowska, A. M., Hillebrand, H., Lengfellner, K. & Sommer, U. 2014. Temperature effects on phytoplankton diversity - The zooplankton link. *Journal of Sea Research,* 85**,** 359-364.
Li, P., Tao, J., Lin, J., He, C., Shi, Q., Li, X. & Zhang, C. 2019. Stratification of dissolved organic matter in the upper 2000 m water column at the Mariana Trench. *Sci Total Environ,* 668**,** 1222-1231.
Li, Z., Groeskamp, S., Cerovecki, I. & England, M. H. 2022. The Origin and Fate of Antarctic Intermediate Water in the Southern Ocean. *Journal of Physical Oceanography,* 52**,** 2873-2890.
Liefer, J. D., Garg, A., Fyfe, M. H., Irwin, A. J., Benner, I., Brown, C. M., Follows, M. J., Omta, A. W. & Finkel, Z. V. 2019. The Macromolecular Basis of Phytoplankton C:N:P Under Nitrogen Starvation. *Front Microbiol,* 10**,** 763.
Lin, Y., Moreno, C., Marchetti, A., Ducklow, H., Schofield, O., Delage, E., Meredith, M., Li, Z., Eveillard, D., Chaffron, S. & Cassar, N. 2021. Decline in plankton diversity and carbon flux with reduced sea ice extent along the Western Antarctic Peninsula. *Nat Commun,* 12**,** 4948.
Litchman, E. & Klausmeier, C. A. 2008. Trait-Based Community Ecology of Phytoplankton. *Annual Review of Ecology Evolution and Systematics,* 39**,** 615-639.

Litchman, E., Klausmeier, C. A., Miller, J. R., Schofield, O. M. & Falkowski, P. G. 2006. Multi-nutrient, multi-group model of present and future oceanic phytoplankton communities. *Biogeosciences,* 3**,** 585-606.

Liu, D., Fang, Y., Tu, Y. & Pan, Y. 2014. Chemical method for nitrogen isotopic analysis of ammonium at natural abundance. *Anal Chem,* 86**,** 3787-92.

Lizotte, M. P. 2001. The Contributions of Sea Ice Algae to Antarctic Marine Primary Production1. *American Zoologist,* 41**,** 57-73.

Llort, J., Lévy, M., Sallée, J. B. & Tagliabue, A. 2019. Nonmonotonic Response of Primary Production and Export to Changes in Mixed-Layer Depth in the Southern Ocean. *Geophysical Research Letters,* 46**,** 3368-3377.

Loh, A. N. & Bauer, J. E. 2000. Distribution, partitioning and fluxes of dissolved and particulate organic C, N and P in the eastern North Pacific and Southern Oceans. *Deep-Sea Research Part I-Oceanographic Research Papers,* 47**,** 2287-2316.

Lomas, M. W. & Glibert, P. M. 1999. Temperature regulation of nitrate uptake: A novel hypothesis about nitrate uptake and reduction in cool-water diatoms. *Limnology and Oceanography,* 44**,** 556-572.

Lønborg, C., Carreira, C., Jickells, T. & Álvarez-Salgado, X. A. 2020. Impacts of Global Change on Ocean Dissolved Organic Carbon (DOC) Cycling. *Frontiers in Marine Science,* 7.

Long, M. C., Moore, J. K., Lindsay, K., Levy, M., Doney, S. C., Luo, J. Y., Krumhardt, K. M., Letscher, R. T., Grover, M. & Sylvester, Z. T. 2021. Simulations With the Marine Biogeochemistry Library (MARBL). *Journal of Advances in Modeling Earth Systems,* 13**,** e2021MS002647.

Lopez-Urrutia, A., San Martin, E., Harris, R. P. & Irigoien, X. 2006. Scaling the metabolic balance of the oceans. *Proc Natl Acad Sci U S A,* 103**,** 8739-44.

Lueker, T. J., Dickson, A. G. & Keeling, C. D. 2000. Ocean pCO2 calculated from dissolved inorganic carbon, alkalinity, and equations for K1 and K2: validation based on laboratory measurements of CO2 in gas and seawater at equilibrium. *Marine Chemistry,* 70**,** 105-119.

Luo, Y. W., Doney, S. C., Anderson, L. A., Benavides, M., Berman-Frank, I., Bode, A., Bonnet, S., Boström, K. H., Böttjer, D., Capone, D. G., Carpenter, E. J., Chen, Y. L., Church, M. J., Dore, J. E., Falcón, L. I., Fernández, A., Foster, R. A., Furuya, K., Gómez, F., Gundersen, K., Hynes, A. M., Karl, D. M., Kitajima, S., Langlois, R. J., Laroche, J., Letelier, R. M., Marañón, E., Mcgillicuddy, D. J., Moisander, P. H., Moore, C. M., Mourino-Carballido, B., Mulholland, M. R., Needoba, J. A., Orcutt, K. M., Poulton, A. J., Rahav, E., Raimbault, P., Rees, A. P., Riemann, L., Shiozaki, T., Subramaniam, A., Tyrrell, T., Turk-Kubo, K. A., Varela, M., Villareal, T. A., Webb, E. A., White, A. E., Wu, J. & Zehr, J. P. 2012. Database of diazotrophs in global ocean: abundance, biomass and nitrogen fixation rates. *Earth System Science Data,* 4**,** 47-73.

Mackey, M. D., Mackey, D. J., Higgins, H. W. & Wright, S. W. 1996. CHEMTAX - A program for estimating class abundances from chemical markers: Application to HPLC measurements of phytoplankton. *Marine Ecology Progress Series,* 144**,** 265-283.

Maniscalco, M. A., Brzezinski, M. A., Lampe, R. H., Cohen, N. R., Mcnair, H. M., Ellis, K. A., Brown, M., Till, C. P., Twining, B. S., Bruland, K. W., Marchetti, A. & Thamatrakoln, K. 2022. Diminished carbon and nitrate assimilation drive changes in diatom elemental stoichiometry independent of silicification in an iron-limited assemblage. *ISME Commun,* 2**,** 57.

Maranger, R., Bird, D. F. & Price, N. M. 1998. Iron acquisition by photosynthetic marine phytoplankton from ingested bacteria. *Nature,* 396**,** 248-251.
Marchetti, A., Schruth, D. M., Durkin, C. A., Parker, M. S., Kodner, R. B., Berthiaume, C. T., Morales, R., Allen, A. E. & Armbrust, E. V. 2012. Comparative metatranscriptomics identifies molecular bases for the physiological responses of phytoplankton to varying iron availability. *Proc Natl Acad Sci U S A,* 109**,** E317-25.
Marchetti, A., Varela, D. E., Lance, V. P., Lance, V. P., Palmucci, M., Giordano, M. & Virginia Armbrust, E. 2009. Iron and silicic acid effects on phytoplankton productivity, diversity, and chemical composition in the central equatorial Pacific Ocean. *Limnology and Oceanography,* 55**,** 11-29.
Martinson, D. G. & Mckee, D. C. 2012. Transport of warm Upper Circumpolar Deep Water onto the western Antarctic Peninsula continental shelf. *Ocean Science,* 8**,** 433-442.
Martiny, A. C., Pham, C. T. A., Primeau, F. W., Vrugt, J. A., Moore, J. K., Levin, S. A. & Lomas, M. W. 2013. Strong latitudinal patterns in the elemental ratios of marine plankton and organic matter. *Nature Geoscience,* 6**,** 279-283.
Mascioni, M., Almandoz, G. O., Cefarelli, A. O., Cusick, A., Ferrario, M. E. & Vernet, M. 2019. Phytoplankton composition and bloom formation in unexplored nearshore waters of the western Antarctic Peninsula. *Polar Biology,* 42**,** 1859-1872.
Masson-Delmotte, V., Zhai, P., Pirani, A., Connors, S. L., Péan, C., Berger, S., Caud, N., Chen, Y., Goldfarb, L. & Gomis, M. 2021. Climate change 2021: the physical science basis. *Contribution of working group I to the sixth assessment report of the intergovernmental panel on climate change,* 2.
Mathis, J. T., Hansell, D. A., Kadko, D., Bates, N. R. & Cooper, L. W. 2007. Determining net dissolved organic carbon production in the hydrographically complex western Arctic Ocean. *Limnology and Oceanography,* 52**,** 1789-1799.
Matsuoka, K., Skoglund, A., Roth, G., De Pomereu, J., Griffiths, H., Headland, R., Herried, B., Katsumata, K., Le Brocq, A., Licht, K., Morgan, F., Neff, P. D., Ritz, C., Scheinert, M., Tamura, T., Van De Putte, A., Van Den Broeke, M., Von Deschwanden, A., Deschamps-Berger, C., Van Liefferinge, B., Tronstad, S. & Melvær, Y. 2021. Quantarctica, an integrated mapping environment for Antarctica, the Southern Ocean, and sub-Antarctic islands. *Environmental Modelling & Software,* 140**,** 105015.
Mayzaud, P. & Pakhomov, E. A. 2014. The role of zooplankton communities in carbon recycling in the Ocean: the case of the Southern Ocean. *Journal of Plankton Research,* 36**,** 1543-1556.
Mccain, J. S. P., Tagliabue, A., Susko, E., Achterberg, E. P., Allen, A. E. & Bertrand, E. M. 2021. Cellular costs underpin micronutrient limitation in phytoplankton. *Sci Adv,* 7**,** eabg6501.
Mcdonnell, A. M. P. & Buesseler, K. O. 2010. Variability in the average sinking velocity of marine particles. *Limnology and Oceanography,* 55**,** 2085-2096.
Mckie-Krisberg, Z. M., Gast, R. J. & Sanders, R. W. 2015. Physiological responses of three species of Antarctic mixotrophic phytoflagellates to changes in light and dissolved nutrients. *Microb Ecol,* 70**,** 21-9.
Mcminn, A. & Hodgson, D. 1993. Summer Phytoplankton Succession in Ellis Fjord, Eastern Antarctica. *Journal of Plankton Research,* 15**,** 925-938.
Mcneil, B. I. & Matear, R. J. 2008. Southern Ocean acidification: A tipping point at 450-ppm atmospheric CO2. *Proceedings of the National Academy of Sciences of the United States of America,* 105**,** 18860-18864.

Mdutyana, M., Marshall, T., Sun, X., Burger, J. M., Thomalla, S. J., Ward, B. B. & Fawcett, S. E. 2022. Controls on nitrite oxidation in the upper Southern Ocean: insights from winter kinetics experiments in the Indian sector. *Biogeosciences,* 19**,** 3425-3444.

Mdutyana, M., Thomalla, S. J., Philibert, R., Ward, B. B. & Fawcett, S. E. 2020. The Seasonal Cycle of Nitrogen Uptake and Nitrification in the Atlantic Sector of the Southern Ocean. *Global Biogeochemical Cycles,* 34**,** e2019GB006363.

Medeiros, P. M., Seidel, M., Powers, L. C., Dittmar, T., Hansell, D. A. & Miller, W. L. 2015. Dissolved organic matter composition and photochemical transformations in the northern North Pacific Ocean. *Geophysical Research Letters,* 42**,** 863-870.

Mendes, C. R. B., Costa, R. R., Ferreira, A., Jesus, B., Tavano, V. M., Dotto, T. S., Leal, M. C., Kerr, R., Islabao, C. A., Franco, A., Mata, M. M., Garcia, C. a. E. & Secchi, E. R. 2023. Cryptophytes: An emerging algal group in the rapidly changing Antarctic Peninsula marine environments. *Glob Chang Biol,* 29**,** 1791-1808.

Mendes, C. R. B., Tavano, V. M., Dotto, T. S., Kerr, R., De Souza, M. S., Garcia, C. a. E. & Secchi, E. R. 2018a. New insights on the dominance of cryptophytes in Antarctic coastal waters: A case study in Gerlache Strait. *Deep-Sea Research Part Ii-Topical Studies in Oceanography,* 149**,** 161-170.

Mendes, C. R. B., Tavano, V. M., Kerr, R., Dotto, T. S., Maximiano, T. & Secchi, E. R. 2018b. Impact of sea ice on the structure of phytoplankton communities in the northern Antarctic Peninsula. *Deep-Sea Research Part Ii-Topical Studies in Oceanography,* 149**,** 111-123.

Menezes, V. V., Macdonald, A. M. & Schatzman, C. 2017. Accelerated freshening of Antarctic Bottom Water over the last decade in the Southern Indian Ocean. *Sci Adv,* 3**,** e1601426.

Merder, J., Freund, J. A., Feudel, U., Hansen, C. T., Hawkes, J. A., Jacob, B., Klaproth, K., Niggemann, J., Noriega-Ortega, B. E., Osterholz, H., Rossel, P. E., Seidel, M., Singer, G., Stubbins, A., Waska, H. & Dittmar, T. 2020. ICBM-OCEAN: Processing Ultrahigh-Resolution Mass Spectrometry Data of Complex Molecular Mixtures. *Anal Chem,* 92**,** 6832-6838.

Meredith, M. 2019. The global importance of the Southern Ocean, and the key role of its freshwater cycle. *Ocean Challenge,* 23**,** 27-32.

Meredith, M., Sommerkorn, M., Cassotta, S., Derksen, C., Ekaykin, A., Hollowed, A., Kofinas, G., Mackintosh, A., Melbourne-Thomas, J. & Muelbert, M. 2019. Chapter 3: polar regions. *IPCC special report on the ocean and cryosphere in a changing climate,* 5.

Meredith, M. P. & Brandon, M. A. 2017. Oceanography and sea ice in the Southern Ocean. *Sea Ice*.

Meredith, M. P., Brandon, M. A., Wallace, M. I., Clarke, A., Leng, M. J., Renfrew, I. A., Van Lipzig, N. P. M. & King, J. C. 2008. Variability in the freshwater balance of northern Marguerite Bay, Antarctic Peninsula: Results from δ18O. *Deep Sea Research Part II: Topical Studies in Oceanography,* 55**,** 309-322.

Meredith, M. P. & Hogg, A. M. 2006. Circumpolar response of Southern Ocean eddy activity to a change in the Southern Annular Mode. *Geophysical Research Letters,* 33.

Moberg, E. A. & Sosik, H. M. 2012. Distance maps to estimate cell volume from two-dimensional plankton images. *Limnology and Oceanography-Methods,* 10**,** 278-288.

Moffat, C., Beardsley, R. C., Owens, B. & Van Lipzig, N. 2008. A first description of the Antarctic Peninsula Coastal Current. *Deep-Sea Research Part Ii-Topical Studies in Oceanography,* 55**,** 277-293.

Moffat, C. & Meredith, M. 2018. Shelf-ocean exchange and hydrography west of the Antarctic Peninsula: a review. *Philos Trans A Math Phys Eng Sci,* 376**,** 20170164.
Moffat, C., Owens, B. & Beardsley, R. C. 2009. On the characteristics of Circumpolar Deep Water intrusions to the west Antarctic Peninsula Continental Shelf. *Journal of Geophysical Research-Oceans,* 114.
Moline, M. A., Claustre, H., Frazer, T. K., Schofield, O. & Vernet, M. 2004. Alteration of the food web along the Antarctic Peninsula in response to a regional warming trend. *Global Change Biology,* 10**,** 1973-1980.
Moline, M. A., Karnovsky, N. J., Brown, Z., Divoky, G. J., Frazer, T. K., Jacoby, C. A., Torrese, J. J. & Fraser, W. R. 2008. High latitude changes in ice dynamics and their impact on polar marine ecosystems. *Year in Ecology and Conservation Biology 2008,* 1134**,** 267-319.
Moline, M. A. & Prezelin, B. B. 1996. Long-term monitoring and analyses of physical factors regulating variability in coastal Antarctic phytoplankton biomass, in situ productivity and taxonomic composition over subseasonal, seasonal and interannual time scales. *Marine Ecology Progress Series,* 145**,** 143-160.
Mongwe, N. P., Vichi, M. & Monteiro, P. M. S. 2018. The seasonal cycle of CO2 and CO2 fluxes in the Southern Ocean: diagnosing anomalies in CMIP5 Earth system models. *Biogeosciences,* 15**,** 2851-2872.
Montes-Hugo, M., Doney, S. C., Ducklow, H. W., Fraser, W., Martinson, D., Stammerjohn, S. E. & Schofield, O. 2009. Recent changes in phytoplankton communities associated with rapid regional climate change along the western Antarctic Peninsula. *Science,* 323**,** 1470-3.
Montes-Hugo, M. A., Vernet, M., Martinson, D., Smith, R. & Iannuzzi, R. 2008. Variability on phytoplankton size structure in the western Antarctic Peninsula (1997-2006). *Deep-Sea Research Part Ii-Topical Studies in Oceanography,* 55**,** 2106-2117.
Moore, C. M., Mills, M. M., Arrigo, K. R., Berman-Frank, I., Bopp, L., Boyd, P. W., Galbraith, E. D., Geider, R. J., Guieu, C., Jaccard, S. L., Jickells, T. D., La Roche, J., Lenton, T. M., Mahowald, N. M., Marañón, E., Marinov, I., Moore, J. K., Nakatsuka, T., Oschlies, A., Saito, M. A., Thingstad, T. F., Tsuda, A. & Ulloa, O. 2013. Processes and patterns of oceanic nutrient limitation. *Nature Geoscience,* 6**,** 701-710.
Moore, J. K., Doney, S. C. & Lindsay, K. 2004. Upper ocean ecosystem dynamics and iron cycling in a global three-dimensional model. *Global Biogeochemical Cycles,* 18.
Moorthi, S., Caron, D. A., Gast, R. J. & Sanders, R. W. 2009. Mixotrophy: a widespread and important ecological strategy for planktonic and sea-ice nanoflagellates in the Ross Sea, Antarctica. *Aquatic Microbial Ecology,* 54**,** 269-277.
Moreau, S., Boyd, P. W. & Strutton, P. G. 2020. Remote assessment of the fate of phytoplankton in the Southern Ocean sea-ice zone. *Nat Commun,* 11**,** 3108.
Moreau, S., Hattermann, T., De Steur, L., Kauko, H. M., Ahonen, H., Ardelan, M., Assmy, P., Chierici, M., Descamps, S., Dinter, T., Falkenhaug, T., Fransson, A., Gronningsaeter, E., Hallfredsson, E. H., Huhn, O., Lebrun, A., Lowther, A., Lubcker, N., Monteiro, P., Peeken, I., Roychoudhury, A., Rozanska, M., Ryan-Keogh, T., Sanchez, N., Singh, A., Simonsen, J. H., Steiger, N., Thomalla, S. J., Van Tonder, A., Wiktor, J. M. & Steen, H. 2023. Wind-driven upwelling of iron sustains dense blooms and food webs in the eastern Weddell Gyre. *Nat Commun,* 14**,** 1303.
Moreau, S., Mostajir, B., Belanger, S., Schloss, I. R., Vancoppenolle, M., Demers, S. & Ferreyra, G. A. 2015. Climate change enhances primary production in the western Antarctic Peninsula. *Glob Chang Biol,* 21**,** 2191-205.

Moreau, S., Schloss, I. R., Mostajir, B., Demers, S., Almandoz, G. O., Ferrario, M. E. & Ferreyra, G. A. 2012. Influence of microbial community composition and metabolism on air-sea ΔpCO2 variation off the western Antarctic Peninsula. *Marine Ecology Progress Series,* 446**,** 45-59.

Moreno, C. M., Bernish, M., Meyer, M. G., Li, Z., Waite, N., Cohen, N. R., Schofield, O. & Marchetti, A. 2024. Molecular physiology of Antarctic diatom natural assemblages and bloom event reveal insights into strategies contributing to their ecological success. *mSystems,* 9**,** e0130623.

Moschonas, G., Gowen, R. J., Paterson, R. F., Mitchell, E., Stewart, B. M., Mcneill, S., Glibert, P. M. & Davidson, K. 2017. Nitrogen dynamics and phytoplankton community structure: the role of organic nutrients. *Biogeochemistry,* 134**,** 125-145.

Murphy, E. J., Johnston, N. M., Hofmann, E. E., Phillips, R. A., Jackson, J. A., Constable, A. J., Henley, S. F., Melbourne-Thomas, J., Trebilco, R., Cavanagh, R. D., Tarling, G. A., Saunders, R. A., Barnes, D. K. A., Costa, D. P., Corney, S. P., Fraser, C. I., Höfer, J., Hughes, K. A., Sands, C. J., Thorpe, S. E., Trathan, P. N. & Xavier, J. C. 2021. Global Connectivity of Southern Ocean Ecosystems. *Frontiers in Ecology and Evolution,* 9.

Nardelli, B. B., Guinehut, S., Verbrugge, N., Cotroneo, Y., Zambianchi, E. & Iudicone, D. 2017. Southern Ocean Mixed-Layer Seasonal and Interannual Variations From Combined Satellite and In Situ Data. *Journal of Geophysical Research-Oceans,* 122**,** 10042-10060.

Nardelli, S. C., Gray, P. C., Stammerjohn, S. E. & Schofield, O. 2023. Characterizing coastal phytoplankton seasonal succession patterns on the West Antarctic Peninsula. *Limnology and Oceanography,* 68**,** 845-861.

Nelson, D. M., Smith Jr., W. O., Gordon, L. I. & Huber, B. A. 1987. Spring distributions of density, nutrients, and phytoplankton biomass in the ice edge zone of the Weddell-Scotia Sea. *Journal of Geophysical Research: Oceans,* 92**,** 7181-7190.

Nicholson, S. A., Lévy, M., Llort, J., Swart, S. & Monteiro, P. M. S. 2016. Investigation into the impact of storms on sustaining summer primary productivity in the Sub-Antarctic Ocean. *Geophysical Research Letters,* 43**,** 9192-9199.

Nicholson, S. A., Whitt, D. B., Fer, I., Du Plessis, M. D., Lebehot, A. D., Swart, S., Sutton, A. J. & Monteiro, P. M. S. 2022. Storms drive outgassing of CO2 in the subpolar Southern Ocean. *Nat Commun,* 13**,** 158.

Nicol, S., Bowie, A., Jarman, S., Lannuzel, D., Meiners, K. M. & Van Der Merwe, P. 2010. Southern Ocean iron fertilization by baleen whales and Antarctic krill. *Fish and Fisheries,* 11**,** 203-209.

Nissen, C., Gruber, N., Münnich, M. & Vogt, M. 2021. Southern Ocean Phytoplankton Community Structure as a Gatekeeper for Global Nutrient Biogeochemistry. *Global Biogeochemical Cycles,* 35**,** e2021GB006991.

Nissen, C. & Vogt, M. 2021. Factors controlling the competition between Phaeocystis and diatoms in the Southern Ocean and implications for carbon export fluxes. *Biogeosciences,* 18**,** 251-283.

Nissen, C., Vogt, M., Münnich, M., Gruber, N. & Haumann, F. A. 2018. Factors controlling coccolithophore biogeography in the Southern Ocean. *Biogeosciences,* 15**,** 6997-7024.

Nomura, D., Yoshikawa-Inoue, H., Kobayashi, S., Nakaoka, S., Nakata, K. & Hashida, G. 2014. Winter-to-summer evolution of CO2 in surface water and air-sea CO2 lux in the seasonal ice zone of the Southern Ocean. *Biogeosciences,* 11**,** 5749-5761.

Novak, T., Godrijan, J., Pfannkuchen, D. M., Djakovac, T., Mlakar, M., Baricevic, A., Tankovic, M. S. & Gasparovic, B. 2018. Enhanced dissolved lipid production as a response to the sea surface warming. *Journal of Marine Systems,* 180**,** 289-298.

O'neill, B. C., Tebaldi, C., Van Vuuren, D. P., Eyring, V., Friedlingstein, P., Hurtt, G., Knutti, R., Kriegler, E., Lamarque, J. F., Lowe, J., Meehl, G. A., Moss, R., Riahi, K. & Sanderson, B. M. 2016. The Scenario Model Intercomparison Project (ScenarioMIP) for CMIP6. *Geoscientific Model Development,* 9**,** 3461-3482.

Ogawa, H., Fukuda, R. & Koike, I. 1999. Vertical distributions of dissolved organic carbon and nitrogen in the Southern Ocean. *Deep-Sea Research Part I-Oceanographic Research Papers,* 46**,** 1809-1826.

Oksanen, J., Kindt, R., Legendre, P., O'hara, B., Stevens, M. H. H., Oksanen, M. J. & Suggests, M. 2007. The vegan package. *Community ecology package,* 10**,** 719.

Olaizola, M., La Roche, J., Kolber, Z. & Falkowski, P. G. 1994. Non-photochemical fluorescence quenching and the diadinoxanthin cycle in a marine diatom. *Photosynth Res,* 41**,** 357-70.

Olson, R. J. & Sosik, H. M. 2007. A submersible imaging-in-flow instrument to analyze nano- and microplankton: Imaging FlowCytobot. *Limnology and Oceanography-Methods,* 5**,** 195-203.

Osterholz, H., Dittmar, T. & Niggemann, J. 2014. Molecular evidence for rapid dissolved organic matter turnover in Arctic fjords. *Marine Chemistry,* 160**,** 1-10.

Pakhomov, E. A., Froneman, P. W. & Perissinotto, R. 2002. Salp/krill interactions in the Southern Ocean: spatial segregation and implications for the carbon flux. *Deep-Sea Research Part Ii-Topical Studies in Oceanography,* 49**,** 1881-1907.

Palenik, B. & Morel, F. M. M. 1990. Amino-Acid Utilization by Marine-Phytoplankton - a Novel Mechanism. *Limnology and Oceanography,* 35**,** 260-269.

Parkinson, C. L. 2019. A 40-y record reveals gradual Antarctic sea ice increases followed by decreases at rates far exceeding the rates seen in the Arctic. *Proc Natl Acad Sci U S A,* 116**,** 14414-14423.

Parkinson, C. L. & Cavalieri, D. J. 2012. Antarctic sea ice variability and trends, 1979-2010. *Cryosphere,* 6**,** 871-880.

Pauli, N. C., Metfies, K., Pakhomov, E. A., Neuhaus, S., Graeve, M., Wenta, P., Flintrop, C. M., Badewien, T. H., Iversen, M. H. & Meyer, B. 2021. Selective feeding in Southern Ocean key grazers-diet composition of krill and salps. *Commun Biol,* 4**,** 1061.

Pausch, F., Bischof, K. & Trimborn, S. 2019. Iron and manganese co-limit growth of the Southern Ocean diatom Chaetoceros debilis. *PLoS One,* 14**,** e0221959.

Pearce, I., Davidson, A. T., Thomson, P. G., Wright, S. & Van Den Enden, R. 2011. Marine microbial ecology in the sub-Antarctic Zone: Rates of bacterial and phytoplankton growth and grazing by heterotrophic protists. *Deep-Sea Research Part Ii-Topical Studies in Oceanography,* 58**,** 2248-2259.

Pellichero, V., Sallée, J. B., Schmidtko, S., Roquet, F. & Charrassin, J. B. 2017. The ocean mixed layer under Southern Ocean sea-ice: Seasonal cycle and forcing. *Journal of Geophysical Research-Oceans,* 122**,** 1608-1633.

Person, R., Aumont, O. & Lévy, M. 2018. The Biological Pump and Seasonal Variability of pCO2 in the Southern Ocean: Exploring the Role of Diatom Adaptation to Low Iron. *Journal of Geophysical Research-Oceans,* 123**,** 3204-3226.

Petrou, K., Baker, K. G., Nielsen, D. A., Hancock, A. M., Schulz, K. G. & Davidson, A. T. 2019. Acidification diminishes diatom silica production in the Southern Ocean. *Nature Climate Change,* 9**,** 781-+.

Petrou, K., Kranz, S. A., Trimborn, S., Hassler, C. S., Ameijeiras, S. B., Sackett, O., Ralph, P. J. & Davidson, A. T. 2016. Southern Ocean phytoplankton physiology in a changing climate. *J Plant Physiol,* 203**,** 135-150.

Pezza, A. B., Rashid, H. A. & Simmonds, I. 2011. Climate links and recent extremes in antarctic sea ice, high-latitude cyclones, Southern Annular Mode and ENSO. *Climate Dynamics,* 38**,** 57-73.

Philibert, R., Waldron, H. & Clark, D. 2015. A geographical and seasonal comparison of nitrogen uptake by phytoplankton in the Southern Ocean. *Ocean Science,* 11**,** 251-267.

Phillips, A. A., White, M. E., Seidel, M., Wu, F., Pavia, F. F., Kemeny, P. C., Ma, A. C., Aluwihare, L. I., Dittmar, T. & Sessions, A. L. 2022. Novel sulfur isotope analyses constrain sulfurized porewater fluxes as a minor component of marine dissolved organic matter. *Proc Natl Acad Sci U S A,* 119**,** e2209152119.

Poulton, A. J., Daniels, C. J., Esposito, M., Humphreys, M. P., Mitchell, E., Ribas-Ribas, M., Russell, B. C., Stinchcombe, M. C., Tynan, E. & Richier, S. 2016. Production of dissolved organic carbon by Arctic plankton communities: Responses to elevated carbon dioxide and the availability of light and nutrients. *Deep-Sea Research Part Ii-Topical Studies in Oceanography,* 127**,** 60-74.

Poulton, A. J., Moore, C. M., Seeyave, S., Lucas, M. I., Fielding, S. & Ward, P. 2007. Phytoplankton community composition around the Crozet Plateau, with emphasis on diatoms and Phaeocystis. *Deep-Sea Research Part Ii-Topical Studies in Oceanography,* 54**,** 2085-2105.

Prézelin, B. B., Hofmann, E. E., Mengelt, C. & Klinck, J. M. 2000. The linkage between Upper Circumpolar Deep Water (UCDW) and phytoplankton assemblages on the west Antarctic Peninsula continental shelf. *Journal of Marine Research,* 58**,** 165-202.

Purich, A. & Doddridge, E. W. 2023. Record low Antarctic sea ice coverage indicates a new sea ice state. *Communications Earth & Environment,* 4**,** 314.

Purich, A. & England, M. H. 2021. Historical and Future Projected Warming of Antarctic Shelf Bottom Water in CMIP6 Models. *Geophysical Research Letters,* 48**,** e2021GL092752.

Purkey, S. G. & Johnson, G. C. 2013. Antarctic Bottom Water Warming and Freshening: Contributions to Sea Level Rise, Ocean Freshwater Budgets, and Global Heat Gain. *Journal of Climate,* 26**,** 6105-6122.

Quéguiner, B. 2013. Iron fertilization and the structure of planktonic communities in high nutrient regions of the Southern Ocean. *Deep Sea Research Part II: Topical Studies in Oceanography,* 90**,** 43-54.

Raiswell, R., Benning, L. G., Tranter, M. & Tulaczyk, S. 2008. Bioavailable iron in the Southern Ocean: the significance of the iceberg conveyor belt. *Geochem Trans,* 9**,** 7.

Raphael, M. N. & Handcock, M. S. 2022. A new record minimum for Antarctic sea ice. *Nature Reviews Earth & Environment,* 3**,** 215-216.

Ratnarajah, L., Bowie, A. R., Lannuzel, D., Meiners, K. M. & Nicol, S. 2014. The biogeochemical role of baleen whales and krill in Southern Ocean nutrient cycling. *PLoS One,* 9**,** e114067.

Rau, G. H., Riebesell, U. & Wolf-Gladrow, D. 1997. CO2(aq)-dependent photosynthetic 13C fractionation in the ocean: A model versus measurements. *Global Biogeochemical Cycles,* 11**,** 267-278.

Reay, D. S., Priddle, J., Nedwell, D. B., Whitehouse, M. J., Ellis-Evans, J. C., Deubert, C. & Connelly, D. P. 2001. Regulation by low temperature of phytoplankton growth and nutrient uptake in the Southern Ocean. *Marine Ecology Progress Series,* 219**,** 51-64.

Redfield, A., Ketchum, B. & Richards, F. 1963. The influence of organisms on the composition of seawater. *The sea,* 2**,** 26-77.

Redfield, A. C. 1958. The Biological Control of Chemical Factors in the Environment. *American Scientist,* 46**,** 205-221.

Rees, A. P., Owens, N. J. P., Heath, M. R., Plummer, D. H. & Bellerby, R. S. 1995. Seasonal Nitrogen Assimilation and Carbon Fixation in a Fjordic Sea Loch. *Journal of Plankton Research,* 17**,** 1307-1324.

Rees, T. a. V. & Syrett, P. J. 2006. The Uptake of Urea by the Diatom, Phaeodactylum. *New Phytologist,* 82**,** 169-178.

Reigstad, M. & Wassmann, P. 2007. Does Phaeocystis spp. contribute significantly to vertical export of organic carbon? *Phaeocystis, major link in the biogeochemical cycling of climate-relevant elements***,** 217-234.

Riebesell, U., Schulz, K. G., Bellerby, R. G., Botros, M., Fritsche, P., Meyerhofer, M., Neill, C., Nondal, G., Oschlies, A., Wohlers, J. & Zollner, E. 2007. Enhanced biological carbon consumption in a high CO2 ocean. *Nature,* 450**,** 545-8.

Riedel, T. & Dittmar, T. 2014. A method detection limit for the analysis of natural organic matter via Fourier transform ion cyclotron resonance mass spectrometry. *Anal Chem,* 86**,** 8376-82.

Rintoul, S., Hughes, C. & Olbers, D. 2001. Chapter 4.6 The antarctic circumpolar current system. *In:* SIEDLER, G., CHURCH, J. & GOULD, J. (eds.) *Ocean Circulation and Climate - Observing and Modelling the Global Ocean.* Academic Press.

Roach, L. A., Dörr, J., Holmes, C. R., Massonnet, F., Blockley, E. W., Notz, D., Rackow, T., Raphael, M. N., O'farrell, S. P., Bailey, D. A. & Bitz, C. M. 2020. Antarctic Sea Ice Area in CMIP6. *Geophysical Research Letters,* 47**,** e2019GL086729.

Rönner, U., Sörensson, F. & Holm-Hansen, O. 1983. Nitrogen assimilation by phytoplankton in the Scotia Sea. *Polar Biology,* 2**,** 137-147.

Rozema, P. D., Biggs, T., Sprong, P. a. A., Buma, A. G. J., Venables, H. J., Evans, C., Meredith, M. P. & Bolhuis, H. 2017a. Summer microbial community composition governed by upper-ocean stratification and nutrient availability in northern Marguerite Bay, Antarctica. *Deep-Sea Research Part Ii-Topical Studies in Oceanography,* 139**,** 151-166.

Rozema, P. D., Venables, H. J., Van De Poll, W. H., Clarke, A., Meredith, M. P. & Buma, A. G. J. 2017b. Interannual variability in phytoplankton biomass and species composition in northern Marguerite Bay (West Antarctic Peninsula) is governed by both winter sea ice cover and summer stratification. *Limnology and Oceanography,* 62**,** 235-252.

Rysgaard, S., Bendtsen, J., Delille, B., Dieckmann, G. S., Glud, R. N., Kennedy, H., Mortensen, J., Papadimitriou, S., Thomas, D. N. & Tison, J.-L. 2011. Sea ice contribution to the air–sea CO2 exchange in the Arctic and Southern Oceans. *Tellus B: Chemical and Physical Meteorology,* 63**,** 823-830.

Rysgaard, S., Glud, R. N., Sejr, M. K., Bendtsen, J. & Christensen, P. B. 2007. Inorganic carbon transport during sea ice growth and decay: A carbon pump in polar seas. *Journal of Geophysical Research-Oceans,* 112.

Saba, G. K., Fraser, W. R., Saba, V. S., Iannuzzi, R. A., Coleman, K. E., Doney, S. C., Ducklow, H. W., Martinson, D. G., Miles, T. N., Patterson-Fraser, D. L., Stammerjohn, S. E., Steinberg, D. K. & Schofield, O. M. 2014. Winter and spring controls on the summer food web of the coastal West Antarctic Peninsula. *Nat Commun,* 5**,** 4318.

Saggiomo, M., Escalera, L., Saggiomo, V., Bolinesi, F. & Mangoni, O. 2021. Phytoplankton Blooms Below the Antarctic Landfast Ice During the Melt Season Between Late Spring and Early Summer. *J Phycol,* 57**,** 541-550.

Sallee, J. B., Pellichero, V., Akhoudas, C., Pauthenet, E., Vignes, L., Schmidtko, S., Garabato, A. N., Sutherland, P. & Kuusela, M. 2021. Summertime increases in upper-ocean stratification and mixed-layer depth. *Nature,* 591**,** 592-598.

Salter, I., Lampitt, R. S., Sanders, R., Poulton, A., Kemp, A. E. S., Boorman, B., Saw, K. & Pearce, R. 2007. Estimating carbon, silica and diatom export from a naturally fertilised phytoplankton bloom in the Southern Ocean using PELAGRA: A novel drifting sediment trap. *Deep-Sea Research Part Ii-Topical Studies in Oceanography,* 54**,** 2233-2259.

Sanderson, M. P., Bronk, D. A., Nejstgaard, J. C., Verity, P. G., Sazhin, A. F. & Frischer, M. E. 2008. Phytoplankton and bacterial uptake of inorganic and organic nitrogen during an induced bloom of Phaeocystis pouchetii. *Aquatic Microbial Ecology,* 51**,** 153-168.

Sarmiento, J. L., Gruber, N., Brzezinski, M. A. & Dunne, J. P. 2004. High-latitude controls of thermocline nutrients and low latitude biological productivity. *Nature,* 427**,** 56-60.

Sathyendranath, S., Stuart, V., Nair, A., Oka, K., Nakane, T., Bouman, H., Forget, M. H., Maass, H. & Platt, T. 2009. Carbon-to-chlorophyll ratio and growth rate of phytoplankton in the sea. *Marine Ecology Progress Series,* 383**,** 73-84.

Savoye, N., Dehairs, F., Elskens, M., Cardinal, D., Kopczynska, E. E., Trull, T. W., Wright, S., Baeyens, W. & Griffiths, F. B. 2004. Regional variation of spring N-uptake and new production in the Southern Ocean. *Geophysical Research Letters,* 31.

Schoemann, V., Becquevort, S., Stefels, J., Rousseau, W. & Lancelot, C. 2005. Phaeocystis blooms in the global ocean and their controlling mechanisms:: a review. *Journal of Sea Research,* 53**,** 43-66.

Schofield, O., Brown, M., Kohut, J., Nardelli, S., Saba, G., Waite, N. & Ducklow, H. 2018. Changes in the upper ocean mixed layer and phytoplankton productivity along the West Antarctic Peninsula. *Philos Trans A Math Phys Eng Sci,* 376**,** 20170173.

Schofield, O., Saba, G., Coleman, K., Carvalho, F., Couto, N., Ducklow, H., Finkel, Z., Irwin, A., Kahl, A., Miles, T., Montes-Hugo, M., Stammerjohn, S. & Waite, N. 2017. Decadal variability in coastal phytoplankton community composition in a changing West Antarctic Peninsula. *Deep-Sea Research Part I-Oceanographic Research Papers,* 124**,** 42-54.

Sedwick, P. N., Blain, S., Quéguiner, B., Griffiths, F. B., Fiala, M., Bucciarelli, E. & Denis, M. 2002. Resource limitation of phytoplankton growth in the Crozet Basin, Subantarctic Southern Ocean. *Deep-Sea Research Part Ii-Topical Studies in Oceanography,* 49**,** 3327-3349.

Seferian, R., Berthet, S., Yool, A., Palmieri, J., Bopp, L., Tagliabue, A., Kwiatkowski, L., Aumont, O., Christian, J., Dunne, J., Gehlen, M., Ilyina, T., John, J. G., Li, H., Long, M. C., Luo, J. Y., Nakano, H., Romanou, A., Schwinger, J., Stock, C., Santana-Falcon, Y., Takano, Y., Tjiputra, J., Tsujino, H., Watanabe, M., Wu, T., Wu, F. & Yamamoto, A. 2020. Tracking Improvement in Simulated Marine Biogeochemistry Between CMIP5 and CMIP6. *Curr Clim Change Rep,* 6**,** 95-119.

Seidel, M., Beck, M., Riedel, T., Waska, H., Suryaputra, I. G. N. A., Schnetger, B., Niggemann, J., Simon, M. & Dittmar, T. 2014. Biogeochemistry of dissolved organic matter in an anoxic intertidal creek bank. *Geochimica Et Cosmochimica Acta,* 140**,** 418-434.

Seidel, M., Vemulapalli, S. P. B., Mathieu, D. & Dittmar, T. 2022. Marine Dissolved Organic Matter Shares Thousands of Molecular Formulae Yet Differs Structurally across Major Water Masses. *Environ Sci Technol,* 56**,** 3758-3769.

Seidel, M., Yager, P. L., Ward, N. D., Carpenter, E. J., Gomes, H. R., Krusche, A. V., Richey, J. E., Dittmar, T. & Medeiros, P. M. 2015. Molecular-level changes of dissolved organic matter along the Amazon River-to-ocean continuum. *Marine Chemistry,* 177**,** 218-231.

Shadwick, E. H., De Meo, O. A., Schroeter, S., Arroyo, M. C., Martinson, D. G. & Ducklow, H. 2021. Sea Ice Suppression of CO2 Outgassing in the West Antarctic Peninsula: Implications For The Evolving Southern Ocean Carbon Sink. *Geophysical Research Letters,* 48**,** e2020GL091835.

Sheen, K. L., Garabato, A. C. N., Brearley, J. A., Meredith, M. P., Polzin, K. L., Smeed, D. A., Forryan, A., King, B. A., Sallée, J. B., Laurent, L. S., Thurnherr, A. M., Toole, J. M., Waterman, S. N. & Watson, A. J. 2014. Eddy-induced variability in Southern Ocean abyssal mixing on climatic timescales. *Nature Geoscience,* 7**,** 577-582.

Shi, J. R., Talley, L. D., Xie, S. P., Liu, W. & Gille, S. T. 2020. Effects of Buoyancy and Wind Forcing on Southern Ocean Climate Change. *Journal of Climate,* 33**,** 10003-10020.

Shu, Q., Wang, Q., Song, Z. Y., Qiao, F. L., Zhao, J. C., Chu, M. & Li, X. F. 2020. Assessment of Sea Ice Extent in CMIP6 With Comparison to Observations and CMIP5. *Geophysical Research Letters,* 47**,** e2020GL087965.

Signori, C. N., Thomas, F., Enrich-Prast, A., Pollery, R. C. & Sievert, S. M. 2014. Microbial diversity and community structure across environmental gradients in Bransfield Strait, Western Antarctic Peninsula. *Front Microbiol,* 5**,** 647.

Silvano, A., Foppert, A., Rintoul, S. R., Holland, P. R., Tamura, T., Kimura, N., Castagno, P., Falco, P., Budillon, G., Haumann, F. A., Garabato, A. N. C. & Macdonald, A. M. 2020. Recent recovery of Antarctic Bottom Water formation in the Ross Sea driven by climate anomalies. *Nature Geoscience,* 13**,** 780-+.

Slawyk, G., Coste, B., Collos, Y. & Rodier, M. 1997. Isotopic and enzymatic analyses of planktonic nitrogen utilisation in the vicinity of Cape Sines (Portugal) during weak upwelling activity. *Deep-Sea Research Part I-Oceanographic Research Papers,* 44**,** 1-25.

Smith, A. C., Welsh, S., Atkinson, H., Harris, D. & Leng, M. J. 2021a. A new automated method for high-throughput carbon and hydrogen isotope analysis of gaseous and dissolved methane at atmospheric concentrations. *Rapid Communications in Mass Spectrometry,* 35**,** e9086.

Smith Jr, K., Sherman, A., Shaw, T. J. & Sprintall, J. 2013. Icebergs as unique Lagrangian ecosystems in polar seas. *Annual Review of Marine Science,* 5**,** 269-287.

Smith Jr, W. & Nelson, D. M. 1990. Phytoplankton growth and new production in the Weddell Sea marginal ice zone in the austral spring and autumn. *Limnology and Oceanography,* 35**,** 809-821.

Smith, S., Altieri, K. E., Mdutyana, M., Walker, D. R., Parrott, R. G., Gallie, S., Spence, K. a. M., Burger, J. M. & Fawcett, S. E. 2022. Biogeochemical controls on ammonium accumulation in the surface layer of the Southern Ocean. *Biogeosciences,* 19**,** 715-741.

Smith, S., Altieri, K. E., Mdutyana, M., Walker, D. R., Parrott, R. G., Spence, K. a. M., Burger, J. M. & Fawcett, S. E. 2021b. Biogeochemical controls on wintertime ammonium

accumulation in the surface layer of the Southern Ocean. *Biogeosciences Discuss.,* 2021**,** 1-39.
Smith, W. O., Carlson, C. A., Ducklow, H. W. & Hansell, D. A. 1998. Growth dynamics of Phaeocystis antarctica-dominated plankton assemblages from the Ross Sea. *Marine Ecology Progress Series,* 168**,** 229-244.
Smith, W. O. & Comiso, J. C. 2008. Influence of sea ice on primary production in the Southern Ocean: A satellite perspective. *Journal of Geophysical Research-Oceans,* 113.
Smith, W. O., Jr., Ainley, D. G., Arrigo, K. R. & Dinniman, M. S. 2014. The oceanography and ecology of the Ross Sea. *Ann Rev Mar Sci,* 6**,** 469-87.
Solomon, C. M., Collier, J. L., Berg, G. M. & Glibert, P. M. 2010. Role of urea in microbial metabolism in aquatic systems: a biochemical and molecular review. *Aquatic Microbial Ecology,* 59**,** 67-88.
Sosik, H., Futrelle, J., Brownlee, E., Peacock, E., Crockford, T. & Olson, R. 2016. IFCB-Analysis software system, initial formal release at v2 feature stage. Github.
Sosik, H. M. & Olson, R. J. 2007. Automated taxonomic classification of phytoplankton sampled with imaging-in-flow cytometry. *Limnology and Oceanography-Methods,* 5**,** 204-216.
Stammerjohn, S. E., Martinson, D. G., Smith, R. C., Yuan, X. & Rind, D. 2008. Trends in Antarctic annual sea ice retreat and advance and their relation to El Nino-Southern Oscillation and Southern Annular Mode variability. *Journal of Geophysical Research-Oceans,* 113.
Stefels, J., Van Leeuwe, M. A., Jones, E. M., Meredith, M. P., Venables, H. J., Webb, A. L. & Henley, S. F. 2018. Impact of sea-ice melt on dimethyl sulfide (sulfoniopropionate) inventories in surface waters of Marguerite Bay, West Antarctic Peninsula. *Philos Trans A Math Phys Eng Sci,* 376**,** 20170169.
Steinacher, M., Joos, F., Frölicher, T. L., Bopp, L., Cadule, P., Cocco, V., Doney, S. C., Gehlen, M., Lindsay, K., Moore, J. K., Schneider, B. & Segschneider, J. 2010. Projected 21st century decrease in marine productivity: a multi-model analysis. *Biogeosciences,* 7**,** 979-1005.
Stock, C. A., Dunne, J. P., Fan, S. M., Ginoux, P., John, J., Krasting, J. P., Laufkötter, C., Paulot, F. & Zadeh, N. 2020. Ocean Biogeochemistry in GFDL's Earth System Model 4.1 and Its Response to Increasing Atmospheric CO2. *Journal of Advances in Modeling Earth Systems,* 12**,** e2019MS002043.
Stoecker, D. K., Hansen, P. J., Caron, D. A. & Mitra, A. 2017. Mixotrophy in the Marine Plankton. *Ann Rev Mar Sci,* 9**,** 311-335.
Strzepek, R. F., Boyd, P. W. & Sunda, W. G. 2019. Photosynthetic adaptation to low iron, light, and temperature in Southern Ocean phytoplankton. *Proc Natl Acad Sci U S A,* 116**,** 4388-4393.
Strzepek, R. F. & Harrison, P. J. 2004. Photosynthetic architecture differs in coastal and oceanic diatoms. *Nature,* 431**,** 689-92.
Strzepek, R. F., Maldonado, M. T., Hunter, K. A., Frew, R. D. & Boyd, P. W. 2011. Adaptive strategies by Southern Ocean phytoplankton to lessen iron limitation: Uptake of organically complexed iron and reduced cellular iron requirements. *Limnology and Oceanography,* 56**,** 1983-2002.
Stubbins, A. & Dittmar, T. 2015. Illuminating the deep: Molecular signatures of photochemical alteration of dissolved organic matter from North Atlantic Deep Water. *Marine Chemistry,* 177**,** 318-324.

Sunagawa, S., Acinas, S. G., Bork, P., Bowler, C., Tara Oceans, C., Eveillard, D., Gorsky, G., Guidi, L., Iudicone, D., Karsenti, E., Lombard, F., Ogata, H., Pesant, S., Sullivan, M. B., Wincker, P. & De Vargas, C. 2020. Tara Oceans: towards global ocean ecosystems biology. *Nat Rev Microbiol,* 18**,** 428-445.

Sunda, W. G. 2012. Feedback Interactions between Trace Metal Nutrients and Phytoplankton in the Ocean. *Front Microbiol,* 3**,** 204.

Suttle, C. A. 2007. Marine viruses--major players in the global ecosystem. *Nat Rev Microbiol,* 5**,** 801-12.

Swadling, K. M., Constable, A. J., Fraser, A. D., Massom, R. A., Borup, M. D., Ghigliotti, L., Granata, A., Guglielmo, L., Johnston, N. M., Kawaguchi, S., Kennedy, F., Kiko, R., Koubbi, P., Makabe, R., Martin, A., Mcminn, A., Moteki, M., Pakhomov, E. A., Peeken, I., Reimer, J., Reid, P., Ryan, K. G., Vacchi, M., Virtue, P., Weldrick, C. K., Wongpan, P. & Wotherspoon, S. J. 2023. Biological responses to change in Antarctic sea ice habitats. *Frontiers in Ecology and Evolution,* 10.

Sylvester, Z., Long, M. & Brooks, C. 2021. Detecting Climate Signals in Southern Ocean Krill Growth Habitat. *Frontiers in Marine Science,* 8**,** 669508.

Syrett, P. J. 1981. Nitrogen-Metabolism of Microalgae. *Canadian Bulletin of Fisheries and Aquatic Sciences,* 210**,** 182-210.

Tagliabue, A., Aumont, O., Death, R., Dunne, J. P., Dutkiewicz, S., Galbraith, E., Misumi, K., Moore, J. K., Ridgwell, A., Sherman, E., Stock, C., Vichi, M., Völker, C. & Yool, A. 2016. How well do global ocean biogeochemistry models simulate dissolved iron distributions? *Global Biogeochemical Cycles,* 30**,** 149-174.

Tagliabue, A., Bopp, L. & Aumont, O. 2008. Ocean biogeochemistry exhibits contrasting responses to a large scale reduction in dust deposition. *Biogeosciences,* 5**,** 11-24.

Tagliabue, A., Bopp, L. & Aumont, O. 2009. Evaluating the importance of atmospheric and sedimentary iron sources to Southern Ocean biogeochemistry. *Geophysical Research Letters,* 36.

Tagliabue, A., Kwiatkowski, L., Bopp, L., Butenschön, M., Cheung, W., Lengaigne, M. & Vialard, J. 2021. Persistent Uncertainties in Ocean Net Primary Production Climate Change Projections at Regional Scales Raise Challenges for Assessing Impacts on Ecosystem Services. *Frontiers in Climate,* 3.

Takao, S., Nakaoka, S. I., Hashihama, F., Shimada, K., Yoshikawa-Inoue, H., Hirawake, T., Kanda, J., Hashida, G. & Suzuki, K. 2020. Effects of phytoplankton community composition and productivity on sea surface CO2 variations in the Southern Ocean. *Deep-Sea Research Part I-Oceanographic Research Papers,* 160**,** 103263.

Takeda, S. 1998. Influence of iron availability on nutrient consumption ratio of diatoms in oceanic waters. *Nature,* 393**,** 774-777.

Talley, L. D., Pickard, G. L., Emery, W. J. & Swift, J. H. 2011. Southern Ocean. *In:* TALLEY, L. D., PICKARD, G. L., EMERY, W. J. & SWIFT, J. H. (eds.) *Descriptive Physical Oceanography*. Boston: Academic Press.

Tanioka, T., Garcia, C. A., Larkin, A. A., Garcia, N. S., Fagan, A. J. & Martiny, A. C. 2022. Global patterns and predictors of C:N:P in marine ecosystems. *Commun Earth Environ,* 3**,** 271.

Taucher, J., Bach, L. T., Prowe, A. E. F., Boxhammer, T., Kvale, K. & Riebesell, U. 2022. Enhanced silica export in a future ocean triggers global diatom decline. *Nature,* 605**,** 696-700.

Terhaar, J., Frölicher, T. L. & Joos, F. 2022. Observation-constrained estimates of the global ocean carbon sink from Earth system models. *Biogeosciences,* 19**,** 4431-4457.

Thomalla, S. J., Waldron, H. N., Lucas, M. I., Read, J. F., Ansorge, I. J. & Pakhomov, E. 2011. Phytoplankton distribution and nitrogen dynamics in the southwest indian subtropical gyre and Southern Ocean waters. *Ocean Science,* 7**,** 113-127.

Thomson, P. G., Davidson, A. T., Van Den Enden, R., Pearce, I., Seuront, L., Paterson, J. S. & Williams, G. D. 2010. Distribution and abundance of marine microbes in the Southern Ocean between 30 and 80°E. *Deep-Sea Research Part Ii-Topical Studies in Oceanography,* 57**,** 815-827.

Thornton, D. C. O. 2014. Dissolved organic matter (DOM) release by phytoplankton in the contemporary and future ocean. *European Journal of Phycology,* 49**,** 20-46.

Timmermans, K. R., Gerringa, L. J., De Baar, H. J., Van Der Wagt, B., Veldhuis, M. J., De Jong, J. T., Croot, P. L. & Boye, M. 2001. Growth rates of large and small Southern Ocean diatoms in relation to availability of iron in natural seawater. *Limnology and Oceanography,* 46**,** 260-266.

Timmermans, K. R., Gledhill, M., Nolting, R. F., Veldhuis, M. J. W., De Baar, H. J. W. & Van Den Berg, C. M. G. 1998. Responses of marine phytoplankton in iron enrichment experiments in the northern North Sea and northeast Atlantic Ocean. *Marine Chemistry,* 61**,** 229-242.

Timmermans, K. R., Van Der Wagt, B. & De Baar, H. J. W. 2004. Growth rates, half-saturation constants, and silicate, nitrate, and phosphate depletion in relation to iron availability of four large, open-ocean diatoms from the Southern Ocean. *Limnology and Oceanography,* 49**,** 2141-2151.

Tortell, P. D., Payne, C. D., Li, Y., Trimborn, S., Rost, B., Smith, W. O., Riesselman, C., Dunbar, R. B., Sedwick, P. & Ditullio, G. R. 2008. CO2 sensitivity of Southern Ocean phytoplankton. *Geophysical Research Letters,* 35.

Touzé-Peiffer, L., Barberousse, A. & Le Treut, H. 2020. The Coupled Model Intercomparison Project: History, uses, and structural effects on climate research. *Wiley Interdisciplinary Reviews: Climate Change,* 11**,** e648.

Tréguer, P., Bowler, C., Moriceau, B., Dutkiewicz, S., Gehlen, M., Aumont, O., Bittner, L., Dugdale, R., Finkel, Z., Iudicone, D., Jahn, O., Guidi, L., Lasbleiz, M., Leblanc, K., Levy, M. & Pondaven, P. 2017. Influence of diatom diversity on the ocean biological carbon pump. *Nature Geoscience,* 11**,** 27-37.

Trimborn, S., Thoms, S., Karitter, P. & Bischof, K. 2019. Ocean acidification and high irradiance stimulate the photo-physiological fitness, growth and carbon production of the Antarctic cryptophyte Geminigera cryophila. *Biogeosciences,* 16**,** 2997-3008.

Trivelpiece, W. Z., Hinke, J. T., Miller, A. K., Reiss, C. S., Trivelpiece, S. G. & Watters, G. M. 2011. Variability in krill biomass links harvesting and climate warming to penguin population changes in Antarctica. *Proc Natl Acad Sci U S A,* 108**,** 7625-8.

Trull, T. W. & Armand, L. 2001. Insights into Southern Ocean carbon export from the δ13C of particles and dissolved inorganic carbon during the SOIREE iron release experiment. *Deep-Sea Research Part Ii-Topical Studies in Oceanography,* 48**,** 2655-2680.

Tsakalakis, I., Follows, M. J., Dutkiewicz, S., Follett, C. L. & Vallino, J. J. 2022. Diel light cycles affect phytoplankton competition in the global ocean. *Global Ecology and Biogeography,* 31**,** 1838-1849.

Tupas, L. M., Koike, I., Karl, D. M. & Holmhansen, O. 1994. Nitrogen-Metabolism by Heterotrophic Bacterial Assemblages in Antarctic Coastal Waters. *Polar Biology,* 14**,** 195-204.

Turner, J., Barrand, N. E., Bracegirdle, T. J., Convey, P., Hodgson, D. A., Jarvis, M., Jenkins, A., Marshall, G., Meredith, M. P., Roscoe, H., Shanklin, J., French, J., Goosse, H., Guglielmin, M., Gutt, J., Jacobs, S., Kennicutt, M. C., Masson-Delmotte, V., Mayewski, P., Navarro, F., Robinson, S., Scambos, T., Sparrow, M., Summerhayes, C., Speer, K. & Klepikov, A. 2014. Antarctic climate change and the environment: an update. *Polar Record,* 50**,** 237-259.

Turner, J. & Comiso, J. 2017. Solve Antarctica's sea-ice puzzle. *Nature,* 547**,** 275-277.

Turner, J., Holmes, C., Harrison, T. C., Phillips, T., Jena, B., Reeves-Francois, T., Fogt, R., Thomas, E. R. & Bajish, C. C. 2022. Record Low Antarctic Sea Ice Cover in February 2022. *Geophysical Research Letters,* 49**,** e2022GL098904.

Uchida, T., Balwada, D., R, P. A., G, A. M., S, K. S. & Levy, M. 2020. Vertical eddy iron fluxes support primary production in the open Southern Ocean. *Nat Commun,* 11**,** 1125.

Van Boekel, J., Stefels, W., Stefels, J. & Van Boekel, W. 1993. Production of DMS from dissolved DMSP in axenic cultures of the marine phytoplankton species Phaeocystis spp. *Mar. Ecol. Prog. Ser,* 97**,** 11-18.

Van Leeuwe, M., Scharek, R., De Baar, H. J., De Jong, J. & Goeyens, L. 1997. Iron enrichment experiments in the Southern Ocean: physiological responses of plankton communities. *Deep Sea Research Part II: Topical Studies in Oceanography,* 44**,** 189-207.

Venables, H. J., Clarke, A. & Meredith, M. P. 2013. Wintertime controls on summer stratification and productivity at the western Antarctic Peninsula. *Limnology and Oceanography,* 58**,** 1035-1047.

Virtanen, P., Gommers, R., Oliphant, T. E., Haberland, M., Reddy, T., Cournapeau, D., Burovski, E., Peterson, P., Weckesser, W. & Bright, J. 2020. SciPy 1.0: fundamental algorithms for scientific computing in Python. *Nature methods,* 17**,** 261-272.

Wadley, M. R., Jickells, T. D. & Heywood, K. J. 2014. The role of iron sources and transport for Southern Ocean productivity. *Deep-Sea Research Part I-Oceanographic Research Papers,* 87**,** 82-94.

Walker, O. S., Jr., Craig, A. C., Hugh, W. D. & Dennis, A. H. 1998. Growth dynamics of Phaeocystis antarctica-dominated plankton assemblages from the Ross Sea. *Marine Ecology Progress Series,* 168**,** 229-244.

Wang, S. & Moore, J. K. 2011. Incorporating Phaeocystisis nto a Southern Ocean ecosystem model. *Journal of Geophysical Research,* 116.

Wang, X. D., Wang, Y. & Smith, W. O. 2011. The role of nitrogen on the growth and colony development of Phaeocystis globosa (Prymnesiophyceae). *European Journal of Phycology,* 46**,** 305-314.

Ward, B. A. & Follows, M. J. 2016. Marine mixotrophy increases trophic transfer efficiency, mean organism size, and vertical carbon flux. *Proc Natl Acad Sci U S A,* 113**,** 2958-63.

Waters, K. J. & Smith, R. C. 1992. Palmer LTER: A sampling grid for the Palmer LTER program. *Antarctic Journal of the United States,* 27**,** 236-239.

Watson, A. J., Bakker, D. C., Ridgwell, A. J., Boyd, P. W. & Law, C. S. 2000. Effect of iron supply on Southern Ocean CO2 uptake and implications for glacial atmospheric CO2. *Nature,* 407**,** 730-3.

Watts, J., Bell, T. G., Anderson, K., Butterworth, B. J., Miller, S., Else, B. & Shutler, J. 2022. Impact of sea ice on air-sea CO2 exchange – A critical review of polar eddy covariance studies. *Progress in Oceanography,* 201**,** 102741.

Weber, T. S. & Deutsch, C. 2010. Ocean nutrient ratios governed by plankton biogeography. *Nature,* 467**,** 550-4.

Westwood, K. J., Thomson, P. G., Van Den Enden, R. L., Maher, L. E., Wright, S. W. & Davidson, A. T. 2018. Ocean acidification impacts primary and bacterial production in Antarctic coastal waters during austral summer. *Journal of Experimental Marine Biology and Ecology,* 498**,** 46-60.

Wilkins, D., Van Sebille, E., Rintoul, S. R., Lauro, F. M. & Cavicchioli, R. 2013a. Advection shapes Southern Ocean microbial assemblages independent of distance and environment effects. *Nat Commun,* 4**,** 2457.

Wilkins, D., Yau, S., Williams, T. J., Allen, M. A., Brown, M. V., Demaere, M. Z., Lauro, F. M. & Cavicchioli, R. 2013b. Key microbial drivers in Antarctic aquatic environments. *FEMS Microbiol Rev,* 37**,** 303-35.

Wohlers, J., Engel, A., Zollner, E., Breithaupt, P., Jurgens, K., Hoppe, H. G., Sommer, U. & Riebesell, U. 2009. Changes in biogenic carbon flow in response to sea surface warming. *Proc Natl Acad Sci U S A,* 106**,** 7067-72.

Woodward, E. M. S. & Rees, A. P. 2001. Nutrient distributions in an anticyclonic eddy in the northeast Atlantic Ocean, with reference to nanomolar ammonium concentrations. *Deep-Sea Research Part Ii-Topical Studies in Oceanography,* 48**,** 775-793.

Wright, S. W., Van Den Enden, R. L., Pearce, I., Davidson, A. T., Scott, F. J. & Westwood, K. J. 2010. Phytoplankton community structure and stocks in the Southern Ocean (30–80 E) determined by CHEMTAX analysis of HPLC pigment signatures. *Deep Sea Research Part II: Topical Studies in Oceanography,* 57**,** 758-778.

Wu, M., Mccain, J. S. P., Rowland, E., Middag, R., Sandgren, M., Allen, A. E. & Bertrand, E. M. 2019. Manganese and iron deficiency in Southern Ocean Phaeocystis antarctica populations revealed through taxon-specific protein indicators. *Nat Commun,* 10**,** 3582.

Xu, K., Fu, F. X. & Hutchins, D. A. 2014. Comparative responses of two dominant Antarctic phytoplankton taxa to interactions between ocean acidification, warming, irradiance, and iron availability. *Limnology and Oceanography,* 59**,** 1919-1931.

Yadav, J., Kumar, A. & Mohan, R. 2020. Dramatic decline of Arctic sea ice linked to global warming. *Natural Hazards,* 103**,** 2617-2621.

Yang, E. J., Jiang, Y. & Lee, S. 2016. Microzooplankton herbivory and community structure in the Amundsen Sea, Antarctica. *Deep-Sea Research Part Ii-Topical Studies in Oceanography,* 123**,** 58-68.

Yang, X., Wynn-Edwards, C. A., Strutton, P. G. & Shadwick, E. H. 2024. Drivers of Air-Sea CO2 Flux in the Subantarctic Zone Revealed by Time Series Observations. *Global Biogeochemical Cycles,* 38**,** e2023GB007766.

Yao, W. J., Shi, J. X. & Zhao, X. L. 2017. Freshening of Antarctic Intermediate Water in the South Atlantic Ocean in 2005-2014. *Ocean Science,* 13**,** 521-530.

Yentsch, C. S. & Vaccaro, R. F. 2003. Phytoplankton Nitrogen in the Oceans. *Limnology and Oceanography,* 3**,** 443-448.

Yuan, X. J. 2004. ENSO-related impacts on Antarctic sea ice: a synthesis of phenomenon and mechanisms. *Antarctic Science,* 16**,** 415-425.

Zheng, B., Lucas, A. J., Franks, P. J. S., Schlosser, T. L., Anderson, C. R., Send, U., Davis, K., Barton, A. D. & Sosik, H. M. 2023. Dinoflagellate vertical migration fuels an intense red tide. *Proc Natl Acad Sci U S A,* 120**,** e2304590120.

Zhu, Z., Xu, K., Fu, F. X., Spackeen, J. L., Bronk, D. A. & Hutchins, D. A. 2016. A comparative study of iron and temperature interactive effects on diatoms and Phaeocystis antarctica from the Ross Sea, Antarctica. *Marine Ecology Progress Series,* 550**,** 39-51.
Zhuang, J., Dussin, R., Jüling, A. & Rasp, S. 2018. xESMF: Universal regridder for geospatial data. *Zenodo [code],* 10.